

*marine drugs*

# Bioactive Molecules from Extreme Environments

---

Edited by

Daniela Giordano

Printed Edition of the Special Issue Published in *Marine Drugs*



Review

# Deep-Sea Fungi Could Be the New Arsenal for Bioactive Molecules

Muhammad Zain ul Arifeen, Yu-Nan Ma, Ya-Rong Xue and Chang-Hong Liu \*

State Key Laboratory of Pharmaceutical Biotechnology, School of Life Sciences, Nanjing University, Nanjing 210023, China; m.z.arifeen@gmail.com (M.Z.u.A.); mayunan994727@163.com (Y.-N.M.); xueyr@nju.edu.cn (Y.-R.X.)

\* Correspondence: chliu@nju.edu.cn; Tel./Fax: +86-25-8968-5469

Received: 28 November 2019; Accepted: 17 December 2019; Published: 20 December 2019

**Abstract:** Growing microbial resistance to existing drugs and the search for new natural products of pharmaceutical importance have forced researchers to investigate unexplored environments, such as extreme ecosystems. The deep-sea (>1000 m below water surface) has a variety of extreme environments, such as deep-sea sediments, hydrothermal vents, and deep-sea cold region, which are considered to be new arsenals of natural products. Organisms living in the extreme environments of the deep-sea encounter harsh conditions, such as high salinity, extreme pH, absence of sun light, low temperature and oxygen, high hydrostatic pressure, and low availability of growth nutrients. The production of secondary metabolites is one of the strategies these organisms use to survive in such harsh conditions. Fungi growing in such extreme environments produce unique secondary metabolites for defense and communication, some of which also have clinical significance. Despite being the producer of many important bioactive molecules, deep-sea fungi have not been explored thoroughly. Here, we made a brief review of the structure, biological activity, and distribution of secondary metabolites produced by deep-sea fungi in the last five years.

**Keywords:** deep-sea; extreme; ecosystem; fungi; bioactive compounds; secondary metabolites

---

## 1. Deep-Sea Fungi: A Novel Source of Bioactive Molecules

Antibiotics and antifungal drugs are the most commonly used drugs in the world, but their role in treating human diseases has been greatly reduced due to the development of pathogen resistance against these drugs. Scientists are now looking for new, untapped and renewable resources for the isolation of novel compounds to with clinical importance. Despite the fact that the ocean provides habitats to a huge number of microbes, both fungi and bacteria for thousands of years, the microbes of these extreme ecosystems and their potential for new drug discovery have not yet been fully realized due to methodological and technical limitations. Fungi are the most diverse and abundant eukaryotic organisms on the planet, and their presence in all possible extreme ecosystems make them an ideal source for investigations of new drug development. Scientists are interested in the extraction of novel and unique natural products, having clinical importance, from different organisms living in the extreme environments. In addition to terrestrial extreme environments, the ocean could also be considered a good reservoir of bioactive metabolites [1–4]. Fungi living in the deep-sea environments are known to produce novel bioactive compounds. Although, it is not fully understood why the fungi living in the extreme environments produce unique and novel products, it is assumed that fungal genome has evolved to make necessary adjustments in order to sustain life in such harsh conditions and might be involved in chemical defense and communication [5].

The ocean is considered to be one of the most diverse ecosystems. Compared to terrestrial and coastal ecosystems, the deep-sea (water depths below 1000 m) has a variety of extreme environments, such as temperatures ranging from 0 to 400 °C, lack of light and oxygen, high hydrostatic pressure

up to 400 atm, and limited supply of nutrient substrates, making these habitats extremely difficult for life [6,7]. In order to inhabit such extreme ecosystems, organisms should have the potential to adjust to these conditions with different mechanism, such as regulating temperature, pH, and solute concentration, as well as the production of biomolecules to control DNA, protein, and lipid damage. This may be why microorganisms growing in these environments produce special metabolites.

Previously, drug investigators mainly considered bacteria, especially actinomycetes, as an important source of antifungal and antibacterial drugs. Cephalosporin C was the first compound derived from the marine fungus *Cephalosporium* sp. in 1949. After that, a number of important drugs—for instance, polyketide griseofulvin, terpenoid fusidic acid, cephalosporins, etc.—have been isolated from the marine fungi. Despite being the source of such important products, deep-sea fungi have not received full attention [8]. With the increasing demand for new drugs, scientists are now looking for new and unexplored resources for bioactive compounds, and the deep-sea consists of some extreme ecosystems that are worth exploring for new metabolites. Studies about isolating new bioactive molecules from marine environments are growing at an increasing rate, and hundreds of new compounds are reported every year; for instance, in 2017, a total of 448 new compounds were reported [9].

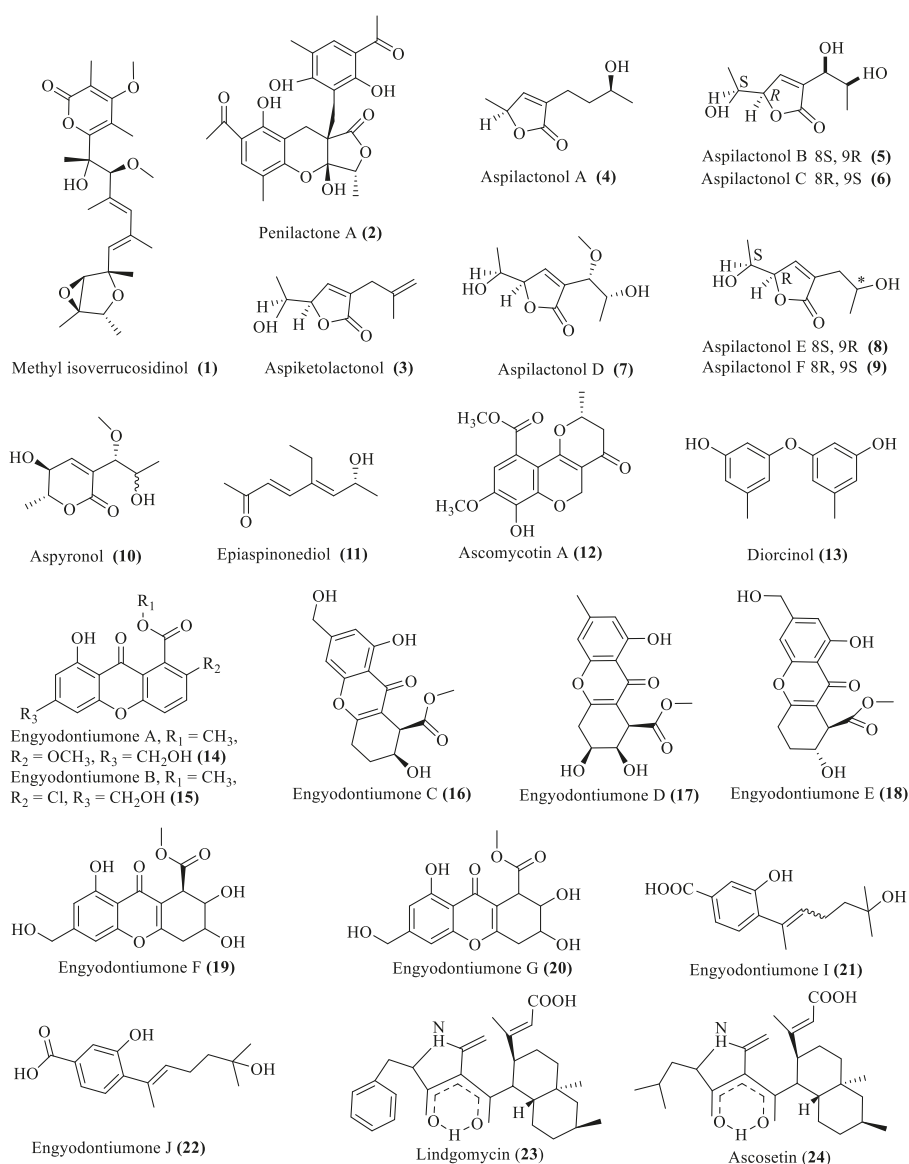
In this review, we present an overview of all those new and important bioactive metabolites isolated from deep-sea fungi during the last five years. We include only those molecules which were extracted from the deep-sea fungi associated with some kind of extreme environments, irrespective of its isolation from terrestrial counterparts, while all those compounds were excluded which were isolated from marine fungi and were not associated with extreme environments. This review will benefit all those who are interested in extreme-marine-environment fungi and their bioactive molecules. For more detailed information about other important secondary metabolites extracted from marine fungi, one should refer to our previous review papers [10–12].

## 2. Bioactive Compounds from Deep-Sea Fungi

According to the literature survey, we found 151 novel bioactive compounds isolated from marine fungi extracted from different extreme environments in the last five years. The majority of these compounds were isolated from two fungal genera i.e., *Penicillium* (63, 41.2% of the total compounds) and *Aspergillus* (43, 28.1% of the total compounds). Table 1 lists the detail of these compounds, which fall into different categories according to their structure.

### 2.1. Polyketide Compounds

Twenty-four polyketide compounds (1–24; Figure 1) with important biological activities were isolated from fungi extracted from different deep-sea environments. Among them, compounds 1 and 2 were isolated from *Penicillium* spp., which showed antibiotic activity (MIC of 32 µg/mL against *Bacillus subtilis*) and nuclear factor NF-κB inhibition activity, respectively [13,14]. Compounds 3–11 were from *Aspergillus* sp. 16-02-1, which exhibited cytotoxicity (with a 10%–80% inhibition rate at 100 µg/mL against various cancer cell lines i.e., K562, HL-60, HeLa, and BGC-823) [15]. Similarly, compounds 12–24 were isolated from the species belonging to *Ascomycetes*, *Engyodontium*, and *Lindgomycetaceae*, out of which compounds 12–13 and 23–24 showed strong antibiotic activities against *Bacillus subtilis*, *Acinetobacter baumannii*, *Escherichia coli*, *Staphylococcus aureus*, *Enterococcus faecalis*, *Staphylococcus epidermidis*, and *Propionibacterium acnes*, while compounds 14–22 exhibited strong cytotoxic activity (IC<sub>50</sub> 4.9 µM) against U937 cells (Table 1) [16–18].

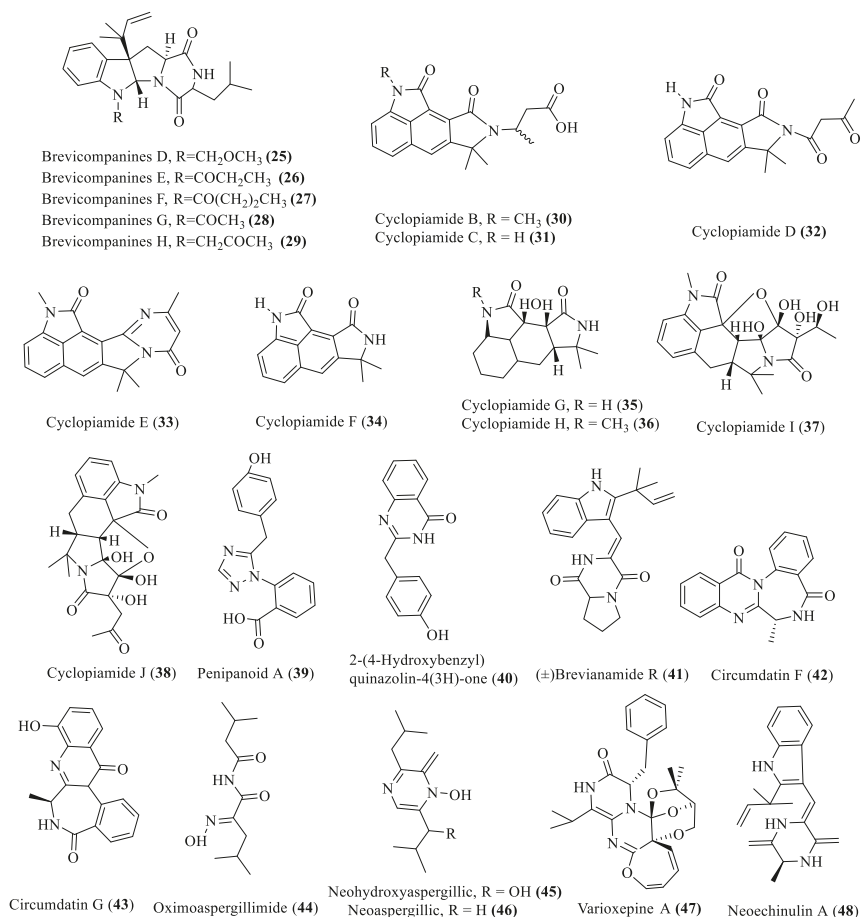


**Figure 1.** Structures of polyketide secondary metabolites obtained from deep-sea fungi.

## 2.2. Nitrogen-Containing Compounds

Twenty-four novel alkaloid-bioactive compounds (25–48; Figure 2) have been reported from deep-sea fungi since 2013, out of which compounds 25–40 were isolated from *Penicillium* spp., and showed cytotoxic activities against BV2 cell ( $\text{IC}_{50}$  of 27–45  $\mu\text{g/mL}$ ), brine shrimp ( $\text{IC}_{50}$  of 14.1 to 38.5  $\mu\text{g/mL}$ ), SMMC-7721 ( $\text{IC}_{50}$  of 54.2  $\mu\text{M}$ ), BEL-7402 ( $\text{IC}_{50}$  of 17.5  $\mu\text{M}$ ), and BEL-7402 ( $\text{IC}_{50}$  of 19.8  $\mu\text{M}$ ) [19–21]. Compounds 41–46 were identified from *Aspergillus* spp., in which compounds 41 and 45–46 displayed antibiotic activity (MIC of 30 to 40  $\mu\text{g/mL}$ ) against BCG, *Candida albicans*, *Bacillus subtilis*, *Staphylococcus aureus*, *Pseudomonas aeruginosa*, *Bacillus cereus*, *Klebsiella pneumoniae*, and *Escherichia coli*,

while compounds **47** and **48** were extracted from other genera and showed antimicrobial activity (MIC between 16 and 64  $\mu\text{g/mL}$  against *Escherichia coli*, *Aeromonas hydrophila*, *Micrococcus luteus*, *Staphylococcus aureus*, *Vibrio anguillarum*, *Vibrio harveyi*, and *Vibrio parahaemolyticus*) and cytotoxic activity against human cervical carcinoma HeLa, respectively [22–26].

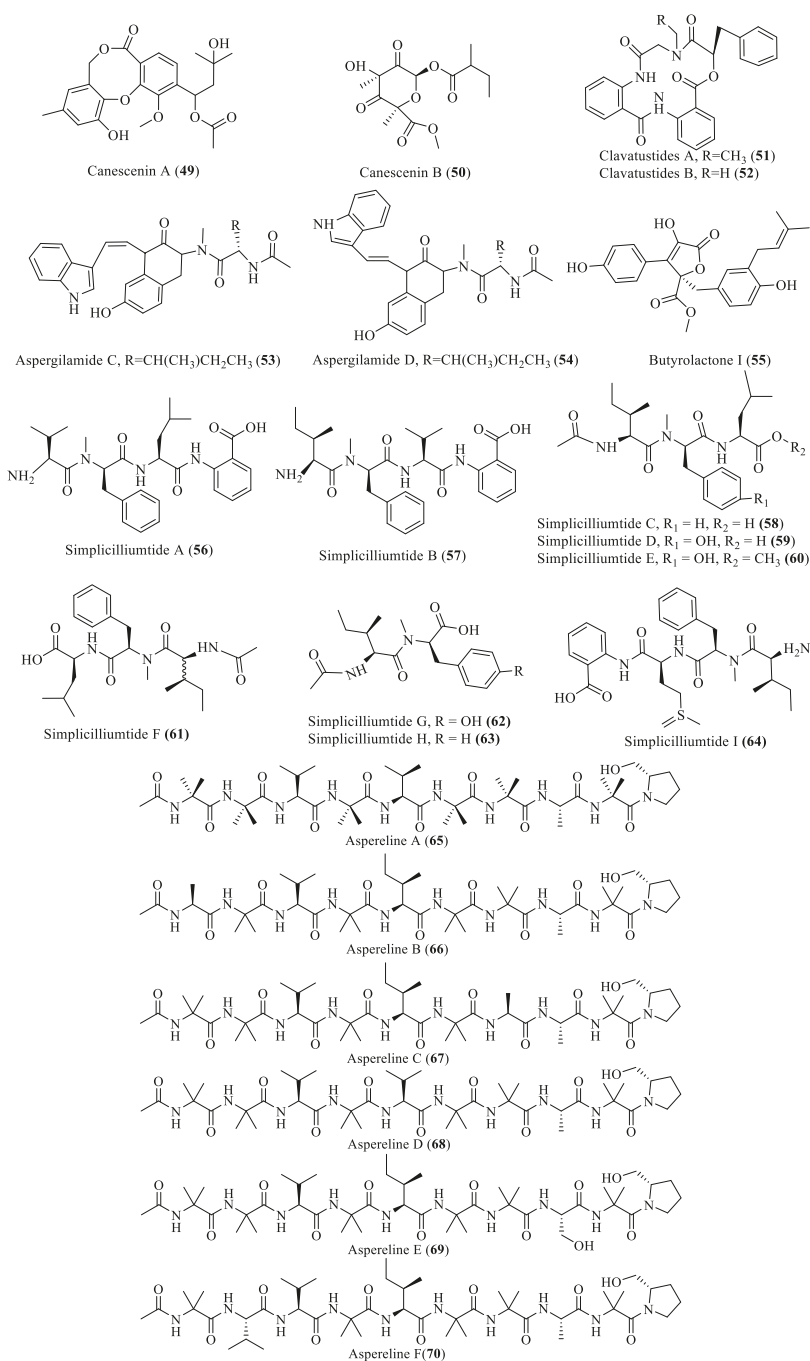


**Figure 2.** Bioactive alkaloid compounds isolated from deep-sea fungi.

### 2.3. Polypeptides

Twenty-two polypeptides with novel structures (**49–70**; Figure 3) were reported from fungi inhabiting different marine environments during 2013–2019. Compounds **49** and **50** were isolated from *Penicillium canescens* and displayed antibiotic activity against *Bacillus amyloliquefaciens* and *Pseudomonas aeruginosa* at 100  $\mu\text{M}$ , while compounds **51–55** were extracted from *Aspergillus* spp., in which **51–54** showed cytotoxic activity (IC<sub>50</sub> of 15–25  $\mu\text{g/mL}$ ) against HepG2, SMMC-7721, Bel-7402, and human glioma U87 cell lines, while compound **55** showed inhibitory effects (IC<sub>50</sub> value of 5.11  $\mu\text{mol/L}$ ) against *Mycobacterium tuberculosis* protein tyrosine phosphatase B (MtpB) [27–30]. However, compounds **56–64**, which were obtained from *Simplicillium obclavatum*, and **65–70**, obtained from *Trichoderma asperellum*, displayed cytotoxicity (IC<sub>50</sub> of 39.4–100  $\mu\text{M}$ ) against human leukemia HL-60 and K562 cell lines and antibiotic activity (IC<sub>50</sub> of 39.4–100  $\mu\text{M}$ ) against Gram-positive bacteria

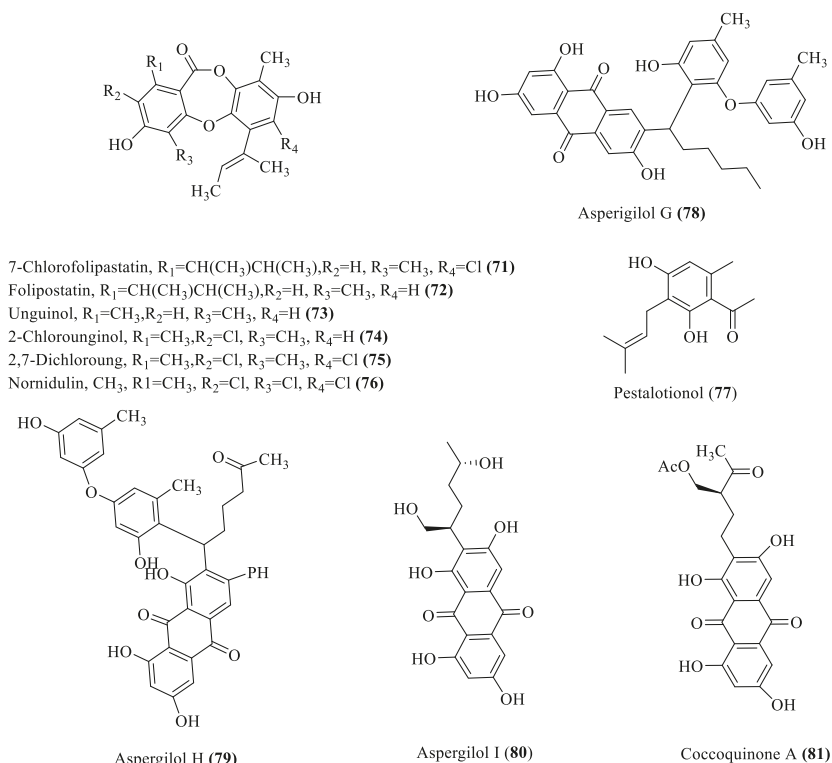
(e.g., *Bacillus amyloliquefaciens*, *Staphylococcus aureus*) and Gram-negative bacteria (e.g., *Pseudomonas aeruginosa* and *Escherichia coli*), respectively [28,31].



**Figure 3.** Bioactive polypeptides isolated from deep-sea fungi.

## 2.4. Ester and Phenolic Derivatives

Six new ester derivatives (**71–76**; Figure 4) were extracted from *Aspergillus ungui* NKH-007 and showed inhibition of sterol O-acyltransferase (SOAT) enzymes in Chinese hamster ovary (CHO) cells and are thus considered to be good candidates for an anti-atherosclerotic agent [32]. Five new phenolic compounds (**77–81**; Figure 4) isolated from *Penicillium* sp. and *Aspergillus versicolor* showed potent activity against *Staphylococcus aureus* and *Bacillus subtilis*, with MIC values of 2–8 µg/mL [33,34]. However, compounds **78–81** expressed antiviral activity toward HSV-1, with EC<sub>50</sub> values of 3.12–6.25 µM [34].



**Figure 4.** Ester and phenolic derivatives obtained from deep-sea fungi.

## 2.5. Piperazine Derivatives

Fourteen new piperazine derivatives (**82–95**; Figure 5) reported from marine fungi during the last five years. These derivatives were isolated from genera of *Penicillium*, *Aspergillus*, and *Dichotomomyces* collected from deep-sea sediments. Compounds **82–84** showed strong cytotoxicity with IC<sub>50</sub> of 1.7 and 2 µM against K562 and mouse lymphoma cell line, respectively; similarly, compounds **91–95** also showed strong cytotoxic activity [35–37]. Compounds **85–89** showed antibacterial activity against *Staphylococcus aureus* with the MIC values of 6.25–12.5 µg/mL [21]. The new compound **90** also showed stronger inhibition activity against α-glucosidase with IC<sub>50</sub> value of 138 µM [37].



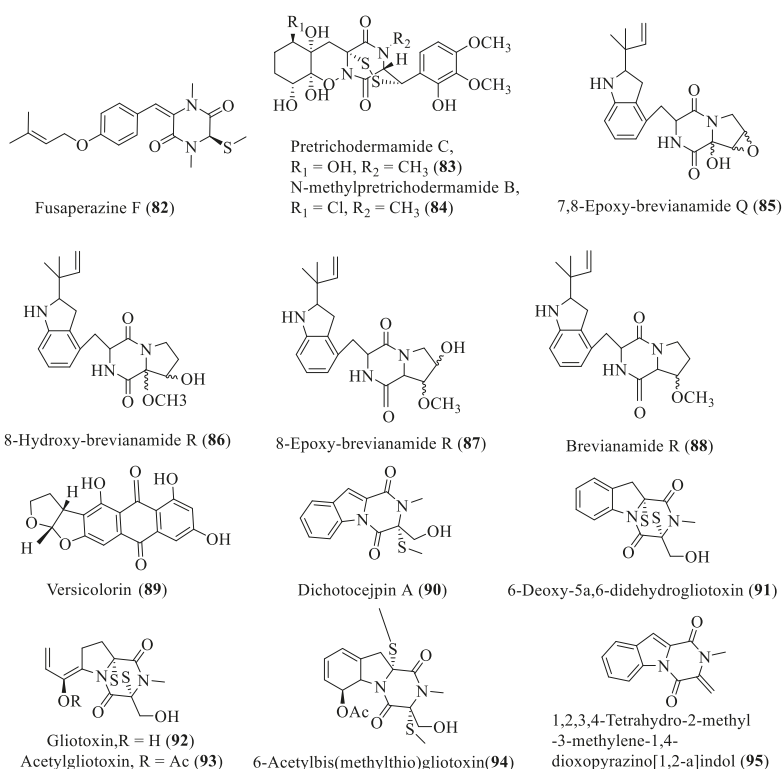
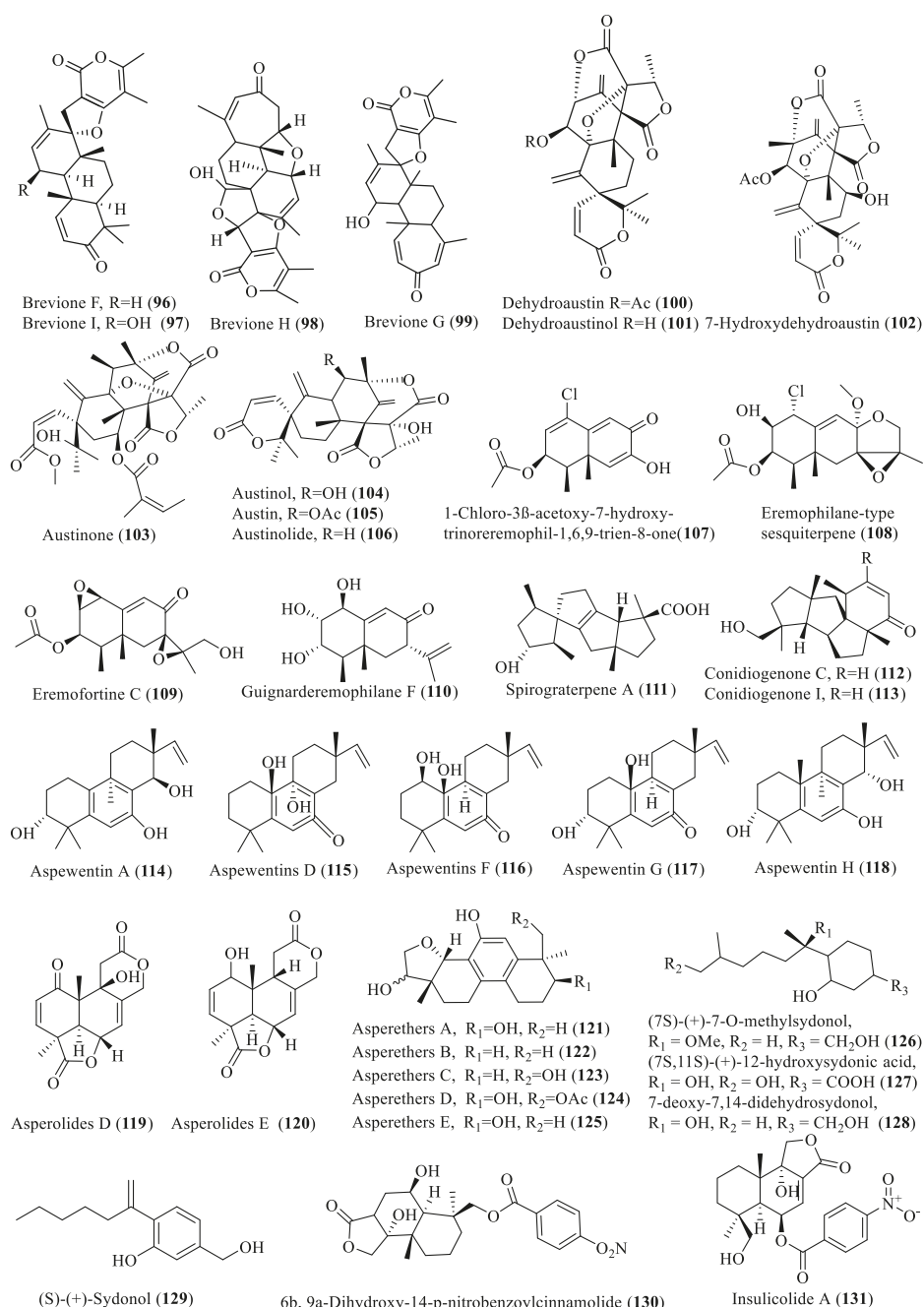


Figure 5. Piperazine derivatives isolated from deep-sea fungi.

## 2.6. Terpenoid Compounds

Thirty-six new and important bioactive terpenoids (96–131; Figure 6) have been isolated from marine fungi extracted from the deep-sea sediments since 2013. Compounds 96–113 were isolated from *Penicillium* spp., while compounds 114–131 were extracted from *Aspergillus* spp. Breviones (96–99), isolated from the deepest sediment-derived fungus *Penicillium* sp. (5115 m depth), displayed diverse activities, such as cytotoxicity against HeLa, MCF-7, and A549 cells with  $\text{IC}_{50}$  values of 7.44 to 32.5  $\mu\text{M}$ , respectively, and growth inhibition of HIV-1 with  $\text{EC}_{50}$  value of 14.7  $\mu\text{M}$  against C8166 cells [22,38]. Compounds 100–110 showed antibiotic and inhibition activities against silkworm, while 20-nor-isopimarane diterpenoids, including aspewentins (114–118), asperethers (121–125), asperoloids (119–120), and compounds 130 and 131, showed cytotoxic activities [33,39–45]. However, the spirocyclic diterpenes (111–113) exhibited strong anti-allergic effect with 18% inhibition at 20  $\mu\text{g/mL}$  [46]. Interestingly, four new compounds (126–129) were extracted from hydrothermal vent-derived *Aspergillus sydowii*, through activation of a new pathway for secondary metabolite production by the addition of a 5-azacytidine (a DNA methyltransferase inhibitor). These compounds showed anti-inflammatory and antidiabetic activities and are thus the first secondary metabolites isolated from fungi which have both antidiabetic and anti-inflammatory activities [47].

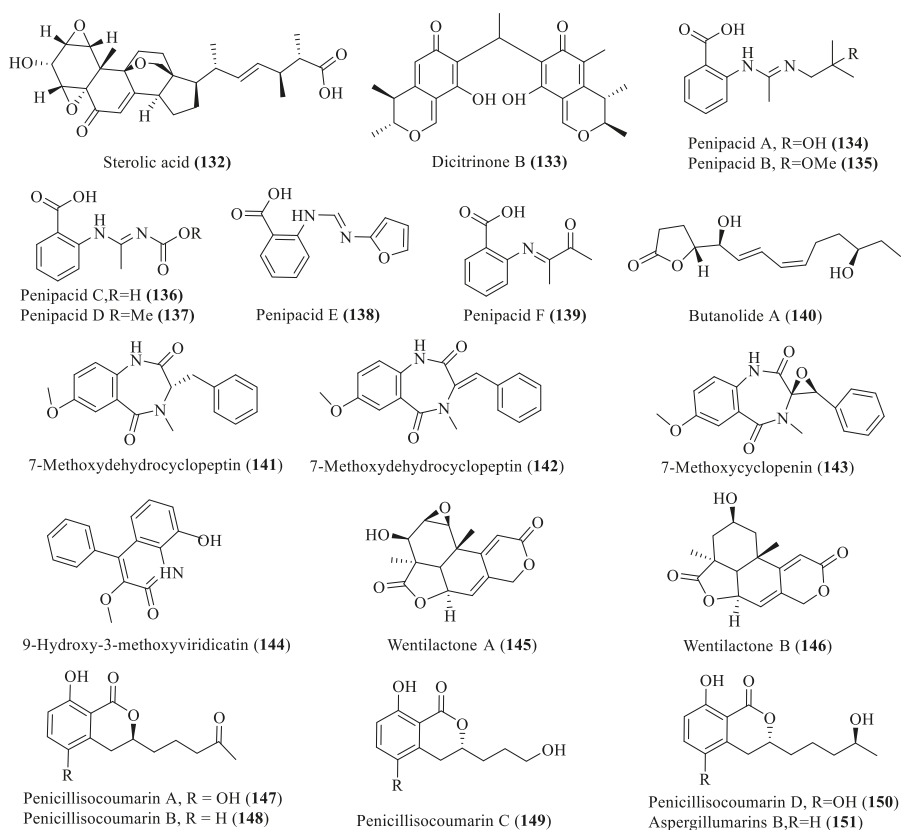


**Figure 6.** Structures of terpenoid secondary metabolites obtained from deep-sea fungi.

## 2.7. Other Unrelated Compounds

Twenty secondary metabolites with different structures were isolated from deep-sea fungi, mainly from *Penicillium* spp. and *Aspergillus* spp. (132–151; Figure 7). Penipacids A–F (134–139),

polyoxygenated sterol (**132**), dicitrinone B (**133**) and butanolide A (**140**), which were isolated from deep-sea sediments-derived *Penicillium* spp., showed cytotoxic activities against RKO, MCF-7, PTP1B and A375 cancer cell lines with IC<sub>50</sub> values of 8.4–28.4  $\mu$ M [38,42,48,49]. Similarly, four isocoumarins, penicillisocoumarin A–D (**147**–**150**), and an isocoumarins aspergillumarin B (**151**) were also isolated from *Penicillium* which showed weak antibacterial activities [33]. Four antibiotic cyclophenin derivatives compounds (**141**–**144**) and a series of antitumor wentilactones (**145**,**146**) were isolated from *Aspergillus* spp. [50,51].



**Figure 7.** Bioactive metabolites derived from deep-sea fungi.

Table 1. Secondary metabolites extracted from deep-sea fungi during 2013–2019.

Metabolites	Fungal Species	Source	Location	Depth (m) *	Bioactivity	Ref.
Methyl-isoverrucosidinol (1)	<i>Penicillium</i> sp. Y-50-10	Sulfur-rich Sediment	hydrothermal vent, Taiwan	–	Antibiotic	[13]
	<i>Penicillium crustosum</i> PRB-2	Sediment	Prydz Bay, Antarctica	526	NF- $\kappa$ B inhibition	[14]
Aspiketolactonol (3)	<i>Aspergillus</i> sp. 16-02-1	Hydrothermal vent water	Lau Basin, Southwest Pacific Ocean,	2255	Cytotoxic	[15]
Aspilactonols A–F (4–9)						
Aspyronol (10)						
Epispinonediol (11)						
Ascomycin A (12)	<i>Ascomycolta</i> sp. Ind19F07	Sediment	Indian Ocean	3614	Antibiotic	[16]
Diocinol (13)	<i>Engyodontium album</i> DFFCS021	Sediment	South China Sea	3739	Cytotoxic	[18]
Engyodontiumones A–J (14–22)	<i>Lindogmycetaceae</i> strains KF970 and LF327	Sediment	Greenland Sea, Baltic Sea	3650	Antibiotic	[17]
Lindogmycin (23)						
Ascosetin (24)						
Nitrogen-containing compounds						
Brevicompanines D–H (25–29)	<i>Penicillium</i> sp. F1	Sediment	–	5080	LPS-induced inflammation	[22]
Cyclopiamide B–J (30–38)	<i>Penicillium commune</i> DFFCS026	Sediment	South China Sea	3563	Cytotoxic	[24]
Penipanoid A (39)	<i>Penicillium paneum</i> SD-44	Sediment	South China Sea	201	Cytotoxic	[23]
Quinazolinone (40)						
(±) Brevianamide R (41)	<i>Aspergillus versicolor</i> MF180151	Sediment	Bohai Sea, China	–	Antibacterial	[21]
Circumdatin F and G (42–43)	<i>Aspergillus awsterdijkiae</i> SCSIO 05233	Sediment	South China Sea	4593	Cytotoxic	[20]
Oximospergillimide (44)						
Neohydroxyaspergillic (45)	<i>Aspergillus</i> sp. (CH07002)	Water	Pacific Ocean off the coast of Panama		Cytotoxic Antibiotic	[19]
Neosaspergillic (46)						
Varioxepine A (47)	<i>Pactilomyces variotii</i> EN-291	Deep sea water	–	–	Antibiotic	[26]
Neochinulin A (48)	<i>Microsporium</i> sp. (MFS-YL)	Red alga	Guryongpo, Korea	–	Cytotoxic	[25]
Polypeptide						
Canescenin A and B (49–50)	<i>Penicillium canescens</i> SCSIO 2053	Water	East China Sea	2013	Antibacterial	[27]
Clavustide A and B (51–52)	<i>Aspergillus clavatus</i> C2WU	Hydrothermal vent crab	Taiwan Kuishantao	–	Cytotoxic	[29]
Aspergillamides C and D (53–54)	<i>Aspergillus terreus</i> SCSIO 41008	Sponge	Guangdong, China	–	Cytotoxic Antibiotic	[30]
Butyrolactone I (55)						
Simpliciliumitides A–I (56–64)	<i>Simplicillium obclavatum</i> EIODSF 020	Sediment	East Indian Ocean	4571	Cytotoxic	[31]
Asperelines A–F (65–70)	<i>Trichoderma asprellum</i>	Sediment	Antarctic Penguin Island	–	Antibiotic	[28]

Table 1. Cont.

Metabolites	Fungal Species	Source	Location	Depth (m) *	Bioactivity	Ref.
Esters						
7-chlorofolipastatin (71) Folipostatin B (72) Unguinol (73) 2-chlorounginol (74) 2,7-dichlorounginol (75) Noridulin (76)	<i>Aspergillus unguis</i> NKH-007	Sediment	Suruga Bay, Japan	–	Anti-atherosclerotic Cytotoxic Antibiotic	[32]
Phenolic						
Pestalotolol (77)	<i>Penicillium</i> sp. Y-5-2	Hydrothermal vent water	Kueishantao off Taiwan	–	Antibiotic	[33]
Aspergillol G–I (78–80) Coccoquinone A (81)	<i>Aspergillus versicolor</i> SCSIO 41502	Sediment	South China Sea	2326	Anti-HSV-1 Antioxidant Antifouling	[34]
Piperazine						
Fusaperazine F (82)	<i>Penicillium crustosum</i> HDN153086	Sediment	Prydz Bay, Antarctica	–	Cytotoxic	[35]
N-methyl-pretichodermamide B (83) Pretichodermamide C (84)	<i>Penicillium</i> sp. (WN-11-1-3-1-2)	Hypersaline sediment	Wadi El-Natrun, Egypt	–	Cytotoxic	[36]
(±) 7,8-epoxy-brevianamide Q (85) (±) 8-hydroxy-brevianamide R (86) (±) 8-epihydroxy-brevianamide R (87) Brevianamide R (88) Versicolorin B (89)	<i>Aspergillus versicolor</i> MF180151	Sediment	Bohai Sea, China	–	Antibiotic	[21]
Dichotocepsins A (90) 6-deoxy-5a,6-didehydroglutotoxin (91) Glutotoxin (92) Acetylglutotoxin (93) 6-acetylbis(methylthio)-glutotoxin (94) 1,2,3,4-tetrahydro-2-methyl-3-methylene-1,4-dioxypyrazino [1,2-a] indole (95)	<i>Dichotomomyces ceipii</i> FS110	Sediment	South China Sea	3941	α-Glucosidase inhibition Cytotoxic	[37]
Terpenoid						
Brevione F–I (96–99)	<i>Penicillium</i> sp. (MCCC 3A00005)	Sediment	Pacific Ocean	5115	Cytotoxic HIV-1 inhibition	[22,38]
Dehydroaustin (100) Dehydroaustinol (101) 7-hydroxydehydroaustin (102) Austinone (103) Austinol (104) Austin (105) Austinolide (106)	<i>Penicillium</i> sp. Y-5-2	Hydrothermal vent water	Kueishantao off Taiwan	8	Antibacterial Anti-insectal	[33]

Table 1. Cont.

Metabolites	Fungal Species	Source	Location	Depth (m) *	Bioactivity	Ref.
1-chloro-3 $\beta$ -acetoxy-7-hydroxytrimeremophil-1,6,9-trien-8-one (107)	<i>Penicillium</i> sp. PR19N-1	Sediment	Prydz Bay, Antarctica	526	Cytotoxic	[40,41]
Eremophilane-type sesquiterpenes (108)						
Eremofortine C (109)						
Guignardemophilane F (110)	<i>Penicillium</i> sp. S-1-18	Sediment	Antarctic	1393	Antibacterial	[42]
Spirograterpene A (111)	<i>Penicillium granulatum</i> MCCC 3A00475	Water	Prydz Bay of Antarctica	2284	Antiallergic	[46]
Conidigenone C and I (112-113)						
Aspewentin A and D-H (114-118)						
Asperethers A-E (121-125)	<i>Aspergillus wentii</i> SD-310	Sediment	South China Sea	2038	Antimicrobial Cytotoxic Anti-inflammatory	[39,43,44]
Asperolides D and E (119-120)						
(7S)-(+)-7-O-methylsydonol (126)	<i>Aspergillus sydowii</i>	Sediment	Hsinchu, Taiwan	–	Anti-inflammatory	[47]
(7S,11S)-(+)-12-hydroxysydonic acid (127)						
7-deoxy-7,14-didehydroxydonol (128)						
(S)-(+)-sydonol (129)						
6 $\beta$ ,9 $\alpha$ -dihydroxy-14-p-nitrobenzoylcinnamamide (130)	<i>Aspergillus ochraceus</i> Jcm1F17	Marine alga	South China Sea	–	Antiviral Cytotoxic	[45]
Insulicolide A (131)						
Other compounds						
Sterolic acid (132)	<i>Penicillium</i> sp. MCCC 3A00005	Sediment	East Pacific Ocean	5115	Cytotoxic	[38]
Dicitrinone B (133)	<i>Penicillium citrinum</i>	Sediment	Langqi Island, Fujian, China	–	Antitumor	[49]
Penipacids A-F (134-139)	<i>Penicillium paneum</i> SD-44	Sediment	South China Sea	–	Cytotoxic	[48]
Butanolide A (140)	<i>Penicillium</i> sp. S-1-18	Sediment	Antarctic seabed	1393	Cytotoxic	[42]
7-Methoxycyclopeptin (141)						
7-Methoxy dehydro cyclopeptin (142)	<i>Aspergillus versicolor</i> XZ-4	Hydrothermal vent crab	Kueishantao, Taiwan		Antibiotic	[50]
7-Methoxy cyclophenin (143)						
9-Hydroxy-3-methoxyviridicatin (144)						
Wentilactone A and B (145-146)	<i>Aspergillus dimorphicus</i> SD317	Sediment	South China Sea	2038	Antitumor	[51]
Penicillioscoumarin A-D (147-150)	<i>Penicillium</i> sp. Y-5-2	Hydrothermal vent water	Kueishantao off Taiwan	8	Antibacterial	[33]
Aspergillumarins B (151)						

\* Depth represents water depth below the surface.

### 3. Conclusions and Perspective

The results of current studies indicate that the deep-sea extreme environmental fungi are one of the rich and unexploited sources of important medicinal lead compounds. Most of the fungi (e.g., *Penicillium* spp. and *Aspergillus* spp.) living in the extreme environments of the deep-sea have the potential to synthesize new bioactive compounds. However, the research on deep-sea fungi and their metabolites is very limited due to the difficulty of sampling and the limitation of culture technology. Thanks to the advances in genome technology and the implementation of the deep-sea drilling program, novel compounds with great biological activities are expected from these fungi in the near future. From the literature review, we can say these fungi from the extreme environments have the potential to produce clinically important natural products. The compounds we discussed in this review show strong bioactivities and might have the potential to be a future anticancer drug. Among them, terpenoid derivatives were the most important and abundant compound category which were mainly isolated from deep-sea derived *Penicillium* spp. and *Aspergillus* spp. This class of compounds showed strongest antibiotic and cytotoxic activities as compared to other classes of compounds and has the potential to be a future candidate for anticancer drugs, especially brevione, which was isolated from the deepest part of the sea and showed the strongest cytotoxic activity.

**Author Contributions:** Writing—original draft preparation, M.Z.u.A.; writing—review and editing, Y.-N.M., Y.-R.X. and C.-H.L. All authors have read and agreed to the published version of the manuscript.

**Funding:** This work was financially supported by the National Natural Science Foundation of China (General Program: 41773083, 41973073; Major Program: 91951121).

**Conflicts of Interest:** The authors declare that they have no competing interests.

### References

- König, G.M.; Kehraus, S.; Seibert, S.F.; Abdel-Lateff, A.; Müller, D. Natural products from marine organisms and their associated microbes. *Chem. Bio. Chem.* **2006**, *7*, 229–238. [\[CrossRef\]](#) [\[PubMed\]](#)
- Chen, G.; Wang, H.-F.; Pei, Y.-H. Secondary metabolites from marine-derived microorganisms. *J. Asian Nat. Prod. Res.* **2014**, *16*, 105–122. [\[CrossRef\]](#) [\[PubMed\]](#)
- Agrawal, S.; Adholeya, A.; Deshmukh, S.K. The pharmacological potential of non-ribosomal peptides from marine sponge and tunicates. *Front. Pharmacol.* **2016**, *7*, 333. [\[CrossRef\]](#) [\[PubMed\]](#)
- Deshmukh, S.K.; Prakash, V.; Ranjan, N. Recent advances in the discovery of bioactive metabolites from *Pestalotiopsis*. *Phytochem. Rev.* **2017**, *16*, 883–920. [\[CrossRef\]](#)
- Deshmukh, S.K.; Prakash, V.; Ranjan, N. Marine fungi: A source of potential anticancer compounds. *Front. Microbiol.* **2018**, *8*, 2536. [\[CrossRef\]](#)
- Danovaro, R.; Corinaldesi, C.; Dell’Anno, A.; Snelgrove, P.V. The deep-sea under global change. *Curr. Biol.* **2017**, *27*, R461–R465. [\[CrossRef\]](#)
- Barone, G.; Varrella, S.; Tangherlini, M.; Rastelli, E.; Dell’Anno, A.; Danovaro, R.; Corinaldesi, C. Marine fungi: Biotechnological perspectives from deep-hypersaline anoxic basins. *Diversity* **2019**, *11*, 113. [\[CrossRef\]](#)
- Hamilton-Miller, J. Development of the semi-synthetic penicillins and cephalosporins. *Int. J. Antimicrob.* **2008**, *31*, 189–192. [\[CrossRef\]](#)
- Carroll, A.R.; Copp, B.R.; Davis, R.A.; Keyzers, R.A.; Prinsep, M.R. Marine natural products. *Nat. Prod. Rep.* **2019**, *36*, 122–173. [\[CrossRef\]](#)
- Wang, Y.-T.; Xue, Y.-R.; Liu, C.-H. A brief review of bioactive metabolites derived from deep-sea fungi. *Mar. Drugs* **2015**, *13*, 4594–4616. [\[CrossRef\]](#)
- Arifeen, M.Z.U.; Liu, C.-H. Novel enzymes isolated from marine-derived fungi and its potential applications. *United J. Biochem. Biotechnol.* **2018**, *1*, 1–11.
- Arifeen, M.Z.U.; Xue, Y.-R.; Liu, C.-H. Deep-sea fungi: Diversity, enzymes, and bioactive metabolites. In *Fungi in Extreme Environments: Ecological Role and Biotechnological Significance*; Springer: Berlin, Germany, 2019; pp. 331–347.

13. Pan, C.; Shi, Y.; Auckloo, B.; Chen, X.; Chen, C.-T.; Tao, X.; Wu, B. An unusual conformational isomer of verrucosidin backbone from a hydrothermal vent fungus, *Penicillium* sp. Y-50-10. *Mar. Drugs* **2016**, *14*, 156. [\[CrossRef\]](#)
14. Wu, G.; Ma, H.; Zhu, T.; Li, J.; Gu, Q.; Li, D. Penilactones A and B, two novel polyketides from Antarctic deep-sea derived fungus *Penicillium crustosum* PRB-2. *Tetrahedron* **2012**, *68*, 9745–9749. [\[CrossRef\]](#)
15. Chen, X.-W.; Li, C.-W.; Cui, C.-B.; Hua, W.; Zhu, T.-J.; Gu, Q.-Q. Nine new and five known polyketides derived from a deep sea-sourced *Aspergillus* sp. 16-02-1. *Mar. Drugs* **2014**, *12*, 3116–3137. [\[CrossRef\]](#)
16. Tian, Y.-Q.; Lin, X.-P.; Liu, J.; Kaliyaperumal, K.; Ai, W.; Ju, Z.-R.; Yang, B.; Wang, J.; Yang, X.-W.; Liu, Y. Ascomycin, a new citromycin analogue produced by *Ascomycota* sp. Ind19F07 isolated from deep sea sediment. *Nat. Prod. Res.* **2015**, *29*, 820–826. [\[CrossRef\]](#)
17. Wu, B.; Wiese, J.; Labes, A.; Kramer, A.; Schmaljohann, R.; Imhoff, J. Lindgomycin, an unusual antibiotic polyketide from a marine fungus of the *Lindgomycetaceae*. *Mar. Drugs* **2015**, *13*, 4617–4632. [\[CrossRef\]](#)
18. Yao, Q.; Wang, J.; Zhang, X.; Nong, X.; Xu, X.; Qi, S. Cytotoxic polyketides from the deep-sea-derived fungus *Engyodontium album* DFFSCS021. *Mar. Drugs* **2014**, *12*, 5902–5915. [\[CrossRef\]](#)
19. Cardoso-Martínez, F.; de la Rosa, J.M.; Díaz-Marrero, A.R.; Darias, J.; D’Croz, L.; Cerella, C.; Diederich, M.; Cueto, M. Oximoaspergillimide, a fungal derivative from a marine isolate of *Aspergillus* sp. *Eur. J. Org. Chem.* **2015**, *2015*, 2256–2261. [\[CrossRef\]](#)
20. Fredimoses, M.; Zhou, X.; Ai, W.; Tian, X.; Yang, B.; Lin, X.; Xian, J.-Y.; Liu, Y. Westerdijkian A, a new hydroxyphenylacetic acid derivative from deep sea fungus *Aspergillus westerdijkiae* SCSIO 05233. *Nat. Prod. Res.* **2015**, *29*, 158–162. [\[CrossRef\]](#)
21. Hu, J.; Li, Z.; Gao, J.; He, H.; Dai, H.; Xia, X.; Liu, C.; Zhang, L.; Song, F. New diketopiperazines from a marine-derived fungus strain *Aspergillus versicolor* MF180151. *Mar. Drugs* **2019**, *17*, 262. [\[CrossRef\]](#)
22. Zhang, X.; Li, S.-J.; Li, J.-J.; Liang, Z.-Z.; Zhao, C.-Q. Novel natural products from extremophilic fungi. *Mar. Drugs* **2018**, *16*, 194. [\[CrossRef\]](#) [\[PubMed\]](#)
23. Li, C.-S.; An, C.-Y.; Li, X.-M.; Gao, S.-S.; Cui, C.-M.; Sun, H.-F.; Wang, B.-G. Triazole and dihydroimidazole alkaloids from the marine sediment-derived fungus *Penicillium paneum* SD-44. *J. Nat. Prod.* **2011**, *74*, 1331–1334. [\[CrossRef\]](#) [\[PubMed\]](#)
24. Xu, X.; Zhang, X.; Nong, X.; Wei, X.; Qi, S. Oxindole alkaloids from the fungus *Penicillium commune* DFFSCS026 isolated from deep-sea-derived sediments. *Tetrahedron* **2015**, *71*, 610–615. [\[CrossRef\]](#)
25. Wijesekara, I.; Li, Y.-X.; Vo, T.-S.; Van Ta, Q.; Ngo, D.-H.; Kim, S.-K. Induction of apoptosis in human cervical carcinoma HeLa cells by neoechinulin A from marine-derived fungus *Microsporium* sp. *Process Biochem.* **2013**, *48*, 68–72. [\[CrossRef\]](#)
26. Zhang, P.; Mandi, A.; Li, X.-M.; Du, F.-Y.; Wang, J.-N.; Li, X.; Kurtan, T.; Wang, B.-G. Varioxepine A, a 3 H-oxepine-containing alkaloid with a new oxa-cage from the marine algal-derived endophytic fungus *Paecilomyces variotii*. *Org. Lett.* **2014**, *16*, 4834–4837. [\[CrossRef\]](#)
27. Dasanayaka, S.; Nong, X.-H.; Liang, X.; Liang, J.-Q.; Amin, M.; Qi, S.-H. New dibenzodioxocinone and pyran-3, 5-dione derivatives from the deep-sea-derived fungus *Penicillium canescens* SCSIO z053. *J. Asian Nat. Prod. Res.* **2019**, *1*–8. [\[CrossRef\]](#)
28. Ren, J.; Xue, C.; Tian, L.; Xu, M.; Chen, J.; Deng, Z.; Proksch, P.; Lin, W. Asperelines A–F, peptaibols from the marine-derived fungus *Trichoderma asperellum*. *J. Nat. Prod.* **2009**, *72*, 1036–1044. [\[CrossRef\]](#)
29. Jiang, W.; Ye, P.; Chen, C.-T.; Wang, K.; Liu, P.; He, S.; Wu, X.; Gan, L.; Ye, Y.; Wu, B. Two novel hepatocellular carcinoma cycle inhibitory cyclodepsipeptides from a hydrothermal vent crab-associated fungus *Aspergillus clavatus* C2WU. *Mar. Drugs* **2013**, *11*, 4761–4772. [\[CrossRef\]](#)
30. Luo, X.W.; Yun, L.; Liu, Y.J.; Zhou, X.F.; Liu, Y.H. Peptides and polyketides isolated from the marine sponge-derived fungus *Aspergillus terreus* SCSIO 41008. *Chin. J. Nat. Med.* **2019**, *17*, 149–154. [\[CrossRef\]](#)
31. Liang, X.; Zhang, X.-Y.; Nong, X.-H.; Wang, J.; Huang, Z.-H.; Qi, S.-H. Eight linear peptides from the deep-sea-derived fungus *Simplicillium obclavatum* EIODSF 020. *Tetrahedron* **2016**, *72*, 3092–3097. [\[CrossRef\]](#)
32. Uchida, R.; Nakajyo, K.; Kobayashi, K.; Ohshiro, T.; Terahara, T.; Imada, C.; Tomoda, H. 7-Chlorofolipastatin, an inhibitor of sterol O-acyltransferase, produced by marine-derived *Aspergillus ungui* NKH-007. *J. Antibiot.* **2016**, *69*, 647. [\[CrossRef\]](#) [\[PubMed\]](#)
33. Pan, C.; Shi, Y.; Auckloo, B.N.; ul Hassan, S.S.; Akhter, N.; Wang, K.; Ye, Y.; Chen, C.-T.A.; Tao, X.; Wu, B. Isolation and antibiotic screening of fungi from a hydrothermal vent site and characterization of secondary metabolites from a *Penicillium* isolate. *Mar. Biotechnol.* **2017**, *19*, 469–479. [\[CrossRef\]](#) [\[PubMed\]](#)



34. Huang, Z.; Nong, X.; Ren, Z.; Wang, J.; Zhang, X.; Qi, S. Anti-HSV-1, antioxidant and antifouling phenolic compounds from the deep-sea-derived fungus *Aspergillus versicolor* SCSIO 41502. *Bioorg. Med. Chem. Lett.* **2017**, *27*, 787–791. [\[CrossRef\]](#) [\[PubMed\]](#)
35. Liu, C.-C.; Zhang, Z.-Z.; Feng, Y.-Y.; Gu, Q.-Q.; Li, D.-H.; Zhu, T.-J. Secondary metabolites from Antarctic marine-derived fungus *Penicillium crustosum* HDN153086. *Nat. Prod. Res.* **2019**, *33*, 414–419. [\[CrossRef\]](#) [\[PubMed\]](#)
36. Orfali, R.S.; Aly, A.H.; Ebrahim, W.; Abdel-Aziz, M.S.; Müller, W.E.; Lin, W.; Daletos, G.; Proksch, P. Pretrichodermamide C and N-methylpretrichodermamide B, two new cytotoxic epidithiodiketopiperazines from hyper saline lake derived *Penicillium* sp. *Phytochem. Lett.* **2015**, *11*, 168–172. [\[CrossRef\]](#)
37. Fan, Z.; Sun, Z.-H.; Liu, Z.; Chen, Y.-C.; Liu, H.-X.; Li, H.-H.; Zhang, W.-M. Dichotocejpins A–C: New diketopiperazines from a deep-sea-derived fungus *Dichotomomyces cejpui* FS110. *Mar. Drugs* **2016**, *14*, 164. [\[CrossRef\]](#)
38. Li, Y.; Ye, D.; Shao, Z.; Cui, C.; Che, Y. A sterol and spiroditerpenoids from a *Penicillium* sp. isolated from a deep sea sediment sample. *Mar. Drugs* **2012**, *10*, 497–508. [\[CrossRef\]](#)
39. Li, X.-D.; Li, X.-M.; Li, X.; Xu, G.-M.; Liu, Y.; Wang, B.-G. Aspewentins D–H, 20-nor-isopimarane derivatives from the deep sea sediment-derived fungus *Aspergillus wentii* SD-310. *J. Nat. Prod.* **2016**, *79*, 1347–1353. [\[CrossRef\]](#)
40. Wu, G.; Lin, A.; Gu, Q.; Zhu, T.; Li, D. Four new chloro-eremophilane sesquiterpenes from an Antarctic deep-sea derived fungus, *Penicillium* sp. PR19N-1. *Mar. Drugs* **2013**, *11*, 1399–1408. [\[CrossRef\]](#)
41. Lin, A.; Wu, G.; Gu, Q.; Zhu, T.; Li, D. New eremophilane-type sesquiterpenes from an antarctic deep-sea derived fungus, *Penicillium* sp. PR19 N-1. *Arch. Pharm. Res.* **2014**, *37*, 839–844. [\[CrossRef\]](#)
42. Zhou, Y.; Li, Y.-H.; Yu, H.-B.; Liu, X.-Y.; Lu, X.-L.; Jiao, B.-H. Furanone derivative and sesquiterpene from antarctic marine-derived fungus *Penicillium* sp. S-1-18. *J. Asian Nat. Prod. Res.* **2018**, *20*, 1108–1115. [\[CrossRef\]](#) [\[PubMed\]](#)
43. Li, X.-D.; Li, X.; Li, X.-M.; Xu, G.-M.; Zhang, P.; Meng, L.-H.; Wang, B.-G. Tetranorlabdane diterpenoids from the deep sea sediment-derived fungus *Aspergillus wentii* SD-310. *Planta Med.* **2016**, *82*, 877–881. [\[CrossRef\]](#) [\[PubMed\]](#)
44. Li, X.; Li, X.-M.; Li, X.-D.; Xu, G.-M.; Liu, Y.; Wang, B.-G. 20-Nor-isopimarane cycloethers from the deep-sea sediment-derived fungus *Aspergillus wentii* SD-310. *RSC Adv.* **2016**, *6*, 75981–75987. [\[CrossRef\]](#)
45. Fang, W.; Lin, X.; Zhou, X.; Wan, J.; Lu, X.; Yang, B.; Ai, W.; Lin, J.; Zhang, T.; Tu, Z. Cytotoxic and antiviral nitrobenzoyl sesquiterpenoids from the marine-derived fungus *Aspergillus ochraceus* Jcma1F17. *MedChemComm* **2014**, *5*, 701–705. [\[CrossRef\]](#)
46. Niu, S.; Fan, Z.-W.; Xie, C.-L.; Liu, Q.; Luo, Z.-H.; Liu, G.; Yang, X.-W. Spirograterpene A, a tetracyclic spiro-diterpene with a fused 5/5/5 ring system from the deep-sea-derived fungus *Penicillium granulatum* MCCC 3A00475. *J. Nat. Prod.* **2017**, *80*, 2174–2177. [\[CrossRef\]](#)
47. Chung, Y.-M.; Wei, C.-K.; Chuang, D.-W.; El-Shazly, M.; Hsieh, C.-T.; Asai, T.; Oshima, Y.; Hsieh, T.-J.; Hwang, T.-L.; Wu, Y.-C. An epigenetic modifier enhances the production of anti-diabetic and anti-inflammatory sesquiterpenoids from *Aspergillus sydowii*. *Bioorg. Med. Chem.* **2013**, *21*, 3866–3872. [\[CrossRef\]](#)
48. Li, C.-S.; Li, X.-M.; Gao, S.-S.; Lu, Y.-H.; Wang, B.-G. Cytotoxic anthranilic acid derivatives from deep sea sediment-derived fungus *Penicillium paneum* SD-44. *Mar. Drugs* **2013**, *11*, 3068–3076. [\[CrossRef\]](#)
49. Chen, L.; Gong, M.-W.; Peng, Z.-F.; Zhou, T.; Ying, M.-G.; Zheng, Q.-H.; Liu, Q.-Y.; Zhang, Q.-Q. The marine fungal metabolite, dicitrinone B, induces A375 cell apoptosis through the ROS-related caspase pathway. *Mar. Drugs* **2014**, *12*, 1939–1958. [\[CrossRef\]](#)
50. Pan, C.; Shi, Y.; Chen, X.; Chen, C.-T.A.; Tao, X.; Wu, B. New compounds from a hydrothermal vent crab-associated fungus *Aspergillus versicolor* XZ-4. *Org. Biomol. Chem.* **2017**, *15*, 1155–1163. [\[CrossRef\]](#)
51. Xu, R.; Xu, G.-M.; Li, X.-M.; Li, C.-S.; Wang, B.-G. Characterization of a newly isolated marine fungus *Aspergillus dimorphicus* for optimized production of the anti-tumor agent wentilactones. *Mar. Drugs* **2015**, *13*, 7040–7054. [\[CrossRef\]](#)





Review

# Halophiles and Their Biomolecules: Recent Advances and Future Applications in Biomedicine

Paulina Corral <sup>1,2</sup>, Mohammad A. Amoozegar <sup>3</sup> and Antonio Ventosa <sup>2,\*</sup>

<sup>1</sup> Department of Biology, University of Naples Federico II, 80126 Naples, Italy; pcv@us.es

<sup>2</sup> Department of Microbiology and Parasitology, Faculty of Pharmacy, University of Sevilla, 41012 Sevilla, Spain

<sup>3</sup> Department of Microbiology, School of Biology, College of Science, University of Tehran, Tehran 14155-6955, Iran; amoozegar@ut.ac.ir

\* Correspondence: ventosa@us.es; Tel.: +34-954556765

Received: 30 November 2019; Accepted: 28 December 2019; Published: 30 December 2019

**Abstract:** The organisms thriving under extreme conditions better than any other organism living on Earth, fascinate by their hostile growing parameters, physiological features, and their production of valuable bioactive metabolites. This is the case of microorganisms (bacteria, archaea, and fungi) that grow optimally at high salinities and are able to produce biomolecules of pharmaceutical interest for therapeutic applications. As long as the microbiota is being approached by massive sequencing, novel insights are revealing the environmental conditions on which the compounds are produced in the microbial community without more stress than sharing the same substratum with their peers, the salt. In this review are reported the molecules described and produced by halophilic microorganisms with a spectrum of action in vitro: antimicrobial and anticancer. The action mechanisms of these molecules, the urgent need to introduce alternative lead compounds and the current aspects on the exploitation and its limitations are discussed.

**Keywords:** halophilic bacteria; archaea and fungi; biomolecules; biomedicine; antimicrobial compounds; anticancer compounds

## 1. Halophilic Microorganisms

Halophiles are organisms represented by archaea, bacteria, and eukarya for which the main characteristic is their salinity requirement, halophilic “salt-loving”. Halophilic microorganisms constitute the natural microbial communities of hypersaline ecosystems, which are widely distributed around the world [1]. They require sodium ions for their growth and metabolism. Thus, based on the NaCl optimal requirement for growth the halophiles are classified in three different categories: slight (1–3%); moderate (3–15%); and extreme (15–30%) [2,3]. In contrast to halotolerant organisms, obligate halophiles require NaCl concentrations higher than 3% NaCl or above of seawater, with about 3.5% NaCl [4]. The tolerance parameters and salt requirements are dependent on temperature, pH, and growth medium. In this way, the halophiles are adapted and limited by specific environmental factors. Those microorganisms able to survive and optimally thrive under a wide spectrum of extreme environmental factors are designed polyextremophiles [5,6]. In fact, a halophilic microorganism can also be alkaliphile, designated as haloalkaliphile, growing optimally or very well at pH values above 9.0, but cannot grow at the near neutral pH value of 6.5 [7].

The general features of halophilic microorganisms are the low nutritional requirements and resistance to high concentrations of salt with the capacity to balance the osmotic pressure of the environment [8]. Their mechanisms of haloadaptation are based on the intracellular storage of KCl over 37% (5 M) (salt-in strategy) or the accumulation of compatible solutes (salt-out strategy) to keep the balance of sodium into the cytoplasm and counteract the osmotic pressure of the external environment given by the high salinity [9].

They are physiologically diverse; mostly aerobic and as well anaerobic, heterotrophic, phototrophic, and chemoautotrophic [10,11]. Ecologically, the halophilic microorganisms inhabit different ecosystems characterized by a salinity higher than seawater, i.e., 3.5% NaCl, these niches go from hypersaline soils, springs, salt lakes, sabkhas, and other naturally-occurring coastal saline habitats, marshes, marine abyssal sediments to endophytes [12]. Other known habitats are the result of human intervention like salted foods, brines, oil fields, saltern ponds and tanneries [13]. The high salinity reduces the number of organisms where just halophilic or halotolerant ones can survive in such hypersaline ecosystem, with archaea typically dominating the higher salinity environments. The predominant natural habitats better studied are the hypersaline lakes of oceanic (thalassohaline) or non-oceanic (athalassohaline) origin and solar salterns [14–16]. The better known hypersaline environments are the Great Salt Lake and the Dead Sea, with pH values around 7, and soda lakes with highly alkaline values of pH 9–11, among them are the Lake Magadi in Kenya, the Wadi Natrun lakes in Egypt, Mono Lake, Big Soda Lake, Soap Lake in Western USA, and Kulunda Steppe soda lakes in Russia [17]. Many new species of bacteria and archaea have been reported from various hypersaline regions located in different countries, mainly China, Spain, USA, Austria, Australia, Egypt, Korea, Japan, Iran, Thailand, Indonesia, Russia, Argentina, Kenya, Mexico, France, Poland, Philippines, Taiwan, Romania, and India [10,18,19]. The vast majority of halophilic bacteria and archaea produce carotenoid pigments, present in high amount in their membranes. The dense community of halophiles and the algae *Dunaliella*, also producer of carotenoids, are the responsible of the typical pink, red, and purple coloration of the hypersaline environments [20].

## 2. Biotechnological Importance/Interest of Haloarchaea and Halophilic Bacteria

The exploitation of extremophiles is having special importance in the development of new molecules with potential applications in biomedicine. Current efforts are focused primarily to cover the urgent health needs, especially those that represent the main global threats, cancer and antibiotic resistance. The great metabolic versatility of halophilic microorganisms, their low nutritional requirements and their genetic machineries of adaptation to harsh conditions, like nutrient starvation, desiccation, high sun radiation, and high ionic strength, make them promising candidates and a hope for drug discovery [21]. Continuous advances in “omics” and bioinformatic tools are revealing uncountable encoding genes for the production of several active compound in response to the extreme conditions [22,23]. The concomitant application of cutting-edge technologies is helping to deciphering the molecular, physiological, and metabolic mechanisms for the production of new bioactive compounds [24].

Halophilic microorganisms are recognized producers of carotenoid pigments, retinal proteins, hydrolytic enzymes, and compatible solutes as macromolecules stabilizers, biopolymers, and biofertilizers [19,25]. Halophilic bacteria and extremely halophilic aerobic archaea, also known as haloarchaea, play a significant role in the industry with a large number of applications like fermented food products, cosmetics, preservatives, manufacturing of bioplastics, photoelectric devices, artificial retinas, holograms, biosensors, etc. [26–31].

In this review, we focus on the biomolecules described as antimicrobial or anticancer compounds produced by halophilic bacteria, archaea, or fungi and discuss current and future perspectives in this field.

## 3. Antimicrobial Compounds

The current situation of antibiotic resistance propagation poses a global threat to public health. Over the past decades, antibiotics have saved millions of lives, but their misuse has led to the emergence of multi-drug resistant bacteria (MDR), reducing or nullifying their effectiveness. Recently, the continuous increase in antibiotic resistance is reaching critical levels, which implies an increase in morbidity in the healthy population and an imminent risk for hospitalized patients [32,33]. In fact, the main cause of death of inpatients are attributable to complications due to MDR infections [34]. Preventing the return to the pre-antibiotic era is one of the main challenges for science. The urgent need to introduce new effective antimicrobial therapies is leading to the exploitation of all possible

natural and sustainable resources, including extreme environments as a promising resource for new antibiotic discovery.

The first antimicrobial compounds from halophilic microorganisms were reported in 1982 by Rodriguez-Valera et al. Halocin was the term coined for substances secreted by several members of the genus *Halobacterium* capable of causing death and lysis of the surrounding microbiota. Halocins are the proteins and antimicrobial peptides (AMPs) produced by haloarchaea [35,36]. Despite the ecological and environmental role of several halocins, their action against human pathogens has been less studied.

In the fight against time, the clinical significance of halophilic microorganisms is minorly reported and the antimicrobial action against the most important risk group of human pathogens ESKAPE: *Enterococcus faecium*, *Staphylococcus aureus*, *Klebsiella pneumoniae*, *Acinetobacter baumannii*, and *Pseudomonas aeruginosa*, still remains as a potential.

According to the data inferred, the antagonistic action identified and the production of bioactive compounds by halophilic microorganisms are derived from bacteria, archaea, and fungi. In the chronology of AMPs discovery, several authors have gone beyond the primary screenings deciphering the chemical structure of the molecules in bacteria (Table 1), while the vast majority of inhibitory studies are solely limited to the activity (Table 2).

### 3.1. Bacteria

Members of the phylum *Actinobacteria* are mainly responsible for the inhibitory activity against human pathogens with clinical significance. As in non-extreme environments, in saline and hypersaline environments heterotrophic bacteria are also present in soils, being *Actinobacteria* frequently isolated from solar salterns, mangroves, and seafloor sediments [37,38]. The most frequent producers of metabolites reported come from species of the genus *Nocardiopsis* and *Streptomyces*, hence constituting the main producers of bioactive compounds. In fact, members of the genus *Streptomyces* are widely recognized as fruitful producers of natural compounds [39]. The chemical elucidation of molecules known from halophilic members of *Nocardiopsis* are: (i) pyrrolo (1,2-A (pyrazine-1,4-dione, hexahydro-3-[2-methylpropyl])- and Actinomycin C2, two compounds produced by the haloalkaliphilic strain *Nocardiopsis* sp. AJ1, isolated from saline soil of Kovalam solar salterns in India [40]; (ii) Angucyclines and Angucyclinones are produced by *Nocardiopsis* sp. HR-4, isolated from a salt lake soil in Algerian Sahara, the new natural compound was established as 7-deoxy-8-O-methyltetrangomycin, which is also effective against Methicillin-Resistant *Staphylococcus aureus* (MRSA) ATCC 43300 [41]; (iii) Borrelidin C and D are produced by *Nocardiopsis* sp. HYJ128, isolated from topsoil saltern in Jeungdo, Jeollanamdo, Republic of Korea, exhibited antimicrobial action against *Salmonella enterica* ATCC 14028 [42]; (iv) Quinoline alkaloid (4-oxo-1,4-dihydroquinoline-3-carboxamide) was identified as a new natural product from *Nocardiopsis terrae* YIM 90022 isolated from saline soils in China. The antibacterial activity of the quinolone was reported in *S. aureus*, *B. subtilis* and *E. coli*; the quinolone has also antifungal activity against the pathogenic fungi, as it was observed against *Pyricularia oryzae*. Another five known compounds were also produced by *N. terrae* YIM 90022 [43]; (v) new p-terphenyls: p-terphenyl 1 and a novel p-terphenyl derivative bearing a benzothiazole moiety are produced by halophilic actinomycete *Nocardiopsis gilva* YIM 90087, isolated from a hypersaline soil Xinjiang, China. Furthermore, of the antimicrobial activity against clinical strains, these compounds exhibit antifungal activity against species of *Fusarium*, *Trichophyton*, *Aspergillus*, *Candida*, and *Pyricularia*. Known molecules like p-terphenyl 2, novobiocin, cyclodipeptides, and aromatic acids are also produced by *N. gilva* YIM 90087, which is considered as a new source for novobiocin [44].

Regarding the metabolites produced by members of the genus *Streptomyces*, only a low number of strains has been isolated from hypersaline environments; however, members of this genus are frequently isolated from marine deep or coastal sediments where the salinity is higher than that of seawater. Among the molecules identified are: (i) 1-hydroxy-1-norresistomycin, this quinone-related antibiotic was extracted from *Streptomyces chibaensis* AUBN1/7, isolated from marine sediment samples of the Bay of Bengal, India. This compound exhibited antibacterial activities against Gram-positive and Gram-negative bacteria, besides of a potent in vitro cytotoxic activity against cell lines HMO2 (gastric

adenocarcinoma) and HePG2 (hepatic carcinoma) [45]; (ii) Himalomycin A and Himalomycin B, two new anthracycline antibiotics produced by *Streptomyces* sp. strain B692, isolated from sandy sediment of a coastal site of Mauritius (Indian Ocean). In addition, known metabolites like rabelomycin, fridamycin D, N benzylacetamide, and N-(2'-phenylethyl) acetamide were also produced by *Streptomyces* sp. strain B692 [46]; (iii) 7-demethoxy rapamycin was produced by a moderately halophilic strain *Streptomyces hygroscopicus* BDUS 49, isolated from seashore of Bigeum Island, South West coast of South Korea; the molecule displayed a broad spectrum antimicrobial activity against Gram-positive and Gram-negative bacteria. Antifungal and cytotoxic action was also identified on this strain [47]; (iv) Streptomonicin (STM) is an antibiotic lasso peptide from *Streptomonospora alba* YIM 90003, isolated from a soil sample in Xinjiang province, China. STM is active against several Gram-positive bacteria, in particular species of *Bacillus*, *Listeria*, *Enterococcus*, *Mycobacterium* and *Staphylococcus*. Despite that STM has an inhibitory action against a wide panel of Gram-positive pathogens, the activity against fungi and Gram-negative bacteria was not evidenced [48].

In addition to the mentioned genera of *Actinobacteria* (*Nocardiopsis* and *Streptomyces*), recognized as the more prolific producers of natural substances, other halophilic species belonging to different genera have also been described as producers of molecules like: (i) cyclic antimicrobial lipopeptides: Gramicidin S and four cyclic dipeptides (CDPs), named cyclo(L-4-OH-Pro-L-Leu), cyclo(L-Tyr-L-Pro), cyclo(L-Phe-L-Pro), and cyclo(L-Leu-L-Pro), were extracted from *Paludifilum halophilum* strain SMBg3, which constitute a new genus of the family *Thermoactinomycetaceae*, isolated from superficial sediment collected from Sfax marine solar saltern in Tunisia. These CDPs possess an inhibitory effect against the plant pathogen *Agrobacterium tumefaciens* and the human pathogens *Staphylococcus aureus*, *Salmonella enterica*, *Escherichia coli*, and *Pseudomonas aeruginosa* [49]; (ii) A semi synthetic derivative N-(4-aminocyclooctyl)-3,5-dinitrobenzamide, obtained from the precursor of the novel natural product cyclooctane-1,4-diamine and a known compound 3-([1H-indol-6-yl] methyl) hexahydropyrrolo [1,2-a] pyrazine-1,4-dione were obtained from *Pseudonocardia endophytica* VUK-10, isolated from sediment of Nizampatnam mangrove ecosystem in Bay of Bengal, India. The new compound, semi synthetic derivative N-(4-aminocyclooctyl)-3,5-dinitrobenzamide showed a strong antimicrobial and antifungal activity against *Streptococcus mutans*, *Pseudomonas aeruginosa*, *Candida albicans*, and *Aspergillus niger*. Significant anticancer activities at nanomolar concentrations were also observed in carcinoma cell lines MDA-MB-231 (breast), HeLa (cervical), OAW-42 (ovarian), and MCF-7 (breast) reported as resistant to cancer drugs [50]. In minor grade, other halophilic bacteria not belonging to the phylum *Actinobacteria* produce antimicrobial compounds, as for example halophilic strains of the genus *Vibrio*, like *Vibrio* sp. A1SM3-36-8, isolated from Colombian solar salterns, which produces 13-cis-docosenamide with special antimicrobial action against Methicillin-resistant *Staphylococcus aureus* (MRSA) and cytotoxic activity against cervical adenocarcinoma (SiHa) and lung carcinoma (A-549) [51]. Within this genus, *Vibrio parahaemolyticus* strain B2 is recognized by producing Vibrindole A, and was also effective against *Staphylococcus aureus* [52].

Finally, *Bacillus* sp. BS3 [53] and *Halomonas salifodinae* MPM-TC [54] showed antimicrobial action against *Pseudomonas aeruginosa*. Both strains were isolated from solar salterns in Thamaraiikulam, Tamil Nadu, India. In the case of *Halomonas salifodinae* MPM-TC, besides of the inhibition of bacterial growth also exhibits an antiviral action against the White Spot Syndrome Virus (WSSV) in the white shrimp *Penaeus monodon*. The effect suppressor of the virus and the boosting of immune system of the shrimps make of the extracted compound a feasible alternative to commercially banned antibiotics and excellent candidate to develop new antiviral drugs against shrimp viruses such as WSSV.

A genome-mining study conducted on 2699 genomes across the three domains of life demonstrated the widespread distribution of non-ribosomal peptide synthetase (NRPSs) and modular polyketide synthase (PKSs) biosynthetic pathways. Among 31 phyla of bacteria inferred, *Actinobacteria* is the most representative exhibiting the presence of 1225 gene clusters between NRPS, PKS and hybrids from a total of the 271 genomes studied. It was observed that *Salinispora arenicola* CNS-205 and *Salinispora tropica* CNB-440 harbor PKS and NRPS gene clusters, respectively. The halophilic bacterium *Halomonas elongata* DSM 2581 also contains NRPS [55].

**Table 1.** Chronological report of halophilic bacteria and their molecules with antimicrobial activity in vitro against human pathogens.

Isolation Source	Genus	Antimicrobial Activity	Molecule	Formula	Reference
Saline soil of Kovalam solar salterns India	<i>Nocardopsis</i> sp. AJ1	<i>E. coli</i> , <i>S. aureus</i> , <i>P. aeruginosa</i> , <i>V. parahaemolyticus</i> , <i>A. hydrophila</i>	Pyrolo (1,2-A (pyrazine-1,4-dione, hexahydro-3-(2-methylpropyl)-)	C <sub>11</sub> H <sub>18</sub> N <sub>2</sub> O <sub>2</sub>	[40]
			Actinomycin C2	C <sub>63</sub> H <sub>88</sub> N <sub>12</sub> O <sub>16</sub>	
Sfax solar saltern, Tunisia	<i>Paludifilum halophilum</i> SMB <sub>83</sub>	<i>E. coli</i> BW25113, <i>S. henoxaz</i> ATCC43972, <i>P. aeruginosa</i> ATCC 49189 Gram-positive <i>M. luteus</i> LB 14110, <i>S. aureus</i> ATCC6538, and <i>L. ranoan</i> BUG #96	Cyclic lipopeptide:		[49]
			Gramicidin S	C <sub>60</sub> H <sub>82</sub> N <sub>12</sub> O <sub>10</sub>	
			Cyclic dipeptides (CDPs):		
			Cyclo(-4-OH-Pro-L-Leu)	C <sub>11</sub> H <sub>18</sub> N <sub>2</sub> O <sub>3</sub>	
			Cyclo(-Tyr-L-Pro)	C <sub>14</sub> H <sub>16</sub> N <sub>2</sub> O <sub>3</sub>	
			Cyclo(-Phe-L-Pro)	C <sub>14</sub> H <sub>16</sub> N <sub>2</sub> O <sub>2</sub>	
Brine and sediments from Manauare solar saltern. La Guajira, Colombia	<i>Vibrio</i> sp. AISM3-36-8	Methicillin-resistant <i>S. aureus</i> (MRSA) ATCC BAA-44, <i>B. subtilis</i> ATCC 21556	Cyclo(-L-Leu-L-Pro)	C <sub>11</sub> H <sub>18</sub> N <sub>2</sub> O <sub>2</sub>	[51]
			13- <i>cis</i> -docosenamide	C <sub>22</sub> H <sub>43</sub> NO	
Salt lake soil, Algerian Sahara. Algeria	<i>Nocardopsis</i> sp. HR-4	<i>S. aureus</i> ATCC 25923, Methicillin-Resistant <i>S. aureus</i> (MRSA) ATCC 43300, <i>M. luteus</i> ATCC 4698, <i>E. faecalis</i> ATCC 29212	Angucyclines and angucyclinones:		[41]
			Compound 1: (-)-8-O-methyltetrangomycin	C <sub>20</sub> H <sub>16</sub> O <sub>5</sub>	
			Compound 2: (-)-7-deoxy-8-O methyltetrangomycin	C <sub>20</sub> H <sub>18</sub> O <sub>5</sub>	
Topsoil saltern in Jeungdo, Jeollanam-do, Republic of Korea	<i>Nocardopsis</i> sp. HYJ128	<i>Salmonella enterica</i> ATCC 14028	Borrelidin C	C <sub>28</sub> H <sub>43</sub> NO <sub>7</sub>	[42]
			Borrelidin D	C <sub>28</sub> H <sub>43</sub> NO <sub>7</sub>	
			N-(4-aminocyclooctyl)-3,5-dinitrobenzamide	C <sub>15</sub> H <sub>20</sub> N <sub>4</sub> O <sub>5</sub>	
Sediments of mangrove Nizampatnam, Bay of Bengal, Andhra Pradesh, India	<i>Pseudonocardia endophytica</i> VUK-10	<i>B. cereus</i> (MTCC 430), <i>S. mutans</i> (MTCC 497), <i>S. aureus</i> (MTCC 3160), <i>S. epidermis</i> (MTCC 120), <i>B. subtilis</i> (ATCC 6633), <i>B. megaterium</i> (NCIM 2187), <i>E. coli</i> (ATCC 35218), <i>P. aeruginosa</i> (ATCC 9027), <i>P. vulgaris</i> (MTCC 7299), <i>S. marcescens</i> (MTCC 118), <i>X. campestris</i> (MTCC 2286), <i>X. maltacumarum</i> (NCIM 2954) and <i>S. typhi</i> (ATCC 14028)	3-(1H-indol-6-yl) methyl) hexahydropyrrulo [1,2- <i>al</i> ] pyrazine-1,4-dione	C <sub>16</sub> H <sub>17</sub> N <sub>5</sub> O <sub>2</sub>	[50]

Table 1. Cont.

Isolation Source	Genus	Antimicrobial Activity	Molecule	Formula	Reference
Soil sample, Xinjiang Province, China	<i>Streptomonospora alba</i> YIM 9003	<i>B. anthracis</i> , <i>B. halodurans</i> , <i>B. cereus</i> ATCC 4342, ATCC 13472, <i>B. subtilis</i> , <i>L. monocytogenes</i> , <i>E. faecalis</i> , <i>S. aureus</i> and <i>M. smegmatis</i>	Streptomonomycin (STM)	$C_{107}H_{160}N_{22}O_{39}$	[48]
Great Barrier Reef (GBR) sponges, Queensland, Australia	<i>Salinispongomonacola</i>	<i>M. aurum</i> , <i>M. lepreae</i> , <i>M. tuberculosis</i>	Rifamycin B	$C_{39}H_{49}NO_{14}$	[56]
			Rifamycin S	$C_{37}H_{46}NO_{12}$	
			Rifamycin W	$C_{35}H_{46}NO_{11}$	
			Quinoloid alkaloid 4-oxo-1,4-dihydroquinoline-3-carboxamide	$C_{10}H_7N_2O_2$	
Saline soil, Qaidam Basin, north-west China	<i>Noctardiopsis terrae</i> YIM 90022	<i>S. aureus</i> , <i>E. coli</i> and <i>B. subtilis</i>	<i>p</i> -hydroxybenzoic acid	$C_7H_6O_3$	[43]
			<i>N</i> -acetyl-L-anthranilic acid	$C_9H_9NO$	
			Indole-3-carboxylic acid	$C_9H_7NO_2$	
			Cyclo (Trp-Gly)	$C_{13}H_{13}N_5O_2$	
			Cyclo (Leu-Ala)	$C_9H_{16}N_2O_2$	
			Lipopeptide biosurfactants		
Condenser water, solar salt works in Thamarakulam, Kanyakumari district, Tamil Nadu, India	<i>Bacillus</i> sp. BS3	<i>E. coli</i> , <i>S. aureus</i> , <i>P. aeruginosa</i> and <i>S. typhi</i>	I3-Docosenamide, (Z)	$CH_3(CH_2)_7CH=CH(CH_2)_{11}CONH_2$	[53]
			Mamosamine	$C_6H_{13}NO_5.HCl$	
			9-Octadecenamide, (Z)	$C_{18}H_{35}NO$	
			2-Octanol, 2-methyl-6-methylene	$C_{12}H_{22}O_2$	
			Cylohex-1,4,5-triol-3-one-1-carbo	$C_5H_8FN_3$	
			2-Butanamine, 2-methyl-	$C_5H_{13}N$	
			1,2-Ethanediamine, <i>N,N,N',N'</i> -tetramethyl-	$C_6H_{16}N_2$	
			<i>p</i> -Terphenyl:	$C_{22}H_{22}O_5$	
			6'-Hydroxy-4,2',3',4'-tetramethoxy- <i>p</i> -terphenyl		
Hypersaline soil, Xinjiang, China	<i>Noctardiopsis gilva</i> YIM 90087	<i>B. subtilis</i> , <i>S. aureus</i>	<i>p</i> -Terphenyl derivative:		[44]
			4,7-bis(4-methoxyphenyl)-6-hydroxy-5-methoxybenzo[d]thiazole	$C_{22}H_{19}NO_4S$	



Table 1. Cont.

Isolation Source	Genus	Antimicrobial Activity	Molecule	Formula	Reference
Solar salt condenser, Thamaraikulam solar saltern, Kanyakumari district, Tamil Nadu, India	<i>Halomonas salifodinae</i> MPM-1C	<i>V. harveyi</i> , <i>V. parahaemolyticus</i> , <i>P. aeruginosa</i> and <i>A. hydrophila</i>	Perfluorotributylamine	C <sub>12</sub> F <sub>27</sub> N	[54]
			Cyclopentane, 1-butyl-2-ethyl-	C <sub>11</sub> H <sub>22</sub>	
			1,1'-Biphenyl]-3-amine	C <sub>12</sub> H <sub>11</sub> N	
			Pyridine, 4-(phenylmethyl)-	C <sub>12</sub> H <sub>11</sub> N	
			Hexadecane, 2-methyl-	C <sub>17</sub> H <sub>36</sub>	
			Nonadecane	C <sub>19</sub> H <sub>40</sub>	
			Phytol	C <sub>20</sub> H <sub>40</sub> O	
Seashore soil, Bigeum Island, South West coast of South Korea	<i>Streptomyces hygrosopicus</i> BDUS 49	<i>B. subtilis</i> , <i>S. aureus</i> , <i>E. coli</i> , <i>S. typhi</i>	7-Deoxy rapamycin	C <sub>50</sub> H <sub>75</sub> NO <sub>12</sub>	[47]
Marine sediment of Mission Bay, San Diego, South California	<i>Marrinispora</i> sp. NPS12745	<i>S. aureus</i> ATCC 29213-MSSA, <i>S. aureus</i> ATCC 43300-MRSA, <i>S. epidermidis</i> ATCC 70576,  <i>S. epidermidis</i> ATCC 70582,  <i>S. pneumoniae</i> ATCC 49619-Penicillin sensitive, <i>S. pneumoniae</i> ATCC 51915-Penicillin resistant, <i>E. faecalis</i> ATCC 29212-Vancomycin sensitive, <i>E. faecium</i> ATCC 700221-Vancomycin resistant, <i>Haemophilus influenzae</i> ATCC 49247, <i>Haemophilus influenzae</i> ATCC 49766 <i>E. coli</i> permeable mutant	Chlorinated bisindole pyrroles:		[57]
			Lynamycin A	C <sub>22</sub> H <sub>16</sub> N <sub>5</sub> O <sub>2</sub> Cl <sub>2</sub>	
			Lynamycin B	C <sub>22</sub> H <sub>14</sub> N <sub>5</sub> O <sub>2</sub> Cl <sub>3</sub> Na	
			Lynamycin C	C <sub>20</sub> H <sub>12</sub> N <sub>5</sub> Cl <sub>4</sub>	
			Lynamycin D	C <sub>24</sub> H <sub>18</sub> N <sub>5</sub> O <sub>4</sub> Cl <sub>2</sub>	
			Lynamycin E	C <sub>24</sub> H <sub>19</sub> N <sub>5</sub> O <sub>4</sub> Cl	
Platinum Coast on the Mediterranean Sea, north of Egypt	<i>Streptomyces</i> sp. Merv8102	<i>P. aeruginosa</i> ATCC 10145), <i>B. subtilis</i> ATCC 6051, <i>S. aureus</i> ATCC 6538 and <i>M. luteus</i> ATCC 9341	Esramycin Triazolopyrimidine [1,2,4] Triazolol[1,5-a]pyrimidin-7(4H)-one, 5-methyl-2-(2-oxo-2-phenylethyl)-	C <sub>14</sub> H <sub>12</sub> N <sub>4</sub> O <sub>2</sub>	[58]
Marine sediment, La Jolla, California	<i>Streptomyces</i> sp. CNQ-418	Methicillin-resistant <i>S. aureus</i> (MRSA)	Marinopyrroles A Marinopyrroles B	C <sub>22</sub> H <sub>12</sub> Cl <sub>4</sub> N <sub>2</sub> O <sub>4</sub> C <sub>22</sub> H <sub>11</sub> BrCl <sub>4</sub> N <sub>2</sub> O <sub>4</sub>	[59]

Table 1. Cont.

Isolation Source	Genus	Antimicrobial Activity	Molecule	Formula	Reference
Sediment of Bay of Bengal, India	<i>Streptomyces chibaensis</i> sp. AUBN17	<i>B. subtilis</i> ATCC 6633, <i>B. pumilus</i> ATCC 19164, <i>S. aureus</i> ATCC 29213, <i>E. coli</i> ATCC 25922, <i>P. aeruginosa</i> ATCC 27853 <i>P. vulgaris</i> ATCC 6897	1-Hydroxy-1-norresistomycin	$C_{21}H_{14}O_7$	[45]
			Resistomycin	$C_{21}H_{14}O_7$	
Sediment of the Lagoon de Terminos at the Gulf of Mexico	<i>Streptomyces</i> B80055/ <i>Streptomyces</i> B4842	<i>E. coli</i> , <i>S. aureus</i> , <i>S. viridochromogenes</i>	1-Hydroxy-1-norresistomycin	$C_{21}H_{14}O_7$	[60]
			Resistoflavin Resistoflavin methyl ether	$C_{23}H_{18}O_7$	
Marine sediment from Scripps Canyon, La Jolla, California, Pacific Coast, United States	<i>Streptomyces nodosus</i> NP507994	Drug-sensitive and drug-resistant Gram-positive reaction bacteria	Lajollamycin	$C_{36}H_{53}N_3O_{10}$	[61]
			Nitro-tetraene Spiro- $\beta$ -lactone- $\gamma$ -lactam		
Sediment of Jiaozhou Bay, China	<i>Actinomadura</i> sp. M048	<i>S. aureus</i> , <i>B. subtilis</i> , and <i>S. viridochromogenes</i>	Chandrananinycin A Acetamide, <i>N</i> -(9-hydroxy-3-oxo-3H-phenoxazin-2-yl)-	$C_{14}H_{10}N_2O_4$	[62]
			Chandrananinycin B Acetamide, 2-hydroxy- <i>N</i> -(3-oxo-3H-phenoxazin-2-yl)-	$C_{14}H_{10}N_2O_4$	
			Chandrananinycin C 1-Methoxy-3-methyl-1,2,3,4-tetrahydro-5H-pyrido[3,2- <i>b</i> ]phenoxazin-5-one		
Sandy sediment, coastal site of Mauritius, Indian Ocean	<i>Streptomyces</i> sp. B6921	<i>S. aureus</i> , <i>E. coli</i> , <i>B. subtilis</i> , and <i>S. viridochromogenes</i>	Fridamycin D	$C_{31}H_{52}O_{12}$	[46]
			Himalomycin A	$C_{43}H_{52}O_{16}$	
			Himalomycin B	$C_{43}H_{56}O_{16}$	
Mucus secreted by the box-fish <i>Ostracion cubicus</i> , Israel	<i>Vibrio parahaemolyticus</i> B2	<i>S. aureus</i> , <i>S. albus</i> and <i>B. subtilis</i>	Vibrindole A	$C_{18}H_{16}N_2$	[52]

Table 2. Chronological report of bacteria with antimicrobial activity in vitro against human pathogens which molecules have not been chemically identified.

Isolation Source	Genus	Antimicrobial Activity	Reference
Khewra Salt Range, Punjab, Pakistan	<i>Aquasiliicoccus elongatus</i> MB592,	<i>B. subtilis</i> , <i>B. pumilus</i> , <i>E. faecalis</i> , <i>B. cereus</i> , <i>K. pneumoniae</i> , <i>Ataligenes faecalis</i> , <i>P. septicata</i> , <i>E. faecium</i>	[63]
	<i>Salinococcus seductus</i> MB597, and <i>Halomonas aquamarina</i> MB598		
Hypersaline soils (solonchaks, solonetz and takyrs) from Kostanay, Auliekol and Mendykara. Almaty region, Balkhash, Kazakhstan	<i>Actinomyces</i> spp.	<i>S. aureus</i> MRSA, <i>E. coli</i> (PMG223)	[64]
Marine water, Gujarat, Western India	<i>Kocuria</i> sp. strain rsk4	Antibiotic-resistant <i>S. aureus</i>	[65]
Crystallizer pond sediments of Ribandar saltern, Goa, India	<i>Streptomyces radiopugnans</i>	<i>S. typhimurium</i> , <i>P. vulgaris</i> , <i>E. coli</i>	[66]
	<i>Streptomyces sporocinerus</i>	<i>S. typhimurium</i> , <i>P. vulgaris</i> , <i>E. coli</i>	
	<i>Kocuria palustris</i>	<i>S. aureus</i>	
	<i>Micromonospora</i> sp.	<i>V. cholerae</i>	
	<i>Nocardopsis</i> sp.	<i>S. citreus</i>	
Coastal Solar Saltern, India	<i>Nonomuraea</i> sp. JA18	Methicillin-Resistant <i>S. aureus</i> (MRSA), <i>B. subtilis</i> MTCC441, <i>K. pneumoniae</i> MTCC 109, <i>S. typhi</i> MTCC733, and <i>P. vulgaris</i> MTCC 426	[67]
Sediment of estuarine coastal brackish, Chilika Lake, Khurda Odisha, India	<i>Streptomyces chilikensis</i> RC 1830	<i>E. coli</i> , <i>S. aureus</i> , <i>B. cereus</i> and <i>S. typhi</i>	[67]
Mangrove sediment of Visakhapatnam, Andhra Pradesh, India	<i>Streptomyces</i> sp.	<i>S. aureus</i> , <i>B. subtilis</i> , <i>B. cereus</i> , <i>E. coli</i> , <i>P. aeruginosa</i> , <i>P. vulgaris</i>	[68]
Mangrove sediment, Nizampatnam, Andhra Pradesh, India	<i>Pseudonocardia</i> VUK-10	<i>S. aureus</i> , <i>S. mutans</i> , <i>B. subtilis</i> , <i>E. coli</i> , <i>E. faecalis</i> , <i>P. aeruginosa</i>	[69]

Table 2. Cont.

Isolation Source	Genus	Antimicrobial Activity	Reference
Salt pans Batim and Ribandar, Goa, India		<i>A. baumannii</i> , <i>A. hydrophila</i> , <i>Citrobacter diversus</i> , <i>Citrobacter freundii</i> , <i>E. coli</i> ATCC 25922, <i>K. pneumoniae</i> , <i>Morganella morganii</i> , <i>P. mirabilis</i> , <i>P. ATCC 27855</i> , <i>P. spp.</i> , <i>S. paratyphi A</i> , <i>S. typhi</i> , <i>S. typhimurium</i> , <i>S. boydii</i> , <i>S. flexneri</i> , <i>V. cholerae</i> , Methicillin Resistant <i>S. aureus</i> (MRSA), Methicillin Sensitive <i>S. aureus</i> (MSSA), <i>S. aureus</i> ATCC 25923, <i>S. citreus</i>	[70]
	<i>Bacillus</i> spp. <i>Virgibacillus</i> spp.		
Salt pans, Kodiakarai, Tamil Nadu, India	<i>Streptococcillum album</i>	<i>S. aureus</i> , <i>K. pneumoniae</i> and <i>E. coli</i>	[71]
	<i>Actinopolyspora</i> spp. <i>A. halophila</i> , <i>A. morticallis</i> , <i>A. erythraea</i> , <i>A. xinjiangensis</i> , <i>A. alba</i> , <i>NoCARDiopsis</i> spp. <i>N. litoralis</i> , <i>N. xinjiangensis</i> <i>N. adiformis</i> and <i>N. exhalans</i> <i>Saccharomonospora</i> spp. <i>S. paurometabolica</i> , <i>S. halophila</i> <i>Streptomonospora</i> spp. <i>S. alba</i> , <i>S. amyolytica</i> , <i>S. flavalba</i> <i>Saccharopolyspora</i> sp.	<i>B. subtilis</i> , <i>S. aureus</i> , <i>M. luteus</i> , <i>K. pneumoniae</i> , <i>L. monocytogenes</i>	
Nonrhizospheric soil, Saharan regions, south of Algeria			[72]

Table 2. Cont.

Isolation Source	Genus	Antimicrobial Activity	Reference
Crystallizer pond, Madurai, India	<i>Nocardopsis</i> sp. JA16	<i>S. aureus</i> , <i>B. subtilis</i> , <i>S. typhi</i> , Methicillin-resistant <i>S. aureus</i> (MRSA), <i>K. pneumoniae</i> , <i>Enterobacter</i> sp., and <i>P. aeruginosa</i>	[73]
Bay of Bengal coast of Puducherry and Marakkanam, India	<i>Streptomyces</i> sp. VITSVK9	<i>B. subtilis</i> , <i>Escherichia coli</i> , <i>K. pneumoniae</i> , <i>S. aureus</i> and <i>S. species</i>	[74]
Marine sediment of Marakkanam, Bay of Bengal Coast, Tamil Nadu, India	<i>Saccharopolyspora salina</i> VITSK4	<i>S. aureus</i> ATCC 25923, <i>B. subtilis</i> ATCC 6633, <i>E. coli</i> ATCC 25922, <i>K. pneumoniae</i> ATCC 10273	[75]
Marakkanam coast of Tamil Nadu, India	<i>Streptomyces</i> sp. VITSK1	<i>S. aureus</i> ATCC 25923, <i>B. subtilis</i> ATCC 6633, <i>E. coli</i> ATCC 25922, <i>K. pneumoniae</i> ATCC 10273	[76]
Salt Lake Hani in Xinjiang, China	<i>Actinomyces</i> sp.	<i>B. subtilis</i>	[77]
Salt lakes of Bay of Bengal, India	<i>Actinomyces</i> sp. <i>Streptomyces</i> sp.	<i>P. aeruginosa</i> , <i>B. subtilis</i> , <i>S. epidermidis</i> , <i>E. coli</i>	[78]
Water samples Asen fjord in the Trondheim fjord and Steinvikholmen, Norway	<i>Streptomyces</i> sp.	Gram-negative and Gram-positive bacteria	[79]
Salt Lake Bardawil, Egypt	<i>Streptomyces viriditolucens</i>	<i>E. coli</i> , <i>Edwardsiella tarda</i> , <i>Corynebacterium michiganense</i> B-33, <i>P. solanacearum</i> B-3212 and <i>Staphylococcus</i> spp.	[77]

Table 2. Cont.

Isolation Source	Genus	Antimicrobial Activity	Reference
Soil from salt pan regions of Cuddalore and Parangipettai (Porto-Novo), Tamil Nadu, India	<i>Streptomyces</i> sp., <i>Saccharomonospora</i> sp.	<i>E. coli</i> , <i>K. pneumoniae</i> , <i>P. aeruginosa</i> , <i>V. cholerae</i> , <i>S. typhi</i> , <i>S. aureus</i> , and <i>S. dysenteriae</i>	[80]
	<i>Micromonospora nigra</i> DSM 43818, <i>Micromonospora rhodorangea</i> , <i>Micromonospora halophytica</i> DSM 43171	Multidrug-resistant (MDR) Gram-positive pathogens, vancomycin-resistant enterococci (VRE), and methicillin-resistant <i>S. aureus</i> (MRSA)	
Bismarck and Solomon Sea off the coast of Papua New Guinea	<i>Actinopolyspora</i> spp. AHL, <i>A. halophila</i> , <i>A. mortuialis</i> , <i>A. iruquensis</i>	<i>S. aureus</i> , <i>S. epidermidis</i> , <i>B. subtilis</i>	[82]

Noted: American Type Culture Collection (ATCC); Deutsche Sammlung von Mikroorganismen und Zellkulturen (DSMZ); Multidrug-resistant (MDR); Microbial Type Culture Collection and Gene Bank (MTCC). Microorganisms: *Acinetobacter* (A.): *A. baumannii*, *Aeromonas* (A.): *A. hydrophila*, *Alcaligenes* (A.): *A. faecalis*, *Bacillus* (B.): *B. cereus*, *B. halodurans*, *B. megaterium*, *B. pumilus*, *B. subtilis*, *Burkholderia* (B.): *B. metallica*, *Candida* (C.): *C. albicans*, *Citrobacter* (C.): *C. diversus*, *C. freundii*, *Corynebacterium* (C.): *C. michiganense*, *Edwardsiella* (E.): *E. tarda*, *Enterobacter* (E.): *E. aerogenes*, *Enterococcus* (E.): *E. faecalis*, *E. faecium*, *Vancomycin resistant Enterococcus faecium* (VREF), *Vancomycin sensitive Enterococcus faecalis* (VSEF), *Vancomycin resistant enterococci* (VRE), *Escherichia* (E.): *E. coli*, *Haemophilus* (H.): *H. influenzae*, *Klebsiella* (K.): *K. pneumoniae*, *Listeria* (L.): *L. ivanovii*, *L. monocytogenes*, *Micrococcus* (M.): *M. luteus*, *Morganella* (M.): *M. morganii*, *Mycobacterium* (M.): *M. avium*, *M. leprae*, *M. lepromatosis*, *M. smegmatis*, *M. tuberculosis*, *Proteus* (P.): *P. mirabilis*, *P. vulgaris*, *Pseudomonas* (P.): *P. aeruginosa*, *P. geniculata*, *P. solanacearum*, *Salmonella* (S.): *S. henrici*, *S. paratyphi*, *S. typhi*, *S. typhimurium*, *Serratia* (S.): *S. marcescens*, *Shigella* (S.): *S. boydii*, *S. dysenteriae*, *S. flexneri*, *Staphylococcus* (S.): *S. aureus*, *S. citreus*, *S. epidermidis*, Antibiotic-resistant *Staphylococcus aureus* (ARSA), Methicillin Sensitive *Staphylococcus aureus* (MSSA), Methicillin-resistant *Staphylococcus aureus* (MRSA), *Streptococcus* (S.): *S. mutans*, *S. pneumoniae*, Penicillin resistant *Streptococcus pneumoniae* (PRSP), Penicillin sensitive *Streptococcus pneumoniae* (SPSP), *Streptomyces* (S.): *S. viridochromogenes*, *Vibrio* (V): *V. cholerae*, *V. parahaemolyticus*, *Xanthomonas* (X.): *X. campestris*, *X. maltocearum*.

The biotechnological potential of halophilic bacteria, especially for antimicrobial exploitation, still remains in progress, in spite that the occurrence of new several groups of microorganisms is high, the rate of discovery of new biomolecules is low compared with non-halophilic bacteria. Despite periodic descriptions of new species and attempts to culture hidden microbiota, there are no significant studies focused on the discovery of new bioactive metabolites produced by microorganisms from hypersaline ecosystems. The genome-guided studies are currently the best support to take novel strategies in drug discovery. All the antimicrobial compounds described herein derived from halophilic bacteria in which the molecule has been elucidated are summarized in Table 1 and the strains capable of inhibiting pathogens in primary tests whose molecules are unknown are shown in Table 2.

### 3.2. Archaea

Since the discovery of halocins and their action against the surrounding microbiota in their habitats [35] no new or known antimicrobial compounds derived from archaea capable of inhibiting human pathogens have been reported in the literature to date. At an ecological level, the role of archaeocins in microbial communities is the interspecies competition, the antimicrobial activity of halocins suggests that its function is to dominate a given niche occupied by microorganisms having similar adaptations and nutritional requirements [83–85]. Members of *Halorubrum* and *Haloferax* have been identified as the preponderant halocin-producing genera, the cross-domanin antimicrobial action was observed against bacterial members of the genera *Halomonas*, *Rhodovibrio*, *Salisaeta*, or *Pontibacillus*, all isolated from hypersaline samples [86].

To understand the current situation, it is necessary that a comprehensive analysis of the possible reasons why haloarchaea are under-explored at the biotechnological level and why the antimicrobial exploitation is scarce in comparison with other microorganisms prevalent in non-halophilic environments. The first limitation found is the cultivation time of haloarchaea, observed at around 5 to 30 days to yield colonies or cellular density in broth cultures [12]. Once the cultivation is reached, the upcoming drawback is the evaluation of the inhibitory capacity of haloarchaea against a panel of human pathogens. The main obstacle to overcome is when the primary screening (isolate vs. pathogen) is performed due to the high salinity requirements of haloarchaea to grow, greater than 20% of NaCl until saturation, while in halophilic bacteria the screening can be adapted at lower range of salinity, under 15% of NaCl.

Tests such a direct spot-inoculation of the supernatant, diffusion discs, and cross-streak require the adaptation of an appropriate protocol. Finding the same and suitable conditions to test both microorganisms drive to set-up alternative technical procedures, like dual-media and crude extracts for testing those strains growing above the seawater salinity, ca. 3.5 % [87]. Another possible reason is that the study of extremophilic microbiota has been approached at an ecological level and the vast biotechnological exploitation of these extremophiles is more recognized on their enzymes and compatible solutes. The low metabolic requirements, the hypersaline conditions where they thrive, or the low competition for nutrients with their peers determine their behavior, i.e., the production of halocins, which action is limited to the closest members inhabiting in the same environment [88,89]. This could explain that the production of antimicrobials against the non-halophilic community of microorganisms seems to be unnecessary.

Constituted as a powerful tool, “omics” approaches as metagenomics and genomics effectively support ecological and bioprospecting studies deciphering new insights into halophilic microorganisms [90–92]. Extremely rare is the interdomain horizontal gene transfer (IHGT) across bacteria, archaea, and fungi of homologous DNA. However, a genomic-guided study revealed for the first time a potent antibacterial gene encoding a glycosyl hydrolase 25 muramidases (GH25-muramidase) identified in archaea after co-cultivation with a bacterial competitor [93]. In the genome-mining study conducted by Wang et al. (2014), an atlas of nonribosomal peptide synthetase (NRPSs) and modular polyketide synthase (PKSs) gene clusters was built based on 2699 genomes of bacteria, archaea, and fungi. In this study, were included 25 members of *Halobacteria*: *Haloarcula hispanica* ATCC 33960,

*Halalkalicoccus jeotgali* B3, *Haloarcula marismortui* ATCC 43049, *Halobacterium* sp. NRC-1, *Halobacterium salinarum* R1, *Haloferax mediterranei* ATCC 33500, *Haloferax volcanii* DS2, *Halo geometricum borinquense* DSM 11551, *Halomicrobium mukohataei* DSM 12286, *Halopiger xanaduensis* SH-6, *Haloquadratum walsbyi* C23, *Haloquadratum walsbyi* DSM 16790, *Halorhabdus tiamatea* SARL4B, *Halorhabdus utahensis* DSM 12940, *Halorubrum lacusprofundi* ATCC 49239, *Haloterrigena turkmenica* DSM 5511, *Halovivax ruber* XH-70, *Natrialba magadii* ATCC 43099, *Natrinema* sp. J7-2, *Natrinema pellirubrum* DSM 15624, *Natronobacterium gregoryi* SP2, *Natronococcus occultus* SP4, *Natronomonas moolapensis* 8.8.11, *Natronomonas pharaonis* DSM 2160, *Salinarchaeum* sp. Harcht-Bsk1. Of a total of 3339 cataloged gene clusters, no PKS, NPKS or hybrid in *Halobacteria* were reported. Within the studied archaea, only two and one NRPS were identified in *Methanobacteria* and *Methanomicrobia*, respectively [55]. Despite these results and considering that the class *Halobacteria* is wide represented with seven families, these results do not exclude the biosynthetic capacity of nonribosomal peptide and polyketide, and nor discourage the biotechnological interest of haloarchaea for future natural product discovery.

### 3.3. Fungi

Along the years of research on natural products, fungi represent the basis of antimicrobial discovery. Halotolerant and halophilic fungal communities that inhabit the natural hypersaline environments are not strictly salt requiring, as they can grow and adjust to the whole salinity range, from freshwater to almost saturated NaCl solutions [94,95]. Despite this versatility, the vast majority of antimicrobial molecules from halophilic fungi have been produced under low or moderate salinity conditions since the primary screenings against SKAPE microorganisms are easier without NaCl. The mycobiota of hypersaline environments is dominated by members of *Aspergillus*, *Penicillium*, and other genera, such as *Alternaria*, *Cladosporium*, *Fusarium*, *Debaryomyces*, *Scopulariopsis*, *Chaetomium*, *Wallemia*, and *Hortaea*, which are well represented in ecological and biodiversity studies [96,97]. The species *Gymnoascus halophilus*, *Aspergillus penicillioides*, *Hortaea werneckii*, *Phaeotheca triangularis*, *Aureobasidium pullulans*, *Trimmatostroma salinum*, and some species of the genus *Wallemia*, like *W. ichthyophaga*, are recognized as obligately halophilic, or require high levels of salt above that of seawater [98,99]. However, antimicrobial compounds have not been reported from these species.

The halophilic species of the genus *Aspergillus* are the most prolific and several strains of *Aspergillus* sp. have been isolated from Arctic sub-sea sediments from the Barents Sea (Table 3). In particular, strain 8Na identified as *A. protuberus*, a polyextremophilic fungus able to grow in a wide range of pH, temperature and salinity (up to 25% (w/v)) showed an antimicrobial efficacy against human pathogens. The strongest power inhibitory action was observed against *Staphylococcus aureus*. The molecule responsible of the activity was identified as Bisvertinolone, a compound member of the family Sorbicillinoid [87]. *Aspergillus flocculosus* PT05-1 and *Aspergillus terreus* PT06-2, both isolated from sediment of Putian sea saltern of Fujian, China, showed antimicrobial activity against *Enterobacter aerogenes*, *Pseudomonas aeruginosa*, and *Candida albicans*. Strain PT05-1 produces 11 metabolites among which two are new ergosteroids and pyrrole derivative compounds [100], and strain PT06-2 produces the novel compounds: Terrelactone A and Terremides A and B [101]. Other strains of the genus *Aspergillus*, like *A. terreus* Tsp22 [101–103], *A. flavus*, *A. gracilis*, and *A. penicillioides* [102] have antibacterial and antioxidant activities in crude extracts but the molecule has not been identified. In the atlas of Wang et al. (2014), 360 fungi were genome-mined cataloguing a total of 307 gene clusters from 30 strains of the phylum *Ascomycota*. Within this group, strains of the genus *Aspergillus*: *A. nidulans* FGSC A4, *A. fumigatus*, *A. niger* CBS 513 88, and *A. oryzae* RIB40 harbor NRPSs, PKSs and hybrids gene clusters [55]. These results confirm that the genus *Aspergillus* is among the most prolific producers of antimicrobial metabolites. In spite of the prosperous production of compounds from fungi, the active molecules derived from extremely halophilic fungi are still scarce (Table 3). It is highly probable that through genome-driven studies in halophilic fungi, NRPSs and PKSs are substantially present as their peers providing new insights into the fungal biosynthetic pathways.



Table 3. Halophilic fungi showing antimicrobial activity.

Isolation Source	Species	Antimicrobial Activity	Molecule	Formula	Reference
Abyssal marine sediment. Barents Sea. Arctic Ocean	<i>Aspergillus protuberus</i> MUT 3638	<i>S. aureus</i> , <i>K. pneumoniae</i> , <i>A. baumannii</i> and <i>B. metallica</i>	Bisvertinolone	C <sub>28</sub> H <sub>33</sub> O <sub>9</sub>	[87]
Solar saltern, Phetchaburi, Thailand	<i>Aspergillus flavus</i> , <i>Aspergillus gracilis</i> , and <i>Aspergillus penicillitoides</i>	Antibacterial and antioxidant	Crude extracellular compounds	NR	[102]
Putian saltern of Fujian, China	<i>Aspergillus flocculosus</i> PT05-1	<i>E. aerogenes</i> , <i>P. aeruginosa</i> , and <i>C. albicans</i>	Ergosteroids: (22R,23S)-epoxy-3b,11a,14b,16b-tetrahydroergosta-5,7-dien-12-one  Pyrrole derivatives: 6-(1H-pyrrol-2-yl) hexa-1,3,5-trienyl 4-methoxy-2H-pyran-2-one	C <sub>28</sub> H <sub>42</sub> O <sub>6</sub>   C <sub>16</sub> H <sub>15</sub> NO <sub>3</sub>	[100]
Putian saltern of Fujian, China	<i>Aspergillus terreus</i> PT06-2	<i>E. aerogenes</i> , <i>P. aeruginosa</i> , and <i>C. albicans</i>	Terrenide A Terrenide B Terrelactone A	C <sub>21</sub> H <sub>17</sub> N <sub>3</sub> O <sub>5</sub> C <sub>21</sub> H <sub>15</sub> N <sub>3</sub> O <sub>4</sub> C <sub>24</sub> H <sub>26</sub> O <sub>8</sub>	[101]
Semiarid saltans in Botswana	<i>Aspergillus terreus</i> Tsp22	<i>B. megaterium</i> and <i>S. aureus</i>	Crude extracellular compounds	NR	[103]

Abbreviations: Not reported (NR). Microorganisms: *Achinetobacter* (A); *A. baumannii*. *Bacillus* (B); *B. megaterium*. *Burkholderia* (B); *B. metallica*. *Candida* (C); *C. albicans*. *Enterobacter* (E); *E. aerogenes*. *Escherichia* (E); *E. coli*. *Haemophilus* (H); *H. influenzae*. *Klebsiella* (K); *K. pneumoniae*. *Pseudomonas* (P); *P. aeruginosa*. *Staphylococcus* (S); *S. aureus*.

#### 4. Anticancer Compounds

Natural products are relevant anticancer drugs, which are also called bioactive molecules, produced by organisms. Although, earlier and the well-established anticancer natural products have been obtained from plant cells originally, microorganisms are an excellent alternative, due to the diversity of the microbial world, their easy manipulation, and they can be screened physiologically to discover new natural products with antitumor activity. Although bacterial cells have different communication methods with tumor cells other than metabolites experimentally, bacterial metabolites have been considered the most conventional way against cancer cells viability. Today, more attention is focused on extremophiles as a new source of novel biomolecules [104,105]. Among extremophiles, halophilic and halotolerant microorganisms, which inhabit hypersaline environments, are considered as reliable sources of antitumor metabolites with fewer side effects. In recent years, several studies have been focused on the importance of metabolites from halophilic microorganisms on cancer treatment. The halophilic bacteria, archaea, and fungi involved on the production of anti-cancer biomolecules are summarized in Table 4.

##### 4.1. Bacteria

Since the last two decades, halophilic bacteria have attracted the interests of researchers due to their adaptability to a wide range of salinities. Some studies have been carried out to determine the role of halophilic bacteria in cancer treatment. In one of these studies, Chen et al. (2010) assayed fourteen crude extracts from 45 halophilic bacterial strains and showed cytotoxic activity against human liver cancer cell line Bel 7402 with a half maximal inhibitory concentration (IC<sub>50</sub>) of 500 µg/mL and five of them showed remarkable activities with IC<sub>50</sub> lower than 40 µg/mL [106]. The antineoplastic antibiotic known as tubercidin, was isolated from the halophilic actinobacterium *Actinopolyspora erythraea* YIM 90600, this compound exhibited the capability to stabilize the tumor suppressor Programmed Cell Death Protein 4 (Pdc4), which is known to antagonize critical events in oncogenic pathways. Tubercidin, significantly inhibited proteasomal degradation of a model Pdc4-luciferase fusion protein, with an IC<sub>50</sub> of  $0.88 \pm 0.09$  µM, unveiling a novel biological activity for this well-studied natural product [107].

In two studies on different extracts of halophilic and halotolerant bacteria isolated from brine-seawater interface of the Red Sea, Sagar et al. (2013) tested the cytotoxic and apoptotic activity of their extracts against three human cancer cell lines, including HeLa (cervical carcinoma), MCF-7 (breast adenocarcinoma) and DU145 (prostate carcinoma). In one of their studies, a total of 20 lipophilic (chloroform) and hydrophilic (70% ethanol) extracts from twelve different strains were assessed. Among these, twelve extracts were found to be very active after 24 h of treatment, which were further evaluated for their cytotoxic and apoptotic effects at 48 h. The extracts from the isolates *Halomonas* sp. P1-37B, *Halomonas* sp. P3-37A, and *Sulfitobacter* sp. P1-17B were found to be the most potent against tested cancer cell lines [108]. In the other study, ethyl acetate extracts of 24 strains were assayed and the results showed that most extracts were cytotoxic against one or more cancer cell lines. Out of the thirteen most active microbial extracts, six extracts induced significantly higher apoptosis (>70%) in cancer cells. Molecular studies revealed that extracts from *Chromohalobacter salexigens* strains P3-86A and P3-86B followed the sequence of events of apoptotic pathway involving matrix metalloproteinases (MMP) disruption, Caspase-3/7 activity, Caspase-8 cleavage, polymeric adenosine diphosphate ribose polymerase 1 (PARP-1) cleavage, and phosphatidylserine exposure, whereas the extracts from another *Chromohalobacter salexigens* strain K30 induced Caspase-9 mediated apoptosis. The extracts from *Halomonas meridiana* strain P3-37B and *Idiomarina loihiensis* strain P3-37C were unable to induce any change in MMP in HeLa cancer cells and thus suggested a mitochondria-independent apoptosis induction. However, further detection of a PARP-1 cleavage product and the observed changes in Caspase-8 and Caspase-9 suggested the involvement of caspase-mediated apoptotic pathways [109]. An ethyl acetate extract from *Streptomyces* sp. WH26 showed significant cellular toxicity. Two new compounds, 8-O-methyltetragulol and naphthomycin A, were isolated from this extract via silica gel column chromatography and high-pressure liquid chromatography (HPLC). These

two compounds showed potent cytotoxic activity against several human cancer cell lines including A549, HeLa, BEL-7402, and HT-29 [110]. Novel anticancer molecules, Salternamide A–D, were isolated from a halophilic *Streptomyces* sp. isolated from a saltern on Shinui Island, in the Republic of Korea, and exhibited an extensive viability reduction in several cancer cell lines [111]. Among these molecules, Salternamide A inhibited the hypoxia-induced accumulation of HIF-1 $\alpha$  in several cancer cell lines and suppressed the HIF-1 $\alpha$  by downregulation of its upstream signaling pathways such as PI3K/Akt/mTOR, p42/p44 MAPK, and STAT3. Moreover, in human colorectal cancer cell lines, salternamide A caused cell death by arresting the cells in the G2/M phase and lead to apoptosis [112]. A halophilic bacterium, *Vibrio* sp. strain AISM3-36-8, isolated from Manaure solar saltern in Colombia, showed a high potential to inhibit methicillin-resistant *Staphylococcus aureus* and causing a slight inhibition of lung cancer cell lines [51]. In another study, among nine moderately halophilic bacteria isolated from saline environments of Iran, the supernatant of four strains showed ability to reduce the viability of HUVEC cancer cell line while one of these supernatants induced the proliferation of adipose-derived mesenchymal stem cells [113]. The actinobacterium *Nocardiopsis lucentensis* DSM 44048 isolated from Salt marsh soil in Alicante, Spain produces a new benzoxazole derivatives, Nocarbenzoxazole G. The compound showed cytotoxic activity against liver carcinoma cells (HepG2) and HeLa cancer cells with IC<sub>50</sub> values of 3 and 1  $\mu$ M, respectively [114]. A halotolerant *Bacillus* sp. KCB14S006, which was isolated from a saltern, produced three new lipopeptides with cytotoxic activity. These new lipopeptides lead to a ~30% decrease in the viability of HeLa and src(ts)-NRK cells [115]. In another study, the methanolic extracts of *Bacillus* sp. VITPS14 and *Bacillus* sp. VITPS16 showed cytotoxicity against HeLa cancer cell line but not against A549 cells. These halophilic strains were isolated from soil samples of Marakkanam saltern and Pichavaram mangrove forest, India, respectively. Another halophilic strain, *Bacillus* sp. VITPS7, isolated from this area showed significant antioxidant activity. The presence of  $\beta$ -carotene and flavonoids was confirmed in these extracts [116]. In another study, twenty-four novel halophilic bacteria isolated from the surrounding of active volcanic Barren Island Andaman and the Nicobar Islands in India were examined for their cytotoxic activity against MDA-MB-231 breast cancer cell line. About 65% of these bacterial strains decreased the viability of this cell line to 50% or lower [117]. Metabolites from *Piscibacillus* sp. C12A1 isolated from Sambhar Lake, India, decreased the viability of MDA-MB-231 breast cancer cell line with downregulation of Bcl-xL and CDK-2 expression. Furthermore, cell migration and colony formation of the cells were inhibited in the presence of these metabolites [118].

Biosurfactants produced by microorganisms are active molecules that create an amphipathic surface containing hydrophilic and hydrophobic moieties. In recent years, these biomolecules were also found to possess several interesting properties of therapeutic and biomedical importance. Biosurfactants from the halophilic bacteria *Bacillus* sp. BS3 and *Halomonas* sp. BS4 had the ability to reduce the viability of mammary epithelial carcinoma cells to 24.8% and to 46.8 significantly ( $p < 0.05$ ) at 0.25  $\mu$ g/mL and 2.5  $\mu$ g/mL concentrations, respectively [53,119].

Extracellular polymeric substances (EPS) have recently been attracting considerable attention because of their potential applications in many fields, including biomedicine. EPSs are heterogeneous polymers that contain a wide range of homo- or hetero-carbohydrates as well as organic and inorganic substituents. EPSs produced by both halophilic bacteria and archaea showed remarkable anticancer activity. Also, these polysaccharide polymers have been introduced as important agents for developing nanocarrier systems for anti-cancer drugs. For example, in 2011, Ruiz-Ruiz et al. showed that at a concentration of 500  $\mu$ g/mL, the over sulfated exopolysaccharide of the halophilic bacterium *Halomonas stenophila* strain B100 completely blocked the proliferation of the human T leukemia cells (Jurkat cells) in a dose-response manner. Also, they revealed the positive effect of sulfate groups in viability reduction of Jurkat cells [120]. Moreover, in another study, the anti-cancer activity of the polysaccharide levan and its aldehyde-activated derivatives was reported. This polysaccharide was isolated from *Halomonas smyrnensis* AAD6 and its anticancer activity against human cancer cell lines such as lung (A549), liver (HepG2/C3A), gastric (AGS), and breast (MCF-7) cancer cells (Table 4) has been investigated. In this

study, all evaluated cells were treated with levan samples at a broad concentration ranging from 10 to 1000 µg/mL. All samples were found to display growth inhibition against cancer cell lines at the highest dose (1000 µg/mL). Unmodified levan showed higher anti-cancer effect against AGS cells against other cancer cell lines. Aldehyde-activated levan showed higher anti-tumor activity than unmodified levan against all cancer cell lines. Oxidized levan samples showed higher anticancer activity against A549 and HepG2/C3A cells. By increasing the oxidation degree, the anti-cancer activity also increased. Therefore, it was clearly demonstrated that the introduction of the chemically modified group, aldehydes, into the linear levan molecule could significantly enhance the antitumor activity of levan polysaccharide [121].

Recent preclinical and medicinal studies have shown an inverse relationship between dietary uptake of carotenoids and cancer occurrence. It was reported that the extracted carotenoid from the halotolerant bacterium *Kocuria* sp. QWT-12, isolated from industrial tannery wastewater in Qom, in Iran, had the ability to reduce the viability of human breast cancer cell lines MCF-7, MDA-MB-468, and MDA-MB-231 with an IC<sub>50</sub> of 1, 4, and 8 mg/mL, respectively. Also, this carotenoid decreased the viability of human lung cancer cell line A549, with IC<sub>50</sub> of 4 mg/mL. This carotenoid did not reduce the viability of normal fibroblast cell line at these concentrations [122].

Among all anticancer enzymes, L-asparaginase and L-glutaminase are enzymes with the ability to inhibit acute lymphoblastic leukemia and other cancer cells. Halophilic and halotolerant bacteria are novel sources of these anticancer enzymes. For example, a screening from 85 halophilic strains from the hypersaline Urmia Lake in Iran revealed that 16 (19%) and three strains (3.5%) showed L-asparaginase and L-glutaminase activity, respectively. It was shown that L-asparaginase was produced mainly by strains belonging to the genus *Bacillus*, while L-glutaminase was produced mainly by strains of the genus *Salicola* [27]. In another study, it was reported that from 110 halophilic strains isolated from different saline environments of Iran, a total of 29, four, and two strains produced anticancer enzymes including L-asparaginase, L-glutaminase, and L-arginase, respectively. These strains belonged to the genera *Bacillus*, *Dietzia*, *Halobacillus*, *Rhodococcus*, *Paenibacillus*, and *Planococcus*, as Gram-positive bacteria, and *Pseudomonas*, *Marinobacter*, *Halomonas*, *Idiomarina*, *Vibrio*, and *Stappia* as Gram-negative bacteria [123]. From these strains, the anti-cancer activity of a novel recombinant L-asparaginase enzyme produced by *Halomonas elongata* strain IBRC M10216 was assayed against human lymphoblastic and myeloid leukemia cell lines, Jurkat and U937 (Table 4). This enzyme enhanced the viability of these cancer cell lines with IC<sub>50</sub> values of 2 and 1 U/mL, respectively, but at these concentrations had no effect on the viability of normal HUVEC cell line [124].

Table 4. Halophilic bacteria, archaea, and fungi and their relation to cancer treatment.

Anticancer Activity of:	Isolation Source	Halophilic Strain	Cancer Cell Lines	Molecule	Formula	Reference
Metabolite	Marakkannam saltern and Pichavaram mangrove forests in India	<i>Bacillus</i> sp. VITPS16	Cervical carcinoma	Squalene	C <sub>30</sub> H <sub>50</sub>	[116]
				3-Methyl-2-(2-oxopropyl) furan	C <sub>8</sub> H <sub>10</sub> O <sub>2</sub>	
				Methyl hexadecanoate	C <sub>17</sub> H <sub>34</sub> O <sub>2</sub>	
	Topsail saltern in Jeungdo, Jeollanam-do, Republic of Korea	<i>Nocardopsis</i> sp. HYJ28	Stomach and Leukemia carcinoma	Borrelidin C	C <sub>28</sub> H <sub>43</sub> NO <sub>7</sub>	[42]
				Borrelidin D	C <sub>28</sub> H <sub>43</sub> NO <sub>7</sub>	
				Iturin F <sub>1</sub>	C <sub>51</sub> H <sub>80</sub> N <sub>12</sub> O <sub>15</sub> Na	
	Saltern in Incheon in Korea	<i>Bacillus</i> sp. KCB45006	Cervical carcinoma Myeloid leukemia	Iturin F <sub>2</sub>	C <sub>51</sub> H <sub>80</sub> N <sub>12</sub> O <sub>15</sub> Na	[115]
				Iturin A <sub>8</sub>	C <sub>51</sub> H <sub>80</sub> N <sub>12</sub> O <sub>14</sub> Na	
				Iturin A <sub>9</sub>	C <sub>51</sub> H <sub>80</sub> N <sub>12</sub> O <sub>14</sub> Na	
	A saltern on Shinui Island in Korea	<i>Streptomyces</i> sp.	Colorectal cancer Gastric cancer	Salternamide A	C <sub>23</sub> H <sub>35</sub> ClNO <sub>5</sub>	[111]
	Salt marsh soil, Alicante, Spain	<i>Nocardopsis lucertensis</i> DSM 44048	Liver cancer Cervical cancer cells	Nocarbenezazole G	C <sub>15</sub> H <sub>13</sub> NO <sub>4</sub>	[114]
	Brine-seawater interface of the Red Sea	12 halophilic marine strains	Breast adenocarcinoma Cervical carcinoma Prostate carcinoma	Crude extract	NR	[108]
	Deep-sea brine pools of the Red Sea	24 halophilic marine strains	Breast adenocarcinoma Cervical carcinoma Prostate carcinoma	Crude extract	NR	[109]
	Weihai Solar Saltern in China	<i>Streptomyces</i> sp. WH26	Lung adenocarcinoma Liver hepatocellular adenocarcinoma Cervical carcinoma	8-O-Methylletrangulol Naphthomycin A	C <sub>20</sub> H <sub>14</sub> O <sub>4</sub> C <sub>10</sub> H <sub>16</sub> ClNO <sub>9</sub>	[110]
	Baicheng salt field, Xingjiang Province, China	<i>Actinopolyspora erythraea</i> YIM 90600	Colorectal cancer Tumor suppressor Programmed Cell Death Protein 4 (Pdcd4)	Actinopolysporins A Actinopolysporins B Actinopolysporins C	C <sub>15</sub> H <sub>28</sub> O <sub>4</sub> C <sub>16</sub> H <sub>30</sub> O <sub>4</sub> C <sub>16</sub> H <sub>30</sub> O <sub>2</sub>	[107]
	Weihai Solar Saltern in China	45 moderately halophilic strains	Liver hepatocellular adenocarcinoma	Crude extracts	NR	[106]

Table 4. Cont.

Anticancer Activity of:	Isolation Source	Halophilic Strain	Cancer Cell Lines	Molecule	Formula	Reference
Supernatant metabolite	Sambar Lake in India	<i>Piscibacillus</i> sp. CI2A1	Breast adenocarcinoma	Crude extract	NR	[118]
	Brine and sediment of the Manaure solar saltern in Colombia	<i>Vibrio</i> sp. AISM3-36-8	Lung adenocarcinoma	13- <i>cis</i> -docosanamide	C <sub>22</sub> H <sub>43</sub> NO	[51]
	Different hypersaline lakes in Iran	9 moderately halophilic strains	Umbilical vein endothelial cancer cell	Crude extract	NR	[113]
	Thamarakulam solar salt works in India	<i>Halomonas</i> sp. B54	Mammary epithelial carcinoma	1,2-Ethanediamine, <i>N,N,N',N'</i> -tetra 8-Methyl-6-nonenamide 9-Octadecanamide, (Z) 13-Docosanamide, (Z) Mannosamine 9-Octadecanamide, (Z) 2-Octanol,2-methyl-6-methylene Cyclohex-1,4,5-triol-3-one-1-carbo 2-Butanamine, 2-methyl- 1,2-Ethanediamine, <i>N,N,N',N'</i> -tetramethyl-	C <sub>6</sub> H <sub>16</sub> N <sub>2</sub> C <sub>10</sub> H <sub>19</sub> NO C <sub>18</sub> H <sub>35</sub> NO CH <sub>3</sub> (CH <sub>2</sub> ) <sub>7</sub> CH=CH(CH <sub>2</sub> ) <sub>11</sub> CONH <sub>2</sub> C <sub>6</sub> H <sub>13</sub> NO <sub>3</sub> ·HCl C <sub>18</sub> H <sub>35</sub> NO C <sub>12</sub> H <sub>22</sub> O <sub>2</sub> C <sub>5</sub> H <sub>8</sub> FN <sub>3</sub> C <sub>5</sub> H <sub>13</sub> N C <sub>6</sub> H <sub>16</sub> N <sub>2</sub>	[119]
Biosurfactant	Solar salt works in India	<i>Bacillus</i> sp. BS3	Mammary epithelial carcinoma			[53]
Exopolysaccharide	Çamalti saltern area in Turkey	<i>Halomonas stuyvensis</i> strain AAD6	Breast adenocarcinoma Lung adenocarcinoma Liver hepatocellular adenocarcinoma Gastric adenocarcinoma	Levan	C <sub>18</sub> H <sub>32</sub> O <sub>16</sub>	[121]
	Sabınar saline wetland in Spain	<i>Halomonas stenophila</i> strain B100	Lymphoblastic leukemia	Single acidic exopolysaccharide with glucose, mannose and galactose	NR	[120]
Carotenoid	Industrial lamery wastewater in Iran	<i>Kocuria</i> sp. MA-2	Prostate carcinoma	Neurosporene	C <sub>40</sub> H <sub>58</sub>	[122]
Enzyme	Hypersaline soil in Iran	<i>Halomonas elongata</i> IBRC-M 10216	Lymphoblastic leukemia Myeloid leukemia	L-asparaginase	C <sub>1377</sub> H <sub>2208</sub> N <sub>362</sub> O <sub>42517</sub>	[124]

Table 4. Cont.

Anticancer Activity of:	Isolation Source	Halophilic Strain	Cancer Cell Lines	Molecule	Formula	Reference
Archaea						
Supernatant metabolite	Aran Bidgol hypersaline lake in Iran	<i>Halobacterium salinarum</i> IBRC-M 10715	Prostate carcinoma	Crude extract	NR	[105]
Exopolysaccharide	Urmia Lake in Iran	<i>Halorubrum</i> sp. TBZ112	Gastric adenocarcinoma	Monosaccharide composition mainly composed of mannose, glucosamine, galacturonic acid, arabinose, and glucuronic acid	NR	[125]
Carotenoid	Marine solar saltern in eastern China	<i>Halogeometricum limi</i> strain RO1-6 <i>Haloplantus vossus</i> strain RO5-8	Liver hepatocellular adenocarcinoma	Bacterioruberin	C <sub>50</sub> H <sub>76</sub> O <sub>4</sub>	[127]
	Tunisian solar saltern	<i>Halobacterium halobium</i>	Liver hepatocellular adenocarcinoma	Bacterioruberin	C <sub>50</sub> H <sub>76</sub> O <sub>4</sub>	[126]
Fungi						
Metabolite	Weihai Solar Saltern in China	<i>Aspergillus</i> sp. F1	Lung adenocarcinoma Liver hepatocellular adenocarcinoma Cervical carcinoma Colorectal cancer	Cytochalasin E Ergosterol Rosellichalasin	C <sub>28</sub> H <sub>33</sub> NO <sub>7</sub> C <sub>28</sub> H <sub>44</sub> O C <sub>28</sub> H <sub>33</sub> NO <sub>5</sub>	[128]

Abbreviations: Not reported (NR).

#### 4.2. Archaea

Although most studies in this field have been focused on halophilic bacteria, some studies investigated the potentials of haloarchaea. In one of these studies, among nine haloarchaeal strains isolated from Aran-Bidgol Salt Lake, in Iran, supernatant metabolites from *Halobacterium salinarum* IBRC M10715 had the most potent cytotoxic effect on prostate cancer cell lines (DU145 and PC3, IC<sub>50</sub> = 0.5 mg/mL) without any effects on normal fibroblast cells (HFF-5). Moreover, the selective metabolite significantly increased both early and late apoptosis (about 11% and 9%, respectively) in the androgen-dependent PC3 cell line and reduced sphere formation ability of both cancer cell lines with down-regulation of SOX2 gene expression. Furthermore, prostate cancer cell tumors developed in nude mice significantly shrank post intratumor injection of the metabolite from *Halobacterium salinarum* IBRC M10715 [105]. *Halorubrum* sp. TBZ112 is a haloarchaeal species isolated from the Urmia Lake, Iran. It was reported that this strain could produce EPSs. The isolated EPSs possess a relatively low molecular weight in comparison with those EPSs isolated from other extreme environments (5 vs.  $\geq 100$  kDa, respectively) and the absence of sulfate functional groups in their structure was reported. The anticancer activity of the EPSs from *Halorubrum* sp. TBZ112 was examined and the results did not show any significant changes in the viability of gastric cancer cells (MKN-45) and normal human dermal fibroblast cells (HDF) at concentrations of 100, 250, 500, and 1000  $\mu\text{g/mL}$  after 24 and 48 h of treatment. As the existence of sulfate functional groups and the EPSs bioactivities are directly related, the low cytotoxicity potential of the EPSs from *Halorubrum* sp. TBZ112 was not unexpected [125].

Both in vivo and in vitro studies confirm chemoprevention effects of some carotenoids anticancer activity. Halophilic microorganisms showed great potential toward the production of various carotenoids such as  $\beta$ -carotene, bacterioruberin, and xanthophylls. In recent years, some investigations were carried out to determine the role of carotenoids or other bioactive molecules produced by halophiles on cancer treatment. The effects of *Halobacterium halobium* carotenoid extract on the viability of human hepatoma, HepG2, have been analyzed. This haloarchaeal strain was isolated from a Tunisian solar saltern and the results emphasized that increasing concentrations of the carotenoid extract of this halophilic archaeon decreased significantly the viability of the HepG2 cancer cell line [126]. Carotenoids from the haloarchaea *Halogeometricum limi* strain RO1-6 and *Haloplanus vascus* strain RO5-8 showed a potent antioxidant activity in comparison with  $\beta$ -carotene. In addition, these carotenoid extracts inhibited HepG2 cells in vitro, in a dose-dependent manner. Bacterioruberin was the predominant carotenoid extracted from these haloarchaea [127].

#### 4.3. Fungi

The biotechnological applications of halophilic fungi are remarkably less studied in comparison with halophilic bacteria. There is only one study focused on the cytotoxic effect of metabolites from a moderately halophilic fungal strain, *Aspergillus* sp. F1 [128]. Based on this publication, this strain produced three compounds with anticancer activity including cytochalasin E, ergosterol, and rosellichalasin, and higher salt concentrations increased the production of these compounds. All isolated compounds decreased the viability of A549, Hela, BEL-7402, and RKO human cancer cell lines and the inhibition effect of ergosterol on human colon cancer cell line, RKO, was the most potent cytotoxic report in this study.

Table 4 summarize all the mentioned reports in Section 4, which are related to the anticancer effect of halophilic bacteria, archaea, and fungi isolated from different saline and hypersaline environments in the world.

The following table (Table 5) gathers the most promising new compounds derived from halophilic microorganisms. The minimum inhibitory concentration (MIC) and the half maximal inhibitory concentration (IC<sub>50</sub>) are shown, based on their in vitro bioactivity. The results suggest that these compounds could be candidates for preclinical trials.



Table 5. Promising new compounds derived from halophilic microorganisms candidates for preclinical trials.

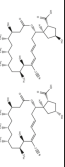
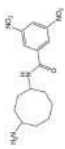
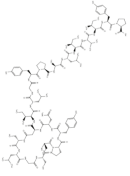

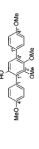
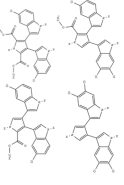
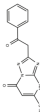
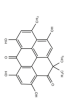
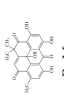
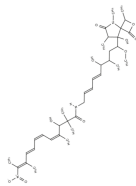
Compound	Structure	Antibiotic Activity		Anticancer Activity		Reference
		Microorganism	MIC (μM)	Cell Lines	IC <sub>50</sub> (μM)	
Borelidin C, D		<i>S. enterica</i>	16–63	Stomach Leukemia	5.5 5.7 6.7	[42]
		<i>S. aureus</i> , <i>S. epidermidis</i> , <i>B. subtilis</i> , <i>P. aeruginosa</i> , <i>P. aeruginosa</i>	16			
Angucyclinone: N-(4-aminocyclooctyl)-3,5-dinitrobenzamide		<i>S. mutans</i>	4	Breast, cervical, ovarian cyst, adenocarcinoma	10 nM	[50]
		<i>X. maltovarum</i> , <i>S. typhi</i> , <i>E. coli</i>	32			
		<i>B. cereus</i>	8			
		<i>C. albicans</i>	16			
		<i>B. anthracis</i>	2–4			
		<i>B. halodurans</i>	4			
		<i>B. cereus</i>	4–7			
		<i>Bacillus</i> sp.	7			
Streptomonomycin STM		<i>B. subtilis</i>	29	NR	NR	[48]
		<i>L. monocytogenes</i>	14			
		<i>E. faecalis</i>	29			
		<i>S. aureus</i>	57			
4-oxo-1,4-dihydroquinoline-3-carboxamide		<i>S. aureus</i>	64	NR	NR	[43]
6'-Hydroxy-4,2',3',4'-tetramethoxy-p-terphenyl		<i>B. subtilis</i>	64	NR	NR	[44]
		<i>C. albicans</i>	32			
Lynamycin A, B, C, and D		<i>S. aureus</i>	1.8–6.2			
		<i>S. epidermidis</i>	2.2–9.5			
		<i>S. pneumoniae</i>	18–57	NR	NR	[57]
		<i>E. faecalis</i>	3.3–19			
		<i>E. faecium</i>	4.4–19			
		<i>H. influenzae</i>	4.4–38			
		<i>E. coli</i>	13–16			

Table 5. Cont.

Compound	Structure	Antibiotic Activity		Anticancer Activity		Reference
		Microorganism	MIC (μM)	Cell Lines	IC <sub>50</sub> (μM)	
Essramycin		<i>E. coli</i>	8			
		<i>P. aeruginosa</i>	3.5			
		<i>B. subtilis</i> , <i>S. aureus</i>	1	NR	NR	[58]
		<i>M. luteus</i>	1.5			
Resistomycin 1-hydroxy-1-Norresistomycin		<i>E. coli</i>				
		<i>S. aureus</i> <i>S. viridochromogenes</i>	40	NR	NR	
Resistoflavin methyl ether		<i>B. subtilis</i>	3.1			[60]
		<i>E. coli</i> , <i>S. aureus</i> , <i>C. albicans</i>	10	NR	NR	
		MSSA	4			
		MRSA	5			
Lajollamycin		SPPS	2			
		PRSP	1.5			
		VSEF	14	Murine melanoma cell line B16-F10	9.6	[61]
		VREF	20			
		<i>E. coli</i>	12			

Note: Not reported (NR). Microorganisms: *Bacillus* (B.): *B. cereus*, *B. lalodurans*, *B. megaterium*, *B. subtilis*, *B. anthracis*, *Candida* (C.): *C. albicans*, *Enterococcus* (E.): *E. faecalis*, *E. faecium*, *Vancomycin resistant Enterococcus faecium* (VREF), *Vancomycin sensitive Enterococcus faecalis* (VSEF), *Vancomycin resistant enterococci* (VRE), *Escherichia* (E.): *E. coli*, *Haemophilus* (H.): *H. influenzae*, *Listeria* (L.): *L. monocytogenes*, *Micrococcus* (M.): *M. luteus*, *Pseudomonas* (P.): *P. aeruginosa*, *Salmonella* (S.): *S. typhi*, *S. enterica*, *Staphylococcus* (S.): *S. aureus*, *S. epidermidis*, *S. mutans*, *Methicillin Sensitive Staphylococcus aureus* (MSSA), *Methicillin-resistant Staphylococcus aureus* (MRSA), *Streptococcus* (S.): *S. pneumoniae*, *Penicillin resistant Streptococcus pneumoniae* (PRSP), *Penicillin sensitive Streptococcus pneumoniae* (SPPS), *Streptomyces* (S.): *S. viridochromogenes*, *Xanthomonas* (X.): *X. maltovorans*.

## 5. Future Perspectives

As the prevalence of antimicrobial resistance increases, researchers are developing new technologies and strategies to find alternatives that reduce the morbidity and mortality caused by the MDR bacteria. Categorizing the need for obtaining new molecules, the most requested by the public health are antimicrobial and anticancer compounds according to the data annually reported by the World Health Organization (WHO). The current and future of natural product discovery is the application of a combination of multi-omics approaches. Depending on the phase of the study, it is foreseen genomics, metagenomics, transcriptomics, proteomics, and metabolomics to reveal the biosynthetic capabilities of a single microorganism or microbial communities in hypersaline environments.

The discovery of novel lead compounds requires more than *in silico* predicted genes and large promising data. The current problem with massive approaches is precisely the lack of concrete results translated in novel lead compound derived of “meta-omics” studies. The heterologous expression of biosynthetic genes is the bottleneck since in several cases the recombinant product and its expression is totally different from what was expected. However, it is important to emphasize that the cultivation of hidden and uncultivable microbiota is improving with the assessment of metagenomic studies [129,130].

Genome mining has been implemented as a mandatory tool widely used to characterize the genetic basis of secondary metabolite biosynthesis based on the features of secondary metabolites organized as biosynthetic gene clusters (BGCs), especially the profile of gene encoding key signature enzymes [131–133]. The application of Next Generation Sequencing (NGS) allows the study of microbial diversity every day more accessible and affordable that allows the prediction of cryptic metabolic pathways and genes involved in the activity. The genome-guided discovery relies on sophisticated methods for identification of new gene families related clusters. The accurate prediction and analysis of relevant genes for secondary metabolite biosynthetic pathways in microbes is performed through the tool based on the Antibiotics and Secondary Metabolites Analysis Shell (antiSMASH) [134].

Due to the high rate of rediscovery of known compounds, the dereplication is an essential approach that allows the identification of duplicate molecules. Dereplication is relying on finding a matching of mass spectra with those present in the mass spectrometry data repository. The development of new computational tools like the algorithm searching spectral, DEREPLICATOR+ is helping to identifying in one order of magnitude peptidic natural products (PNPs) that include nonribosomal peptides (NRPs), and ribosomally synthesized and post-translationally modified peptides (RiPPs). The matching is extended to the identification of polyketides, terpenes, benzenoids, alkaloids, flavonoids, and other classes of natural products. One of the utilities of DEREPLICATOR+ is the enabling of cross-validation of genome-mining and peptidogenomics/glycogenomics results [135].

Several laboratories working in microbial bioprospecting keep their private collection once the antimicrobial, anticancer, antifungal, etc. activity is detected. In many cases, these positive isolates derived from primary screenings are not further studied by genome sequencing and dereplication. A common issue is the obtaining of the purified active compound under laboratory conditions with limited facilities and handling large data with a proper analysis. Moreover, it is important to consider the dereplication costs and time-consuming interpreting. The mentioned facts delay the biodiscovery attempts and constitute the reasonable causing of keeping a stored library of potential compounds. The projection of drug discovery product research is the simplification and accessibility to all these tools faster and with less effort. The power of genome mining in studying natural product biosynthesis by showing the widespread distribution of NRPS/PKS gene clusters and by the elicitation of previously unidentified pathways has been demonstrated. It is clear that coupling genome mining and dereplication will accelerate the biodiscovery at initial steps. The integration and linking of computational approaches are certainly the future of natural product research.

In this review, we have focused in all anticancer molecules reported from halophilic microorganisms. According to the cellular lines used, the focus of primary screenings is addressed to the leading cancer types that affect the global population. However, it is important that further screenings should include cellular lines with intrinsic chemoresistance, like sarcoma and glioblastoma,

characterized by aggressive overproliferation. The future of novel anticancer agents seems to be a combination of high-throughput screening assessed by predictive biomarkers.

**Author Contributions:** A.V. and P.C. designed the review article. P.C., M.A.A., and A.V. prepared and edited the manuscript. P.C. and M.A.A. prepared the tables. All authors revised and contributed to the preparation of the manuscript. All authors have read and agreed to the published version of the manuscript.

**Funding:** This study was supported by the Italian Foundation with the South (Fondazione CON IL SUD) project 2018-PDR-00533 (to P.C.), the Spanish Ministry of Economy and Competitiveness (MINECO) through project CGL2017-83385-P, which included European (FEDER) funds, and Junta de Andalucía (Spain) (to A.V.), and the Iranian National Science Foundation (INSF) (to M.A.A.).

**Conflicts of Interest:** The authors declare that there are no conflicts of interest.

## References

- Oren, A. Microbial life at high salt concentrations: Phylogenetic and metabolic diversity. *Saline Syst.* **2008**, *4*, 2. [[CrossRef](#)]
- Kushner, D.J. Life in high salt and solute concentrations: Halophilic bacteria. In *Microbial Life in Extreme Environments*; Kushner, D.J., Ed.; Academic Press: London, UK, 1978; p. 318.
- Kushner, D.; Kamekura, M. Physiology of halophilic eubacteria. In *Halophilic Bacteria*; Rodriguez-Valera, F., Ed.; CRC Press: Boca Raton, FL, USA, 1988; Volume 1, pp. 109–138.
- Rodriguez-Valera, F.; Ruiz-Berraquero, F.; Ramos-Cormenzana, A. Characteristics of the heterotrophic bacterial populations in hypersaline environments of different salt concentrations. *Microb. Ecol.* **1981**, *7*, 235–243. [[CrossRef](#)] [[PubMed](#)]
- Seckbach, J.; Oren, A.; Stan-Lotter, H. (Eds.) *Polyextremophiles: Life Under Multiple Forms of Stress*; Springer: Heidelberg, Germany, 2013.
- Bowers, K.J.; Mesbah, N.M.; Wiegel, J. Biodiversity of poly-extremophilic bacteria: Does combining the extremes of high salt, alkaline pH and elevated temperature approach a physico-chemical boundary for life? *Saline Syst.* **2009**, *5*, 9. [[CrossRef](#)] [[PubMed](#)]
- Mesbah, N.M.; Wiegel, J. Life under multiple extreme conditions: Diversity and physiology of the halophilic alkalithermophiles. *Appl. Environ. Microbiol.* **2012**, *78*, 4074–4082. [[CrossRef](#)] [[PubMed](#)]
- Ventosa, A.; Nieto, J.J.; Oren, A. Biology of moderately halophilic aerobic bacteria. *Microbiol. Mol. Biol. Rev.* **1998**, *62*, 504–544.
- Bremer, E.; Krämer, R. Responses of microorganisms to osmotic stress. *Annu. Rev. Microbiol.* **2019**, *73*, 313–334. [[CrossRef](#)]
- De la Haba, R.R.; Sánchez-Porro, C.; Marquez, M.C.; Ventosa, A. Taxonomy of halophiles. In *Extremophiles Handbook*; Horikoshi, K., Ed.; Springer Japan: Tokyo, Japan, 2011; pp. 255–308.
- Andrei, A.-Ş.; Banciu, H.L.; Oren, A. Living with salt: Metabolic and phylogenetic diversity of archaea inhabiting saline ecosystems. *FEMS Microbiol. Lett.* **2012**, *330*, 1–9. [[CrossRef](#)]
- Ventosa, A.; Oren, A.; Ma, Y. (Eds.) *Halophiles and Hypersaline Environments*; Springer: Berlin/Heidelberg, Germany, 2011.
- Akpolat, C.; Ventosa, A.; Birbir, M.; Sánchez-Porro, C.; Caglayan, P. Molecular identification of moderately halophilic bacteria and extremely halophilic archaea isolated from salted sheep skins containing red and yellow discolorations. *J. Am. Leather Chem. Assoc.* **2015**, *110*, 211–220.
- Ventosa, A. Unusual micro-organisms from unusual habitats: Hypersaline environments. In *Prokaryotic Diversity*; Logan, N.A., Lappin-Scott, H.M., Oyston, P.C.F., Eds.; Cambridge University Press: Cambridge, UK, 2006; pp. 223–254.
- Ventosa, A.; Fernández, A.B.; León, M.J.; Sánchez-Porro, C.; Rodriguez-Valera, F. The Santa Pola saltern as a model for studying the microbiota of hypersaline environments. *Extremophiles* **2014**, *18*, 811–824. [[CrossRef](#)]
- Ventosa, A.; de la Haba, R.R.; Sánchez-Porro, C.; Papke, R.T. Microbial diversity of hypersaline environments: A metagenomic approach. *Curr. Opin. Microbiol.* **2015**, *25*, 80–87. [[CrossRef](#)]
- Samylina, O.S.; Namsaraev, Z.B.; Grouzdev, D.S.; Slobodova, N.V.; Zelenev, V.V.; Borisenko, G.V.; Sorokin, D.Y. The patterns of nitrogen fixation in haloalkaliphilic phototrophic communities of Kulunda Steppe soda lakes (Altai, Russia). *FEMS Microbiol. Ecol.* **2019**, *95*, fiz174. [[CrossRef](#)] [[PubMed](#)]

18. Naghoni, A.; Emtiazi, G.; Amoozegar, M.A.; Cretoiu, M.S.; Stal, L.J.; Etemadifar, Z.; Shahzadeh Fazeli, S.A.; Bolhuis, H. Microbial diversity in the hypersaline Lake Meyghan, Iran. *Sci. Rep.* **2017**, *7*, 11522. [[CrossRef](#)] [[PubMed](#)]
19. Amoozegar, M.A.; Siroosi, M.; Atashgahi, S.; Smidt, H.; Ventosa, A. Systematics of haloarchaea and biotechnological potential of their hydrolytic enzymes. *Microbiology* **2017**, *163*, 623–645. [[CrossRef](#)] [[PubMed](#)]
20. Oren, A.; Rodriguez-Valera, F. The contribution of halophilic bacteria to the red coloration of saltern crystallizer ponds. *FEMS Microbiol. Ecol.* **2001**, *36*, 123–130. [[CrossRef](#)]
21. Charlesworth, J.C.; Burns, B.P. Untapped resources: Biotechnological potential of peptides and secondary metabolites in archaea. *Archaea* **2015**, *2015*, 1–7. [[CrossRef](#)]
22. Chen, Y.-H.; Lu, C.-W.; Shyu, Y.-T.; Lin, S.-S. Revealing the saline adaptation strategies of the halophilic bacterium *Halomonas beimenensis* through high-throughput omics and transposon mutagenesis approaches. *Sci. Rep.* **2017**, *7*, 13037. [[CrossRef](#)]
23. Das, S.; Dash, H.R. (Eds.) *Microbial Diversity in the Genomic Era*; Academic Press: Cambridge, MA, USA; Elsevier: Amsterdam, The Netherlands, 2018.
24. Vavourakis, C.D.; Mehrshad, M.; Balkema, C.; van Hall, R.; Andrei, A.-Ş.; Ghai, R.; Sorokin, D.Y.; Muyzer, G. Metagenomes and metatranscriptomes shed new light on the microbial-mediated sulfur cycle in a Siberian soda lake. *BMC Biol.* **2019**, *17*, 69. [[CrossRef](#)]
25. DasSarma, P.; Coker, J.A.; Huse, V.; DasSarma, S. Halophiles, industrial applications. In *Encyclopedia of Industrial Biotechnology*; American Cancer Society: Atlanta, GA, USA, 2010; pp. 1–43.
26. Yin, J.; Chen, J.-C.; Wu, Q.; Chen, G.-Q. Halophiles, coming stars for industrial biotechnology. *Biotechnol. Adv.* **2015**, *33*, 1433–1442. [[CrossRef](#)]
27. Shirazian, P.; Asad, S.; Amoozegar, M.A. The potential of halophilic and halotolerant bacteria for the production of antineoplastic enzymes: L-asparaginase and L-glutaminase. *EXCLI J.* **2016**, *15*, 268–279.
28. Kiadehi, M.S.H.; Amoozegar, M.A.; Asad, S.; Siroosi, M. Exploring the potential of halophilic archaea for the decolorization of azo dyes. *Water Sci. Technol.* **2018**, *77*, 1602–1611. [[CrossRef](#)]
29. Giani, M.; Garbayo, I.; Vilchez, C.; Martínez-Espinosa, R.M. Haloarchaeal carotenoids: Healthy novel compounds from extreme environments. *Mar. Drugs* **2019**, *17*, 524. [[CrossRef](#)] [[PubMed](#)]
30. Amoozegar, M.A.; Safarpour, A.; Noghabi, K.A.; Bakhtiary, T.; Ventosa, A. Halophiles and their vast potential in biofuel production. *Front. Microbiol.* **2019**, *10*, 1895. [[CrossRef](#)] [[PubMed](#)]
31. Jin, M.; Gai, Y.; Guo, X.; Hou, Y.; Zeng, R. Properties and applications of extremozymes from deep-sea extremophilic microorganisms: A mini review. *Mar. Drugs* **2019**, *17*, 656. [[CrossRef](#)] [[PubMed](#)]
32. Tseng, W.-P.; Chen, Y.-C.; Chen, S.-Y.; Chen, S.-Y.; Chang, S.-C. Risk for subsequent infection and mortality after hospitalization among patients with multidrug-resistant Gram-negative bacteria colonization or infection. *Antimicrob. Resist. Infect. Control* **2018**, *7*, 93. [[CrossRef](#)] [[PubMed](#)]
33. Peters, L.; Olson, L.; Khu, D.T.K.; Linnros, S.; Le, N.K.; Hanberger, H.; Hoang, N.T.B.; Tran, D.M.; Larsson, M. Multiple antibiotic resistance as a risk factor for mortality and prolonged hospital stay: A cohort study among neonatal intensive care patients with hospital-acquired infections caused by gram-negative bacteria in Vietnam. *PLoS ONE* **2019**, *14*, e0215666. [[CrossRef](#)]
34. Cassini, A.; Högberg, L.D.; Plachouras, D.; Quattrocchi, A.; Hoxha, A.; Simonsen, G.S.; Colomb-Cotinat, M.; Kretzschmar, M.E.; Devleeschauwer, B.; Cecchini, M.; et al. Attributable deaths and disability-adjusted life-years caused by infections with antibiotic-resistant bacteria in the EU and the European Economic Area in 2015: A population-level modelling analysis. *Lancet Infect. Dis.* **2019**, *19*, 56–66. [[CrossRef](#)]
35. Rodriguez-Valera, F.; Juez, G.; Kushner, D.J. Halocins: Salt-dependent bacteriocins produced by extremely halophilic rods. *Can. J. Microbiol.* **1982**, *28*, 151–154. [[CrossRef](#)]
36. Gohel, S.D.; Sharma, A.K.; Dangar, K.G.; Thakrar, F.J.; Singh, S.P. Antimicrobial and biocatalytic potential of haloalkaliphilic actinobacteria. In *Halophiles*; Maheshwari, D.K., Saraf, M., Eds.; Springer: Heidelberg, Germany, 2015; Volume 6, pp. 29–55.
37. Ventosa, A.; Mellado, E.; Sanchez-Porro, C.; Marquez, M.C. Halophilic and halotolerant microorganisms from soils. In *Microbiology of Extreme Soils*; Dion, P., Nautiyal, C.S., Eds.; Springer: Berlin/Heidelberg, Germany, 2008; pp. 87–115.
38. Hamed, J.; Mohammadipanah, F.; Ventosa, A. Systematic and biotechnological aspects of halophilic and halotolerant actinomycetes. *Extremophiles* **2013**, *17*, 1–13. [[CrossRef](#)]

39. Manteca, Á.; Yagüe, P. Streptomyces as a source of antimicrobials: Novel approaches to activate cryptic secondary metabolite pathways. In *Antimicrobial, Antibiotic Resistant, Antibiofilm Strategies and Activity Methods*; Intechopen: London, UK, 2019; pp. 1–21.
40. Adlin Jenifer, J.S.C.; Michaelbabu, M.; Eswaramoorthy Thirumalaikumar, C.L.; Jeraldin Nisha, S.R.; Uma, G.; Citarasu, T. Antimicrobial potential of haloalkaliphilic *Nocardiopsis* sp. AJ1 isolated from solar salterns in India. *J. Basic Microbiol.* **2019**, *59*, 288–301. [[CrossRef](#)]
41. Hadj Rabia-Boukhalfa, Y.; Eveno, Y.; Karama, S.; Selama, O.; Lauga, B.; Duran, R.; Hacène, H.; Eparvier, V. Isolation, purification and chemical characterization of a new angucyclinone compound produced by a new halotolerant *Nocardiopsis* sp. HR-4 strain. *World J. Microbiol. Biotechnol.* **2017**, *33*, 126. [[CrossRef](#)]
42. Kim, J.; Shin, D.; Kim, S.-H.; Park, W.; Shin, Y.; Kim, W.K.; Lee, S.K.; Oh, K.-B.; Shin, J.; Oh, D.-C. Borrelidins C–E: New Antibacterial macrolides from a saltern-derived halophilic *Nocardiopsis* sp. *Mar. Drugs* **2017**, *15*, 166. [[CrossRef](#)] [[PubMed](#)]
43. Tian, S.; Yang, Y.; Liu, K.; Xiong, Z.; Xu, L.; Zhao, L. Antimicrobial metabolites from a novel halophilic actinomycete *Nocardiopsis terrae* YIM 90022. *Nat. Prod. Res.* **2014**, *28*, 344–346. [[CrossRef](#)] [[PubMed](#)]
44. Tian, S.-Z.; Pu, X.; Luo, G.; Zhao, L.-X.; Xu, L.-H.; Li, W.-J.; Luo, Y. Isolation and characterization of new *p*-terphenyls with antifungal, antibacterial, and antioxidant activities from halophilic actinomycete *Nocardiopsis gilva* YIM 90087. *J. Agric. Food Chem.* **2013**, *61*, 3006–3012. [[CrossRef](#)] [[PubMed](#)]
45. Gorajana, A.; Vinjamuri, S.; Poluri, E.; Zeeck, A. 1-Hydroxy-1-norresistomycin, a new cytotoxic compound from a marine actinomycete, *Streptomyces chibaensis*. *J. Antibiot.* **2005**, *8*, 526–529. [[CrossRef](#)] [[PubMed](#)]
46. Maskey, R.P.; Helmke, E.; Laatsch, H. Himalomycin A and B: Isolation and structure elucidation of new fridamycin type antibiotics from a marine *Streptomyces* isolate. *J. Antibiot.* **2003**, *56*, 942–949. [[CrossRef](#)] [[PubMed](#)]
47. Parthasarathi, S.; Sathya, S.; Bupesh, G.; Samy, R.D.; Mohan, M.R.; Kumar, G.S.; Manikandan, M.; Kim, C.J.; Balakrishnan, K. Isolation and characterization of antimicrobial compound from marine *Streptomyces hygroscopicus* BDUS 49. *World J. Fish Mar. Sci.* **2012**, *4*, 268–277.
48. Meteleev, M.; Tietz, J.I.; Melby, J.O.; Blair, P.M.; Zhu, L.; Livnat, I.; Severinov, K.; Mitchell, D.A. Structure, bioactivity, and resistance mechanism of Streptomonicin, an unusual lasso peptide from an understudied halophilic actinomycete. *Chem. Biol.* **2015**, *22*, 241–250. [[CrossRef](#)]
49. Frikha Dammak, D.; Zarai, Z.; Najah, S.; Abdennabi, R.; Belbahri, L.; Rateb, M.E.; Mejdoub, H.; Maalej, S. Antagonistic properties of some halophilic thermoactinomycetes isolated from superficial sediment of a solar saltern and production of cyclic antimicrobial peptides by the novel isolate *Paludifilum halophilum*. *BioMed Res. Int.* **2017**, *2017*, 1–13. [[CrossRef](#)]
50. Mangamuri, U.K.; Vijayalakshmi, M.; Poda, S.; Manavathi, B.; Chitturi, B.; Yenamandra, V. Isolation and biological evaluation of N-(4-aminocyclooctyl)-3,5-dinitrobenzamide, a new semisynthetic derivative from the mangrove-associated actinomycete *Pseudonocardia endophytica* VUK-10. *3 Biotech* **2016**, *6*, 158. [[CrossRef](#)]
51. Conde-Martínez, N.; Acosta-González, A.; Díaz, L.E.; Tello, E. Use of a mixed culture strategy to isolate halophilic bacteria with antibacterial and cytotoxic activity from the Manaure solar saltern in Colombia. *BMC Microbiol.* **2017**, *17*, 230. [[CrossRef](#)]
52. Bell, R.; Carmeli, S.; Sar, N. Vibriindole A, a Metabolite of the marine bacterium, *Vibrio parahaemolyticus*, isolated from the toxic mucus of the boxfish *Ostracion cubicus*. *J. Nat. Prod.* **1994**, *57*, 1587–1590. [[CrossRef](#)] [[PubMed](#)]
53. Donio, M.; Ronica, S.; Viji, V.T.; Velmurugan, S.; Jenifer, J.A.; Michaelbabu, M.; Citarasu, T. Isolation and characterization of halophilic *Bacillus* sp. BS3 able to produce pharmacologically important biosurfactants. *Asian Pac. J. Trop. Med.* **2013**, *6*, 876–883. [[CrossRef](#)]
54. Velmurugan, S.; Raman, K.; Thanga Viji, V.; Donio, M.B.S.; Adlin Jenifer, J.; Babu, M.M.; Citarasu, T. Screening and characterization of antimicrobial secondary metabolites from *Halomonas salifodinae* MPM-TC and its in vivo antiviral influence on Indian white shrimp *Fenneropenaeus indicus* against WSSV challenge. *J. King Saud Univ. Sci.* **2013**, *25*, 181–190. [[CrossRef](#)]
55. Wang, H.; Fewer, D.P.; Holm, L.; Rouhiainen, L.; Sivonen, K. Atlas of nonribosomal peptide and polyketide biosynthetic pathways reveals common occurrence of nonmodular enzymes. *Proc. Natl. Acad. Sci. USA* **2014**, *111*, 9259–9264. [[CrossRef](#)]

56. Bose, U.; Hewavitharana, A.; Ng, Y.; Shaw, P.; Fuerst, J.; Hodson, M. LC-MS-based metabolomics study of marine bacterial secondary metabolite and antibiotic production in *Salinispora arenicola*. *Mar. Drugs* **2015**, *13*, 249–266. [\[CrossRef\]](#)
57. McArthur, K.A.; Mitchell, S.S.; Tsueng, G.; Rheingold, A.; White, D.J.; Grodberg, J.; Lam, K.S.; Potts, B.C.M. Dynamicins A–E, chlorinated bisindole pyrrole antibiotics from a novel marine actinomycete. *J. Nat. Prod.* **2008**, *71*, 1732–1737. [\[CrossRef\]](#)
58. El-Gendy, M.M.A.; Shaaban, M.; Shaaban, K.A.; El-Bondkly, A.M.; Laatsch, H. Essramycin: A first triazolopyrimidine antibiotic isolated from nature. *J. Antibiot.* **2008**, *61*, 149–157. [\[CrossRef\]](#)
59. Hughes, C.C.; Prieto-Davo, A.; Jensen, P.R.; Fenical, W. The Marinopyrroles, antibiotics of an unprecedented structure class from a marine *Streptomyces* sp. *Org. Lett.* **2008**, *10*, 629–631. [\[CrossRef\]](#)
60. Kock, I.; Maskey, R.P.; Biabani, M.A.F.; Helmke, E.; Laatsch, H. 1-Hydroxy-1-norresistomycin and resistoflavin methyl ether: New antibiotics from marine-derived streptomycetes. *J. Antibiot.* **2005**, *58*, 530–534. [\[CrossRef\]](#) [\[PubMed\]](#)
61. Manam, R.R.; Teisan, S.; White, D.J.; Nicholson, B.; Grodberg, J.; Neuteboom, S.T.C.; Lam, K.S.; Mosca, D.A.; Lloyd, G.K.; Potts, B.C.M. Lajollamycin, a nitro-tetraene spiro- $\beta$ -lactone- $\gamma$ -lactam antibiotic from the marine actinomycete *Streptomyces nodosus*. *J. Nat. Prod.* **2005**, *68*, 240–243. [\[CrossRef\]](#) [\[PubMed\]](#)
62. Maskey, R.P.; Li, F.C.; Qin, S.; Fiebig, H.H.; Laatsch, H. Chandrananimycins A–C: Production of novel anticancer antibiotics from a marine *Actinomadura* sp. isolate M048 by variation of medium composition and growth conditions. *J. Antibiot.* **2003**, *56*, 622–629. [\[CrossRef\]](#)
63. Fariq, A.; Yasmin, A.; Jamil, M. Production, characterization and antimicrobial activities of bio-pigments by *Aquasilabacillus elongatus* MB592, *Salinicoccus sesuvii* MB597, and *Halomonas aquamarina* MB598 isolated from Khewra Salt Range, Pakistan. *Extremophiles* **2019**, *23*, 435–449. [\[CrossRef\]](#)
64. Trenozhnikova, L.; Azizan, A. Discovery of actinomycetes from extreme environments with potential to produce novel antibiotics. *Cent. Asian J. Glob. Health* **2018**, *7*, 337. [\[CrossRef\]](#)
65. Kumar, R.R.; Jadeja, V.J. Characterization and partial purification of an antibacterial agent from halophilic actinomycete *Kocuria* sp. strain rsk4. *BiolImpacts* **2018**, *8*, 253–261. [\[CrossRef\]](#)
66. Ballav, S.; Kerkar, S.; Thomas, S.; Augustine, N. Halophilic and halotolerant actinomycetes from a marine saltern of Goa, India producing anti-bacterial metabolites. *J. Biosci. Bioeng.* **2015**, *119*, 323–330. [\[CrossRef\]](#)
67. Ray, L.; Suar, M.; Pattnaik, A.K.; Raina, V. *Streptomyces chilikensis* sp. nov., a halophilic streptomycete isolated from brackish water sediment. *Int. J. Syst. Evol. Microbiol.* **2013**, *63*, 2757–2764. [\[CrossRef\]](#)
68. Rao, K.V.R. Isolation and characterization of antagonistic actinobacteria from mangrove soil. *J. Biochem. Tech.* **2012**, *3*, 361–365.
69. Mangamuri, U.K.; Vijayalakshmi Muvva, V.; Poda, S.; Kamma, S. Isolation, identification and molecular characterization of rare actinomycetes from mangrove ecosystem of Nizampatnam. *Malays. J. Microbiol.* **2012**, *8*, 83–91. [\[CrossRef\]](#)
70. Kamat, T.; Kerkar, S. Bacteria from salt pans: A potential resource of antibacterial metabolites. *RRST-Biotech.* **2011**, *3*, 46–52.
71. Gayathri, A.; Madhanraj, P.; Panneerselvam, A. Diversity, antibacterial activity and molecular characterization of actinomycetes isolated from salt pan region of Kodiakarai, Nagapattinam DT. *Asian J. Pharm. Technol.* **2011**, *1*, 79–81.
72. Meklat, A.; Sabaou, N.; Zitouni, A.; Mathieu, F.; Lebrihi, A. Isolation, taxonomy, and antagonistic properties of halophilic actinomycetes in Saharan soils of Algeria. *Appl. Environ. Microbiol.* **2011**, *77*, 6710–6714. [\[CrossRef\]](#) [\[PubMed\]](#)
73. Jose, A.; Santhi, S.; Solomon, R.D.J. In vitro antimicrobial potential and growth characteristics of *Nocardioopsis* sp. JAJ16 isolated from crystallizer pond. *Int. J. Curr. Res.* **2010**, *3*, 024–026.
74. Saurav, K. Diversity and optimization of process parameters for the growth of *Streptomyces* VITSVK9 spp. isolated from Bay of Bengal, India. *J. Nat. Environ. Sci.* **2010**, *1*, 56–65.
75. Suthindhir, K.; Kannabiran, K. Cytotoxic and antimicrobial potential of actinomycete species *Saccharopolyspora salina* VITSDK4 isolated from the Bay of Bengal coast of India. *Am. J. Infect. Dis.* **2009**, *5*, 90–98. [\[CrossRef\]](#)
76. Suthindhiran, K.; Kannabiran, K. Hemolytic activity of *Streptomyces* VITSDK1 spp. isolated from marine sediments in Southern India. *J. Mycol. Médicale* **2009**, *19*, 77–86. [\[CrossRef\]](#)
77. Cao, L.; Yun, W.; Tang, S.; Zhang, P.; Mao, P.; Jing, X.; Wang, C.; Lou, K. Biodiversity and enzyme screening of actinomycetes from Hami lake. *Wei Sheng Wu Xue Bao* **2009**, *49*, 287–293.



78. Ramesh, S.; Mathivanan, N. Screening of marine actinomycetes isolated from the Bay of Bengal, India for antimicrobial activity and industrial enzymes. *World J. Microbiol. Biotechnol.* **2009**, *25*, 2103–2111. [\[CrossRef\]](#)
79. Hakvåg, S.; Fjærvik, E.; Josefsen, K.; Ian, E.; Ellingsen, T.; Zotchev, S. Characterization of *Streptomyces* spp. isolated from the sea surface microlayer in the Trondheim Fjord, Norway. *Mar. Drugs* **2008**, *6*, 620–635. [\[CrossRef\]](#)
80. Dhanasekaran, D.; Rajakumar, G.; Sivamani, P.; Selvamani, S.; Panneerselvam, A.; Thajuddin, N. Screening of salt pans actinomycetes for antibacterial agents. *Internet J. Microbiol.* **2004**, *1*, 1–4.
81. Magarvey, N.A.; Keller, J.M.; Bernan, V.; Dworkin, M.; Sherman, D.H. Isolation and characterization of novel marine-derived actinomycete taxa rich in bioactive metabolites. *Appl. Environ. Microbiol.* **2004**, *70*, 7520–7529. [\[CrossRef\]](#)
82. Kokare, C.R.; Mahadik, K.R.; Kadam, S.S.; Chopade, B.A. Isolation, characterization and antimicrobial activity of marine halophilic *Actinopolyspora* species AH1 from the west coast of India. *Curr. Sci.* **2004**, *86*, 5.
83. Meseguer, I.; Rodríguez-Valera, F.; Ventosa, A. Antagonistic interactions among halobacteria due to halocin production. *FEMS Microbiol. Lett.* **1986**, *36*, 177–182. [\[CrossRef\]](#)
84. Torreblanca, M.; Meseguer, I.; Ventosa, A. Production of halocins is a practically universal feature of archaeal halophilic rods. *Letts. Appl. Microbiol.* **1994**, *19*, 201–205. [\[CrossRef\]](#)
85. Shand, R.F.; Leyva, K.J. Peptide and protein antibiotics from the domain Archaea: Halocins and sulfolobocins. In *Bacteriocins: Ecology and Evolution*; Riley, M.A., Chavan, M.A., Eds.; Springer: Berlin/Heidelberg, Germany, 2007; pp. 93–109.
86. Atanasova, N.S.; Pietilä, M.K.; Oksanen, H.M. Diverse antimicrobial interactions of halophilic archaea and bacteria extend over geographical distances and cross the domain barrier. *MicrobiologyOpen* **2013**, *2*, 811–825. [\[CrossRef\]](#)
87. Corral, P.; Esposito, F.P.; Tedesco, P.; Falco, A.; Tortorella, E.; Tartaglione, L.; Festa, C.; D’Auria, M.V.; Gnani, G.; Varese, G.C.; et al. Identification of a Sorbicillinoid-producing *Aspergillus* strain with antimicrobial activity against *Staphylococcus aureus*: A new polyextremophilic marine fungus from Barents Sea. *Mar. Biotechnol.* **2018**, *20*, 502–511. [\[CrossRef\]](#)
88. Besse, A. Antimicrobial peptides and proteins in the face of extremes: Lessons from archaeocins. *Biochimie* **2015**, *118*, 344–355. [\[CrossRef\]](#)
89. Quadri, I.; Hassani, I.I.; l’Haridon, S.; Chalopin, M.; Hacène, H.; Jebbar, M. Characterization and antimicrobial potential of extremely halophilic archaea isolated from hypersaline environments of the Algerian Sahara. *Microbiol. Res.* **2016**, *186–187*, 119–131. [\[CrossRef\]](#)
90. Pi, B.; Yu, D.; Dai, F.; Song, X.; Zhu, C.; Li, H.; Yu, Y. A Genomics based discovery of secondary metabolite biosynthetic gene clusters in *Aspergillus ustus*. *PLoS ONE* **2015**, *10*, e0116089. [\[CrossRef\]](#)
91. Kjærboelling, I.; Vesth, T.C.; Frisvad, J.C.; Nybo, J.L.; Theobald, S.; Kuo, A.; Bowyer, P.; Matsuda, Y.; Mondo, S.; Lyhne, E.K.; et al. Linking secondary metabolites to gene clusters through genome sequencing of six diverse *Aspergillus* species. *Proc. Natl. Acad. Sci. USA* **2018**, *115*, E753–E761. [\[CrossRef\]](#)
92. Wolfender, J.-L.; Litaudon, M.; Touboul, D.; Queiroz, E.F. Innovative omics-based approaches for prioritisation and targeted isolation of natural products—New strategies for drug discovery. *Nat. Prod. Rep.* **2019**, *36*, 855–868. [\[CrossRef\]](#)
93. Metcalf, J.A.; Funkhouser-Jones, L.J.; Brileya, K.; Reysenbach, A.-L.; Bordenstein, S.R. Antibacterial gene transfer across the tree of life. *eLife* **2014**, *25*, 3. [\[CrossRef\]](#) [\[PubMed\]](#)
94. Plemenitaš, A.; Lenassi, M.; Konte, T.; Kežžar, A.; Zajc, J.; Gostinčar, C.; Gunde-Cimerman, N. Adaptation to high salt concentrations in halotolerant/halophilic fungi: A molecular perspective. *Front. Microbiol.* **2014**, *5*, 199. [\[CrossRef\]](#) [\[PubMed\]](#)
95. Gunde-Cimerman, N.; Plemenitaš, A.; Oren, A. Strategies of adaptation of microorganisms of the three domains of life to high salt concentrations. *FEMS Microbiol. Rev.* **2018**, *42*, 353–375. [\[CrossRef\]](#) [\[PubMed\]](#)
96. Plemenitaš, A.; Vaupotič, T.; Lenassi, M.; Kogej, T.; Gunde-Cimerman, N. Adaptation of extremely halotolerant black yeast *Hortaea werneckii* to increased osmolarity: A molecular perspective at a glance. *Stud. Mycol.* **2008**, *61*, 67–75. [\[CrossRef\]](#)
97. Moubasher, A.-A.H.; Abdel-Sater, M.A.; Soliman, Z.S.M. Yeasts and filamentous fungi associated with some dairy products in Egypt. *J. Mycol. Médicale* **2018**, *28*, 76–86. [\[CrossRef\]](#)



98. Chamekh, R.; Deniel, F.; Donot, C.; Jany, J.-L.; Nodet, P.; Belabid, L. Isolation, identification and enzymatic activity of halotolerant and halophilic fungi from the Great Sebkh of Oran in Northwestern of Algeria. *Mycobiology* **2019**, *47*, 230–241. [\[CrossRef\]](#)
99. Chung, D.; Kim, H.; Choi, H.S. Fungi in salterns. *J. Microbiol.* **2019**, *57*, 717–724. [\[CrossRef\]](#)
100. Zheng, J.; Wang, Y.; Wang, J.; Liu, P.; Li, J.; Zhu, W. Antimicrobial ergosteroids and pyrrole derivatives from halotolerant *Aspergillus flocculosus* PT05-1 cultured in a hypersaline medium. *Extremophiles* **2013**, *17*, 963–971. [\[CrossRef\]](#)
101. Wang, Y.; Zheng, J.; Liu, P.; Wang, W.; Zhu, W. Three new compounds from *Aspergillus terreus* PT06-2 grown in a high salt medium. *Mar. Drugs* **2011**, *9*, 1368–1378. [\[CrossRef\]](#)
102. Ali, I.; Siwarungson, N.; Punnapayak, H.; Lotrakul, P.; Prasongsuk, S.; Bankeeree, W.; Rakshit, S.K. Screening of potential biotechnological applications from obligate halophilic fungi, isolated from a man-made solar saltern located in Phetchaburi province, Thailand. *Pak. J. Bot.* **2014**, *46*, 983–988.
103. Lebogang, L.; Taylor, J.E.; Mubyana-John, T. A preliminary study of the fungi associated with salt pans in Botswana and their anti-microbial properties. *Bioremediation Biodivers. Bioavail.* **2009**, *3*, 61–71.
104. Safarpour, A.; Amoozgar, M.A.; Ventosa, A. Hypersaline environments of Iran: Prokaryotic biodiversity and their potentials in microbial biotechnology. In *Extremophiles in Eurasian Ecosystems: Ecology, Diversity, and Applications*; Egamberdieva, D., Birkeland, N.-K., Panosyan, H., Li, W.-J., Eds.; Springer: Singapore, 2018; Volume 8, pp. 265–298.
105. Safarpour, A.; Ebrahimi, M.; Shahzadeh Fazeli, S.A.; Amoozgar, M.A. Supernatant metabolites from halophilic archaea to reduce tumorigenesis in prostate cancer in-vitro and in-vivo. *Iran. J. Pharm. Res.* **2019**, *18*, 241–253. [\[PubMed\]](#)
106. Chen, L.; Wang, G.; Bu, T.; Zhang, Y.; Wang, Y.; Liu, M.; Lin, X. Phylogenetic analysis and screening of antimicrobial and cytotoxic activities of moderately halophilic bacteria isolated from the Weihai Solar Saltern (China). *World J. Microbiol. Biotechnol.* **2010**, *26*, 879–888. [\[CrossRef\]](#)
107. Zhao, L.-X.; Huang, S.-X.; Tang, S.-K.; Jiang, C.-L.; Duan, Y.; Beutler, J.A.; Henrich, C.J.; McMahon, J.B.; Schmid, T.; Bles, J.S.; et al. Actinopolysporins A–C and tubercidin as a Pcd4 stabilizer from the halophilic actinomycete *Actinopolyspora erythraea* YIM 90600. *J. Nat. Prod.* **2011**, *74*, 1990–1995. [\[CrossRef\]](#) [\[PubMed\]](#)
108. Sagar, S.; Esau, L.; Hikmawan, T.; Antunes, A.; Holtermann, K.; Stingl, U.; Bajic, V.B.; Kaur, M. Cytotoxic and apoptotic evaluations of marine bacteria isolated from brine-seawater interface of the Red Sea. *BMC Complement. Altern. Med.* **2013**, *13*, 29. [\[CrossRef\]](#) [\[PubMed\]](#)
109. Sagar, S.; Esau, L.; Holtermann, K.; Hikmawan, T.; Zhang, G.; Stingl, U.; Bajic, V.B.; Kaur, M. Induction of apoptosis in cancer cell lines by the Red Sea brine pool bacterial extracts. *BMC Complement. Altern. Med.* **2013**, *13*, 344. [\[CrossRef\]](#)
110. Liu, H.; Xiao, L.; Wei, J.; Schmitz, J.C.; Liu, M.; Wang, C.; Cheng, L.; Wu, N.; Chen, L.; Zhang, Y.; et al. Identification of *Streptomyces* sp. nov. WH26 producing cytotoxic compounds isolated from marine solar saltern in China. *World J. Microbiol. Biotechnol.* **2013**, *29*, 1271–1278. [\[CrossRef\]](#)
111. Kim, S.-H.; Shin, Y.; Lee, S.-H.; Oh, K.-B.; Lee, S.K.; Shin, J.; Oh, D.-C. Salternamides A–D from a halophilic *Streptomyces* sp. actinobacterium. *J. Nat. Prod.* **2015**, *78*, 836–843. [\[CrossRef\]](#)
112. Bach, D.-H.; Kim, S.-H.; Hong, J.-Y.; Park, H.J.; Oh, D.-C.; Lee, S.K. Salternamide A suppresses hypoxia-induced accumulation of HIF-1 $\alpha$  and induces apoptosis in human colorectal cancer cells. *Mar. Drugs* **2015**, *13*, 6962–6976. [\[CrossRef\]](#)
113. Sarvari, S.; Seyedjafari, E.; Amoozgar, M.A.; Bakhshandeh, B. The effect of moderately halophilic bacteria supernatant on proliferation and apoptosis of cancer cells and mesenchymal stem cells. *Cell. Mol. Biol. Noisy Gd. Fr.* **2015**, *61*, 30–34.
114. Sun, M.; Zhang, X.; Hao, H.; Li, W.; Lu, C. Nocarbenzoxazoles A–G, benzoxazoles produced by halophilic *Nocardiopsis lucentensis* DSM 44048. *J. Nat. Prod.* **2015**, *78*, 2123–2127. [\[CrossRef\]](#) [\[PubMed\]](#)
115. Son, S.; Ko, S.-K.; Jang, M.; Kim, J.; Kim, G.; Lee, J.; Jeon, E.; Futamura, Y.; Ryoo, I.-J.; Lee, J.-S.; et al. New cyclic lipopeptides of the iturin class produced by saltern-derived *Bacillus* sp. KCB14S006. *Mar. Drugs* **2016**, *14*, 72. [\[CrossRef\]](#) [\[PubMed\]](#)
116. Prathiba, S.; Jayaraman, G. Evaluation of the anti-oxidant property and cytotoxic potential of the metabolites extracted from the bacterial isolates from mangrove forest and saltern regions of South India. *Prep. Biochem. Biotechnol.* **2018**, *48*, 750–758. [\[CrossRef\]](#) [\[PubMed\]](#)

117. Lawrance, A.; Balakrishnan, M.; Gunasekaran, R.; Srinivasan, R.; Valsalan, V.N.; Gopal, D.; Ramalingam, K. Unexplored deep sea habitats in active volcanic Barren Island, Andaman and Nicobar Islands are sources of novel halophilic eubacteria. *Infect. Genet. Evol.* **2018**, *65*, 1–5. [\[CrossRef\]](#)
118. Neelam, D.K.; Agrawal, A.; Tomer, A.K.; Bandyopadhyaya, S.; Sharma, A.; Jagannadham, M.V.; Mandal, C.C.; Dadheech, P.K. A *Piscibacillus* sp. isolated from a soda lake exhibits anticancer activity against breast cancer MDA-MB-231 cells. *Microorganisms* **2019**, *7*, 34. [\[CrossRef\]](#)
119. Donio, M.B.S.; Ronica, F.A.; Viji, V.T.; Velmurugan, S.; Jenifer, J.S.C.A.; Michaelbabu, M.; Dhar, P.; Citarasu, T. *Halomonas* sp. BS4, a biosurfactant producing halophilic bacterium isolated from solar salt works in India and their biomedical importance. *SpringerPlus* **2013**, *2*, 149. [\[CrossRef\]](#)
120. Ruiz-Ruiz, C.; Srivastava, G.K.; Carranza, D.; Mata, J.A.; Llamas, I.; Santamaría, M.; Quesada, E.; Molina, I.J. An exopolysaccharide produced by the novel halophilic bacterium *Halomonas stenophila* strain B100 selectively induces apoptosis in human T leukaemia cells. *Appl. Microbiol. Biotechnol.* **2011**, *89*, 345–355. [\[CrossRef\]](#)
121. Sarilmiser, H.K.; Ozlem, A.; Gonca, O.; Arga, K.Y.; Toksoy Oner, E. Effective stimulating factors for microbial levan production by *Halomonas smyrnensis* AAD6T. *J. Biosci. Bioeng.* **2015**, *119*, 455–463. [\[CrossRef\]](#)
122. Rezaeeyan, Z.; Safarpour, A.; Amoozegar, M.A.; Babavalian, H.; Tebyanian, H.; Shakeri, F. High carotenoid production by a halotolerant bacterium, *Kocuria* sp. strain QWT-12 and anticancer activity of its carotenoid. *EXCLI J.* **2017**, *16*, 840–851.
123. Zolfaghar, M.; Amoozegar, M.A.; Khajeh, K.; Babavalian, H.; Tebyanian, H. Isolation and screening of extracellular anticancer enzymes from halophilic and halotolerant bacteria from different saline environments in Iran. *Mol. Biol. Rep.* **2019**, *46*, 3275–3286. [\[CrossRef\]](#)
124. Ghasemi, A.; Asad, S.; Kabiri, M.; Dabirmanesh, B. Cloning and characterization of *Halomonas elongata* L-asparaginase, a promising chemotherapeutic agent. *Appl. Microbiol. Biotechnol.* **2017**, *101*, 7227–7238. [\[CrossRef\]](#) [\[PubMed\]](#)
125. Hamidi, M.; Mirzaei, R.; Delattre, C.; Khanaki, K.; Pierre, G.; Gardarin, C.; Petit, E.; Karimitabar, F.; Faezi, S. Characterization of a new exopolysaccharide produced by *Halorubrum* sp. TBZ112 and evaluation of its anti-proliferative effect on gastric cancer cells. *3 Biotech* **2019**, *9*, 1. [\[CrossRef\]](#) [\[PubMed\]](#)
126. Abbes, M.; Baati, H.; Guermazi, S.; Messina, C.; Santulli, A.; Gharsallah, N.; Ammar, E. Biological properties of carotenoids extracted from *Halobacterium halobium* isolated from a Tunisian solar saltern. *BMC Complement. Altern. Med.* **2013**, *13*, 255. [\[CrossRef\]](#) [\[PubMed\]](#)
127. Hou, J.; Cui, H.-L. *In vitro* antioxidant, antihemolytic, and anticancer activity of the carotenoids from halophilic archaea. *Curr. Microbiol.* **2018**, *75*, 266–271. [\[CrossRef\]](#)
128. Xiao, L.; Liu, H.; Wu, N.; Liu, M.; Wei, J.; Zhang, Y.; Lin, X. Characterization of the high cytochalasin E and rosellichalasin producing *Aspergillus* sp. nov. F1 isolated from marine solar saltern in China. *World J. Microbiol. Biotechnol.* **2013**, *29*, 11–17. [\[CrossRef\]](#)
129. León, M.J.; Fernández, A.B.; Ghai, R.; Sánchez-Porro, C.; Rodríguez-Valera, F.; Ventosa, A. From metagenomics to pure culture: Isolation and characterization of the moderately halophilic bacterium *Spiribacter salinus* gen. nov., sp. nov. *Appl. Environ. Microbiol.* **2014**, *80*, 3850–3857. [\[CrossRef\]](#)
130. Hamm, J.N.; Erdmann, S.; Eloë-Fadrosh, E.A.; Angeloni, A.; Zhong, L.; Brownlee, C.; Williams, T.J.; Barton, K.; Carswell, S.; Smith, M.A.; et al. Unexpected host dependency of Antarctic nanohaloarchaeota. *Proc. Natl. Acad. Sci. USA* **2019**, *116*, 14661–14670. [\[CrossRef\]](#)
131. Blin, K.; Kim, H.U.; Medema, M.H.; Weber, T. Recent development of antiSMASH and other computational approaches to mine secondary metabolite biosynthetic gene clusters. *Brief. Bioinform.* **2019**, *20*, 1103–1113. [\[CrossRef\]](#)
132. Wang, S.; Zheng, Z.; Zou, H.; Li, N.; Wu, M. Characterization of the secondary metabolite biosynthetic gene clusters in archaea. *Comput. Biol. Chem.* **2019**, *78*, 165–169. [\[CrossRef\]](#)
133. Zheng, Y.; Saitou, A.; Wang, C.-M.; Toyoda, A.; Minakuchi, Y.; Sekiguchi, Y.; Ueda, K.; Takano, H.; Sakai, Y.; Abe, K.; et al. Genome features and secondary metabolites biosynthetic potential of the class *Ktedonobacteria*. *Front. Microbiol.* **2019**, *10*, 893. [\[CrossRef\]](#)

- 134. Weber, T.; Blin, K.; Duddela, S.; Krug, D.; Kim, H.U.; Bruccoleri, R.; Lee, S.Y.; Fischbach, M.A.; Müller, R.; Wohlleben, W.; et al. antiSMASH 3.0—A comprehensive resource for the genome mining of biosynthetic gene clusters. *Nucleic Acids Res.* **2015**, *43*, W237–W243. [[CrossRef](#)] [[PubMed](#)]
- 135. Mohimani, H.; Gurevich, A.; Shlemov, A.; Mikheenko, A.; Korobeynikov, A.; Cao, L.; Shcherbin, E.; Nothias, L.-F.; Dorrestein, P.C.; Pevzner, P.A. Dereplication of microbial metabolites through database search of mass spectra. *Nat. Commun.* **2018**, *9*, 4035. [[CrossRef](#)] [[PubMed](#)]



© 2019 by the authors. Licensee MDPI, Basel, Switzerland. This article is an open access article distributed under the terms and conditions of the Creative Commons Attribution (CC BY) license (<http://creativecommons.org/licenses/by/4.0/>).



## Article

# Characterization of Carotenoid Biosynthesis in Newly Isolated *Deinococcus* sp. AJ005 and Investigation of the Effects of Environmental Conditions on Cell Growth and Carotenoid Biosynthesis

Jun Young Choi, Kunjoong Lee and Pyung Cheon Lee \*

Department of Molecular Science and Technology and Department of Applied Chemistry and Biological Engineering, Ajou University, Woncheon-dong, Yeongtong-gu, Suwon 16499, Korea; custom@ajou.ac.kr (J.Y.C.); digh0724@ajou.ac.kr (K.L.)

\* Correspondence: pclee@ajou.ac.kr; Tel.: +82-31-219-2461

Received: 29 November 2019; Accepted: 11 December 2019; Published: 14 December 2019

**Abstract:** Our purpose was to characterize the structures of deinoxanthin from *Deinococcus* sp. AJ005. The latter is a novel reddish strain and was found to synthesize two main acyclic carotenoids: deinoxanthin and its derivative. The derivative (2-keto-deinoxanthin) contains a 2-keto functional group instead of a 2-hydroxyl group on a  $\beta$ -ionone ring. A deinoxanthin biosynthesis pathway of *Deinococcus* sp. AJ005 involving eight putative enzymes was proposed according to genome annotation analysis and chemical identification of deinoxanthin. Optimal culture pH and temperature for *Deinococcus* sp. AJ005 growth were pH 7.4 and 20 °C. Sucrose as a carbon source significantly enhanced the cell growth in comparison with glucose, glycerol, maltose, lactose, and galactose. When batch fermentation was performed in a bioreactor containing 40g/L sucrose, total carotenoid production was 650% higher than that in a medium without sucrose supplementation. The culture conditions found in this study should provide the basis for the development of fermentation strategies for the production of deinoxanthin and of its derivative by means of *Deinococcus* sp. AJ005.

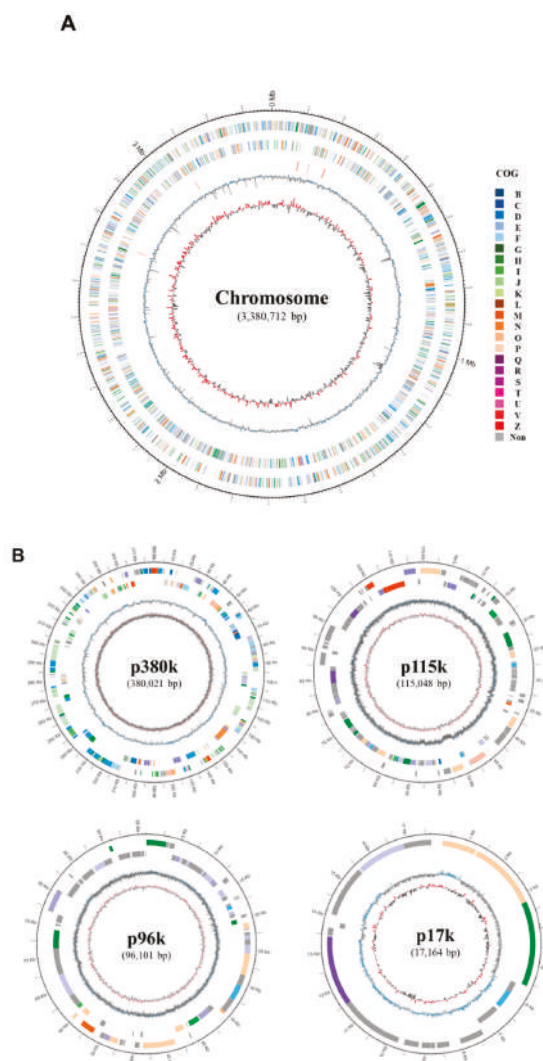
**Keywords:** *Deinococcus*; deinoxanthin; carotenoid

## 1. Introduction

*Deinococcus* strains are Gram-positive bacteria having a variety of metabolic pathways. Their habitats range from common environments, such as air, soils, and seas [1–3], to extremes such as high altitudes: stratosphere and alpine conditions [4–6]. Novel *Deinococcus* strains have been continuously isolated from Antarctic and marine fishes in extreme environments [7,8]. Notably, *Deinococcus* strains are known for their survival under strong  $\gamma$ -rays or UV radiation and desiccation conditions [9]. Several studies have shown that, to withstand these extreme environments, *Deinococcus* strains have unique metabolic capabilities including redundant DNA repair systems and biosynthesis of antioxidants such as the carotenoid deinoxanthin [10,11].

The latter is a major monocyclic carotenoid present in many *Deinococcus* strains, and its chemical structure was first characterized using deinoxanthin from *D. radiodurans* featuring high resistance to radiation [12,13]. Deinoxanthin has been reported to be more effective in scavenging very reactive singlet oxygen species (which fatally damage cellular metabolic pathways) than  $\beta$ -carotene, lutein, and lycopene [14,15]. Furthermore, deinoxanthin has anticancer activity [16] and can serve as a biomarker of a living organism in space research [17]. Given that carotenoids, including deinoxanthin, are being used as antioxidants, cosmetic ingredients, and food or feed additives [18,19], carotenoid-producing *Deinococcus* strains have aroused interest as microbial producers of bioactive carotenoids.

Recently, a novel reddish *Deinococcus* strain, AJ005, was isolated from seawater near King George Island, and the AJ005 genome was completely sequenced and made publicly available [20]. *Deinococcus* sp. AJ005 synthesizes red carotenoids, and its complete genome consists of a single circular chromosome (3.3 Mbp) and four circular plasmids (p380k, p115k, p96k, and p17k; Figure 1).



**Figure 1.** Circular representation of the chromosome and four plasmids of *Deinococcus* sp. AJ005. (A) From the outer to inner circle: predicted protein-coding sequences (colored according to Clusters of Orthologous Groups (COGs) categories) on the plus strand, predicted protein-coding sequences (colored by COGs categories) on the minus strand, RNA genes (transfer RNAs (tRNAs): blue, ribosomal RNAs (rRNAs): red), GC content (blue/black), and a GC skew (red/black). (B). From the outer to inner circle: predicted protein-coding sequences (colored by COGs categories) on the plus strand, predicted protein-coding sequences (colored by COGs categories) on the minus strand, GC content (blue/black), and a GC skew (red/black).

In this study, our purpose was to characterize the structures of deinoxanthin from *Deinococcus* sp. AJ005. We proposed that a deinoxanthin biosynthetic pathway exists in *Deinococcus* sp. AJ005 on the basis of genome annotation analysis and chemical identification of isolated carotenoids. In addition, we investigated the effects of culture conditions on the deinoxanthin biosynthesis in this strain.

## 2. Results and Discussion

### 2.1. Characterization of Carotenoids of *Deinococcus* Sp. AJ005

To identify carotenoids of *Deinococcus* sp. AJ005, total carotenoids were extracted and analyzed by C18 reverse-phase high-performance liquid chromatography (HPLC). The HPLC analysis of the carotenoid profile yielded two main polar peaks (Figure 2A). After purification by silica chromatography, the two polar carotenoids were analyzed by liquid chromatography with mass spectrometry (MS) in positive APCI (atmospheric-pressure chemical ionization) mode. According to our analysis of mass spectra and UV/Vis spectra, a carotenoid corresponding to peak 1 had a molecular ion  $(M+H)^+$  with  $m/z$  581.4 and  $\lambda_{\max} = 453$  (shoulder), 475, and 492 (shoulder) nm (Figure 2B), whereas the carotenoid corresponding to peak 2 had a molecular ion  $(M+H)^+$  of  $m/z$  583.4 and  $\lambda_{\max} = 453$  (shoulder), 475, and 492 (shoulder) nm (Figure 2C). The mass fragmentation pattern of peak 2 was similar to the reported pattern of deinoxanthin [21,22]: 565.3  $((M+H)^+ - 18$ ; loss of  $H_2O$ ), 547.4  $((M+H)^+ - 18 - 18$ ; loss of 2 molecules of  $H_2O$ ), and 523.3  $((M+H)^+ - 60$ ; loss of the acyclic end containing a hydroxyl group). On the basis of the molecular ion, UV/Vis spectra, and the mass fragmentation pattern, the carotenoid corresponding to peak 2 is proposed to be deinoxanthin. The carotenoid corresponding to peak 1 had the same UV/Vis spectrum as that of deinoxanthin and a mass fragmentation pattern similar to that of deinoxanthin with a difference of  $-2$   $m/z$ : 561.3  $((M+H)^+ - 18)$  in peak 1 versus 565.3  $((M+H)^+ - 18)$  in peak 2 and 521.3  $((M+H)^+ - 60)$  in peak 1 versus 523.3  $((M+H)^+ - 60)$  in peak 2. Therefore, the carotenoid corresponding to peak 1 is proposed to be a deinoxanthin derivative (2-keto-deinoxanthin) containing a 2-keto functional group instead of a 2-hydroxyl functional group in the ring structure. The 2-keto group in 2-keto-deinoxanthin did not significantly influence the shape of the UV/Vis spectrum, resulting in the same UV/Vis spectrum of deinoxanthin.

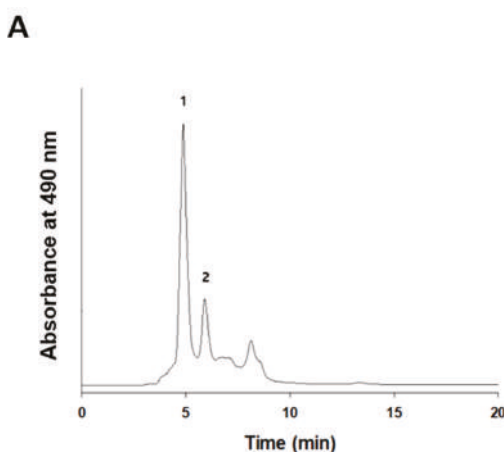
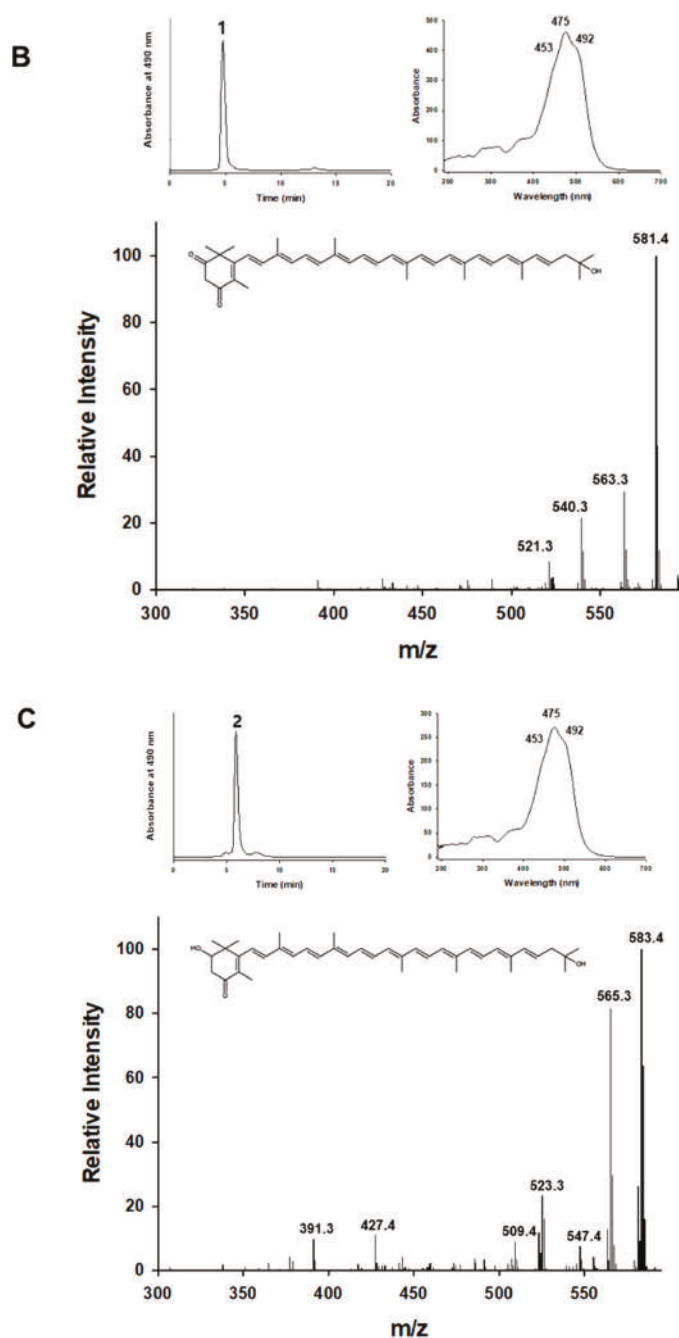


Figure 2. Cont.

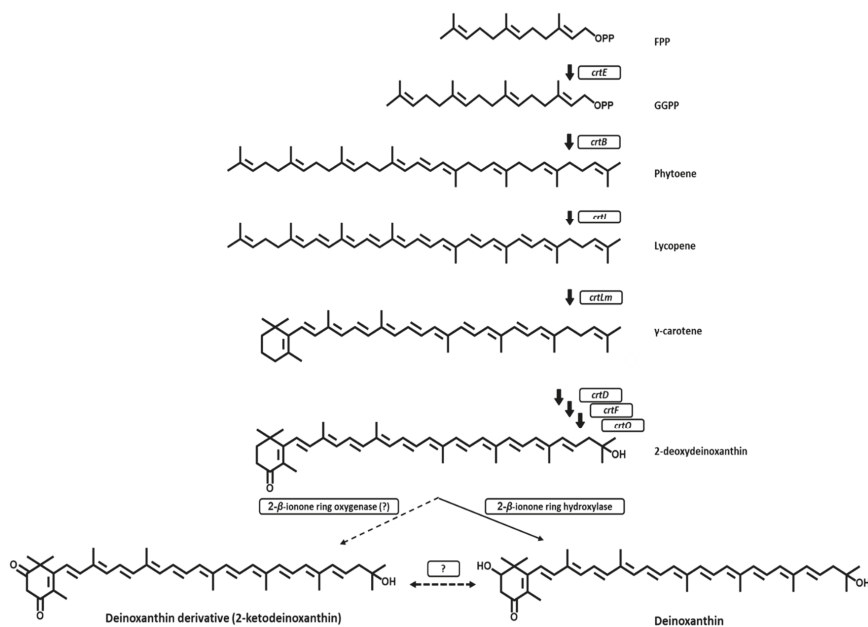


**Figure 2.** The carotenoid profile of *Deinococcus* sp. AJ005 and MS analysis of the carotenoids. (A) The high-performance liquid chromatography (HPLC) profile of a crude carotenoid extract; (B) HPLC/mass spectrometry (MS) chromatograms and the UV/Vis spectrum of the isolated deinoxanthin derivative; (C) HPLC/MS chromatograms and a UV/Vis spectrum of isolated deinoxanthin.



## 2.2. The Proposed Carotenoid Biosynthetic Pathway and Genes Encoding Putative Carotenogenic Enzymes in *Deinococcus* Sp. AJ005

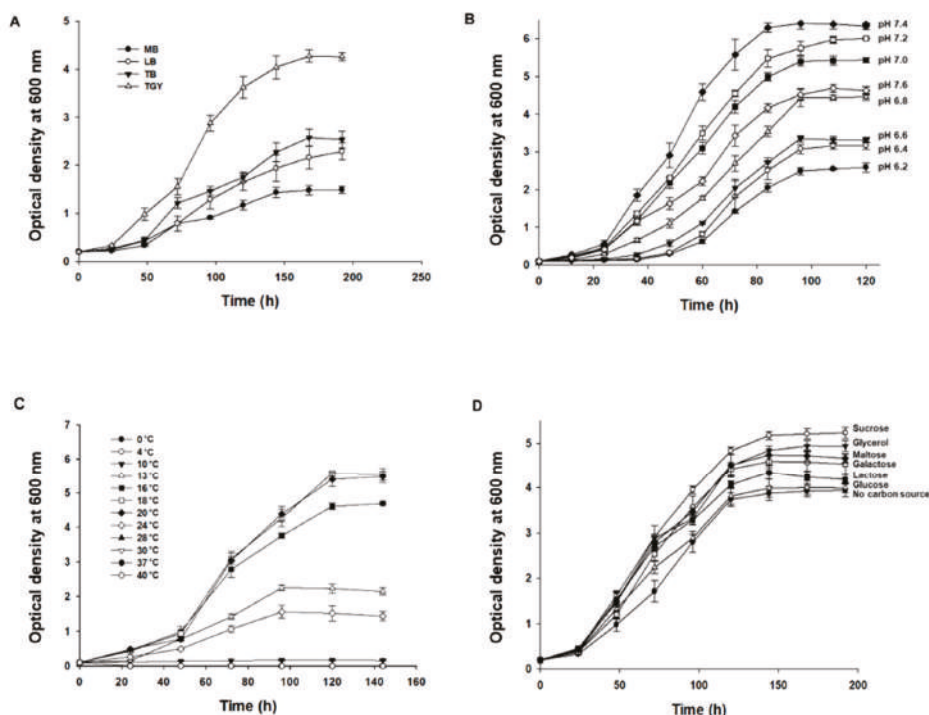
Genome annotation analysis predicted seven genes encoding the putative deinoxanthin pathway enzymes on the chromosome of *Deinococcus* sp. AJ005: GGPP synthase (*crtE*), phytoene synthase (*crtB*), phytoene desaturase (*crtI*), lycopene cyclase (*crtLm*),  $\beta$ -carotene 4-ketolase (*crtO*), C-1',2' hydratase (*cruF*), and C-3',4' desaturase (*crtD*). Unfortunately, a gene encoding 2- $\beta$ -ionone ring hydroxylase for the deinoxanthin biosynthesis and a gene encoding 2- $\beta$ -ionone ring oxygenase for the biosynthesis of the deinoxanthin derivative (2-keto-deinoxanthin) were not found. Nonetheless, there was a gene encoding a putative cytochrome P450 (which might be a 2- $\beta$ -ionone ring hydroxylase) on the chromosome of *Deinococcus* sp. AJ005. A recent study [22] showed that the cytochrome P450 CYP287A1 of *D. radiodurans* R1 is a novel 2- $\beta$ -ionone ring hydroxylase in the deinoxanthin pathway. The BLASTp analysis revealed that there is a 70% amino acid identity between the putative cytochrome P450 of *Deinococcus* sp. AJ005 and the cytochrome P450 CYP287A1 of *D. radiodurans* R1. In addition to the above eight genes, one gene coding for a putative lycopene elongase (*crtEb*), two genes encoding a putative phytoene dehydrogenase, two genes encoding a putative cytochrome P450 hydroxylase, and one gene encoding a possible cytochrome P450 were predicted on the chromosome of *Deinococcus* sp. AJ005. According to the chemical identification of deinoxanthin and of the deinoxanthin derivative from the crude carotenoid extract of *Deinococcus* sp. AJ005 and according to the putative carotenogenic enzymes, a carotenoid pathway of *Deinococcus* sp. AJ005 was proposed (Figure 3). Functional analysis of the putative enzymes (in particular three cytochrome P450s) needs to be performed to elucidate the proposed carotenoid pathway.



**Figure 3.** Proposed biosynthetic pathways for deinoxanthin and for its derivative in *Deinococcus* sp. AJ005<sup>T</sup>. The following enzymes are involved in these biosynthetic pathways: *CrtE*, GGPP synthase; *CrtB*, phytoene synthase; *CrtI*, phytoene desaturase; *CrtLm*, lycopene cyclase; *CrtO*,  $\beta$ -carotene 4-ketolase; *CruF*, C-1',2' hydratase; *CrtD*, C-3',4' desaturase; 2- $\beta$ -ionone ring hydroxylase; and 2- $\beta$ -ionone ring oxygenase (unidentified). The ? mark represents the possibility of oxido-reduction catalyzed by an unknown enzyme.

### 2.3. Effects of Culture Media, Culture pH, and Temperature on Cell Growth

To investigate the effects of culture media, culture pH, temperature, and a carbon source on the growth of *Deinococcus* sp. AJ005 cells, 100 mL flask cultures were carried out. Among several media (Luria–Bertani (LB), Terrific Broth (TB), Marine Broth 2216 (MB), and Tryptone–Glucose–Yeast extract (TGY) broth) containing 1 g/L glucose and with pH adjusted to 7.5, the growth of *Deinococcus* sp. AJ005 cells reached the highest OD<sub>600</sub> of  $4.3 \pm 0.1$  in the TGY medium at 20 °C, followed by the TB, LB, and MB media (Figure 4A). Next, the effects of culture pH and temperature on the growth of *Deinococcus* sp. AJ005 cells were studied in the TGY medium containing 1 g/L glucose. An initial culture pH of 7.4 at 20 °C was found to be optimal for cell growth (OD<sub>600</sub> of  $6.4 \pm 0.1$ ), and pH values above 7.6 or below 6.8 significantly reduced the cell growth (Figure 4B). At culture temperatures of 18 °C and 20 °C, the cell growth reached the highest OD<sub>600</sub> of  $5.5 \pm 0.3$  in the TGY medium containing 1 g/L glucose and with pH adjusted to 7.4. No growth was observed below 4 °C or above 28 °C (Figure 4C). Carbon sources significantly affected the growth of *Deinococcus* sp. AJ005 cells. When *Deinococcus* sp. AJ005 was grown in the TGY medium containing 10 g/L one of six carbon sources (i.e., glucose, glycerol, maltose, lactose, galactose, or sucrose); the greatest cell growth (OD<sub>600</sub> of  $5.3 \pm 0.2$ ) was observed in the TGY medium containing sucrose, followed by glycerol, maltose, galactose, lactose, and glucose (Figure 4D).

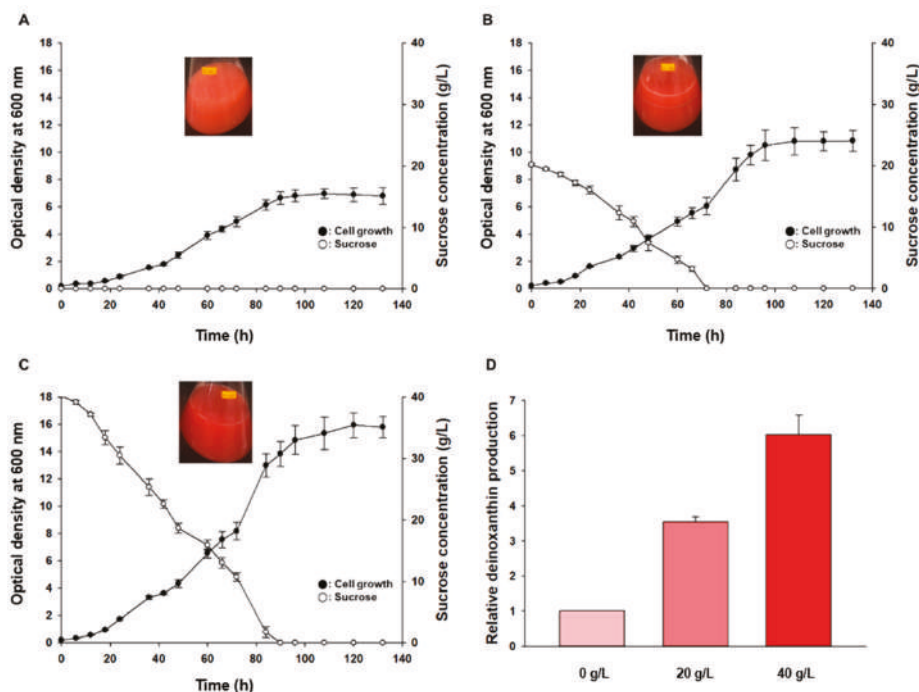


**Figure 4.** Cell growth of *Deinococcus* sp. AJ005<sup>T</sup> in flask cultures under different culture conditions. (A) Four culture media (pH 7.5 and 20 °C); (B) eight culture pH values (20 °C); (C) 12 culture temperatures (pH 7.4); and (D) six carbon sources (10 g/L, 20 °C, and pH 7.4).

### 2.4. Batch Fermentation Involving *Deinococcus* sp. AJ005 for Carotenoid Production

To achieve high production of deinoxanthin and of the deinoxanthin derivative, bioreactor fermentation with *Deinococcus* sp. AJ005 was performed at 20 °C and pH 7.4 in the TGY medium containing 0, 20, or 40 g/L sucrose. In the TGY medium containing 0 g/L sucrose, the cell growth

reached an  $OD_{600}$  of  $7.3 \pm 0.3$ , and the maximum specific growth rate was  $0.085 \text{ h}^{-1}$  (Figure 5A). In the TGY medium containing 20 g/L sucrose, the cell growth reached an  $OD_{600}$  of  $11.2 \pm 0.7$ , and the maximum specific growth rate was  $0.12 \text{ h}^{-1}$  (Figure 5B). We noticed that 20 g/L sucrose was completely consumed in 72 h. In the TGY medium containing 40 g/L sucrose, the cell growth reached an  $OD_{600}$  of  $16.1 \pm 0.6$ , and the maximum specific growth rate was  $0.18 \text{ h}^{-1}$  (Figure 5C), whereas 40 g/L sucrose was completely consumed in 90 h. Total carotenoid production was proportional to the cell growth (Figure 5D). Total carotenoid production in the TGY medium containing 40 g/L sucrose was 650% higher than that in the TGY medium containing 0 g/L sucrose and 80% higher than that in the TGY medium containing 20 g/L sucrose.



**Figure 5.** Bioreactor batch fermentation of the TGY (medium (containing different concentrations of sucrose) by *Deinococcus* sp. AJ005. (A) 0 g/L sucrose (B); 20 g/L sucrose; (C) 40 g/L sucrose; (D) relative carotenoid production in the medium containing 0, 20, or 40 g/L sucrose.

### 3. Materials and Methods

#### 3.1. Flask Fermentation Involving *Deinococcus* Sp. AJ005

*Deinococcus* sp. AJ005, isolated from seawater near King George Island, was grown in 100 mL of a culture medium in a 500 mL baffled flask with rotary shaking at 250 rpm at various pH levels and temperatures as described below. Luria-bertani, TB, MB, and TGY media containing 1 g/L glucose were used for growing *Deinococcus* sp. AJ005 at  $20^\circ\text{C}$  and pH 7.5. To investigate the influence of culture pH on the cell growth, *Deinococcus* sp. AJ005 was grown in 100 mL of the TGY medium containing 1 g/L glucose and with pH adjusted to 6.2–7.6 in increments of 0.2 by means of the phosphate buffer system. To investigate the impact of culture temperature on the cell growth, *Deinococcus* sp. AJ005 was grown at 0, 2, 4, 10, 13, 16, 18, 20, 24, 28, 30, 37, or  $40^\circ\text{C}$  in 100 mL of the TGY medium containing 1 g/L glucose and with pH adjusted to 7.4. Glucose, glycerol, maltose, lactose, galactose, and sucrose (Sigma–Aldrich) served as a carbon source (10 g/L) in the TGY medium with pH adjusted to 7.4.

### 3.2. Bioreactor Fermentation by *Deinococcus* Sp. AJ005

Bioreactor batch fermentation was carried out with 1.5 L of the TGY medium containing sucrose (0, 20, or 40 g/L) as a carbon source in 5 L jar BioFlo 320 (Eppendorf, Hamburg, Germany). Pre-cultures (100 mL) were grown in the TGY medium at 20 °C for 1 day and inoculated into a bioreactor. The temperature was maintained at 20 °C, and pH was automatically maintained at 7.4 by adding 2.0 N HCl or 2.0 N NaOH. The dissolved oxygen level was maintained at 30% by supplying air and by adjusting agitation between 200 and 500 rpm.

### 3.3. Extraction and Analysis of Carotenoids

*Deinococcus* sp. AJ005 was grown in 1 L of the TGY medium. Carotenoids were repeatedly extracted from cell pellets of *Deinococcus* sp. AJ005 by means of 10 mL of methanol. The colored supernatants were concentrated to 10 mL in an EZ-2 Plus centrifugal evaporator (Genevac Inc., Ipswich, United Kingdom), and an equal volume of ethyl acetate and of a 5N NaCl solution was added. The upper colored phase was collected, washed with distilled water, passed through an anhydrous magnesium sulfate column, and completely dried with nitrogen gas. Carotenoids were purified from the crude carotenoid extract by silica chromatography (10 × 50 cm) based on silica gel 60 (Merck, Darmstadt, Germany). Elution was performed with hexane:acetone (6.5:3.5 v/v). Each purified carotenoid was completely dried and dissolved in methanol. Next, 10 µL of a carotenoid was injected into an Agilent 1200 HPLC system equipped with a ZORBAX SB-C18 column (4.6 × 250 mm, 5-micron, Agilent Technologies, Santa Clara, California, USA) and with a photodiode array detector (Agilent Technologies, USA). Each carotenoid was subjected to diode array detection at 480 nm wavelength. The HPLC conditions were as follows: 23 °C column temperature, a 0.8 mL/min flow rate, and an isocratic mobile phase of acetonitrile, methanol, and isopropyl alcohol (40:50:10 v/v/v). The mass fragmentation spectra of carotenoids were monitored in the positive ion mode of an Agilent LC/MS 6150 Quadrupole system equipped with an atmospheric-pressure chemical ionization interface (Agilent Technologies). The MS conditions were as follows: 3 kV capillary voltage, 4.0 µA corona current, 12 L/min drying gas flow, 35 psi<sub>g</sub> nebulizer pressure, and 350 °C drying gas temperature and vaporizer temperature.

### 3.4. Monitoring Cell Growth and Quantification of Carbohydrates and Carotenoids

Cell growth was monitored by measuring the absorbance at 600 nm (OD<sub>600</sub>) with a SPECTRAMax Plus384 spectrophotometer (Molecular Devices, San Jose, California, USA). The concentrations of glucose, glycerol, maltose, lactose, galactose, and sucrose were determined using an Agilent 1100 HPLC system equipped with a refractive index detector (Agilent, Santa Clara, California, USA) and an Aminex HPX-87H column (Bio-Rad, Hercules, California, USA) at a flow rate of 0.7 mL/min and column temperature of 50 °C, with 4 mM H<sub>2</sub>SO<sub>4</sub> as the mobile phase. The total-carotenoid amount was measured via the absorbance of the methanol extract at a wavelength of 475 nm on the SPECTRAMax Plus384 spectrophotometer.

## 4. Conclusions

*Deinococcus* sp. AJ005 synthesizes two main types of acyclic carotenoids: deinoxanthin and a deinoxanthin derivative (2-keto-deinoxanthin). Genome sequence analysis of deinoxanthin-producing *Deinococcus* sp. AJ005 uncovered eight genes encoding putative deinoxanthin biosynthesis enzymes. The culture conditions found in this study should provide the basis for the development of fermentation strategies for the production of deinoxanthin and of its derivative by means of *Deinococcus* sp. AJ005.

**Author Contributions:** J.Y.C., K.L., and P.C.L. planned and designed the experiments. J.Y.C. and K.L. performed the experiments and analyzed data. P.C.L. drafted the manuscript. P.C.L. coordinated the study and finalized the manuscript. All authors read and approved the final manuscript.

**Funding:** This research was funded by the National Research Foundation of Korea, grant number 2012M1A2A2026562, and by the Priority Research Centers Program through the National Research Foundation of Korea, grant number 2019R1A6A1A11051471.

**Conflicts of Interest:** The authors declare no conflict of interest. The funders had no role in the design of the study; in the collection, analyses, or interpretation of data; in the writing of the manuscript, or in the decision to publish the results.

## References

1. Yoo, S.H.; Weon, H.Y.; Kim, S.J.; Kim, Y.S.; Kim, B.Y.; Kwon, S.W. *Deinococcus aerolatus* sp. nov. and *Deinococcus aerophilus* sp. nov., isolated from air samples. *Int. J. Syst. Evol. Microbiol.* **2010**, *60*, 1191–1195. [[CrossRef](#)] [[PubMed](#)]
2. Dong, N.; Li, H.R.; Yuan, M.; Zhang, X.H.; Yu, Y. *Deinococcus antarcticus* sp. nov., isolated from soil. *Int. J. Syst. Evol. Microbiol.* **2015**, *65*, 331–335. [[CrossRef](#)] [[PubMed](#)]
3. Rainey, F.A.; Ray, K.; Ferreira, M.; Gatz, B.Z.; Nobre, F.; Bagaley, D.; Rash, B.A.; Park, M.J.; Earl, A.M.; Shank, N.C.; et al. Extensive Diversity of Ionizing-Radiation-Resistant Bacteria Recovered from Sonoran Desert Soil and Description of Nine New Species of the Genus *Deinococcus* Obtained from a Single Soil Sample. *Appl. Environ. Microbiol.* **2005**, *71*, 5225–5235. [[CrossRef](#)] [[PubMed](#)]
4. Yang, Y.; Itoh, T.; Yokobori, S.; Itahashi, S.; Shimada, H.; Satoh, K.; Ohba, H.; Narumi, I.; Yamagishi, A. *Deinococcus aerius* sp. nov., isolated from the high atmosphere. *Int. J. Syst. Evol. Microbiol.* **2009**, *59*, 1862–1866. [[CrossRef](#)]
5. Yang, Y.; Itoh, T.; Yokobori, S.; Shimada, H.; Itahashi, S.; Satoh, K.; Ohba, H.; Narumi, I.; Yamagishi, A. *Deinococcus aetherius* sp. nov., isolated from the stratosphere. *Int. J. Syst. Evol. Microbiol.* **2010**, *60*, 776–779. [[CrossRef](#)]
6. Callegan, R.P.; Nobre, M.F.; McTernan, P.M.; Battista, J.R.; Navarro-Gonzalez, R.; McKay, C.P.; da Costa, M.S.; Rainey, F.A. Description of four novel psychrophilic, ionizing radiation-sensitive *Deinococcus* species from alpine environments. *Int. J. Syst. Evol. Microbiol.* **2008**, *58*, 1252–1258. [[CrossRef](#)]
7. Shashidhar, R.; Bandekar, J.R. *Deinococcus piscis* sp. nov., a radiation-resistant bacterium isolated from a marine fish. *Int. J. Syst. Evol. Microbiol.* **2009**, *59*, 2714–2717. [[CrossRef](#)]
8. Hirsch, P.; Gallikowski, C.A.; Siebert, J.; Peissl, K.; Kroppenstedt, R.; Schumann, P.; Stackebrandt, E.; Anderson, R. *Deinococcus frigens* sp. nov., *Deinococcus saxicola* sp. nov., and *Deinococcus marmoris* sp. nov., low temperature and draught-tolerating, UV-resistant bacteria from continental Antarctica. *Int. J. Syst. Evol. Microbiol.* **2004**, *27*, 636–645. [[CrossRef](#)]
9. Cox, M.M.; Keck, J.L.; Battista, J.R. Rising from the Ashes: DNA Repair in *Deinococcus radiodurans*. *PLoS Genet.* **2010**, *6*, e1000815. [[CrossRef](#)]
10. Lange, C.C.; Wackett, L.P.; Minton, K.W.; Daly, M.J. Engineering a recombinant *Deinococcus radiodurans* for organopollutant degradation in radioactive mixed waste environments. *Netw. Address Transl.* **1998**, *16*, 929–933. [[CrossRef](#)]
11. Brim, H.; Osborne, J.P.; Kostandarithes, H.M.; Fredrickson, J.K.; Wackett, L.P.; Daly, M.J. *Deinococcus radiodurans* engineered for complete toluene degradation facilitates Cr(VI) reduction. *Microbiology* **2006**, *152*, 2469–2477. [[CrossRef](#)] [[PubMed](#)]
12. Lemee, L.; Peuchant, E.; Clerc, M.; Brunner, M.; Pfander, H. Deinoxanthin: A new carotenoid isolated from *Deinococcus Radiodurans*. *Tetrahedron Lett.* **1997**, *53*, 919–926. [[CrossRef](#)]
13. Bamji, M.S.; Krinsky, N.I. The carotenoid pigments of a radiation-resistant *Micrococcus* species. *Biochim. Biophys. Acta* **1966**, *115*, 276–284. [[CrossRef](#)]
14. Ji, H.F. Insight into the strong antioxidant activity of deinoxanthin, a unique carotenoid in *Deinococcus radiodurans*. *Int. J. Mol. Sci.* **2010**, *11*, 4506–4510. [[CrossRef](#)] [[PubMed](#)]
15. Tian, B.; Xu, Z.; Sun, Z.; Lin, J.; Hua, Y. Evaluation of the antioxidant effects of carotenoids from *Deinococcus radiodurans* through targeted mutagenesis, chemiluminescence, and DNA damage analyses. *Biochim. Biophys. Acta* **2007**, *1770*, 902–911. [[CrossRef](#)] [[PubMed](#)]
16. Choi, Y.J.; Hur, J.M.; Lim, S.; Jo, M.; Kim, D.H.; Choi, J.I. Induction of apoptosis by deinoxanthin in human cancer cells. *Anticancer Res.* **2014**, *34*, 1829–1835. [[PubMed](#)]

17. Leuko, S.; Bohmeier, M.; Hanke, F.; Boettger, U.; Rabbow, E.; Parpart, A.; Rettberg, P.; de Vera, J.P. On the Stability of Deinoxanthin Exposed to Mars Conditions during a Long-Term Space Mission and Implications for Biomarker Detection on Other Planets. *Front. Microbiol.* **2017**, *8*, 1680. [\[CrossRef\]](#)
18. Schmidt, R. Deactivation of O<sub>2</sub>(<sup>1</sup>Δg) Singlet Oxygen by Carotenoids: Internal Conversion of Excited Encounter Complexes. *J. Phys. Chem. A* **2004**, *108*, 5509–5513. [\[CrossRef\]](#)
19. Mayne, S.T. Beta-carotene, carotenoids, and disease prevention in humans. *FASEB J.* **1996**, *10*, 690–701. [\[CrossRef\]](#)
20. Choi, J.Y.; Lee, K.; Lee, P.C. Complete genome sequence of the carotenoid-producing *Deinococcus* sp. strain AJ005. *Microbiol. Resour. Announc.* **2019**, *8*, e01245-19. [\[CrossRef\]](#)
21. Hansler, A.; Chen, Q.; Ma, Y.; Gross, S.S. Untargeted metabolite profiling reveals that nitric oxide bioynthesis is an endogenous modulator of carotenoid biosynthesis in *Deinococcus radiodurans* and is required for extreme ionizing radiation resistance. *Arch. Biochem.* **2016**, *589*, 38–52. [\[CrossRef\]](#) [\[PubMed\]](#)
22. Zhou, Z.; Zhang, W.; Su, S.; Chen, M.; Lu, W.; Lin, M.; Molnar, I.; Xu, Y. CYP287A1 is a carotenoid 2-beta-hydroxylase required for deinoxanthin biosynthesis in *Deinococcus radiodurans* R1. *Appl. Microbiol. Biotechnol.* **2015**, *99*, 10539–10546. [\[CrossRef\]](#) [\[PubMed\]](#)



© 2019 by the authors. Licensee MDPI, Basel, Switzerland. This article is an open access article distributed under the terms and conditions of the Creative Commons Attribution (CC BY) license (<http://creativecommons.org/licenses/by/4.0/>).

## Article

# Synthesis of Bioactive Silver Nanoparticles by a *Pseudomonas* Strain Associated with the Antarctic Psychrophilic Protozoon *Euplotes focardii*

Maria Sindhura John <sup>1</sup>, Joseph Amruthraj Nagoth <sup>1</sup>, Kesava Priyan Ramasamy <sup>1</sup>, Alessio Mancini <sup>1</sup>, Gabriele Giuli <sup>2</sup>, Antonino Natalello <sup>3</sup>, Patrizia Ballarini <sup>1</sup>, Cristina Miceli <sup>1</sup> and Sandra Pucciarelli <sup>1,\*</sup>

<sup>1</sup> School of Biosciences and Veterinary Medicine, University of Camerino, 62032 Camerino, Italy; sindhuramaria@gmail.com (M.S.J.); amruthjon@gmail.com (J.A.N.); kesavanlife@gmail.com (K.P.R.); alessio.mancini@unicam.it (A.M.); patrizia.ballarini@unicam.it (P.B.); cristina.miceli@unicam.it (C.M.)

<sup>2</sup> School of Sciences and Technology, University of Camerino, 62032 Camerino, Italy; gabriele.giuli@unicam.it

<sup>3</sup> Department of Biotechnology and Biosciences, University of Milano-Bicocca, 20126 Milano, Italy; antonino.natalello@unimib.it

\* Correspondence: sandra.pucciarelli@unicam.it; Tel.: +39-0737-403231

Received: 30 November 2019; Accepted: 31 December 2019; Published: 3 January 2020

**Abstract:** The synthesis of silver nanoparticles (AgNPs) by microorganisms recently gained a greater interest due to its potential to produce them in various sizes and morphologies. In this study, for AgNP biosynthesis, we used a new *Pseudomonas* strain isolated from a consortium associated with the Antarctic marine ciliate *Euplotes focardii*. After incubation of *Pseudomonas* cultures with 1 mM of AgNO<sub>3</sub> at 22 °C, we obtained AgNPs within 24 h. Scanning electron (SEM) and transmission electron microscopy (TEM) revealed spherical polydispersed AgNPs in the size range of 20–70 nm. The average size was approximately 50 nm. Energy dispersive X-ray spectroscopy (EDS) showed the presence of a high intensity absorption peak at 3 keV, a distinctive property of nanocrystalline silver products. Fourier transform infrared (FTIR) spectroscopy found the presence of a high amount of AgNP-stabilizing proteins and other secondary metabolites. X-ray diffraction (XRD) revealed a face-centred cubic (fcc) diffraction spectrum with a crystalline nature. A comparative study between the chemically synthesized and *Pseudomonas* AgNPs revealed a higher antibacterial activity of the latter against common nosocomial pathogen microorganisms, including *Escherichia coli*, *Staphylococcus aureus* and *Candida albicans*. This study reports an efficient, rapid synthesis of stable AgNPs by a new *Pseudomonas* strain with high antimicrobial activity.

**Keywords:** green synthesis biomaterials; silver nitrate; antibiotics; nanotechnology

## 1. Introduction

Nanotechnology has become an emerging field in the area of biotechnology, dealing with the synthesis, design and manipulation of particles with approximate sizes from 1 to 100 nm. Nanoparticles (NPs) are used in biomedical sciences, healthcare, drug–gene delivery, space industries, cosmetics, chemical industries, optoelectronics, etc. [1]. Various physiochemical methods have been used for AgNP synthesis, including microwave, biochemical and electrochemical synthesis, chemical reduction (aqueous and non-aqueous), irradiation, ultrasonic-associated, photo-induced, photo-catalytic and microemulsion methods. However, these methodologies have various disadvantages because they imply high energy consumption and the use of toxic reagents with the generation of hazardous waste, which causes potential risks to the environment and human health [2,3]. In these days, there is a growing need to develop simple, cost-effective, reliable, bio-compatible and eco-friendly approaches



for the synthesis of nanomaterials, which do not contain toxic chemicals in the synthesis protocols. For mining the metallic nanomaterials, microbial-mediated green synthesis has recently been considered as a promising source [4]. Green synthesis of nanoparticles represents a cost-effective and environmentally friendly method with advantages over conventional methods that involve chemical, potentially toxic solvents. For green NP synthesis, the most important issues are the solvent medium combined with the selection of ecologically nontoxic, reducing and stabilizing agents [5]. There are different green methods for nanoparticle synthesis, but the most commonly appreciated is through bacteria, because bacteria are usually easy to grow [6]. Capping agents are considered fundamental for nanoparticles stabilization. Capped AgNPs are known to exhibit better antibacterial activity with respect to uncapped AgNPs [7]. Biologically synthesized nanoparticles have remarkable potential since they can be easily coated with a lipid/protein layer, which confers physiological solubility and stability useful for applications in biomedicine [8].

AgNPs possess general antibacterial and bactericidal properties. These are mostly against methicillin-resistant strains [9]. Gram-negative and Gram-positive bacteria are relevant causes of numerous infections in hospitals. Due to the increased microbial resistance to multiple antibiotics [10], many researchers are interested in developing novel and effective antimicrobial agents [11]. Furthermore, AgNPs exhibit anti-biofilm activities [12] and synergistic activities with diverse antibiotics, such as  $\beta$ -lactams, macrolides and lincosamides [13]. The use of silver-coated antiseptics shows a broad-spectrum activity and a far lower chance than antibiotics in inducing the typical microbial resistance [14].

The mechanism at the basis of the extracellular synthesis of nanoparticles using microbes appears based on enzymes such as the secreted nitrate reductase that helps in the production of metal nanoparticles from metal ions [15]. Such mechanism was shown in *Bacillus licheniformis* [16]. The biosynthesis and stabilization of nanoparticles in *Stenotrophomonas maltophilia* via charge capping, involving the electron shuttle enzymatic metal reduction process produced by the Nicotinamide Adenine Dinucleotide Phosphate (NADPH)-dependent reductase enzyme, has also been reported [17]. In *Pseudomonas* spp., a possible process for the biosynthesis of AgNPs is described, to be performed by a Nicotinamide Adenine Dinucleotide (NADH)-dependent nitrate reductase [18,19]. The enzyme may be responsible for the reduction of  $\text{Ag}^+$  to  $\text{Ag}^0$  and the subsequent formation of AgNPs, where the NADH-dependent reductase is expected to act as a carrier while the bioreduction occurs by means of the electrons from NADH [18,19].

The aim of this study is to develop a simple and low-cost approach for AgNP intracellular synthesis using a new *Pseudomonas* strain isolated from a consortium associated with the psychrophilic marine ciliated protozoan *Euplotes focardii* [20], which we named *Pseudomonas* sp. ef1 [21]. *E. focardii* is a free-swimming ciliate endemic of the oligotrophic coastal sediments of the Antarctic Terra Nova Bay [22]. It has been maintained in cultures for more than 20 years after the first isolation. *E. focardii*'s optimal growing temperature is about 4–5 °C, with a drop at 8–10 °C and not surviving if exposed to temperatures over 10 °C [22]. We showed that the AgNPs produced by *Pseudomonas* sp. ef1 possess higher antimicrobial activity with respect to those chemically synthesized, which could be used against common pathogenic microorganisms.

## 2. Results and Discussion

### 2.1. Biosynthesis of AgNPs and UV–Vis Spectroscopy Characterization

We primarily investigated the biosynthesis of AgNPs by *Pseudomonas* sp. ef1 through the observation of the culture medium colour change by incubation of the bacterial biomass with 1 mM  $\text{AgNO}_3$  at 22 °C (the optimal growing temperature of *Pseudomonas* sp. ef1). A change in colour from white to brown occurred within 24 h in the presence of light (Figure S1). The change to a brown colour of the culture was maintained for 72 h (Figure S1A,B). No colour change was observed in the control culture containing the heat-killed bacterial biomass with 1 mM  $\text{AgNO}_3$  (data not shown).



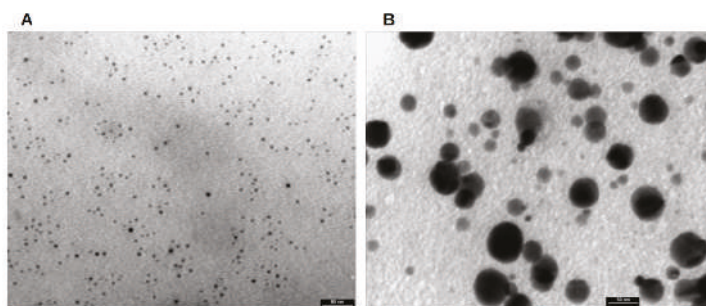
Medium colour change related to extracellular synthesis of AgNPs has been previously reported in another *Pseudomonas* culture [23], as well as in *Bacillus methylotrophicus* [24] and *Actinobacteria* SL19 and SL24 strains, and in fungi as *Fusarium semitectum*, *Aspergillus fumigatus* [25] and *Streptomyces* sp. The culture medium colour change is attributed to the excitation of the surface plasmon resonance of AgNPs [26,27].

*Pseudomonas* sp. ef1 AgNPs formation was confirmed by UV–vis spectroscopy, considered one of the most valuable methods for the characterization of the optical response of metal nanoparticles, including AgNPs. This method has been demonstrated to be appropriately sensitive to check AgNPs' intense surface plasmon resonances (SPRs) [28] in the range of 350–600 nm [29–31]. A 0.1 mL aliquot of the *Pseudomonas* sp. ef1 culture was diluted with 0.9 mL of ddH<sub>2</sub>O and UV–visible spectra was recorded from 300 to 800 nm wavelength at room temperature: A relevant peak at about 420 nm was found (Figure S1C), as also reported for AgNPs produced by *Pseudomonas putida* NCIM 2650 [32] and *Pseudomonas* sp. (JQ989348) [33]. By contrast, *Pseudomonas* sp. “ram bt-1” AgNPs showed absorbance spectra at 430 nm [34]. The presence of a single SPR peak suggests AgNPs of spherical shape [35].

## 2.2. Morphology and Chemical Composition of *Pseudomonas* sp. ef1 AgNPs

We performed scanning electron microscopy (SEM) to define the size and shape of the AgNPs synthesized by *Pseudomonas* sp. ef1. SEM images (Figure S2A,A') revealed polydispersed (i.e., non-uniform in size) AgNPs of spherical shape. Their size ranged from 20 to about 100 nm.

To better understand the surface morphology and for getting additional information on the size, a TEM investigation was conducted (Figure 1). Aliquots of AgNP solution were placed onto a nitrocellulose- and Formvar-coated copper grid and maintained to dry under room conditions. TEM micrographs suggested particle sizes around 10 nm (clearly visible in Figure 1A) to 70 nm (Figure 1B), with the average size being 50 nm. The particles showed a spherical shape, well separated from each other even when these formed aggregates, suggesting the presence of capping peptides around each particle, whose role is to stabilize the nanoparticles.

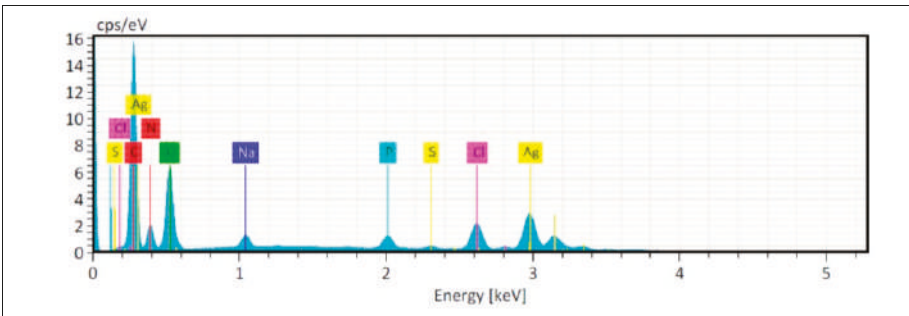


**Figure 1.** Transmission electron microscopy (TEM) micrographs of *Pseudomonas* sp. ef1 silver nanoparticles (AgNPs). The particles show a spherical shape with size from 10 nm (A) to 70 nm (B), with the average size being 50 nm. Bars: 50 nm

*Pseudomonas* sp. ef1 AgNPs appear similar to those produced by other *Pseudomonas* [36–42]. The TEM grid analysis of *Pseudomonas* sp. ef1 bio-AgNPs revealed smooth-surfaced polydispersed particles, approximately spherical in shape with the size ranging from 12.5 to 100 nm. By contrast, bio-AgNPs from *Pseudomonas putida* were monodispersed and smaller in size (6 to 16 nm) [43].

The chemical composition of the *Pseudomonas* sp. ef1 AgNPs was obtained by energy dispersive X-ray (EDX) spectrum analysis (Figure 2). We observed an intense signal of Ag at 3 keV, which confirmed the presence of AgNPs. Metallic AgNPs are typically reported to show a strong signal peak at 3 keV, due to surface plasmon resonance [44,45]. However, other element (C, N and O) signals were detected at normal mode (Figure 2 and Table 1). These elements probably derive from the emissions of

the capping proteins. The EDX spectrum analysis of *Pseudomonas fluorescens* CA 417 AgNPs also showed the presence of a high intensity absorption peak at 3 keV [46].



**Figure 2.** EDAX investigation of *Pseudomonas* sp. ef1 AgNPs. A: EDAX spectrum of AgNPs; Ag, C, N and O indicate the silver (the highest peak, recorded at 3 keV), carbon, nitrogen and oxygen signals (the relative amounts are reported in Table 1).

**Table 1.** Quantitative EDAX results of *Pseudomonas* sp. ef1 AgNPs.

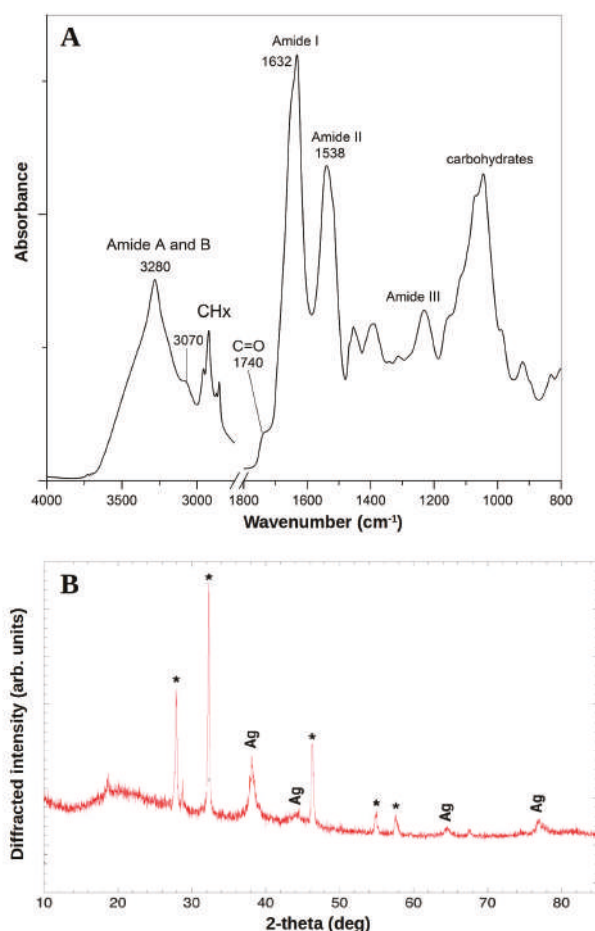
Element	At.No	Netto	Mass [%]	Mass Norm [%]	Atom [%]	Abs. err [%] 1 sigma	rel err [%] 1 sigma
Carbon	6	197121	22.22	29.78	48.86	2.45	11.01
Nitrogen	7	27658	7.08	9.49	13.35	0.90	12.76
Oxygen	8	90933	15.84	21.22	26.15	1.82	11.48
Sodium	11	16435	1.20	1.61	1.38	0.10	8.09
Phosphorus	15	22015	1.45	1.95	1.24	0.08	5.60
Sulfur	16	4429	0.32	0.43	0.26	0.04	11.83
Chlorine	17	51613	4.53	6.07	3.38	0.18	4.02
Silver	47	127532	21.98	29.46	5.38	0.76	3.45
Sum		74.64		100.00	100.00		

2.3. Capping Proteins and Crystalline Structure of *Pseudomonas* sp. AgNPs

To confirm the potential interactions between the silver salts and the capping proteins, which could account for the reduction of Ag<sup>+</sup> ions with consequent stabilization of AgNPs, we performed FTIR measurements (Figure 3A). The amide linkages between the amino acid residues in proteins produce a typical signature in the infrared spectral region [47].

The FTIR spectrum of *Pseudomonas* sp. ef1 AgNPs is characterized by the protein Amide A, B, I, II and III bands (Figure 3). In particular, the peaks around 3280 cm<sup>−1</sup> (Amide A) and 3070 cm<sup>−1</sup> (Amide B) are mainly assigned to the NH vibrations. The absorption maximum of the Amide I band, due to the C=O stretching of the peptide bond, occurs around 1632 cm<sup>−1</sup>. The Amide II band, mainly due to the amide NH bending, peaked around 1538 cm<sup>−1</sup>. The complex absorption in the 1200–950 cm<sup>−1</sup> spectral region can be tentatively assigned to carbohydrate absorption. The 1740 cm<sup>−1</sup> peak is characteristic of C=O carbonyl groups [48].

The overall FTIR pattern confirms that capping proteins are present in the AgNPs and that these proteins are not extensively aggregated. Protein–nanoparticle interactions are produced either through free amine groups or cysteine residues and through the electrostatic attraction of negatively charged carboxylate groups, specifically in enzymes [49]. The free amine and carbonyl groups of bacterial proteins could possibly be responsible for the formation and stabilization of AgNPs [50,51].



**Figure 3.** (A) FTIR absorption spectrum of *Pseudomonas* sp. ef1 AgNPs. The peak position and the assignment of the main components are reported. (B) XRD spectrum recorded for *Pseudomonas* sp. ef1 AgNPs. Four intense peaks at 38.95°, 45.12°, 65.39° and 78.12° correspond to plane values of (1 1 1), (2 0 0), (2 2 0) and (3 1 1) at the 2 $\theta$  angle, which were consistent with the standard data JCPDS file no. 01-087-0717, indicated by asterisks.

The capping proteins prevent aggregation and provide nanoparticle stability [52]. Fourier transform infrared spectrum applied to the deep-sea bacterium *Pseudomonas* sp. JQ989348 AgNPs showed the presence of proteins in large amounts, as well as other secondary metabolites [33].

The crystalline structure of *Pseudomonas* sp. ef1 AgNPs was confirmed by XRD analysis (Figure 3B). The AgNPs diffraction spectrum showed a face-centred cubic (fcc) crystalline nature, including peaks at 38.95°, 45.12°, 65.39° and 78.12° (labelled as Ag in Figure 3B), which corresponded to plane values of (1 1 1), (2 0 0), (2 2 0) and (3 1 1) at the 2 $\theta$  angle. These were consistent with the standard data JCPDS file no. 01-087-0717. Peaks indicated by asterisks in Figure 3B probably correspond to the crystallization of the bio-organic phase occurring on the AgNPs surface, as also reported in [53–57]. Alternatively, these peaks may be due to AgNO<sub>3</sub>, which has not been reduced by *Pseudomonas* sp. ef1.

X-ray diffraction (XRD) analysis of *Pseudomonas fluorescens* CA 417 AgNPs also revealed well-defined peaks at 38° 44°, 64° and 78°, thus showing the face-centred cubic (fcc) metallic crystal

corresponding to the (111), (200), (220) and (311) facets of the crystal planes at the  $2\theta$  angle [46]. The crystalline structure of biogenic AgNPs of *Pseudomonas putida* MVP2 was also confirmed by XRD [43].

#### 2.4. *Pseudomonas sp. ef1* AgNPs Antimicrobial Activity

The antibacterial activity of *Pseudomonas sp. ef1* AgNPs was tested against pathogenic Gram-positive and Gram-negative bacteria, as well as fungi, and compared with that of chemically synthesized AgNPs and AgNO<sub>3</sub> (Table S1 and Figure 4). In the comparative study, the biosynthesized AgNPs exhibited a stronger antibacterial property than the chemically synthesized AgNPs and AgNO<sub>3</sub> (Figure 4). Among Gram-negative bacteria, the larger inhibition zone ( $\varnothing$  19.0 mm) was against *Escherichia coli* and the smallest ( $\varnothing$  14.0 mm) was against *Pseudomonas aeruginosa* and *Serratia marcescens*. Among Gram-positive bacteria, the highest zone of 15 mm was formed against *Staphylococcus aureus*. Among fungi, the larger zone was against *Candida albicans* ( $\varnothing$  15.0 mm).

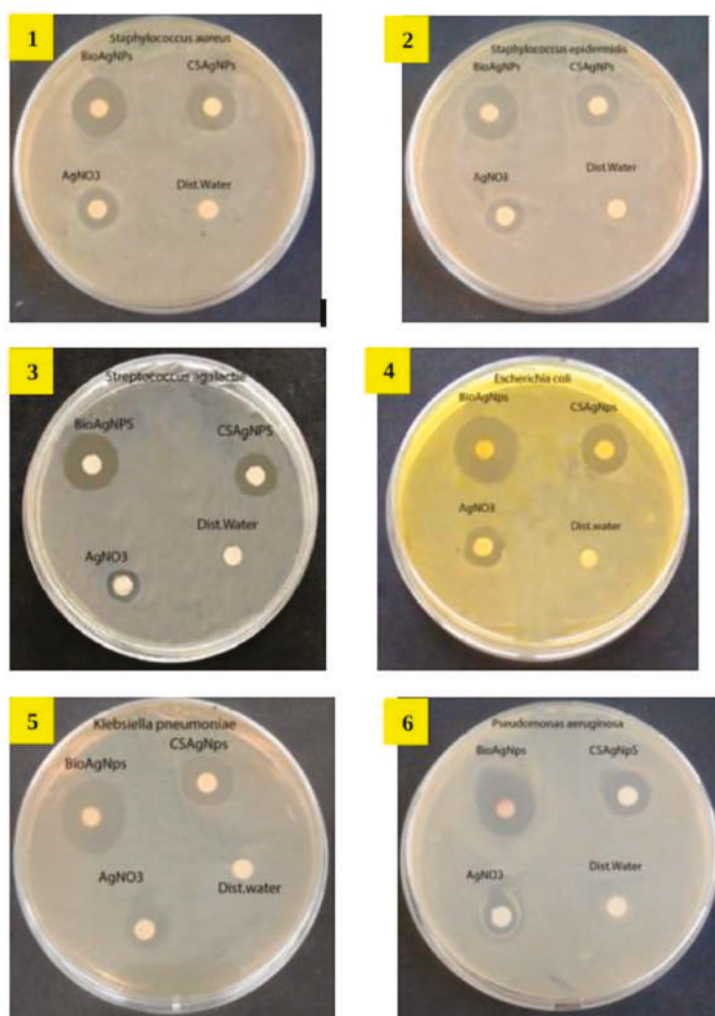
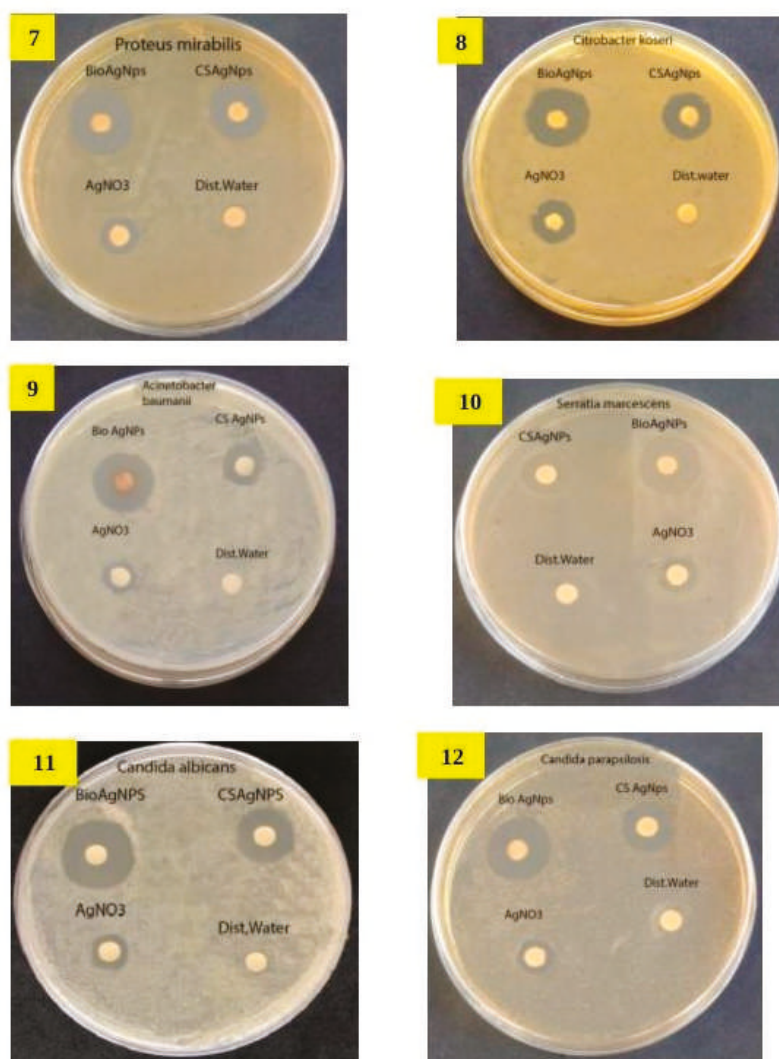


Figure 4. Cont.



**Figure 4.** Antimicrobial activity of *Pseudomonas* sp. ef1 AgNPs tested against twelve human pathogens. The bio AgNPs disks were compared with chemically synthesized AgNPs disks. AgNO<sub>3</sub> disks and distilled water disks were used as control. The human pathogens are: 1. *Staphylococcus aureus*, 2. *Staphylococcus epidermidis*, 3. *Streptococcus agalactiae*, 4. *Escherichia coli*, 5. *Klebsiella pneumoniae*, 6. *Pseudomonas aeruginosa*, 7. *Proteus mirabilis*, 8. *Citrobacter koseri*, 9. *Acinetobacter baumannii*, 10. *Serratia marcescens*, 11. *Candida albicans*, 12. *Candida parapsilosis*.

It has been reported that *E. coli* showed a greater sensitivity by comparison with that of *Bacillus cereus* and *Streptococcus pyogenes*, probably due to the narrow cell walls of Gram-negative bacteria with respect to Gram-positive bacteria [58].

The use of the biosynthesized AgNPs may be one of the promising approaches to overcome bacterial resistance and could also play a new key role in pharmacotherapeutics. The mechanism of the AgNP-mediated bactericidal property is still to be understood. A mechanism proposed by other



studies is that AgNPs attach to the cell wall, thus modifying the membrane integrity and disturbing its permeability and cell respiration functions [59,60]. Most likely, the antibacterial activity of AgNPs is size dependent. This means that smaller AgNPs that have a large surface area available for interactions function as more efficient antimicrobial agents than larger ones. It is also possible that AgNPs can penetrate inside the bacteria and not only interact with the membrane of the cell [60]. Another possible process responsible of AgNPs antimicrobial activity may be the release of  $\text{Ag}^+$  ions, since they may play a partial but relevant role in the bactericidal effect [60].

### 3. Materials and Methods

#### 3.1. Synthesis of AgNPs by *Pseudomonas* sp. ef1

The bacterial biomass was produced by inoculating *Pseudomonas* sp. ef1 into Luria-Bertani (LB) medium (10 g of Tryptone, 10 g of NaCl and 5 g of yeast extract, dissolved in 1 L of ddH<sub>2</sub>O). The culture flasks were incubated on an orbital shaker set at 220 rpm, at 22 °C. After 24 h the biomass was harvested by centrifuging at 5000 rpm for 30 min. After removal of the supernatant, approximately 2 mg of the bacterial biomass was transferred into an Erlenmeyer flask containing a solution of 1 mM AgNO<sub>3</sub>. The mixture was placed in the orbital shaker set at 200 rpm for 24 h at 22 °C. The heat-killed biomasses incubated with silver nitrate were maintained as control. Biosynthesis was carried out in bright condition as visible light irradiation is known to increase the biosynthetic rate of AgNPs formation. The bioreduction of  $\text{Ag}^+$  ions were monitored by changes in colour of the bacterial biomass reaction mixture containing the AgNO<sub>3</sub> (Figure S1) and by UV–visible spectroscopy (UV-1800, Shimadzu): a 0.1 mL aliquot of the sample was diluted with 0.9 mL of ddH<sub>2</sub>O and UV–visible spectra was recorded from 300 to 800 nm wavelength. ddH<sub>2</sub>O was used as blank.

#### 3.2. Purification of AgNPs

Bacterial biomass was collected by centrifugation at 5000 rpm for 30 min. The resulting pellet was then suspended in ddH<sub>2</sub>O and ultra-sonicated at a pulse rate of 6V at intervals of 30 s for ten cycles. Afterwards, the solution was centrifuged again at 5000 rpm for 30 min and the supernatant loaded on a Sephadex G-50 resin equilibrated in 10 mM Tris buffer (pH 7.0) to remove contaminating debris and proteins. AgNPs were finally extracted from the buffered solution by adding 3 volumes of isopropanol to the obtained nanoparticle solution. Isopropyl alcohol is known to dissolve a wide range of non-polar compounds and to evaporate quickly compared to ethanol. The mixture was rotated on the orbital shaker overnight and subjected to evaporation to obtain a purified powdered highly enriched in NPs.

#### 3.3. Chemical Synthesis of AgNPs

A solution of 1 mM of AgNO<sub>3</sub> was heated to boil. As the solution started to boil, a sodium citrate solution was added drop-by-drop until the solution turned into a greyish-yellow color, indicating  $\text{Ag}^+$  ion formation. Heating was continued for 60 s. The solution was then chilled to room temperature.

#### 3.4. Scanning Electron Microscopy (SEM), Transmission Electron Microscopy (TEM) and Energy Dispersive X-ray Analysis (EDAX)

For SEM (ZIESSA, Sigma 300) analysis, purified AgNPs were sonicated for 15 min to reach a uniform distribution. A drop of the solution was loaded on carbon-coated copper grids and allowed to evaporate under infrared light for 30 min.

TEM (PHILIPS EM208S) analysis was performed using an acceleration voltage of 100 kV. Drops of an AgNP solution were loaded on nitrocellulose- and Formvar-coated copper TEM grids. After 2 min, the extra solution was removed, and the grids were allowed to dry at room temperature. The acquired data were analysed by Statistical Software (StatSoft, Tulsa, Okla., United States) using the variability plot of average methods. After 100 measurements the size distribution of the AgNPs was estimated using TEM imaging and analysis software (TIA).

EDAX analysis of AgNPs was performed using Field Emission Scanning Electron Microscope (FESEM) equipped with an EDAX attachment.

### 3.5. Fourier Transform Infrared Spectroscopy (FTIR) Analysis

AgNPs were deposited on the single reflection diamond element of the attenuated total reflection (ATR) device (Quest, Specac) and dried at room temperature. The ATR/FTIR spectrum was collected by the Varian 670-IR spectrometer, equipped with a nitrogen-cooled Mercury Cadmium Telluride detector, under the following conditions: triangular apodization, scan speed of 25 kHz, resolution of  $2\text{ cm}^{-1}$  and 512 scan co-additions [61].

### 3.6. X-ray Diffraction Analysis (XRD)

X-ray Diffraction measurements were performed by scanning drop-coated films of AgNPs in a wide range of Bragg angle  $2\theta$  at a rate of  $2\text{ min}^{-1}$ . A Philips PW 1830 instrument was used, and it was operated at a voltage of 40 kV with a current of 30 mA using monochromatic Cu K $\alpha$  radiation ( $\lambda = 1.5405\text{ \AA}$ ). The diffracted intensities were recorded in the  $2\theta$  range of  $10^\circ$ – $80^\circ$ . To elucidate the crystalline structure, the resulting images were compared with the Joint Committee on Powder Diffraction Standards (JCPDS) library.

### 3.7. Screening of Antimicrobial Activity of Biosynthesized AgNPs

The evaluation of the biosynthesized AgNPs antibacterial activity was carried out by the Kirby–Bauer disc diffusion method on the following twelve stains: *Staphylococcus aureus*, *Staphylococcus epidermidis*, *Streptococcus agalactiae* (Gram-positive bacteria); *Escherichia coli*, *Klebsiella pneumoniae*, *Pseudomonas* sp., *Proteus mirabilis*, *Citrobacter koseri*, *Acinetobacter baumannii*, *Serratia marcescens* (Gram-negative bacteria); and *Candida albicans* and *Candida parapsilosis* (fungi).

The biosynthesized AgNPs were tested for antibacterial activity by the Kirby–Bauer disc diffusion method. The pathogenic cultures were subcultured into peptone broth and incubated at  $37^\circ\text{C}$  to reach  $10^5$ – $10^6\text{ CFU ml}^{-1}$ . The fresh cultures of pathogens were plated using a sterile cotton swab on Petri dishes containing Muller Hinton Agar. Six millimetre filter paper disks impregnated with 25  $\mu\text{L}$  of biosynthesized AgNPs using a sterile micropipette were placed on the pathogen-plated agar. Bio-AgNPs disks were compared with chemically synthesized AgNPs disks.  $\text{AgNO}_3$  disks and distilled water disks were used as control. The plates were incubated at  $37^\circ\text{C}$  for 18–24 h to measure the zone of inhibition.

## 4. Conclusions

In this study we reported an easy and efficient biological method to synthesize AgNPs using the biomass of a novel *Pseudomonas* strain isolated from a bacterial consortium found in association with the Antarctic ciliate *E. focardii*. We also characterized these AgNPs. Their stability makes the present method a viable alternative to chemical synthesis methods. Due to the lesser specificity of the reaction parameters, this process can be explored for large-scale synthesis of AgNPs. The study highlights an efficient strategy to obtain bionanomaterial that can be used against a large number of drug resistant pathogenic bacteria, thus contributing to solve this globally serious concern, especially given there being a limited choice of antibiotic treatment [62]. Furthermore, these AgNPs show the highest antimicrobial activity with respect to those that are chemically synthesized. The *Pseudomonas* strain here used can also be exploited to remove silver nitrate contamination from the environment, allowing to associate its potential in bioremediation and in antibiotics production.

## 5. Patents

The results of this paper are related to the patent number 102019000014121 deposited in 06/08/2019.

**Supplementary Materials:** The following are available online at <http://www.mdpi.com/1660-3397/18/1/38/s1>, Figure S1: AgNP synthesis by *Pseudomonas* sp. ef1. Table S1: Antimicrobial activity of AgNPs synthesized by *Pseudomonas* sp. against various pathogenic organisms. Supplementary references.

**Author Contributions:** All authors contributed to the conception and design of this study; material preparation, collection and analysis of data were performed by M.S.J., J.A.N. and K.P.R.; The draft of the manuscript was prepared by M.S.J., J.A.N. and A.M.; all authors contributed to the improvement of the previous versions of the manuscript; all authors read and approved the final version. All authors have read and agreed to the published version of the manuscript.

**Funding:** This work was supported by the EC MSCA H2020 RISE Metable-645693.

**Acknowledgments:** We thanks Laura Petetta (University of Camerino) for the support in SEM analysis.

**Conflicts of Interest:** The authors declare no conflict of interest.

## References

1. Khan, I.; Saeed, K.; Khan, I. Nanoparticles: Properties, applications and toxicities. *Arab. J. Chem.* **2019**, *12*, 908–931. [\[CrossRef\]](#)
2. Irvani, S.; Korbekandi, H.; Mirmohammadi, S.V.; Zolfaghari, B. Synthesis of silver nanoparticles: Chemical, physical and biological methods. *Res. Pharm. Sci.* **2014**, *9*, 385–406. [\[PubMed\]](#)
3. Gandhi, H.; Khan, S. Biological Synthesis of Silver Nanoparticles and Its Antibacterial Activity. *J. Nanomed. Nanotechnol.* **2016**, *7*, 1–3. [\[CrossRef\]](#)
4. Gurunathan, K.; Kalishwaralal, R.; Vaidyanathan, V.; Deepak, S.R.K.; Pandian, J.; Muniyandi, N.; Hariharan, S.H.E. Biosynthesis, purification and characterization of silver nanoparticles using *Escherichia coli*. *Colloids Surf.* **2009**, *74*, 328–335. [\[CrossRef\]](#) [\[PubMed\]](#)
5. Badr, Y.; Wahed, E.; Mahmoud, M.G. Photo catalytic degradation of methyl red dye by silica nanoparticles. *J. Hazard. Mater.* **2008**, *154*, 245–253. [\[CrossRef\]](#) [\[PubMed\]](#)
6. Parikh, R.Y.; Singh, S.; Prasad, B.L.V.; Patole, M.S.; Sastry, M.; Shouche, Y.S. Extracellular synthesis of crystalline silver nanoparticles and molecular evidence of silver resistance from *Morganella* sp.: Towards understanding biochemical synthesis mechanism. *Chembiochem* **2008**, *9*, 1415–1422. [\[CrossRef\]](#) [\[PubMed\]](#)
7. Abdel-Mohsen, A.M.; Hrdina, R.; Burgert, L.; Abdel, R.M.; Rahman, M.; Hasova, D.; Smejkalova, M.; Kolar, M.; Pekar, A.S. Antibacterial activity and cell viability of hyaluronan fiber with silver nanoparticles. *Carbohydr. Polym.* **2013**, *92*, 1177–1187. [\[CrossRef\]](#) [\[PubMed\]](#)
8. Emerich, D.F.; Thanos, C.G. The pinpoint promise of nanoparticle-based drug delivery and molecular diagnosis. *Biomol. Eng.* **2006**, *23*, 171–184. [\[CrossRef\]](#)
9. Shahverdi, A.R.; Fakhimi, A.; Shahverdi, H. Synthesis and effect of silver nanoparticles on the antibacterial activity of different antibiotics against *Staphylococcus aureus* and *Escherichia coli*. *Nanomed. Nanotechnol.* **2007**, *3*, 168–171. [\[CrossRef\]](#)
10. Criswell, D. The “evolution of antibiotic resistance”. *Acta Facts* **2004**, *33*, 1–4.
11. Fayaz, A.M.; Balaji, K.; Girilal, M.; Yadav, R.; Kalaichelvan, P.T.; Venketesan, R. Biogenic synthesis of silver nanoparticles and their synergistic effect with antibiotics: A study against Gram-positive and Gram-negative bacteria. *Nanomed. Nanotechnol.* **2010**, *6*, 103–109. [\[CrossRef\]](#) [\[PubMed\]](#)
12. Kalishwaralal, K.; Barath Mani Kanth, S.; Pandian, S.R.K.; Deepak, V.; Gurunathan, S. Silver nanoparticles impede the biofilm formation by *Pseudomonas* sp and *Staphylococcus epidermidis*. *Colloids Surf.* **2010**, *79*, 340–344. [\[CrossRef\]](#) [\[PubMed\]](#)
13. Panacek, A.; Kvitek, L.; Prucek, R.; Kolar, M.; Vecerova, R.; Pizurova, N.; Sharma, V.K.; Nevecna, T.; Zboril, R. Silver colloid nanoparticles: Synthesis, characterization, and their antibacterial activity. *J. Phys. Chem.* **2006**, *110*, 6248–6253. [\[CrossRef\]](#) [\[PubMed\]](#)
14. Jones, S.A.; Bowler, P.G.; Walker, M.; Parsons, D. Controlling wound bio burden with a novel silver containing hydrofiber dressing. *Wound Repair Regen.* **2004**, *12*, 288–294. [\[CrossRef\]](#) [\[PubMed\]](#)
15. Duran, N.; Marcato, D.P.; Alves, L.O.; de Souza, G.; Esposito, E. Mechanical aspect of biosynthesis of silver nanoparticles by several *Fusarium oxysporum* strains. *J. Nanobiotechnol.* **2005**, *3*, 8–15. [\[CrossRef\]](#) [\[PubMed\]](#)
16. Kalimuthu, K.; Babu, R.S.; Venkataraman, D.; Bilal, M.; Gurunathan, S. Biosynthesis of silver nanocrystals by *Bacillus licheniformis*. *Colloids Surf.* **2008**, *65*, 150–153. [\[CrossRef\]](#)



17. Nangia, Y.; Wangoo, N.; Goyal, N.; Shekhawat, G.; Suri, C.R. A novel bacterial isolate *Stenotrophomonas maltophilia* as living factory for synthesis of gold nanoparticles. *Microb. Cell Factories* **2009**, *8*, 39. [\[CrossRef\]](#)
18. Eckhardt, S.; Brunetto, P.S.; Gagnon, J.; Priebe, M.; Giese, B.; Fromm, K.M. Nanobio silver: Its interactions with peptides and bacteria, and its uses in medicine. *Chem. Rev.* **2013**, *113*, 4708–4754. [\[CrossRef\]](#)
19. Hulkoti, N.I.; Taranath, T.C. Biosynthesis of nanoparticles using microbes—A review. *Colloids Surf. Biointerfaces* **2014**, *121*, 474–483. [\[CrossRef\]](#)
20. Pucciarelli, S.; Devaraj, R.R.; Mancini, A.; Ballarini, P.; Castelli, M.; Schrallhammer, M.; Petroni, G.; Miceli, C. Microbial Consortium Associated with the Antarctic Marine Ciliate *Euplotes focardii*: An Investigation from Genomic Sequences. *Microb. Ecol.* **2015**, *70*, 484–497. [\[CrossRef\]](#)
21. Ramasamy, K.P.; Telatin, A.; Mozzicafreddo, M.; Miceli, C.; Pucciarelli, S. Draft Genome Sequence of a New *Pseudomonas* sp. Strain, ef1, Associated with the Psychrophilic Antarctic Ciliate *Euplotes Focardii*. *Microbiol. Resour. Announc.* **2019**, *10*, 8. [\[CrossRef\]](#) [\[PubMed\]](#)
22. Pucciarelli, S.; La Terza, A.; Ballarini, P.; Barchetta, S.; Yu, T.; Marziale, F.; Passini, V.; Methé, B.; Detrich, H.W., 3rd; Miceli, C. Molecular cold-adaptation of protein function and gene regulation: The case for comparative genomic analyses in marine ciliated protozoa. *Mar. Genom.* **2009**, *2*, 57–66. [\[CrossRef\]](#) [\[PubMed\]](#)
23. Quinteros, M.A.; Aiassa Martínez, I.M.; Dalmasso, P.R.; Páez, L.R. Silver Nanoparticles: Biosynthesis Using an ATCC Reference Strain of *Pseudomonas* sp and Activity as Broad Spectrum Clinical Antibacterial Agents. *Int. J. Biomater.* **2016**, *2016*, 1–7. [\[CrossRef\]](#) [\[PubMed\]](#)
24. Wang, C.; Kim, Y.J.; Singh, P.; Mathiyalagan, R.; Jin, Y.; Yang, D.C. Green synthesis of silver nanoparticles by *Bacillus methylotrophicus*, and their antimicrobial activity. *Artif. Cells Nanomed. Biotechnol.* **2015**, *6*, 1–6.
25. Alani, F.; Moo-Young, M.; Anderson, W. Biosynthesis of silver nanoparticles by a new strain of *Streptomyces* sp. compared with *Aspergillus fumigatus*. *World J. Microbiol. Biotechnol.* **2012**, *28*, 1081–1086. [\[CrossRef\]](#)
26. Ahmad, A.; Mukherjee, P.; Senapati, S.; Mandal, D.; Khan, M.I.; Kumar, R. Extracellular biosynthesis of silver nanoparticles using the fungus *Fusarium oxysporum*. *Colloids Surf.* **2003**, *28*, 313–318. [\[CrossRef\]](#)
27. Duran, N.; Marcato, P.D.; Souza, G.; Alves, G.O.L.; Esposito, E. Antibacterial Effect of Silver Nanoparticles Produced by Fungal Process on Textile Fabrics and Their Effluent Treatment. *J. Biomed. Nanotechnol.* **2007**, *3*, 203–208. [\[CrossRef\]](#)
28. Mulvaney, P. Surface plasmon spectroscopy of nanosized metal particles. *Langmuir* **1996**, *12*, 788–800. [\[CrossRef\]](#)
29. Sastry, M.; Patil, V.; Sainkar, S.R. Electrostatically controlled diffusion of carboxylic acid derivatized silver colloidal particles in thermally evaporated fatty amine films. *J. Phys. Chem.* **1998**, *102*, 1404–1410. [\[CrossRef\]](#)
30. Henglein, A. Physicochemical properties of small metal particles in solution: “Microelectrode” reactions, chemisorption, composite metal particles, and the atom-to-metal transition. *J. Phys. Chem.* **1993**, *97*, 5457–5471. [\[CrossRef\]](#)
31. Ravindra, B.K.; Rajasab, A.H. A comparative study on biosynthesis of silver nanoparticles using four different fungal species. *Int. J. Pharm. Pharm. Sci.* **2014**, *6*, 372–376.
32. Thamilselvi, V.; Radha, K.V. Synthesis of silver nanoparticles from *Pseudomonas putida* ncim 2650 in silver nitrate supplemented growth medium and optimization using response surface methodology. *Dig. J. Nanomater. Biostruct.* **2013**, *8*, 1101–1111.
33. Ramalingam, V.; Rajaram, R.; Prem Kumar, C.; Santhanam, P.; Dhinesh, P.; Vinothkumar, S.; Kaleshkumar, K. Biosynthesis of silver nanoparticles from deep sea bacterium *Pseudomonas* sp JQ989348 for antimicrobial, antibiofilm, and cytotoxic activity. *J. Basic Microbiol.* **2014**, *54*, 928–936. [\[CrossRef\]](#) [\[PubMed\]](#)
34. Rammohan, M.; Balakrishnan, K. Rapid Synthesis and Characterization of Silver Nano Particles by Novel *Pseudomonas* sp. “ram bt-1”. *J. Ecobiotechnol.* **2011**, *3*, 24–28.
35. Kanchana, A.; Agarwal, I.; Sunkar, S.; Nellore, J.; Namasivayam, K. Biogenic silver nanoparticles from *Spinacia oleracea* and *Lactuca sativa* and their potential antimicrobial activity. *Dig. J. Nanomater. Biostruct.* **2011**, *6*, 1741–1750.
36. Shivakrishna, P.; Ram Prasad, M.; Krishna, G.; Singara Charya, M.A. Synthesis of Silver Nano Particles from Marine Bacteria *Pseudomonas aeruginosa*. *Octa J. Biosci.* **2013**, *1*, 108–114.
37. Busi, S.; Rajkumari, J.; Ranjan, B.; Karuganti, S. Green rapid biogenic synthesis of bioactive silver nanoparticles (AgNPs) using *Pseudomonas* sp. ET. *Nanobiotechnol.* **2014**, *8*, 267–274. [\[CrossRef\]](#)

38. Shahverdi, A.R.; Minaeian, S.; Shahverdi, H.R.; Jamalifar, H.; Nohi, A.A. Rapid synthesis of silver nanoparticles using culture supernatants of Enterobacteria: A novel biological approach. *Process. Biochem.* **2007**, *42*, 919–923. [\[CrossRef\]](#)
39. Das, V.L.; Thomas, R.; Varghese, R.T.; Soniya, E.V.; Mathew, J.; Radhakrishnan, E.K. Extracellular synthesis of silver nanoparticles by the *Bacillus* strain CS 11 isolated from industrialized area. *Biotech* **2014**, *4*, 121–126. [\[CrossRef\]](#)
40. Dipak, P.; Narayan Sinha, S. Extracellular Synthesis of Silver Nanoparticles Using *Pseudomonas* sp KUPSB12 and Its Antibacterial Activity. *Jordan J. Biol. Sci.* **2014**, *7*, 245–250.
41. Klaus, T.; Joerger, R.; Olsson, E.; Granquist, C.G. Silver based crystalline nanoparticles, microbially fabricated. *Proc. Natl. Acad. Sci. USA* **1999**, *96*, 13611–13614. [\[CrossRef\]](#) [\[PubMed\]](#)
42. Nair, B.; Pradeep, T. Coalescence of nanoclusters and formation of sub-micron crystallites assisted by *Lactobacillus* strains. *Cryst. Growth Des.* **2002**, *4*, 295–298.
43. Gopinath, V.; Priyadarshini, S.; FaiLoke, M.; Arunkumar, J.; Marsili, E.; Mubarak, D.; Vadivelu, A.J. Biogenic synthesis, characterization of antibacterial silver nanoparticles and its cell cytotoxicity. *Arab. J. Chem.* **2017**, *10*, 1107–1117. [\[CrossRef\]](#)
44. Magudapatty, P.; Gangopadhyay, P.; Panigrahi, B.K.; Nair, K.G.M.; Dhara, S. Electrical transport studies of Ag nanoclusters embedded in glass matrix. *Phys. B Condens. Matter* **2001**, *299*, 142–146. [\[CrossRef\]](#)
45. Kaviya, S.; Santhanalakshmi, J.; Viswanathan, B.; Muthumany, J.; Srinivasan, K. Biosynthesis of silver nanoparticles using citrus sinensis peel extract and its antibacterial activity. *Spectrochim. Acta Part A* **2011**, *79*, 594–598. [\[CrossRef\]](#)
46. Syed, B.; Prasad, N.; Dhananjaya, M.N.; Mohan, B.L.; Kumar, K.; Yallappa, S.; Satish, S. Synthesis of silver nanoparticles by endosymbiont *Pseudomonas fluorescens* CA 417 and their bactericidal activity. *Enzym. Microb. Technol.* **2016**, *95*, 128–136. [\[CrossRef\]](#)
47. Barth, A. Infrared spectroscopy of proteins. *BBA- Bioenerg.* **2007**, *1767*, 1073–1101. [\[CrossRef\]](#)
48. Baker, M.J.; Hussain, S.R.; Lovergne, L.; Untereiner, V.; Hughes, C.; Lukaszewski, R.A.; Thiéfin, G.; Sockalingum, G.D. Developing and understanding biofluid vibrational spectroscopy: A critical review. *Chem. Soc. Rev.* **2017**, *45*, 1803–1818. [\[CrossRef\]](#)
49. Gole, A.; Dash, C.; Ramakrishnan, V.; Sainkar, S.R.; Mandale, A.B.; Rao, M.; Sastry, M. Pepsin—Gold Colloid Conjugates: Preparation, Characterization, and Enzymatic Activity. *Langmuir* **2001**, *17*, 1674–1679. [\[CrossRef\]](#)
50. Babu, M.M.G.; Gunasekaran, P. Production and structural characterization of crystalline silver nanoparticles from *Bacillus cereus* isolate. *Colloids Surf.* **2009**, *74*, 191–195. [\[CrossRef\]](#)
51. Balaji, D.S.; Basavaraja, S.; Deshpande, R.; Mahesh, D.; Prabhakar, B.K.; Venkataraman, A. Extracellular biosynthesis of functionalized silver nanoparticles by strains of *Cladosporium cladosporioides* fungus. *Colloids Surf. B* **2009**, *68*, 88–92. [\[CrossRef\]](#) [\[PubMed\]](#)
52. Afreen, R.V.; Rathod, V.; Ranganath, E. Synthesis of monodispersed silver nanoparticles by *Rhizopus stolonifer* and its antibacterial activity against MDR strains of *Pseudomonas* sp from burnt patients. *Int. J. Environ. Sci.* **2011**, *1*, 1582–1592.
53. Sathyavathi, R.; Krishna, M.B.M.; Rao, S.V.; Saritha, R.; Rao, D.N. Biosynthesis of silver nanoparticles using coriandrum sativum leaf extract and their application in nonlinear optics. *Adv. Sci. Lett.* **2010**, *3*, 1–6. [\[CrossRef\]](#)
54. Mickymaray, S. One-step Synthesis of Silver Nanoparticles Using Saudi Arabian Desert Seasonal Plant *Sisymbrium irio* and Antibacterial Activity Against Multidrug-Resistant Bacterial Strains. *Biomolecules* **2019**, *9*, 662. [\[CrossRef\]](#)
55. Shaik, M.R.; Khan, M.; Kuniyil, M.; Al-Warthan, A.; Alkhathlan, H.Z.; Siddiqui, M.R.H.; Shaik, J.P.; Ahamed, A.; Mahmood, A.; Khan, M.; et al. Plant-Extract-Assisted Green Synthesis of Silver Nanoparticles Using *Origanum vulgare* L. Extract and Their Microbicidal Activities. *Sustainability* **2018**, *10*, 913.
56. Das, G.; Patra, J.K.; Debnath, T.; Ansari, A.; Shin, H.-S. Investigation of antioxidant, antibacterial, antidiabetic, and cytotoxicity potential of silver nanoparticles synthesized using the outer peel extract of *Ananas comosus* (L.). *PLoS ONE* **2019**, *14*, e0220950. [\[CrossRef\]](#)
57. Bibi, N.; Ali, Q.; Tanveer, Z.I.; Rahman, H.; Anees, M. Antibacterial efficacy of silver nanoparticles prepared using *Fagonia cretica* L. leaf extract. *Inorgan. Nano-Met. Chem.* **2019**, *49*, 260–266. [\[CrossRef\]](#)

58. Priyadarshini, S.; Gopinath, V.; Priyadharsshini, N.M.; Mubarak, A.D.; Velusamy, P. Synthesis of anisotropic silver nanoparticles using novel strain, *Bacillus flexus* and its biomedical application. *Colloids Surf.* **2013**, *102*, 232–237. [\[CrossRef\]](#)
59. Lin, Y.S.E.; Vidic, R.D.; Stout, J.E.; McCartney, C.A.; Yu, V.L. Inactivation of *Mycobacterium avium* by copper and silver ions. *Water Res.* **1998**, *32*, 1997–2000. [\[CrossRef\]](#)
60. Rai, M.; Yadav, A.; Gade, A. Silver nanoparticles as a new generation of antimicrobials. *Biotechnol. Adv.* **2009**, *27*, 76–83. [\[CrossRef\]](#)
61. Natalello, A.; Mangione, P.P.; Giorgetti, S.; Porcari, R.; Marchese, L.; Zorzoli, I.; Relini, A.; Ami, D.; Faravelli, G.; Valli, M.; et al. Co-fibrillogenesis of Wild-type and D76N  $\beta$ 2-Microglobulin: THE CRUCIAL ROLE OF FIBRILLAR SEEDS. *J. Biol. Chem.* **2016**, *291*, 9678–9689. [\[CrossRef\]](#) [\[PubMed\]](#)
62. Mancini, A.; Pucciarelli, S. Antibiotic activity of the antioxidant drink effective Microorganism-X (EM-X) extracts against common nosocomial pathogens: An in vitro study. *Nat. Prod. Res.* **2018**, *4*, 1–6. [\[CrossRef\]](#) [\[PubMed\]](#)



© 2020 by the authors. Licensee MDPI, Basel, Switzerland. This article is an open access article distributed under the terms and conditions of the Creative Commons Attribution (CC BY) license (<http://creativecommons.org/licenses/by/4.0/>).



## Article

# New Discorhabdin Alkaloids from the Antarctic Deep-Sea Sponge *Latrunculia biformis*

Fengjie Li <sup>1</sup>, Christian Peifer <sup>2</sup>, Dorte Janussen <sup>3</sup> and Deniz Tasdemir <sup>1,4,\*</sup>
<sup>1</sup> GEOMAR Centre for Marine Biotechnology (GEOMAR-Biotech), Research Unit Marine Natural Products Chemistry, GEOMAR Helmholtz Centre for Ocean Research Kiel, Am Kiel-Kanal 44, 24106 Kiel, Germany

<sup>2</sup> Pharmaceutical Chemistry, Kiel University, Gutenbergstraße 76, 24118 Kiel, Germany

<sup>3</sup> Senckenberg Research Institute and Natural History Museum, Senckenberganlage 25, D-60325 Frankfurt, Germany

<sup>4</sup> Faculty of Mathematics and Natural Sciences, Kiel University, Christian-Albrechts-Platz 4, 24118 Kiel, Germany

\* Correspondence: dtasdemir@geomar.de; Tel.: +49-431-600-4430

Received: 14 June 2019; Accepted: 22 July 2019; Published: 25 July 2019

**Abstract:** The sponge genus *Latrunculia* is a prolific source of discorhabdin type pyrroloiminoquinone alkaloids. In the continuation of our research interest into this genus, we studied the Antarctic deep-sea sponge *Latrunculia biformis* that showed potent in vitro anticancer activity. A targeted isolation process guided by bioactivity and molecular networking-based metabolomics yielded three known discorhabdins, (–)-discorhabdin L (**1**), (+)-discorhabdin A (**2**), (+)-discorhabdin Q (**3**), and three new discorhabdin analogs (–)-2-bromo-discorhabdin D (**4**), (–)-1-acetyl-discorhabdin L (**5**), and (+)-1-octacosatrienoyl-discorhabdin L (**6**) from the MeOH-soluble portion of the organic extract. The chemical structures of **1–6** were elucidated by extensive NMR, HR-ESIMS, FT-IR,  $[\alpha]_D$ , and ECD (Electronic Circular Dichroism) spectroscopy analyses. Compounds **1**, **5**, and **6** showed promising anticancer activity with IC<sub>50</sub> values of 0.94, 2.71, and 34.0  $\mu$ M, respectively. Compounds **1–6** and the enantiomer of **1** ((+)-discorhabdin L, **1e**) were docked to the active sites of two anticancer targets, topoisomerase II- $\alpha$  and indoleamine 2,3-dioxygenase (IDO1), to reveal, for the first time, the binding potential of discorhabdins to these proteins. Compounds **5** and **6** are the first discorhabdin analogs with an ester function at C-1 and **6** is the first discorhabdin bearing a long-chain fatty acid at this position. This study confirms *Latrunculia* sponges to be excellent sources of chemically diverse discorhabdin alkaloids.

**Keywords:** *Latrunculia*; Antarctica; deep-sea sponge; molecular networking; molecular docking; discorhabdin

## 1. Introduction

*Latrunculia* species are cold-adapted sponges commonly found in the coastlines of the southern hemisphere [1–3]. The genus *Latrunculia* has proven to be a prolific source of structurally intriguing compounds from different classes, such as norsesterterpenes [4,5], callipeltins [6,7], and various types of pyrroloiminoquinone alkaloids [8–10]. Discorhabdins represent a large and unique subclass of pyrroloiminoquinone alkaloids that have been associated with the chemical defense and greenish to brownish coloration of the sponge [11,12]. Discorhabdins exhibit strong anticancer activity against many cancer types, such as human colon cancer, adenocarcinoma, and leukemia [13–15]. However, the mechanism of their anticancer action has been poorly studied. Indeed, only the farnesyltransferase enzyme [16] and hypoxia-inducible factor 1 $\alpha$  (HIF-1 $\alpha$ ) and transcriptional coactivator p300 interaction [17] have been shown as potential targets of discorhabdins.

As part of our research interest into deep-sea *Latrunculia* sponges from Antarctica [18], herein we investigated the in-depth chemistry of *Latrunculia biformis*, which was collected from the Antarctic Weddell Sea shelf at 291 m depth. The crude organic extract of the sponge exhibited significant in vitro anticancer activity against six cancer cell lines. A molecular networking (MN)-based metabolomics study on fractions obtained from the MeOH-soluble portion of the sponge indicated the presence of a large discorhabdin cluster with many nodes belonging to potentially new discorhabdins. Guided by anticancer activity and MN-based dereplication, six discorhabdin-type alkaloids were isolated from the MeOH subextract, including three known compounds (–)-discorhabdin L (1), (+)-discorhabdin A (2), (+)-discorhabdin Q (3) and three new discorhabdin derivatives, namely (–)-2-bromo-discorhabdin D (4), (–)-1-acetyl-discorhabdin L (5), and (+)-1-octacosatrienoyl-discorhabdin L (6). Since the amounts of the isolated compounds were very minor, only compounds 1, 5 and 6 could be tested for their anticancer activity against the human colon cancer cell line HCT-116. We applied a structure-based docking approach on all isolated compounds and the enantiomer of 1 (1e) against two cancer targets reported for pyrroloiminoquinone alkaloids, i.e., topoisomerase I–II and indoleamine 2,3-dioxygenase IDO1 [19–21] to predict their anticancer potential and to suggest potential molecular mechanism(s) of action. This study reports MN and bioactivity-guided isolation of compounds 1–6, their structure elucidation, and biological activities with potential target identification for their anticancer activity.

## 2. Results

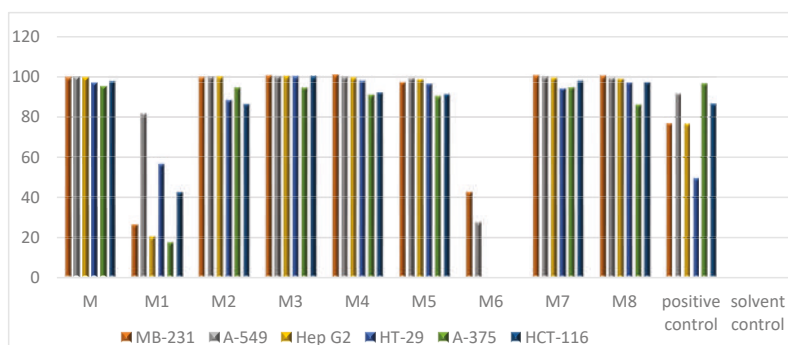
### 2.1. Bioactivity and Molecular Networking-guided Purification and Structural Elucidation

The olive green-colored sponge material was freeze-dried and successively extracted with water, MeOH, and dichloromethane (DCM) subsequently. The combined organic extract was submitted to bioactivity screening against six cancer cell lines, where it showed significant activity with IC<sub>50</sub> values ranging from 4.0 to 56.2 µg/mL (Table 1). The solvent partitioning of the crude organic extract between MeOH and *n*-hexane yielded the MeOH (M) and the *n*-hexane subextracts. The M subextract demonstrated strong anticancer activity (Figure 1) and was further fractionated over a C18 SPE cartridge. The anticancer activity was tracked to six SPE fractions, M2–M5, M7, and M8 (Figure 1).

**Table 1.** Anticancer activity of the *L. biformis* crude extract. The IC<sub>50</sub> values are in µg/mL. Positive control doxorubicine.

Sample	A-375	HCT-116	A-549	MB-231	Hep G2	HT-29
Crude extract	17.4	4.8	56.2	46.8	18.2	4.0
Positive control	0.13	10.6	31.4	15.2	14.6	3.0

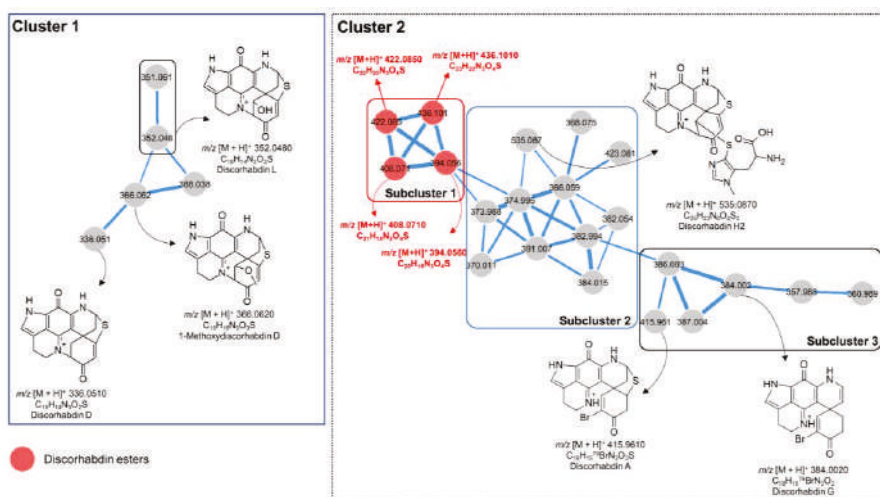
In order to prioritize the isolation workflow towards undescribed molecules with potential anticancer properties, we acquired tandem UPLC-QToF-MS/MS (positive-ion mode) data on these six active fractions. The generated MS/MS (MS<sup>2</sup>) data were uploaded to the publicly available Global Natural Product Social Molecular Networking (GNPS) platform (<http://gnps.ucsd.edu>) and analyzed following the molecular networking (MN) online workflow [22]. Software Cytoscape (Version 3.61) was used to visualize the resulting networks. The automated dereplication on GNPS platform did not annotate any pyrroloiminoquinone alkaloids. Hence, compound annotation was based on manual dereplication by comparing the predicted molecular formulae against multiple public or commercially available databases.



**Figure 1.** In vitro activity of MeOH subextract (M) and its C18 solid phase extraction (SPE) fractions (M1–M8) against six cancer cell lines. Test concentration: 100  $\mu\text{g/mL}$ . Positive control: Doxorubicine. Solvent control: 0.5% DMSO.

After a comprehensive examination of the global MN of the SPE fractions, two clusters attracted our attention (Figure 2). Cluster 1 contained five nodes, four of which were annotated as known molecules discorhabdin L [13], its analog, discorhabdin D [23], and 1-methoxydiscorhabdin D [19], leaving the node at  $m/z$  368.0380 to be a putatively new derivative (Figure 2). From this cluster, we were able to purify (–)-discorhabdin L (1), but failed to purify the potentially new discorhabdin analog ( $m/z$  368.0380) due to its very minor quantity.

With 21 nodes, cluster 2 was the biggest in the generated MN, which can be further divided into three subclusters (Figure 2). Based on the elemental composition analysis, MS/MS fragmentation patterns, and biological source, two brominated alkaloids discorhabdin A [24] and discorhabdin G [25] were identified in subcluster 3. However, only discorhabdin A (2) was isolated in sufficient amounts for NMR and other spectroscopic analyses. Discorhabdin H2 [26] was the only annotated compound in subcluster 2. Unfortunately, neither this compound nor the remaining nodes that represent potentially new discorhabdin analogs could be purified in sufficient quantity.



**Figure 2.** Molecular cluster observed in SPE fractions of *L. bififormis* MeOH subextract. Numbers within the nodes indicate parent ions, and edge thickness represents the cosine similarity between nodes. Red nodes: Discorhabdin esters; Grey nodes: Other discorhabdin analogs.

The subcluster 1 (of cluster 2) contained four nonbrominated nodes at  $m/z$  394.0560, 408.0710, 422.085, and 436.1010 connected with thick edges, indicating their high structural similarity. Elemental composition analysis revealed the difference of a  $\text{CH}_2$  unit between these ions (Figure 2, in red). In-depth analysis of their MS/MS spectra revealed the presence of the same MS fragment ( $m/z$  352.0766,  $\text{C}_{18}\text{H}_{14}\text{N}_3\text{O}_3\text{S}$ ) in all four compounds, suggesting these compounds to be discorhabdin alkaloids bearing an alkyl chain with varying lengths. From subcluster 1, we isolated the compound with  $m/z$  394.0560 and identified it as a new metabolite, (–)-1-acetyl-discorhabdin L (5), as discussed later.

In addition, we purified three compounds, namely the known compound (+)-discorhabdin Q (3) as well as two new compounds, namely (–)-2-bromo-discorhabdin D (4) and (+)-1-octacosatrienoyl-discorhabdin L (6), which did not appear in the MN because of the low intensity of their MS fragments. The enantiopurity of all purified compounds was further checked individually by RP-DAD-HPLC on an analytical chiral column. The sharp single peak in the UV chromatograms confirmed the enantiopurity of 1–6.

The structure of compound 1 was elucidated as (–)-(1*R*,2*S*,6*R*,8*S*)-discorhabdin L [13], based on comparison of its 1D and 2D NMR data including NOESY spectrum (Tables 2 and 3, Supplementary Figures S1–S6). The specific rotation of compound 1 ( $[\alpha]^{20}_{\text{D}} = -71$ ,  $c$  0.1, MeOH) showed the same sign as that reported for (–)-discorhabdin L ( $[\alpha]^{20}_{\text{D}} = -240$ ,  $c$  0.0125, MeOH) [26]. In order to confirm the absolute configuration of compound 1, the ECD (Electronic Circular Dichroism) spectrum was run. The experimental ECD spectrum of 1 (Supplementary Figure S8) was essentially identical to the ECD spectrum of (–)-(1*R*,2*S*,6*R*,8*S*)-discorhabdin L [26]. Hence, compound 1 was unambiguously characterized as (–)-(1*R*,2*S*,6*R*,8*S*)-discorhabdin L.

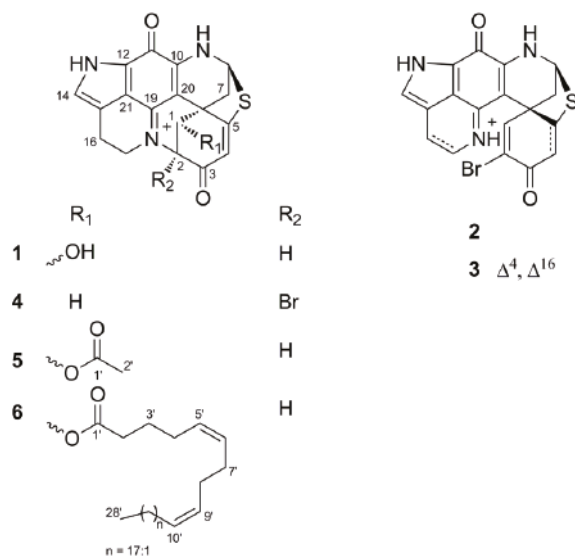


Figure 3. Chemical structures of compounds 1–6.

Compound 2 exhibited the same  $^1\text{H}$  and  $^{13}\text{C}$  NMR resonances (Supplementary Figures S9 and S10) as (+)-discorhabdin A [24,27]. The analysis of its COSY, HSQC, and HMBC spectra (Supplementary Figures S10–S12) supported the same planar structure as discorhabdin A and NOESY spectrum confirmed the relative configuration of three stereocenters (Supplementary Figure S13). The specific rotation of compound 2 ( $[\alpha]^{20}_{\text{D}} = +197$ ,  $c$  0.01, MeOH) exhibited the same sign as (+)-discorhabdin A ( $[\alpha]^{20}_{\text{D}} = +400$ ,  $c$  0.05, MeOH) [24]. An early X-ray crystal analysis has confirmed the configuration of



the chiral centers within (+)-discorhabdin A as 5R,6S,8S [27]. Thus, compound **2** was identified as (+)-(5R,6S,8S)-discorhabdin A (Figure 3).

Compound **3** was identified as the known compound discorhabdin Q, based on its 1D and 2D NMR data (Supplementary Figures S15–S20), which were in good agreement with those reported in the literature [26]. The examination of the  $^1\text{H}$ - $^1\text{H}$  NOESY spectrum of **3** (Supplementary Figure S19) allowed the assignment of the relative configuration of two stereocenters. Compound **3** exhibited a specific rotation value ( $[\alpha]^{20}_{\text{D}} = +568$ ,  $c$  0.1, MeOH), which was similar both in the magnitude and sign to that observed for (+)-(6S,8S)-discorhabdin Q ( $[\alpha]^{20}_{\text{D}} = +720$ ,  $c$  0.025, MeOH) [26], hence we concluded compound **3** as (+)-(6S,8S)-discorhabdin Q.

**Table 2.**  $^1\text{H}$  NMR data of compounds **1**, **4**, **5**, and **6** in  $\text{CD}_3\text{OD}$  (trifluoroacetic acid (TFA) salts, 600 MHz,  $\delta$  in ppm).

NO.	1	4	5	6
	$\delta_{\text{H}}$ , Mult. (J in Hz)	$\delta_{\text{H}}$ , Mult. (J in Hz)	$\delta_{\text{H}}$ , Mult. (J in Hz)	$\delta_{\text{H}}$ , Mult. (J in Hz)
1	4.63 d (3.6)	3.58 d (13.3)	5.79 d (3.6)	5.79 d (3.6)
2	4.15 d (3.6)	3.23 d (13.3)		
4	6.14 s	6.14 s	4.36 d (3.6)	4.35 d (3.6)
7 $\alpha$	2.57 dd (1.3, 12.0)	2.66 dd (1.5, 12.1)	6.23 s	6.23 s
7 $\beta$	2.96 dd (3.6, 12.0)	2.84 dd (3.5, 12.1)	2.63 dd (1.4, 12.1)	2.64 d (1.2, 12.1)
8	5.59 dd (1.3, 3.6)	5.68 dd (1.5, 3.5)	2.81 dd (3.7, 12.1)	2.76 dd (3.6, 12.1)
14	7.11 s	7.14 s	5.61 dd (1.4, 3.7)	5.61 dd (1.2, 3.6)
16	3.19 ddd (7.5, 13.0, 16.7)	3.10 m	7.13 s	7.13 s
	3.06 ddd (3.0, 6.9, 16.7)		3.21 ddd (6.9, 7.5, 16.6)	3.22 ddd (6.8, 7.3, 16.6)
17	4.02 ddd (3.0, 7.5, 14.2)	4.62 ddd (2.1, 5.6, 13.8)	3.08 ddd (2.9, 6.9, 16.6)	3.08 ddd (2.7, 6.8, 16.6)
	3.91 ddd (6.9, 13.0, 14.2)	3.66 td (6.3, 13.8)	4.04 ddd (2.9, 7.5, 13.8)	4.04 ddd (2.7, 7.3, 13.7)
2'	-	-	3.93 td (6.9, 13.8)	3.93 td (6.8, 13.7)
3'	-	-	2.15 s	2.44 td (1.5, 7.5)
4'	-	-	-	1.69 m
5'	-	-	-	2.10 m
6'	-	-	-	5.34 m
7'	-	-	-	5.44 m
8'	-	-	-	2.08 m
9'	-	-	-	2.08 m
10'	-	-	-	5.37 m
11'-27'	-	-	-	5.34 m
				1.25–1.40 m;
28'	-	-	-	2.00–2.06 m; 5.36 m
				0.90 t (7.0)

Compound **4** was obtained as a greenish film. The isotopic pattern of the molecule ion peaks (1:1 ratio) was indicative for the presence of one bromine atom in this molecule. The molecular formula of  $\text{C}_{18}\text{H}_{13}^{79}\text{BrN}_3\text{O}_2\text{S}$  was established by the pseudo-molecular ion peak at  $m/z$  413.9913  $[\text{M} + \text{H}]^+$  in the HR-ESIMS (Supplementary Figure S27) spectrum, requiring 14 degrees of unsaturation. The  $^1\text{H}$  NMR data (Table 2, Supplementary Figure S22) together with HSQC spectrum (Supplementary Figure S23) revealed the presence of three methine resonances at  $\delta_{\text{H}}$  7.14 (H-14, s),  $\delta_{\text{H}}$  6.14 (H-4, s), and  $\delta_{\text{H}}$  5.68 (H-8, dd,  $J = 1.5, 3.5$  Hz), four methylene groups corresponding to H<sub>2</sub>-17 ( $\delta_{\text{H}}$  3.66 and 4.62), H<sub>2</sub>-1 ( $\delta_{\text{H}}$  3.23 and 3.58), H<sub>2</sub>-16 ( $\delta_{\text{H}}$  3.10), and H<sub>2</sub>-7 ( $\delta_{\text{H}}$  2.66 and 2.84). The  $^{13}\text{C}$  NMR spectrum (Table 3) showed 18 carbon signals including 4 methylenes ( $\delta_{\text{C}}$  20.0, 38.7, 42.4, and 50.2), 3 methines ( $\delta_{\text{C}}$  63.1, 110.9, and 126.0), and 11 quaternary carbons ( $\delta_{\text{C}}$  44.5, 78.1, 100.4, 119.3, 122.2, 124.0, 148.2, 150.2, 165.4, 172.8, and 176.4). By comparison with the data reported for discorhabdins [13,23], the three low-field quaternary carbon signals at  $\delta_{\text{C}}$  176.4, 172.8, and 165.4 were tentatively assigned to C-3, C-5, and C-11, respectively, while the high-field quaternary carbon at  $\delta_{\text{C}}$  44.5 was assigned to C-6. The COSY correlation between H<sub>2</sub>-16 and H<sub>2</sub>-17, together with the additional  $^1\text{H}$  -  $^{13}\text{C}$  HMBC correlations between H-14/C-12, C-21, C-11; H<sub>2</sub>-16/C-14, C-21; H<sub>2</sub>-17/C-15, C-19 confirmed the pyrroloiminoquinone motif [13,23]. Similarly, the homonuclear COSY correlation between H<sub>2</sub>-7 and H-8, and the HMBC correlations between H<sub>2</sub>-1/C-2, C-3, C-6, C-20; H-4/C-2, C-3, C-6; and H<sub>2</sub>-7/C-5, C-6, C-20 suggested the position of the carbonyl group

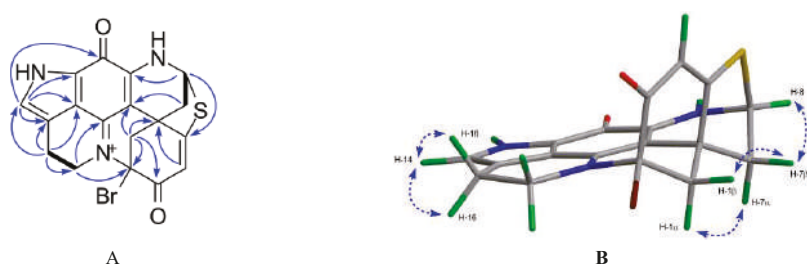
( $\delta_C$  176.4) at C-3, and the position of the methylene ( $\delta_C$  42.4) at C-1 (Figure 4A). A further HMBC coupling between H-8 and C-5 was indicative of a thioether bridge between C-8 and C-5, while the HMBC correlation between H<sub>2</sub>-17 and C-2 established the bridge between N-18 and C-2 (Figure 4A). All these data, plus the lack of any further spin coupling observed for H<sub>2</sub>-1, allowed the placement of the bromine atom on the remaining quaternary carbon, C-2. Thus the planar structure of compound 4 was elucidated as 2-bromo-discorhabdin D.

**Table 3.**  $^{13}\text{C}$  NMR data of compounds 1, 4, 5, and 6 in  $\text{CD}_3\text{OD}$  (150 MHz,  $\delta$  in ppm).

Position	1	4	5	6
	$\delta_C$	$\delta_C^a$	$\delta_C$	$\delta_C$
1	68.5 (CH)	42.4 (CH <sub>2</sub> )	69.6 (CH)	69.5 (CH)
2	67.8 (CH)	78.1 (C)	64.6 (CH)	64.6 (CH)
3	184.8 (C)	176.4 (C)	183.1 (C)	183.0 (C)
4	114.1 (CH)	110.9 (CH)	114.4 (CH)	114.4 (CH)
5	171.5 (C)	172.8 (C)	171.2 (C)	171.1 (C)
6	48.6 (C)	44.5 (C)	47.0 (C)	47.1 (C)
7	37.4 (CH <sub>2</sub> )	38.7 (CH <sub>2</sub> )	37.4 (CH <sub>2</sub> )	37.5 (CH <sub>2</sub> )
8	63.7 (CH)	63.1 (CH)	63.5 (CH)	63.5 (CH)
10	148.6 (C)	148.2 (C)	149.0 (C)	149.1 (C)
11	167.5 (C)	165.4 (C)	167.1 (C)	167.1 (C)
12	125.6 (C)	124.0 (C)	125.6 (C)	125.6 (C)
14	127.2 (CH)	126.0 (CH)	127.4 (CH)	127.4 (CH)
15	119.2 (C)	119.3 (C)	119.4 (C)	119.4 (C)
16	20.6 (CH <sub>2</sub> )	20.0 (CH <sub>2</sub> )	20.7 (CH <sub>2</sub> )	20.7 (CH <sub>2</sub> )
17	52.8 (CH <sub>2</sub> )	50.2 (CH <sub>2</sub> )	52.9 (CH <sub>2</sub> )	52.9 (CH <sub>2</sub> )
19	150.3 (C)	150.2 (C)	150.4 (C)	150.4 (C)
20	101.8 (C)	100.4 (C)	100.6 (C)	100.6 (C)
21	122.7 (C)	122.2 (C)	122.7 (C)	122.7 (C)
1'	-		171.0 (C)	173.6 (C)
2'	-		20.4 (CH <sub>3</sub> )	34.0 (CH <sub>2</sub> )
3'	-		-	25.8 (CH <sub>2</sub> )
4'	-		-	27.5 (CH <sub>2</sub> )
5'	-		-	129.7 (CH)
6'	-		-	131.7 (CH)
7'	-		-	28.4 (CH <sub>2</sub> )
8'	-		-	28.4 (CH <sub>2</sub> )
9'	-		-	130.1 (CH)
10'	-		-	130.8 (CH)
				28.1–30.9 (CH <sub>2</sub> );
11'–25'	-		-	130.9 (CH);
				131.4 (CH)
26'	-		-	32.9 (CH <sub>2</sub> )
27'	-		-	23.7 (CH <sub>2</sub> )
28'	-		-	14.5 (CH <sub>3</sub> )

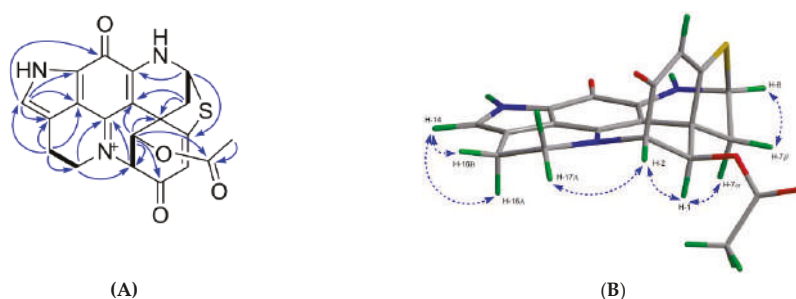
<sup>a</sup> Extracted from HSQC and HMBC spectra.

Compound 4 is a configurationally rigid molecule with seven rings and three stereocenters at C-2, C-6, and C-8. The relative configurations of these stereogenic centers were proposed by the NOE correlations as shown in Figure 4B. The specific rotation value of 4 ( $[\alpha]^{20}_D = -246$ ,  $c$  0.05, MeOH) is opposite to that of (+)-(2S,6R,8S)-discorhabdin D ( $[\alpha]^{20}_D = +80$ ,  $c$  0.025, MeOH) [26]. The experimental ECD spectrum of compound 4 (Supplementary Figure S8) showed the same cotton effects as compound 1 (–)-(1R,2S,6R,8S)-discorhabdin L. So it is reasonable to assume that compound 4 is (–)-(2R,6R,8S)-2-bromodiscorhabdin D.



**Figure 4.** Key 2D NMR correlations observed for compound 4. (A) The COSY (in bold), key H→C HMBC (arrows); (B) key H→H NOESY correlations (dashed line).

Compound 5 was obtained as a green film. Its molecular formula  $C_{20}H_{16}N_3O_4S$  was deduced by HR-ESIMS ( $m/z$  394.0816,  $[M + H]^+$ ) indicating 15 degrees of unsaturation. The FT-IR spectrum of compound 5 displayed the characteristic ester carbonyl absorption band at  $\nu_{\max}$  1747  $\text{cm}^{-1}$  and other similar bands as compound (1) at  $\nu_{\max}$  1653, 1621, 1560, 1528, 1412, and 1201  $\text{cm}^{-1}$ . The  $^1\text{H}$  and  $^{13}\text{C}$  NMR spectra of 5 (Tables 2 and 3) revealed high similarity with 1, with the only difference being the presence of an extra acetyl group in 5 ( $\delta_{\text{H}}$  2.15;  $\delta_{\text{C}}$  171.0 and  $\delta_{\text{C}}$  20.4). The site of esterification was identified as C-1, based on strong HMBC correlations between H-1/C-1' and a weaker HMBC coupling between H-2'/C-1 (Figure 5A). Thus, the planar structure of compound 5 was confirmed as 1-acetyl-disorhabdin L. The analysis of the full 2D NMR dataset (COSY, HSQC, and HMBC) further confirmed that the planar structure of compound 5 (Figure 5A). The relative configuration of compound 5 was elucidated by examining its NOESY spectrum (Figure 5B). The COSY correlation between H-4/H-7 (Supplementary Figure S32) indicated a planar "W" arrangement [28] of the molecule as observed in discorhabdins L [13] and D [23], thus allowing the assignment of the resonance at  $\delta_{\text{H}}$  2.63 to H-7 $\alpha$ . The stereochemistry at C-1 was proposed by the strong NOE correlation (Figure 5B) between H-1/H-7 $\alpha$ . To establish the absolute configuration of (–)-5, its experimental ECD spectrum was compared with that of (–)-(1R,2S,6R,8S)-discorhabdin L (1) (Supplementary Figure S8). The same Cotton effects observed at 290, 360, and 440 nm for both compounds established the absolute configuration of 5 as 1R,2S,6R,8S. Finally, the comparison of the specific rotation values of compounds 1 ( $[\alpha]_{\text{D}}^{20} = -71$ ,  $c$  0.1, MeOH) and 5 ( $[\alpha]_{\text{D}}^{20} = -420$ ,  $c$  0.01, MeOH) identified the structure of 5 as (–)-(1R,2S,6R,8S)-1-acetyl-disorhabdin L.

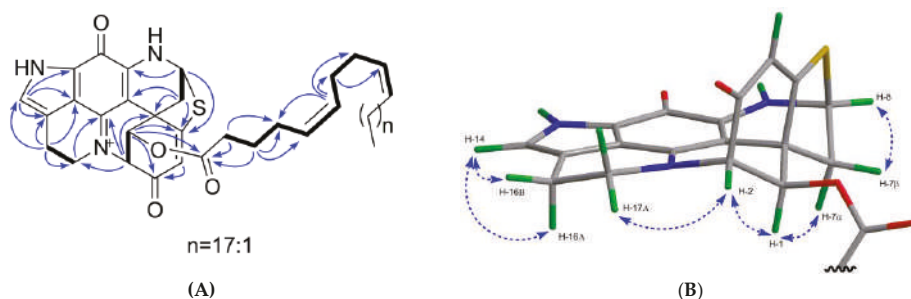


**Figure 5.** Key 2D NMR correlations observed for compound 5. (A) The COSY (in bold), key H→C HMBC (arrows); (B) key H→H NOESY correlations (dashed line).

The most nonpolar component, compound 6, was obtained as a green film with an  $[\alpha]_{\text{D}}^{20}$  value of + 541 ( $c$  0.1, MeOH). It showed a molecular ion peak at  $m/z$  752.4452  $[M + H]^+$  in the HR-ESIMS spectrum. The molecular formula of  $C_{46}H_{62}N_3O_4S$  was deduced from its  $^{13}\text{C}$  NMR and HR-ESIMS data (Table 3 and Supplementary Figure S41), indicating 18 degrees of unsaturation. The FT-IR spectrum contained absorption bands typical of an ester function ( $\nu_{\max}$  1739  $\text{cm}^{-1}$ ) and an alkyl chain ( $\nu_{\max}$  2927

and  $2855\text{ cm}^{-1}$ ,  $-\text{CH}_2$  and  $-\text{CH}_3$  stretching bands). Comparison of the 1D-NMR data of **6** with those of **1** and **5** (Tables 2 and 3) suggested **6** to be another analog of discorhabdin L esterified with a long chain fatty acid ( $\delta_{\text{C}}$  25–35 ppm;  $\delta_{\text{H}}$  1.2–1.4 ppm), which made this molecule very lipophilic. The discorhabdin L core structure that was evident from the 1D and 2D NMR data of **6** (Tables 2 and 3; Figure 6) accounted for 14 degrees of unsaturation. The additional ester carbonyl at  $\delta_{\text{C}}$  173.6 and six  $\text{sp}^2$  carbons belonging to three double bonds at  $\delta_{\text{C}}$  129.7, 130.1, 130.8, 130.9, 131.4, and 131.7 (Supplementary Figure S36) accounted for the remaining 4 degrees of unsaturation. Hence, we concluded that the alkyl chain was an unbranched octacosatriene-oic acid (28:3) (Tables 2 and 3). The HMBC correlation between H-1 ( $\delta_{\text{H}}$  5.79) and C-1' ( $\delta_{\text{C}}$  173.6) supported the attachment of the fatty acid at C-1 (Figure 6A). The geometry of these three double bonds in the fatty acid portion was elucidated by analyzing the  $^{13}\text{C}$  NMR chemical shifts of the six carbons neighboring the double bonds [29]. Carbon atoms adjacent to *cis* double bonds resonate around  $\delta_{\text{C}}$  26.0–28.5, whereas those adjacent to *trans* double bonds appear at higher chemical shift values, namely  $\delta_{\text{C}}$  29.5–38.0 [29]. The observed  $^{13}\text{C}$  NMR shifts in (+)-**6** at  $\delta_{\text{C}}$  27.5, 28.1, 28.2 ( $\times 2$ ), 28.4 ( $\times 2$ ) confirmed the *cis* (Z) configuration of all three double bonds in the fatty acid part (Table 3). The COSY correlations from C-2' to C-10' and HMBC correlations between  $\text{H}_2\text{-2'}/\text{C-1'}$ , C-4';  $\text{H}_2\text{-3'}/\text{C-1'}$ , C-4'; C-5';  $\text{H-6'}/\text{C-4'}$ , C-7'; C-8';  $\text{H}_2\text{-7'}/\text{C-9'}$  (Figure 6A) allowed us to corroborate the position of two unsaturations at C-5' and C-9', and to assign the C-1' to C-10' portion of the fatty acid (Figure 3). Comparison of the 1D NMR data of (+)-**6** with the literature [30] also supports the presence of a  $\Delta^{5,9}$  unsaturated fatty acid. This finding is not surprising since these *cis,cis*-5,9-dienoic lipids are common in sponges [31]. The chemical shift values of C-26', C-27' and C-28' (Table 3) were also assigned by comparison with the literature data [32]. Thus, compound (+)-**6** was identified as C-1 octacosatrienoic acid (C28:3) ester of (–)-discorhabdin L (Figure 3). Due to availability of very minor amount of the compound (0.2 mg) and the failed attempts to improve the highly overlapped NMR signals through different solvents (e.g., MeOD,  $\text{CDCl}_3$ , and  $\text{DMSO-}d_6$ ), we were unable to confirm the position of the third double bond. However, we believe that the lipid residue in **6** is related to the well-known 5Z,9Z demospongiac acids bearing another double bond at C-17, or C-19, or C-23 [31].

On the basis of a strong NOE correlation between H-1 and H-7 $\alpha$  (Figure 6B), as well as the other NOE correlations shown in Figure 6B, the relative configuration of **6** was elucidated to be the same as compounds **1** and **5**. The absolute configuration of **6** was established by comparing its experimental ECD spectrum with those of **1** and **5** (Supplementary Figure S8). Based on the opposite sign of the specific rotation value of **6** ( $[\alpha]_{\text{D}}^{20} = +541$ , *c* 0.1, MeOH) in comparison to compounds **1** ( $[\alpha]_{\text{D}}^{20} = -71$ , *c* 0.1, MeOH) and **5** ( $[\alpha]_{\text{D}}^{20} = -420$ , *c* 0.01, MeOH), **6** was identified as (+)-(1R,2S,6R,8S)-1-octacosatrienoyl-discorhabdin L (Figure 3).



**Figure 6.** Key 2D NMR correlations observed for compound **6**. (A) The COSY (in bold), key H→C HMBC (arrows); (B) key H→H NOESY correlations (dashed line).

## 2.2. In Vitro Bioactivity Tests and Molecular Docking on Purified Compounds

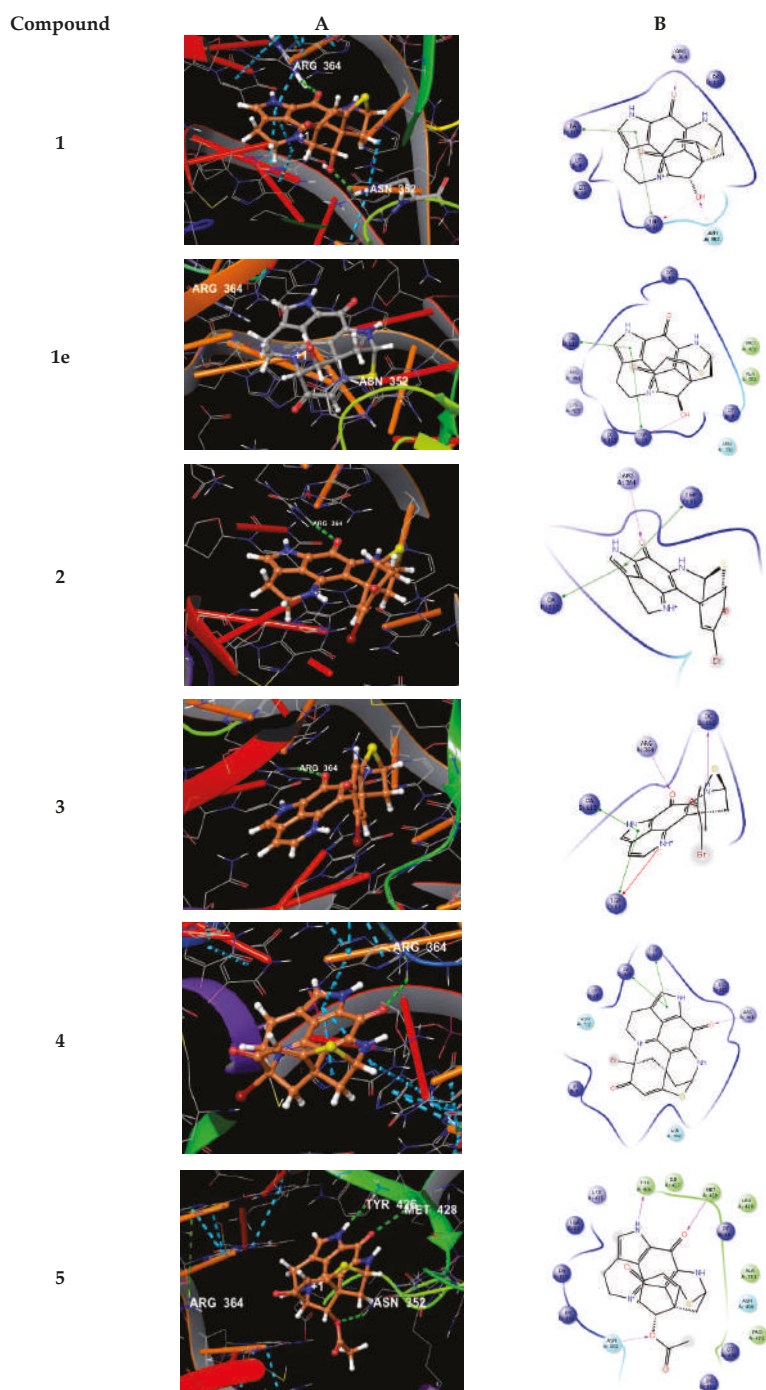
Anticancer activity of the pyrroloiminoquinone-type alkaloids has been the main driving force for isolation of these intriguing structural types. Due to low quantities of the isolated compounds,

we were only able to assess the in vitro anticancer activities of compounds **1**, **5**, and **6** against one cell line. We used HCT-116 colon cancer cells for testing, because of the observed high activity of the MeOH subextract and SPE fractions (Table 1), plus the availability of literature data for (–)-discorhabdin L (**1**) against this cell line (IC<sub>50</sub> value 6.2 µM) [17]. In the current study, compound **1** showed IC<sub>50</sub> value of 0.94 µM (equal to 0.33 µg/mL). The compound **5** displayed promising activity with an IC<sub>50</sub> value of 2.71 µM (= 1.1 µg/mL), while compound **6** was only modestly active against the same cell line (IC<sub>50</sub> value 34.0 µM, equal to 25.6 µg/mL). These results indicate that C-1 OH function is important for anti-colon cancer activity and the substitution of the C-1 OH group, especially with a long chain fatty acyl function is not favored.

Limited by the amounts of the isolated compounds, we performed a molecular modeling study (using Schrödinger software Maestro; [www.schrodinger.com](http://www.schrodinger.com)) on compounds **1–6** and (+)-discorhabdin L (**1e**), the (+) enantiomer of compound **1**, against two known anticancer targets (topoisomerase I/II, indoleamine 2,3-dioxygenase IDO1) to estimate their potential anticancer activity and mechanism(s) of action. Where possible, based on suitable pdb structures, docking experiments were performed. We prepared available relevant pdb protein structures, removed the original ligands, and generated receptor grids. Small molecule 3D structures of the compounds containing a quaternary nitrogen were energetically minimized and possible tautomers/protonated states were evaluated (LigPrep, counter ion not specified). Next, we docked the optimized ligand structures into respective active sites (Glide SP). Calculated 3D binding modes were illustrated, or presented as 2D ligand-interaction diagrams, for clarity.

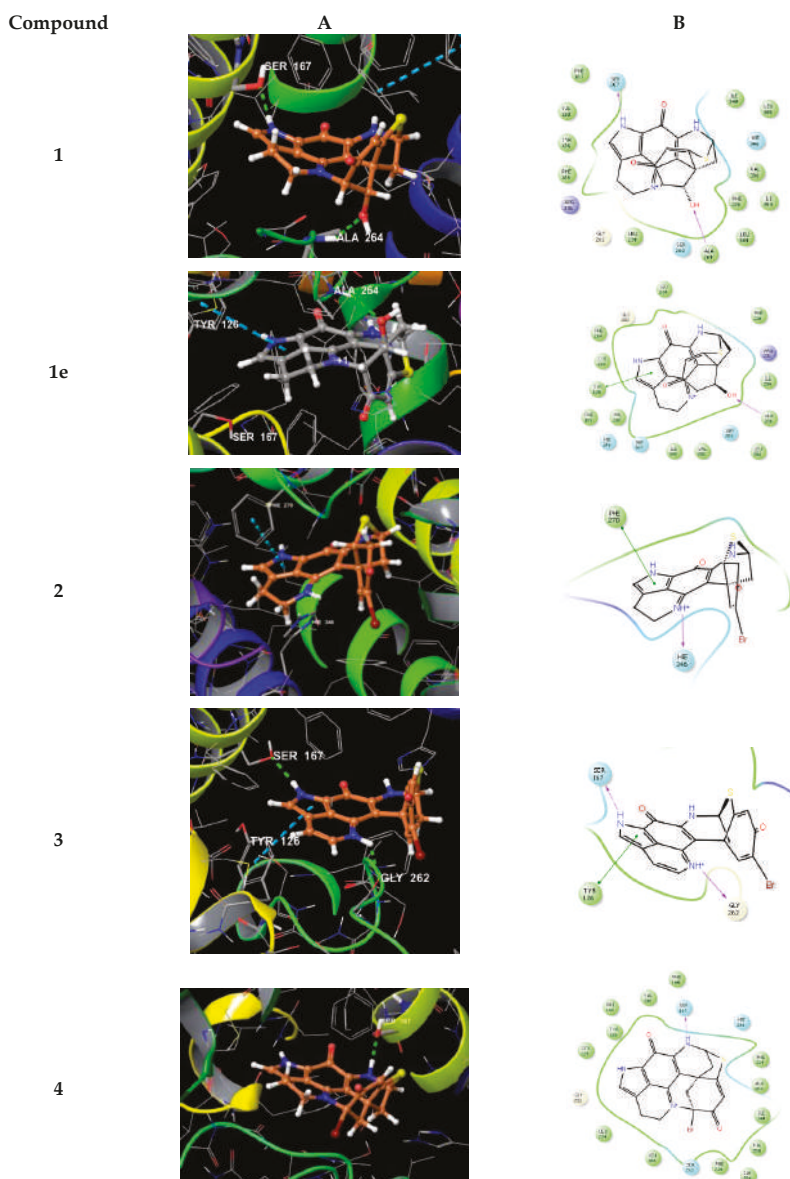
Docking of compounds **1–5** into the active site of topoisomerase I (pdb 1T8I) yielded plausible binding modes (Figure 7), while no binding pose could be calculated for compound **6**, due to the sterically demanding side chain that did not fit into the tight binding pocket). Compared to the original ligand camptothecin, the flat, partly aromatic core of the discorhabdins **1–5** intercalated into the DNA part thereby forming aromatic  $\pi$ - $\pi$ -stacking interactions while also addressing H-bonds towards residues of the topoisomerase I protein. Similar results were obtained by docking experiments with topoisomerase II (pdb 3QX3, original ligand etoposide) suggesting these proteins to be anticancer targets for the compounds **1–5**. Molecular docking study performed (in analogy to the procedure described above) on compound **1e**, which was reported to exhibit strong in vitro cytotoxicity [33], revealed a binding mode in the active site of topoisomerase I, too (Figure 7). Comparable to **1**, the flat core forms a DNA-intercalating complex, but the ligand is distorted by 180°. Thus, the binding modes of both compounds, **1** and **1e**, suggest those ligands to be rather non-specific DNA intercalators.

We also performed docking experiments with another reported target for pyrroloiminoquinone alkaloids, namely the indoleamine 2,3-dioxygenase (IDO1) enzyme for which structural data including ligand–protein complexes are available. As cofactor to mediate physiological substrate oxidation, IDO1 contains a heme moiety and ligands typically form interactions by complexing the iron central atom. Examples for such IDO1 inhibitors and relevant interacting moieties include NLG919 derivative (imidazole-like nitrogen in pdb 5EK2) or ligand INCB14943 (hydroxylamidine moiety in pdb 5XE1). Since the compounds lack comparable nitrogen functionalities to able to interact with heme in a similar manner, docking of the compounds into these active sites revealed no plausible binding modes. However, recent reports demonstrated that another class of potent IDO1 inhibitors such as FXB-001116 (pdb 6AZW) and BMS-978587 (pdb 6AZV) bind to the IDO1 apo structure with high affinity, thereby displacing the heme moiety. Accordingly, we performed docking experiments of compounds **1–6** and **1e** using the apo-protein. This approach suggested possible binding modes for compounds **1–4** and **1e** in the apo active site of IDO1 (Figure 8), but not for the sterically more demanding compounds **5** and **6**.



**Figure 7.** (A) Calculated 3D binding modes of compounds 1–5 and 1e in the active site of topoisomerase I (pdb 1T8I) also containing a DNA molecule (colored in red) with a single strand break; (B) corresponding 2D ligand interaction diagrams showing key interactions of compounds 1–5 and 1e towards topoisomerase I and DNA.





**Figure 8.** 3D binding poses (A) and ligand interaction diagrams (B) of compounds 1–4 and 1e in the active site of IDO1 (pdb 6AZW). Key interactions are shown. The binding pocket is shown in a similar orientation, respectively. Ligand docking revealed plausible binding poses for compounds 1–4 and 1e, but not for compounds 5 and 6.

Inspecting the docking poses of 1 in the above-mentioned protein structures on a molecular level pointed towards a key role for the sterically defined OH-function in 1, as it mediates an H-bond towards Ala264. Another key H-bond interaction occurred between aromatic NH of 1 towards Ser167 (Figure 8). Compound 1 shows a rather planar core, anchoring the ligand with a strong shape-fit into the tight binding pocket. Relative to this core, the thioether bridge sits almost rectangular on top,

occupying a lipophilic area within the binding site, flanked by residues including Val350, Phe226, and Leu384. Within these small sets of compounds, docking of **1** reveals the optimal pose. We also docked (+)-discorhabdin L (**1e**), the enantiomer of **1**, into the active site of IDO1 (in analogy to the procedure described above). Interestingly, the flat core was found to again fill the rather flat pocket. In comparison to **1**, the core sits upside down in **1e**, with the key H-bond towards Ala264 being maintained. Accordingly, the NH-bond towards Ser167 was lost, but the aromatic system formed a  $\pi$ -interaction to Tyr126 (Figure 8). These poses suggest the flat aromatic core of this type of compounds to be the main requisite to bind into the pocket. Furthermore, stereochemistry seems to play a minor role in binding. Thus, it can be assumed the compounds are rather non-specific IDO1-ligands.

The calculated binding mode of compound **4** yielded a shifted orientation of the core, with only one H-bond towards Ser167 (Figure 8). In contrast, compounds **5** and **6** gave no plausible docking solutions, again due to the sterically demanding ester moieties, thus also preventing H-bonding by OH towards Ala264.

In summary, the molecular modeling data suggested plausible binding modes for compounds **1–5** in the target structure of topoisomerase I, and for compounds **1–4** towards IDO1, respectively. However, it is well possible that this class of compounds bind further key anticancer targets, contributing to their cytotoxic potential.

### 3. Discussion

Since the discovery of discorhabdin C from a New Zealand *Latrunculia* sp. in 1986 [8], more than 40 discorhabdin analogs have been reported from different marine sponge genera [34]. Some discorhabdins contain bromination at C-2, C-4, or C-14 positions (e.g., discorhabdin A, discorhabdin C, 14-bromodihydrodiscorhabdin C) [8,23,24,35], some possess a sulfur bridge between C-5 and C-8 (e.g., discorhabdin B, discorhabdin Q) [24,36]. A few discorhabdins (e.g., discorhabdin L, discorhabdin D) are heptacyclic through the formation of an extra bridge between C-2 and N-18 [13,24]. Of the six compounds obtained in the current study, two of them (**5** and **6**) are (–)-discorhabdin L esters. Compound **6** is a triunsaturated C28 fatty acid ester of discorhabdin L. To our knowledge this is the first discorhabdin alkyl ester structure being reported from a marine sponge. Notably, Zou et al. (2013) reported atkamine, a new, large pyrroloiminoquinone scaffold containing a fused epoxybenzazepin and bromophenol groups connected with a cyclic sulfide ring [37]. Between the former and the latter rings, there is a substitution with a monosaturated C20 alkyl chain. The authors suggested this alkyl group to originate from (Z)-15-docosenoic acid, a fatty acid commonly found in sponge species that was possibly incorporated in the very early biosynthesis stages of atkamine [37]. Compounds **5** and **6** isolated in this study instead bear an esterification at C-1 position of the pyrroloiminoquinone ring system. Compound **5** is an acetyl ester of (–)-discorhabdin L, while **6** is an ester of discorhabdin L with an unbranched octacosatrienoic acid. Marine sponges, especially demosponges, are regarded as one of the richest sources of long-chain fatty acids (LCFAs; i.e., C23–34) [38,39]. The octacosatrienoic acid (C28:3) has been reported from marine sponges and corals [40–42], but not from any *Latrunculia* species. The only study that analyzed the FAs composition of Antarctic *Latrunculia* sponges in 2015 showed that Antarctic *L. biformis* contained diverse common and LCFAs (C16, C18), however longer chain unsaturated FAs were not found [43]. This is the first report of a discorhabdin-LCFA ester from nature, and the current study adds three new and intriguing analogs to the list of discorhabdin class alkaloids.

Discorhabdins have been repeatedly studied for their in vitro anticancer activity [10,13,14]. Limited by the strong cytotoxicity and the supply issue, no molecule from this chemical family has ever proceeded to further clinical studies. A few structure–activity relationship studies (SARs) associated with discorhabdins have been conducted, revealing that the ring closure by a bridge between C2 and N18 can significantly reduce the cytotoxicity, while a substitution at C-1 (i.e., OMe, NH<sub>2</sub>) can enhance the anticancer activity [19,26]. The discovery of C-1 esters of discorhabdin L with good to moderate inhibitory activity against HCT-116 cell line here provides further insights for the SARs of discorhabdins.



Although many discorhabdins are associated with anticancer/cytotoxic activity, little is known on their exact mechanism(s) of action. Wada et al. (2011) evaluated (+)-discorhabdin A and its synthetic oxa analog for inhibition against a set of anticancer target enzymes, such as protein kinase, histone deacetylase, farnesyltransferase, telomerase, and proteasome [16]. (+)-Discorhabdin A and its synthetic oxa analog weakly inhibited the farnesyltransferase enzyme ( $IC_{50} > 10 \mu M$ ) [16]. Geoy et al. recently tested the HIF-1 $\alpha$ /p300 inhibition activity of several discorhabdins, including (–)-discorhabdin L ( $IC_{50}$  value  $0.73 \mu M$ ) concluding them to be a novel class of HIF-1 $\alpha$ /p300 inhibitors [17]. In the current study, an *in silico* molecular modeling study revealed the plausible binding modes of discorhabdins in two additional cancer target enzymes, topoisomerase I/II and IDO1.

In summary, guided by the anticancer activity and MN-based metabolomics, the Antarctic deep-sea sponge *L. bififormis* led to the isolation and characterization of three known and three new discorhabdin alkaloids. Despite the small amounts of the extract and fractions that hampered the isolation of many further new discorhabdins, MN-based metabolomics proved useful for identification of chemical inventory of the sponge in early stages. Two compounds were a new type of discorhabdin esters that yielded meaningful SARs in comparison to the parent compound discorhabdin L. Mechanistic studies based on molecular modeling showed, for the first time, the potential binding of discorhabdins to additional anticancer targets that may be involved in their anticancer activity.

## 4. Materials and Methods

### 4.1. General Procedures

Specific rotation of compounds **1–6** were measured on a Jasco P-2000 polarimeter (Jasco, Pfungstadt, Germany). FT-IR spectra were recorded using a PerkinElmer Spectrum Two FT-IR spectrometer (PerkinElmer, Boston, MA, USA). UV spectra were run on a NanoVue Plus spectrophotometer (GE Healthcare, New York, NY, USA). ECD spectra were run in MeOH on a J-810 CD spectrometer (Jasco, Pfungstadt, Germany). NMR spectra were obtained on a Bruker AV 600 spectrometer (600 and 150 MHz for  $^1H$  and  $^{13}C$  NMR, respectively, Bruker®, Billerica, MA, USA) equipped with 5.0 mm Shigemi tube (SHIGEMI, Co., LTD., Tokyo, Japan). The residual solvent signals were used as internal references:  $\delta_H$  3.31/ $\delta_C$  49.0 ppm (MeOD), and  $\delta_H$  2.50/ $\delta_C$  39.51 ppm (DMSO- $d_6$ ). 4-Dimethyl-4-silapentane-1-sulfonic acid (DSS) served as the internal standard. HRMS/MS data were recorded on a Waters Xevo G2-XS QToF Mass Spectrometer (Waters®, Milford, MA, USA) coupled to a Waters Acquity I-Class UPLC system (Waters®, Milford, MA, USA). HR-ESIMS was recorded on micrOTOF II-High-performance TOF-MS system (Bruker®, Billerica, MA, USA) equipped with an electrospray ionization source. Solid phase extraction (SPE) was performed on the Chromabond SPE C18 column cartridges (6 mL/2000 mg, Macherey-Nagel, Duren, Germany). HPLC separations were performed on a VWR Hitachi Chromaster system (VWR International, Allison Park, PA, USA) consisting of a 5430-diode array detector (VWR International, Allison Park, PA, USA), a 5310-column oven, a 5260 autosampler, and a 5110 pump combined in parallel with a VWR evaporative light scattering detector (ELSD 90, VWR International, Allison Park, PA, USA). The eluents used for HPLC separations were H $_2$ O (A) and MeCN (B). Routine HPLC separations were performed on a semi-preparative C18 monolithic column (Onyx, 100  $\times$  10 mm, Phenomenex, Torrance, CA, USA) and an analytical synergi column (250  $\times$  4.6 mm, Phenomenex, Torrance, CA, USA). A chiral cellulose-1 column (Lux 5 $\mu$ , 250  $\times$  4.6 mm, Phenomenex, Torrance, CA, USA) was used for checking the enantiopurity of each purified compound. The organic solvents used for UPLC-QToF-MS/MS analyses were ULC/MS grade (Biosolve BV, North Brabant, Netherlands) and HPLC grade (ITW Reagents, Darmstadt, Germany) for HPLC isolation processes. The water used was MilliQ-water produced by Arium® Water Purification Systems (Sartorius, Göttingen, Germany).

### 4.2. Sponge Material

The sponge was collected in 2015/2016 during the Expedition PS96 of the Research Vessel POLARSTERN to the southern Weddell Sea (Antarctica). The sponge was collected by an Agassiz

trawl at a depth of −291 m, and was fixated immediately after collection. Specimens were cleaned, pre-sorted, photographed, and transferred into buckets with cold seawater as soon as the catch was on deck. Subsamples were transferred into pure ethanol (96%) and the main parts were frozen at −20 °C. The sponges were transported to the Senckenberg Research Institute and Nature Museum in Frankfurt am Main, Germany. Tissue samples were taken and skeletal preparations were made for transmission light microscopy and SEM, according to standard protocols [44]. For taxonomic examination, the sponge spicules were mounted on microscope slides and studied by light microscopy and by SEM. Based on comparative morphology of skeletal characters, the sponge was identified as *Latrunculia biformis*, which is a common species in the Antarctic deeper shelf areas. For identification, the World Porifera Database [45] and relevant literature were used. A specimen (SMF 12109) is deposited in the Porifera collection of Senckenberg Research Institute and Nature Museum, electronically inventoried. The data are online available in the SESAM database.

#### 4.3. Extraction and Isolation

The sponge material (43.615 g, frozen weight) was cut into small pieces and freeze-dried (Martin Christ, Osterode am Harz, Germany). The lyophilized biomass (5.809 g) was extracted at room temperature with water (3 × 200 mL) under agitation to yield the aqueous extract (1.892 g). The remaining sponge residue (3.572 g, dry weight) was extracted with MeOH (3 × 150 mL) and subsequently with DCM (3 × 150 mL) under the same conditions. Combined MeOH and DCM extracts were evaporated to dryness by a rotary evaporator to yield the crude organic extract (328 mg) that showed very strong anticancer activity against multiple cancer cell lines. This extract was partitioned between MeOH (100 mL) and *n*-hexane (100 mL) to yield MeOH (190 mg) and *n*-hexane (120 mg) subextracts. The MeOH-soluble portion, which exhibited strong anticancer activity was fractionated on a Chromabond SPE C18 cartridge. The elution with a step gradient MeOH:H<sub>2</sub>O mixture (0% to 100%) afforded 8 fractions (M1–M8), of which the anticancer activity was tracked to six fractions M2–M5, M7, and M8. RP-HPLC separation of M2 (18 mg) on the analytical Synergi column gradient of H<sub>2</sub>O:MeCN (77:22), with 0.1% TFA, flow 1.0 mL/min yielded compound 1 (1.5 mg, *t<sub>R</sub>* 5.5 min). RP-HPLC analysis of M3 (10 mg) on the same column (gradient of H<sub>2</sub>O:MeCN from 80:20 to 70:30 in 25 min, with 0.1% TFA, flow 1.0 mL/min) afforded compounds 5 (0.3 mg, *t<sub>R</sub>* 15.2 min) and 3 (0.3 mg, *t<sub>R</sub>* 19.0 min). M4 (16 mg) was further fractionated on a Chromabond SPE C18 cartridge to furnish 5 subfractions (M4-1 to M4-5). The subfraction M4-1 (4.4 mg) was further purified by RP-HPLC equipped with an analytical C18 column using a gradient of H<sub>2</sub>O:MeCN (87:13 to 80:20, 0–16 min, 80:20 to 74:26, 16–27 min, with 0.1% TFA, flow 1.0 mL/min) to yield compounds 4 (0.1 mg, *t<sub>R</sub>* 18.9 min) and 2 (0.1 mg, *t<sub>R</sub>* 20.5 min). RP-HPLC separation of the nonpolar fraction M8 (23.9 mg) (gradient of H<sub>2</sub>O:MeCN 25:75 to 0:100, 0–15 min, with 0.1% TFA, flow 1.0 mL/min) on an analytical C18 column yielded compound 6 (0.2 mg, *t<sub>R</sub>* 14.9 min). Each purified compound was further checked, individually, for enantiopurity by RP-DAD-HPLC on a chiral analytical column using a gradient of H<sub>2</sub>O:MeCN (99:1 to 0:100, 0–15 min, with 0.1% TFA, flow 1.5 mL/min).

(−)-(1*R*,2*S*,6*R*,8*S*)-Discorhabdin L (1): Greenish film;  $[\alpha]_D^{20} = -71$  (c 0.1, MeOH); <sup>1</sup>H NMR (CD<sub>3</sub>OD, 600 MHz) and <sup>13</sup>C NMR (CD<sub>3</sub>OD, 150 MHz) Tables 2 and 3; HR-ESIMS found *m/z* [M + H]<sup>+</sup> 352.0748, C<sub>18</sub>H<sub>14</sub>N<sub>3</sub>O<sub>3</sub>S requires 352.0756.

(+)-(5*R*,6*S*,8*S*)-Discorhabdin A (2): Orange film;  $[\alpha]_D^{20} = +197$  (c 0.01, MeOH); HR-ESIMS found *m/z* [M + H]<sup>+</sup> 416.0065, C<sub>18</sub>H<sub>15</sub><sup>79</sup>BrN<sub>3</sub>O<sub>2</sub>S requires 416.0068.

(+)-(6*S*,8*S*)-Discorhabdin Q (3): Orange film;  $[\alpha]_D^{20} = +568$  (c 0.1, MeOH); HR-ESIMS found *m/z* [M + H]<sup>+</sup> 411.9733, C<sub>18</sub>H<sub>11</sub><sup>79</sup>BrN<sub>3</sub>O<sub>2</sub>S requires 411.9759.

(−)-(2*R*,6*R*,8*S*)-2-Bromodiscorhabdin D (4): Greenish film; UV (MeOH) λ<sub>max</sub> 250 (ε 13840), 285 (ε 11184), 325 (ε 7947), 403 (ε 7802) nm;  $[\alpha]_D^{20} = -246$  (c 0.05, MeOH); IR (film) ν<sub>max</sub> 2922, 2852, 1657, 1533,

1514, 1432, 1230  $\text{cm}^{-1}$ ;  $^1\text{H}$  NMR ( $\text{CD}_3\text{OD}$ , 600 MHz) and  $^{13}\text{C}$  NMR ( $\text{CD}_3\text{OD}$  150 MHz) Tables 2 and 3; HR-ESIMS found  $m/z$   $[\text{M} + \text{H}]^+$  413.9913,  $\text{C}_{18}\text{H}_{13}^{79}\text{BrN}_3\text{O}_2\text{S}$  requires 413.9912.

(–)-(1*R*,2*S*,6*R*,8*S*)-1-Acetyl-discorhabdin L (5): Greenish film; UV (MeOH)  $\lambda_{\text{max}}$  250 ( $\epsilon$  24822), 283 ( $\epsilon$  17019), 325 ( $\epsilon$  11700), 403 ( $\epsilon$  11169) nm;  $[\alpha]_{\text{D}}^{20} = -420$  ( $c$  0.01, MeOH); IR (film)  $\nu_{\text{max}}$  2926, 2854, 1747, 1653, 1621, 1560, 1528, 1412, 1201  $\text{cm}^{-1}$ ;  $^1\text{H}$  NMR ( $\text{CD}_3\text{OD}$ , 600 MHz) and  $^{13}\text{C}$  NMR ( $\text{CD}_3\text{OD}$ , 150 MHz) Tables 2 and 3; HR-ESIMS found  $m/z$   $[\text{M} + \text{H}]^+$  394.0816,  $\text{C}_{20}\text{H}_{16}\text{N}_3\text{O}_4\text{S}$  requires 394.0861.

(+)-(1*R*,2*S*,6*R*,8*S*)-1-Octacosatrienoyl-discorhabdin L (6): Greenish film; UV (MeOH)  $\lambda_{\text{max}}$  203 ( $\epsilon$  19890), 249 ( $\epsilon$  19439), 285 ( $\epsilon$  15904), 325 ( $\epsilon$  13122), 403 ( $\epsilon$  11543) nm;  $[\alpha]_{\text{D}}^{20} = +541$  ( $c$  0.1, MeOH); IR (film)  $\nu_{\text{max}}$  3007, 2927, 2855, 1739, 1678, 1621, 1566, 1527, 1441, 1206, 1185, 1135  $\text{cm}^{-1}$ ;  $^1\text{H}$  NMR ( $\text{CD}_3\text{OD}$ , 600 MHz) and  $^{13}\text{C}$  NMR ( $\text{CD}_3\text{OD}$ , 150 MHz) Tables 2 and 3; HR-ESIMS found  $m/z$   $[\text{M} + \text{H}]^+$  752.4452,  $\text{C}_{46}\text{H}_{62}\text{N}_3\text{O}_4\text{S}$  requires 752.4461.

#### 4.4. UPLC-QToF-MS/MS Analysis

The six active C18 SPE fractions of the MeOH soluble portion were analyzed on an ACQUITY UPLC I-Class System coupled to the Xevo G2-XS QToF Mass Spectrometer (Waters®, Milford, Massachusetts, USA) equipped with an electrospray ionization (ESI) source operating with a positive polarity at a mass range of  $m/z$  50–1600 Da. The 0.1 mg/mL MeOH solution of the fractions were filtered through a 0.2  $\mu\text{m}$  PTFE syringe filter (Carl Roth, Karlsruhe, Germany) and then injected (injection volume: 1.0  $\mu\text{L}$ ) into the system equipped with Acquity UPLC HSS T3 column (high-strength silica C18, 1.8  $\mu\text{m}$ , 100  $\times$  2.1 mm I.D., Waters®) operating at 40 °C. Separation was achieved with a binary LC solvent system controlled by MassLynx® (version 4.1) using mobile phase A 99.9% water/0.1% formic acid (ULC/MS grade) and B 99.9% ACN/0.1% formic acid (ULC/MS grade), pumped at a rate of 0.6 mL/min with the following gradient: Initial, 1% B; 0.0–12.0 min to 100% B; 12.0–13.0 min 100% B, and a column reconditioning phase until 15 min.

ESI conditions were set with the capillary voltage at 0.8 kV, sample cone voltage at 40.0 V, source temperature at 150 °C, desolvation temperature at 550 °C, cone gas flow in 50 L/h, and desolvation gas flow in 1200 L/h. MS/MS setting was linear collision energy (CE) at 30 eV. As a control, solvent (methanol) was injected. MassLynx® (Waters®, V4.1) was used to analyze the achieved MS and MS<sup>2</sup> data.

#### 4.5. Molecular Networking

The network was created using the UPLC-HRMS/MS data generated from the six active MeOH subfractions of *L. biformis*. All raw MS/MS data were converted from files (.raw) to mzXML file format using MSConvert (Version 3.6.10051, Vanderbilt University, Nashville, TN, USA). The converted data files were uploaded to the Global Natural Products Social molecular networking (<http://gnps.ucsd.edu>) platform using FileZilla (<https://filezilla-project.org/>) and a molecular network was created using the online workflow at GNPS [22]. The data were filtered by removing all MS/MS peaks within  $\pm 17$  Da of the precursor  $m/z$ . MS/MS spectra were window filtered by choosing only the top 6 peaks in the  $\pm 50$  Da window throughout the spectrum. The data were then clustered with MS-Cluster with a parent mass tolerance of 0.1 Da and an MS/MS fragment ion tolerance of 0.05 Da to create consensus spectra. Further, consensus spectra that contained less than 2 spectra were discarded. A network was then created where edges were filtered to have a cosine score above 0.6 and more than 3 matched peaks. Further edges between two nodes were kept in the network if and only if each of the nodes appeared in each other's respective top 10 most similar nodes. The spectra in the network were then searched against GNPS' spectral libraries. The library spectra were filtered in the same manner as the input data. All matches kept between network spectra and library spectra were required to have a score above 0.7 and at least 6 matched peaks. The output molecular networking data were analyzed and visualized using Cytoscape (ver. 3.61) [46].

#### 4.6. Cytotoxicity Assay

Crude extract of *L. bififormis* and downstream fractions were tested in vitro at a final concentration of 100 µg/mL against 6 human cancer cell lines, Hep G2 (liver cancer cell line, DSMZ, Braunschweig, Germany), HT29 (colorectal adenocarcinoma cell line, DSMZ, Braunschweig, Germany), A375 (malignant melanoma cell line, CLS, Eppelheim, Germany), HCT116 (colon cancer cell line, DSMZ, Braunschweig, Germany), A549 (lung carcinoma cell line, CLS, Eppelheim, Germany), and MDA-MB231 (human breast cancer line, CLS, Eppelheim, Germany). Cells were supplemented at 37 °C and 5% CO<sub>2</sub> in RPMI 1640 medium (Life Technologies, Darmstadt, Germany) with 10% fetal bovine serum, 100 U/mL penicillin and 100 mg/mL streptomycin. A stock solution of 20 mg/mL in DMSO was prepared for each test sample. After 24 h incubation in 96-well plates, the medium in the cells was replaced by 100 µL fresh medium containing the test samples and cells were incubated for another 24 h at 37 °C. Doxorubicin was used as positive control, while 0.5% DMSO and growth media served as negative controls. All samples were prepared in duplicates. The assay was performed according to the manufacturer's instructions (Promega, Madison, WI, USA). Cells were incubated for 2 h at 37 °C and fluorescence at an excitation wavelength of 560 nm and emission at 590 nm was measured. For the determination of IC<sub>50</sub> values, a dilution series of the extracts were tested following the same procedure as described before. IC<sub>50</sub> values were calculated by using Excel to determine the concentration that shows 50% inhibition of the viability.

#### 4.7. Molecular Modeling and Docking

Molecular modeling was performed on a DELL Precision T3610 four core workstation using Schrödinger Maestro (version 11.3, 2017, Schrödinger, LLC, New York, NY, USA). The following RCSB protein data bank (pdb) crystal structures were used for modeling studies: 1T8I, 3QX3, 5EK2, 5XE1, 6AZV, 6AZW. Each protein structure was initially prepared by standard settings of the Protein Preparation Wizard 2015-4 (Epik version 2.4, Schrödinger, LLC, 2015; Impact version 5.9, Schrödinger, LLC, 2015; Prime version 3.2, Schrödinger LLC, 2015). For energy minimizations of the small-molecule ligands, MacroModel (version 11.0, Schrödinger, LLC, 2015) was used. Ionization states and tautomers were generated with LigPrep (version 3.6, Schrödinger, LLC, 2015). Ligand docking and receptor grid generation was performed with Glide (version 6.9, Schrödinger, LLC, 2015). Figures and ligand interaction diagrams (LID) were generated by Maestro.

**Supplementary Materials:** The following are available online at <http://www.mdpi.com/1660-3397/17/8/439/s1>, HR-ESIMS and NMR spectra of compounds 1–6. ECD spectra of compounds 1,4,5, and 6.

**Author Contributions:** Design of the work, D.T. and F.L.; sample provision, D.J.; extraction, purifications of compounds, F.L.; data analysis, F.L. and D.T.; molecular docking experiment, C.P.; writing original manuscript, F.L. and D.T.; editing, D.T.; supervision, D.T.

**Funding:** This research received no external funding.

**Acknowledgments:** Fengjie Li thanks the China Scholarship Council for a Ph.D. fellowship. The Deutsche Forschungsgemeinschaft (DFG) is acknowledged by Dorte Janussen for financial support to her Antarctic sponge research (JA 1063/17-1). We thank Daniel Kersken for his dedicated effort in collection and fixation of these sponges during the PS96 expedition, thanks are due also to the captain and crew of RV POLARSTERN. We are grateful to Arlette Wenzel-Storjohann and Jana Heumann for performing anticancer assays. Joachim Grötzinger is acknowledged for offering the J-810 CD spectrometer for ECD spectrum measurement. We acknowledge financial support by Land Schleswig-Holstein within the funding program Open Access Publikationsfonds.

**Conflicts of Interest:** The authors declare no conflict of interest.

#### References

1. Alvarez, B.; Bergquist, P.R.; Battershill, C.N. Taxonomic revision of the genus *Latrunculia* du Bocage (Porifera: Demospongiae: Latrunculiidae) in New Zealand. *N. Z. J. Mar. Freshw. Res.* **2002**, *36*, 151–184. [CrossRef]

2. Samaai, T.; Gibbons, M.J.; Kelly, M.; Davies-Coleman, M. South African Latrunculiidae (Porifera: Demospongiae: Poecilosclerida): Descriptions of new species of *Latrunculia* du Bocage, *Strongyloidesma* Lévi, and *Tsitsikamma* Samaai & Kelly. *Zootaxa* **2003**, *371*, 1.
3. Kelly, M.; Sim-Smith, C.; Stone, R.; Samaai, T.; Reisch, H.; Austin, W. New taxa and arrangements within the family Latrunculiidae (Demospongiae, Poecilosclerida). *Zootaxa* **2016**, *4121*, 1. [[CrossRef](#)] [[PubMed](#)]
4. Capon, R.; MacLeod, J.K.; Willis, A.C. Trunculins A and B, norsesterterpene cyclic peroxides from a marine sponge, *Latrunculia brevis*. *J. Org. Chem.* **1987**, *52*, 339–342. [[CrossRef](#)]
5. Butler, M.; Capon, R.; Capon, R. Trunculin-F and Contrunculin-A and -B: Novel oxygenated norterpene from a Southern Australian marine sponge, *Latrunculia conulosa*. *Aust. J. Chem.* **1993**, *46*, 1363. [[CrossRef](#)]
6. Zampella, A.; Randazzo, A.; Borbone, N.; Luciani, S.; Trevisi, L.; Debitus, C.; D’Auria, M.V. Isolation of callipeltins A–C and of two new open-chain derivatives of callipeltin A from the marine sponge *Latrunculia* sp. A revision of the stereostructure of callipeltins. *Tetrahedron Lett.* **2002**, *43*, 6163–6166. [[CrossRef](#)]
7. Sepe, V.; D’Orsi, R.; Borbone, N.; D’Auria, M.V.; Bifulco, G.; Monti, M.C.; Catania, A.; Zampella, A. Callipeltins F–I: New antifungal peptides from the marine sponge *Latrunculia* sp. *Tetrahedron* **2006**, *62*, 833–840. [[CrossRef](#)]
8. Perry, N.B.; Blunt, J.W.; McCombs, J.D.; Munro, M.H.G. Discorhabdin C, a highly cytotoxic pigment from a sponge of the genus *Latrunculia*. *J. Org. Chem.* **1986**, *51*, 5476–5478. [[CrossRef](#)]
9. Ford, J.; Capon, R.J. Discorhabdin R: A new antibacterial pyrroloiminoquinone from two latrunculiid marine sponges, *Latrunculia* sp. and *Negombata* sp. *J. Nat. Prod.* **2000**, *63*, 1527–1528. [[CrossRef](#)]
10. Hu, J.-F.; Fan, H.; Xiong, J.; Wu, S.-B. Discorhabdins and pyrroloiminoquinone-related alkaloids. *Chem. Rev.* **2011**, *111*, 5465–5491. [[CrossRef](#)] [[PubMed](#)]
11. Miller, K.; Alvarez, B.; Battershill, C.; Northcote, P.; Parthasarathy, H. Genetic, morphological, and chemical divergence in the sponge genus *Latrunculia* (Porifera: Demospongiae) from New Zealand. *Mar. Biol.* **2001**, *139*, 235–250. [[CrossRef](#)]
12. Furrow, F.B.; Amsler, C.D.; McClintock, J.B.; Baker, B.J. Surface sequestration of chemical feeding deterrents in the Antarctic sponge *Latrunculia apicalis* as an optimal defense against sea star spongivory. *Mar. Biol.* **2003**, *143*, 443–449. [[CrossRef](#)]
13. Reyes, F.; Martín, R.; Rueda, A.; Fernandez, R.; Montalvo, D.; Gomez, C.; Sánchez-Puelles, J.M. Discorhabdins I and L, cytotoxic alkaloids from the sponge *Latrunculia brevis*. *J. Nat. Prod.* **2004**, *67*, 463–465. [[CrossRef](#)] [[PubMed](#)]
14. Gunasekera, S.P.; Zuleta, I.A.; Longley, R.E.; Wright, A.E.; Pomponi, S.A. Discorhabdins S, T, and U, new cytotoxic pyrroloiminoquinones from a deep-water Caribbean sponge of the genus *Batzella*. *J. Nat. Prod.* **2003**, *66*, 1615–1617. [[CrossRef](#)] [[PubMed](#)]
15. Jeon, J.-E.; Na, Z.; Jung, M.; Lee, H.-S.; Sim, C.J.; Nahm, K.; Oh, K.-B.; Shin, J. Discorhabdins from the Korean Marine Sponge *Sceptrella* sp. *J. Nat. Prod.* **2010**, *73*, 258–262. [[CrossRef](#)] [[PubMed](#)]
16. Wada, Y.; Harayama, Y.; Kamimura, D.; Yoshida, M.; Shibata, T.; Fujiwara, K.; Morimoto, K.; Fujioka, H.; Kita, Y. The synthetic and biological studies of discorhabdins and related compounds. *Org. Biomol. Chem.* **2011**, *9*, 4959–4976. [[CrossRef](#)] [[PubMed](#)]
17. Goey, A.K.L.; Chau, C.H.; Sissung, T.M.; Cook, K.M.; Venzon, D.J.; Castro, A.; Ransom, T.R.; Henrich, C.J.; McKee, T.C.; McMahon, J.B.; et al. Screening and biological effects of marine pyrroloiminoquinone alkaloids: Potential inhibitors of the HIF-1 $\alpha$ /p300 interaction. *J. Nat. Prod.* **2016**, *79*, 1267–1275. [[CrossRef](#)]
18. Li, F.; Janussen, D.; Peifer, C.; Pérez-Victoria, I.; Tasdemir, D. Targeted isolation of tsitsikammamines from the antarctic deep-sea sponge *Latrunculia biformis* by molecular networking and anticancer activity. *Mar. Drugs* **2018**, *16*, 268. [[CrossRef](#)]
19. Antunes, E.M.; Beukes, D.R.; Kelly, M.; Samaai, T.; Barrows, L.R.; Marshall, K.M.; Sincich, C.; Davies-Coleman, M.T. Cytotoxic Pyrroloiminoquinones from four new species of South African Latrunculiid Sponges. *J. Nat. Prod.* **2004**, *67*, 1268–1276. [[CrossRef](#)]
20. Delfourne, E. Analogues of marine pyrroloiminoquinone alkaloids: Synthesis and antitumor properties. *Anti-Cancer Agents Med. Chem.* **2008**, *8*, 910–916. [[CrossRef](#)]
21. Dolušić, E.; Larrieu, P.; Meinguet, C.; Colette, D.; Rives, A.; Blanc, S.; Ferain, T.; Pilotte, L.; Stroobant, V.; Wouters, J.; et al. Indoleamine 2,3-dioxygenase inhibitory activity of derivatives of marine alkaloid tsitsikammamine A. *Bioorg. Med. Chem. Lett.* **2013**, *23*, 47–54. [[CrossRef](#)]



22. Wang, M.; Carver, J.J.; Phelan, V.V.; Sanchez, L.M.; Garg, N.; Peng, Y.; Nguyen, D.D.; Watrous, J.; A Kapon, C.; Luzzatto-Knaan, T.; et al. Sharing and community curation of mass spectrometry data with Global Natural Products Social Molecular Networking. *Nat. Biotechnol.* **2016**, *34*, 828–837. [\[CrossRef\]](#)
23. Perry, N.B.; Blunt, J.W.; Munro, M.H.G.; Higa, T.; Sakai, R. Discorhabdin D, an antitumor alkaloid from the sponges *Latrunculia brevis* and *Prianos* sp. *J. Org. Chem.* **1988**, *53*, 4127–4128. [\[CrossRef\]](#)
24. Perry, N.B.; Blunt, J.W.; Munro, M.H.G. Cytotoxic pigments from New Zealand sponges of the genus *Latrunculia*: Discorhabdin A, discorhabdin B and discorhabdin C. *Tetrahedron* **1988**, *44*, 1727–1734. [\[CrossRef\]](#)
25. Yang, A.; Baker, B.J.; Grimwade, J.; Leonard, A.; McClintock, J.B. Discorhabdin Alkaloids from the Antarctic Sponge *Latrunculia apicalis*. *J. Nat. Prod.* **1995**, *58*, 1596–1599. [\[CrossRef\]](#)
26. Grkovic, T.; Pearce, A.N.; Munro, M.H.G.; Blunt, J.W.; Davies-Coleman, M.T.; Copp, B.R. Isolation and characterization of diastereomers of discorhabdins H and K and assignment of absolute configuration to discorhabdins D, N, Q, S, T, and U. *J. Nat. Prod.* **2010**, *73*, 1686–1693. [\[CrossRef\]](#)
27. Kobayashi, J.; Cheng, J.-F.; Ishibashi, M.; Nakamura, H.; Ohizumi, Y.; Hirata, Y.; Sasaki, T.; Lu, H.; Clardy, J. Prianosin A, a novel antileukemic alkaloid from the okinawan marine sponge *Prianos melanos*. *Tetrahedron Lett.* **1987**, *28*, 4939–4942. [\[CrossRef\]](#)
28. Sternhell, S. Correlation of interproton spin-spin coupling constants with structure. *Q. Rev. Chem. Soc.* **1969**, *23*, 236. [\[CrossRef\]](#)
29. Choudhury, S.R.; Traquair, J.A.; Jarvis, W.R. New extracellular fatty acids in culture filtrates of *Sporothrix flocculosa* and *S. rugulosa*. *Can. J. Chem.* **1995**, *73*, 84–87. [\[CrossRef\]](#)
30. Makarieva, T.N.; Santalova, E.A.; Gorshkova, I.A.; Dmitrenok, A.S.; Guzii, A.G.; Gorbach, V.I.; Svetashev, V.I.; Stonik, V.A. A new cytotoxic fatty acid (5Z,9Z)-22-methyl-5,9-tetracosadienoic acid and the sterols from the far Eastern sponge *Geodinella robusta*. *Lipids* **2002**, *37*, 75–80. [\[CrossRef\]](#)
31. Kornprobst, J.-M.; Barnathan, G. Demospongic acids revisited. *Mar. Drugs* **2010**, *8*, 2569–2577. [\[CrossRef\]](#)
32. Gunstone, F.; Pollard, M.; Scrimgeour, C.; Vedanayagam, H. Fatty acids. Part 50. <sup>13</sup>C nuclear magnetic resonance studies of olefinic fatty acids and esters. *Chem. Phys. Lipids* **1977**, *18*, 115–129. [\[CrossRef\]](#)
33. Grkovic, T.; Ding, Y.; Li, X.-C.; Webb, V.L.; Ferreira, D.; Copp, B.R. Enantiomeric discorhabdin alkaloids and establishment of their absolute configurations using theoretical calculations of electronic circular dichroism spectra. *J. Org. Chem.* **2008**, *73*, 9133–9136. [\[CrossRef\]](#)
34. Botić, T.; Defant, A.; Zanini, P.; Žužek, M.C.; Frangež, R.; Janussen, D.; Kersken, D.; Knez, Ž.; Mancini, I.; Sepčić, K. Discorhabdin alkaloids from Antarctic *Latrunculia* spp. sponges as a new class of cholinesterase inhibitors. *Eur. J. Med. Chem.* **2017**, *136*, 294–304.
35. Hooper, G.J.; Davies-Coleman, M.T.; Kelly-Borges, M.; Coetzee, P.S. New alkaloids from a South African *latrunculid* sponge. *Tetrahedron Lett.* **1996**, *37*, 7135–7138. [\[CrossRef\]](#)
36. Djijoux, M.-G.; Gamble, W.R.; Hallock, Y.F.; Cardellina, J.H.; Van Soest, R.; Boyd, M.R. A new discorhabdin from two sponge genera. *J. Nat. Prod.* **1999**, *62*, 636–637. [\[CrossRef\]](#)
37. Zou, Y.; Hamann, M.T. Atkamine: A New Pyrroloiminoquinone scaffold from the cold water Aleutian Islands *Latrunculia* sponge. *Org. Lett.* **2013**, *15*, 1516–1519. [\[CrossRef\]](#)
38. Litchfield, C.; Greenberg, A.J.; Noto, G.; Morales, R.W. Unusually high levels of C24–C30 fatty acids in sponges of the class demospongiae. *Lipids* **1976**, *11*, 567–570. [\[CrossRef\]](#)
39. Řezanka, T.; Sigler, K. Odd-numbered very-long-chain fatty acids from the microbial, animal and plant kingdoms. *Prog. Lipid Res.* **2009**, *48*, 206–238. [\[CrossRef\]](#)
40. Litchfield, C.; Marcantonio, E.E. Occurrence of 5,9,19-octacosatrienoic, 5,9-hexacosadienoic and 17-hexacosenoic acids in the marine sponge *Xestospongia halichondroides*. *Lipids* **1978**, *13*, 199–202. [\[CrossRef\]](#)
41. Imbs, A.B.; Demidkova, D.A.; Dautova, T.N.; Latyshev, N.A. Fatty acid biomarkers of symbionts and unusual inhibition of tetracosapolyenoic acid biosynthesis in corals (*Octocorallia*). *Lipids* **2009**, *44*, 325–335. [\[CrossRef\]](#)
42. Thiel, V.; Blumenberg, M.; Hefter, J.; Pape, T.; Pomponi, S.; Reed, J.; Reitner, J.; Wörheide, G.; Michaelis, W. A chemical view of the most ancient metazoa—Biomarker chemotaxonomy of hexactinellid sponges. *Naturwissenschaften* **2002**, *89*, 60–66. [\[CrossRef\]](#)
43. Botić, T.; Cör, D.; Anesi, A.; Guella, G.; Sepčić, K.; Janussen, D.; Kersken, D.; Knez, Ž. Fatty acid composition and antioxidant activity of Antarctic marine sponges of the genus *Latrunculia*. *Polar Boil.* **2015**, *38*, 1605–1612. [\[CrossRef\]](#)
44. Boury-Esnault, N.; Rützler, K.; Ruetzler, K. Thesaurus of sponge morphology. *Smithson. Contrib. Zool.* **1997**, *596*, 1–55. [\[CrossRef\]](#)

- 45. Samaai, T.; Gibbons, M.J.; Kelly, M. Revision of the genus *Latrunculia* du Bocage, 1869 (Porifera: Demospongiae: Latrunculiidae) with descriptions of new species from New Caledonia and the Northeastern Pacific. *Zootaxa* **2006**, *1127*, 1–71. [[CrossRef](#)]
- 46. Shannon, P.; Markiel, A.; Ozier, O.; Baliga, N.S.; Wang, J.T.; Ramage, D.; Amin, N.; Schwikowski, B.; Ideker, T. Cytoscape: A software environment for integrated models of biomolecular interaction networks. *Genome Res.* **2003**, *13*, 2498–2504. [[CrossRef](#)]



© 2019 by the authors. Licensee MDPI, Basel, Switzerland. This article is an open access article distributed under the terms and conditions of the Creative Commons Attribution (CC BY) license (<http://creativecommons.org/licenses/by/4.0/>).





## Article

# The First Genome Survey of the Antarctic Krill (*Euphausia superba*) Provides a Valuable Genetic Resource for Polar Biomedical Research

Yuting Huang <sup>1,2,3,†</sup>, Chao Bian <sup>2,3,†</sup>, Zhaoqun Liu <sup>1,†</sup>, Lingling Wang <sup>1,†</sup>, Changhu Xue <sup>4</sup>, Hongliang Huang <sup>5</sup>, Yunhai Yi <sup>2,3</sup>, Xinxin You <sup>2,3</sup>, Wei Song <sup>5</sup>, Xiangzhao Mao <sup>4</sup>, Linsheng Song <sup>1,\*</sup> and Qiong Shi <sup>1,2,3,\*</sup>

<sup>1</sup> Liaoning Key Laboratory of Marine Animal Immunology, Dalian Ocean University, Dalian 116023, China; huangyuting@genomics.cn (Y.H.); liuzhaoqun@dlou.edu.cn (Z.L.); wanglingling@dlou.edu.cn (L.W.)

<sup>2</sup> Shenzhen Key Lab of Marine Genomics, Guangdong Provincial Key Lab of Molecular Breeding in Marine Economic Animals, BGI Academy of Marine Sciences, BGI Marine, BGI, Shenzhen 518083, China; bianchao@genomics.cn (C.B.); yiyunhai@genomics.cn (Y.Y.); youxinxin@genomics.cn (X.Y.)

<sup>3</sup> BGI Education Center, University of Chinese Academy of Sciences, Shenzhen 518083, China

<sup>4</sup> Ocean University of China, Qingdao 266100, China; xuech@ouc.edu.cn (C.X.); xzhmao@ouc.edu.cn (X.M.)

<sup>5</sup> East China Sea Fisheries Research Institute, Chinese Academy of Fishery Sciences, Shanghai 200090, China; ecshhl@163.com (H.H.); songw@ecsf.ac.cn (W.S.)

\* Correspondence: lshsong@dlou.edu.cn (L.S.); shiqiong@genomics.cn (Q.S.); Tel.: +86-155-4269-9991 (L.S.); +86-185-6627-9826 (Q.S.); Fax: +86-755-3630-7273 (Q.S.)

† These authors contributed equally to this work.

Received: 29 February 2020; Accepted: 25 March 2020; Published: 31 March 2020

**Abstract:** The world-famous Antarctic krill (*Euphausia superba*) plays a fundamental role in the Antarctic food chain. It resides in cold environments with the most abundant biomass to support the Antarctic ecology and fisheries. Here, we performed the first genome survey of the Antarctic krill, with genomic evidence for its estimated genome size of 42.1 gigabases (Gb). Such a large genome, however, is beyond our present capability to obtain a good assembly, although our sequencing data are a valuable genetic resource for subsequent polar biomedical research. We extracted 13 typical protein-coding gene sequences of the mitochondrial genome and analyzed simple sequence repeats (SSRs), which are useful for species identification and origin determination. Meanwhile, we conducted a high-throughput comparative identification of putative antimicrobial peptides (AMPs) and antihypertensive peptides (AHTPs) from whole-body transcriptomes of the Antarctic krill and its well-known counterpart, the whiteleg shrimp (*Penaeus vannamei*; resident in warm waters). Related data revealed that AMPs/AMP precursors and AHTPs were generally conserved, with interesting variations between the two crustacean species. In summary, as the first report of estimated genome size of the Antarctic krill, our present genome survey data provide a foundation for further biological research into this polar species. Our preliminary investigations on bioactive peptides will bring a new perspective for the in-depth development of novel marine drugs.

**Keywords:** Antarctic krill (*Euphausia superba*); genome survey; mitochondrial genome; whiteleg shrimp (*Penaeus vannamei*); antimicrobial peptide (AMP); antihypertensive peptide (AHTP)

## 1. Introduction

The Antarctic krill (*Euphausia superba*), widely distributed in the Southern Ocean, provides the most abundant biomass for Antarctic ecology and fisheries [1]. It establishes a critical link between primary producers (phytoplankton) and apex predators (such as fishes, squids, penguins, and seals) in the Antarctic food chains [2,3], with an estimated biomass of 100~500 million tons [3]. With such a

large number of Antarctic krill, the Southern Ocean supports an unprecedented abundance of upper trophic-level predators. Field observations have reported that population trends of some krill predators are in part influenced by the abundance changes in Antarctic krill [4]. Human beings are also benefited by many extracted products from the Antarctic krill, such as pharmaceuticals, nutraceutical health foods, and aquaculture feeds [5]. Thus, getting insight into the genetic resources of the Antarctic krill is necessary for species protection, as well as for the development of related fisheries and industry. Studies on the genetic resources of the Antarctic krill primarily focus on transcriptomes [1,3], simple sequence repeats (SSRs) [1], and the mitochondrial genome [6,7]. These data provide valuable foundation for in-depth genetic research on this polar species. However, no complete genome assembly is available for this important crustacean.

Recently, a high-quality genome assembly of its famous counterpart, the whiteleg shrimp (*Penaeus vannamei*), was published [8]. As we know, this shrimp species predominantly inhabits tropical and subtropical areas, and has been extensively cultivated in Asian countries. Resident in such remarkably different environments, the Antarctic krill and the whiteleg shrimp may have undergone differential genetic variances. Since the genome size of the Antarctic krill is huge (over 40 Gb; see more details in our Results), we had to stop our genome project temporarily with only a genome survey available. However, these genomic data are still useful for uncovering short sequences, such as bioactive peptides encoded by entire or partial genes.

For example, antimicrobial peptides (AMPs) are short with broad-spectrum antimicrobial activities; most of them can be classified into either own gene type or proteolysis type (derived from immune related genes) [9]. They are usually less than 10 kDa while acting as the major components of the innate immune defense system in marine invertebrates [10,11], and habitat-related variances in AMPs/AMP precursors are likely to exist in various crustaceans [11]. Although AMPs in the Antarctic krill have received some attention [12], researchers still know little of the overall AMPs in such an important crustacean species and other marine animals from diverse habitats. Looking into the connection between AMPs/AMP precursors and creatures from various environments may help us to identify novel peptides and even apply them for species protection and human health.

Angiotensin converting enzyme (ACE) inhibitors are preferred antihypertensive drugs, and antihypertensive peptides (AHTPs), another important representative with short sequences, are the most effective and popularly studied ACE inhibitory peptides [13]. A lot of AHTPs are usually digested from natural products, and they most frequently contain 2~10 amino acids. Endogenous AHTPs can be hydrolyzed and degraded with assistance of digestive enzymes from in vivo proteins; by binding to ACEs or related receptors, they may adjust the renin angiotensin system for antihypertensive effects [14]. In recent years, several AHTPs have been isolated from Antarctic krill, and some of them have been used for mechanism studies [15,16]. However, general knowledge of *E. superba* AHTPs from the genomic or transcriptomic perspective is still limited. Comparative investigations on AHTPs between the Antarctic krill and the whiteleg shrimp may make contribution to our better understanding of AHTPs in various animals and identification of candidates for practical utilization as pharmaceuticals.

In the present study, we performed the first genome survey of the Antarctic krill. Such a large genome, however, is difficult for us to obtain a good assembly, although our sequencing data are a valuable genetic resource for subsequent polar biomedical research. Partial mitochondrial genome and many SSRs were able to be extracted for species identification and origin determination. Moreover, a comparative study on AMPs and AHTPs, based on available transcriptome and genome sequences from both the Antarctic krill and the whiteleg shrimp, was conducted. Here, our main aim is to establish a basic genomic and genetic foundation for future polar biomedical studies on the Antarctic krill, especially to initiate a preliminary exploration of bioactive peptides in a polar animal for the development of novel marine drugs.

2. Results

2.1. A Genome Survey of the Antarctic Krill

In total, we obtained 911.0 Gb of raw reads sequenced by a BGISEQ500 platform (BGI-Shenzhen, Shenzhen, China) from all the constructed libraries (400 bp in length). A detailed K-mer analysis [14] was performed to estimate the genome size, and a survey peak was visible with high heterozygosity in Antarctic krill (see Figure 1). We calculated the genome size (G) of the Antarctic krill according to the following formula:  $G = K\_num / K\_depth$  [17]. In our present study, the total number of K-mers (K\_num) was 758,531,899,196 and the K\_depth was 18 (Table 1 and Figure 1). Therefore, we estimated that the genome size of *E. superba* was 42.1 Gb; the sequencing depth (X) of the clean data is therefore ~21 of the estimated genome size (Table 1).

Table 1. Statistics of 17-mers for the genome size estimation.

K-mer	K_num	K_depth	Genome Size	Clean Base (bp)	Depth (X)
17	758,531,899,196	18	42,140,661,066	902,660,212,000	21

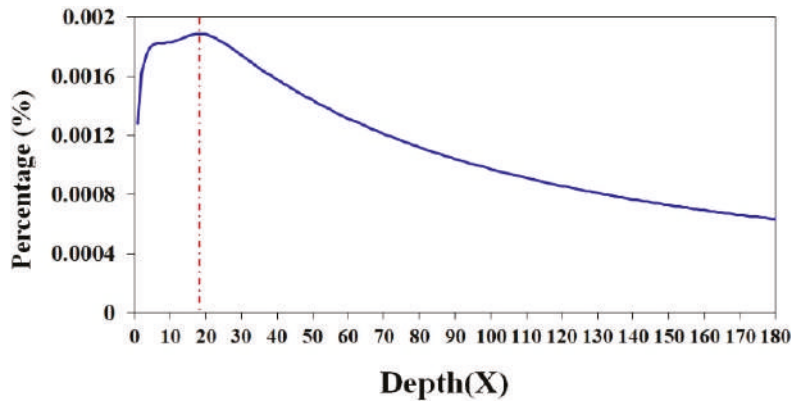


Figure 1. A 17-mer distribution curve of the Antarctic krill (*E. superba*). The x-axis is the sequencing depth (X) of each unique 17-mer, and the y-axis is the percentage of these unique 17-mers.

2.2. Assembly of Extracted Partial Mitochondrial Genome

A roughly complete mitochondrial genome of the Antarctic krill was assembled to be 12,272 bp in length, while the entire length was 15,498 bp in a previous report [6]. Based on these sequences, we extracted all the 13 typical mitochondrial protein-coding genes from our genomic raw sequences, although certain gene sequences are still partial (see File S1). These genes include cytochrome c oxidase subunit I (*coxI*), cytochrome c oxidase subunit II (*coxII*), cytochrome c oxidase subunit III (*coxIII*), ATPase subunit 8 (*atp8*), ATPase subunit 6 (*atp6*), NADH dehydrogenase subunit 3 (*nad3*), NADH dehydrogenase subunit 5 (*nad5*), NADH dehydrogenase subunit 4 (*nad4*), NADH dehydrogenase subunit 4L (*nad4L*), NADH dehydrogenase subunit 6 (*nad6*), cytochrome b (*Cytb*), NADH dehydrogenase subunit 1 (*nad1*), and NADH dehydrogenase subunit 2 (*nad2*). More details about the gene map can be seen in Figure S1, in which the order of these genes was arranged manually, in accordance with the previous report [6].

2.2.1. Annotation and Analysis of Our Extracted Mitochondrial Genes

These mitochondrial genes were assigned into six Kyoto Encyclopedia of Genes and Genomes (KEGG) pathways (see Tables S1 and S2) by using the BLASTp [18] to map against the public KEGG

database [19]. Energy metabolism pathway, as the representative one, consists of 11 genes (Table S2), such as *nad5*, *nad4*, *nad1*, *cox1*, and *cox11* (Figure S2A). The functions of these extracted mitochondrial genes were predicted with classifications by searching the public Gene Ontology (GO) databases [20]. Based on the GO annotation, we assigned them into 13 subcategories under three main categories, including biological process (3), cellular component (7), and molecular function (3). The “catalytic activity” terms (8; 53.3%) were obviously dominant in the “molecular function” (Figure S2B).

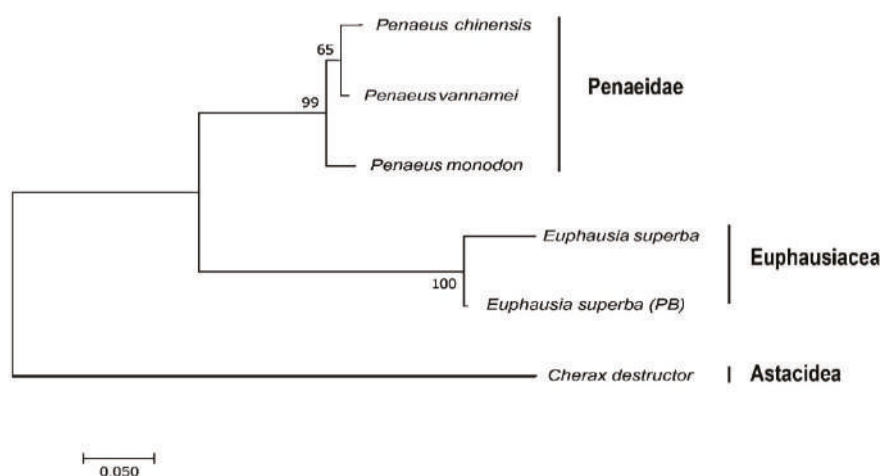
2.2.2. Multiple Sequence Alignment and Phylogenetic Analysis of the Representative Mitochondrial Gene *nad4L*

The representative mitochondrial gene *nad4L* from both Antarctic krill and whiteleg shrimp (a good counterpart from warm waters) were chosen to perform multiple sequence alignment (Figure 2). We observed 6 and 30 different residues between the Antarctic krill in this study and the sample collected from Prydz Bay (*E. superba* PB) [6], and between our Antarctic krill and the whiteleg shrimp, respectively. Obviously, both Antarctic krill samples were more conserved; however, their sequence variances may represent various origins.



**Figure 2.** Multiple sequence alignment of the putative *nad4L* genes. Red circles at the bottom stand for the same residues. Blue and purple colors on the sequences represent the alignment with identity >50% and >80%, respectively.

To confirm the Antarctic krill in the present study is the same species as reported *E. superba* (PB) [6] and to provide more evidence for the phylogenetic relationship between Penaeidae and Euphausiacea, we used the *nad4L* sequence of Australian freshwater crayfish (*Cherax destructor*; NCBI Gene ID: 2827710) as an out-group and constructed a phylogenetic tree of *nad4L* among the Antarctic krill, the whiteleg shrimp, and several other representative shrimps. The established phylogenetic topology was divided into two main groups of Penaeidae and Euphausiacea (Figure 3). The *nad4L* identified for the Antarctic krill in the present study was not surprised to be much closer to the reported *E. superba* (PB)’s [6]. That is to say, the *nad4L* is practicable for the Antarctic krill in species identification and has potential for origin determination.



**Figure 3.** Phylogenetic topology of *nad4L* derived from the Neighbor–Joining method [21]. The bootstrap test employed 1,000 replicates, and the numbers next to branches were replicate percentage of taxa clustering [22]. Corresponding amino acid sequences were analyzed in MEGA7 [23].

### 2.3. Assemblies of Reported Transcriptomes of the Antarctic Krill and the Whiteleg Shrimp

Raw data of the Antarctic krill transcriptomes were downloaded from the National Center for Biotechnology Information (NCBI; accession number PRJNA307639). Total RNA was isolated from six whole specimens that were collected from the Southern Ocean. High-throughput transcriptome sequencing (pair-ended at  $2 \times 150$  bp) on an Illumina HiSeq 3000 platform generated ~77.9 million of raw reads, equal to 11.8 Gb [1]. Here, we assembled these available public transcriptome sequences. After removal of low-quality reads and trimming adapter sequences, we collected 10.6 million of clean reads corresponding to 1.5 Gb, and generated 16,797 unigenes with a GC rate of 37.6% for the Antarctic krill. As summarized in Table 2 for the transcriptome assembly, the average length was 637 bp and the N50 was 923 bp.

**Table 2.** Summary of our de novo assembly of the previously reported *E. superba* transcriptomes [1].

Parameter	Value
Total Number (unigene)	16,797
Total Length (bp)	10,715,598
Mean Length (bp)	637
N50 (bp)	923
GC (%)	37.63

The raw data of the whiteleg shrimp transcriptomes were downloaded from NCBI under the accession number PRJNA288849. In the corresponding report [24], whole-body adult shrimps at three molting stages (including inter-molt, pre-molt and post-molt) were collected from a laboratory culture, and an Illumina HiSeq 2500 platform was used for the sequencing of cDNA libraries. Here, we assembled the publicly available transcriptome sequences. Finally, a total of 90.9 million clean reads (equal to 3.1 Gb) were obtained after data filtering. In the transcriptome assembly, 3,768 unigenes were annotated; the average length was 574 bp and the N50 value was 759 bp, with an average GC content of 51.0% (Table 3).

**Table 3.** Summary of our de novo assembly of the reported *P. vannamei* transcriptomes [24].

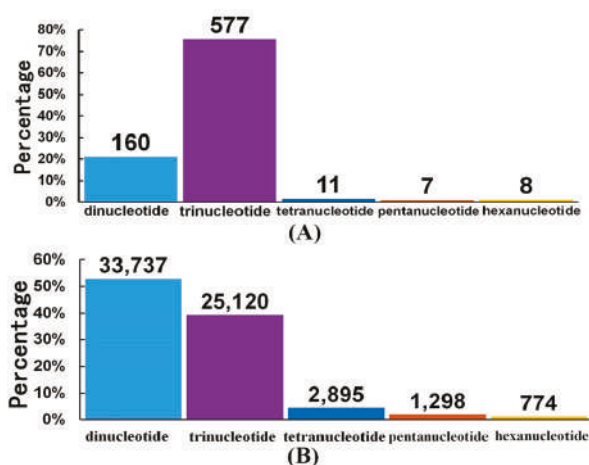
Parameter	Value
Total Number (unigene)	3,768
Total Length (bp)	2,165,058
Mean Length (bp)	574
N50 (bp)	759
GC (%)	50.95

These assemblies of reported transcriptomes were set for high-throughput SSR identification in the Antarctic krill (Section 2.4) and further comparisons of AMPs and AHTPs between the Antarctic krill and the whiteleg shrimp (Sections 2.5 and 2.6).

#### 2.4. High-throughput SSR Identification in the Antarctic Krill

In order to investigate whether genomic data of the Antarctic krill can be used for the development of genetic markers for species identification and origin determination, we picked SSR as a trial example. Interestingly, a total of 1,026 and 74,661 SSRs were identified from our transcriptome (Section 2.3) and partial genome raw data (Section 2.1) of the Antarctic krill, respectively (Table S3). These SSRs ranged from 2 to 6 bp.

In the transcriptome assembly, the most abundant type of SSRs was the trinucleotide repeats. As shown in Figure 4A, the total number of SSRs with trinucleotide repeats was 577, and their percentage reached 75.62%; the second highest number of SSRs, 160, was with dinucleotide repeats. However, in our partial genome raw data, the situation seemed to be different. The most abundant SSRs were with dinucleotide repeats (33,737), accounting for 52.9%; SSRs with trinucleotide repeats were dropped down to the second highest number, 25,120 (see more details in Figure 4B).

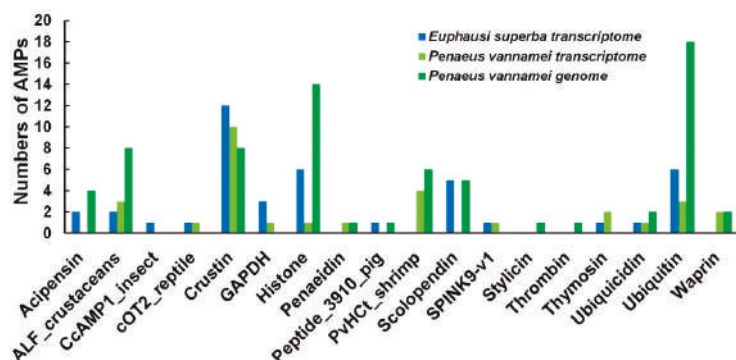


**Figure 4.** SSR classification in the Antarctic krill. Data were analyzed in our transcriptome assembly (A; Section 2.3) and our partial genome raw data (B; Section 2.1). The x-axis is the nucleotide type of each SSR, and the y-axis is the percentages of these SSRs. The number on the top of each bar is the total amount of corresponding SSRs.

#### 2.5. Comparisons of AMPs between the Antarctic Krill and the Whiteleg Shrimp

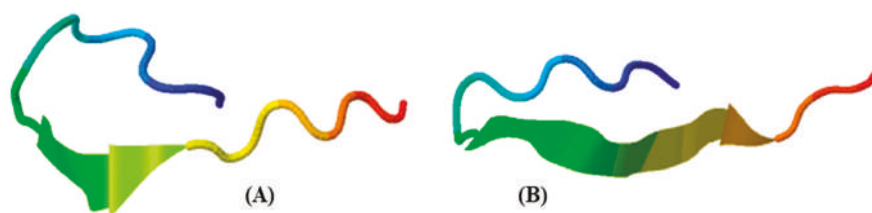
Employing our previously collected list of active AMPs (Table S4) and analysis pipeline [9], we employed BLAST to search the Antarctic krill and the whiteleg shrimp transcripts (Section 2.3) and identified 85 and 78 putative AMPs (Table S5), respectively. These AMPs/AMP precursors were

classified into 16 groups (Figure 5). Interestingly, in the present study, CcAMP1\_insect was only identified in the Antarctic krill transcripts, but not in the transcriptome and genome sequences of the whiteleg shrimp (the third group in Figure 5). We also noted that histone 2 (one of the six histones; with the mapped AMP of Buforin I) and ubiquitin/ribosomal S27 fusion protein (with the mapped AMP of cgUbiquitin) were the top two AMP precursors with the highest transcription values in the Antarctic krill (Table S6; not detectable in the whiteleg shrimp). PvHCt, corresponding to the C-terminal fragment in hemocyanin of *P. vannamei* [25], presented high transcription values in our assembled whiteleg shrimp whole-body transcriptomes (see Table S6).



**Figure 5.** Summary of the identified anti-microbial peptides (AMPs)/AMP precursors from the Antarctic krill transcriptome and the whiteleg shrimp transcriptome and genome assemblies. Blue bars represent those identified in the former (*E. superba*), and green bars represent those retrieved from the latter (*P. vannamei*).

Meanwhile, we observed that the homologous sequence of the CcAMP1\_insect extracted from the Antarctic krill transcriptomes in the present study had one different residue (K) from that of insect *Coridius chinensis*'s (V) (Figure 6). The predicted 3D structure of *E. superba* CcAMP1\_insect (Figure 6B) was different from the *C. chinensis*'s (Figure 6A), although both contained strands and coils.

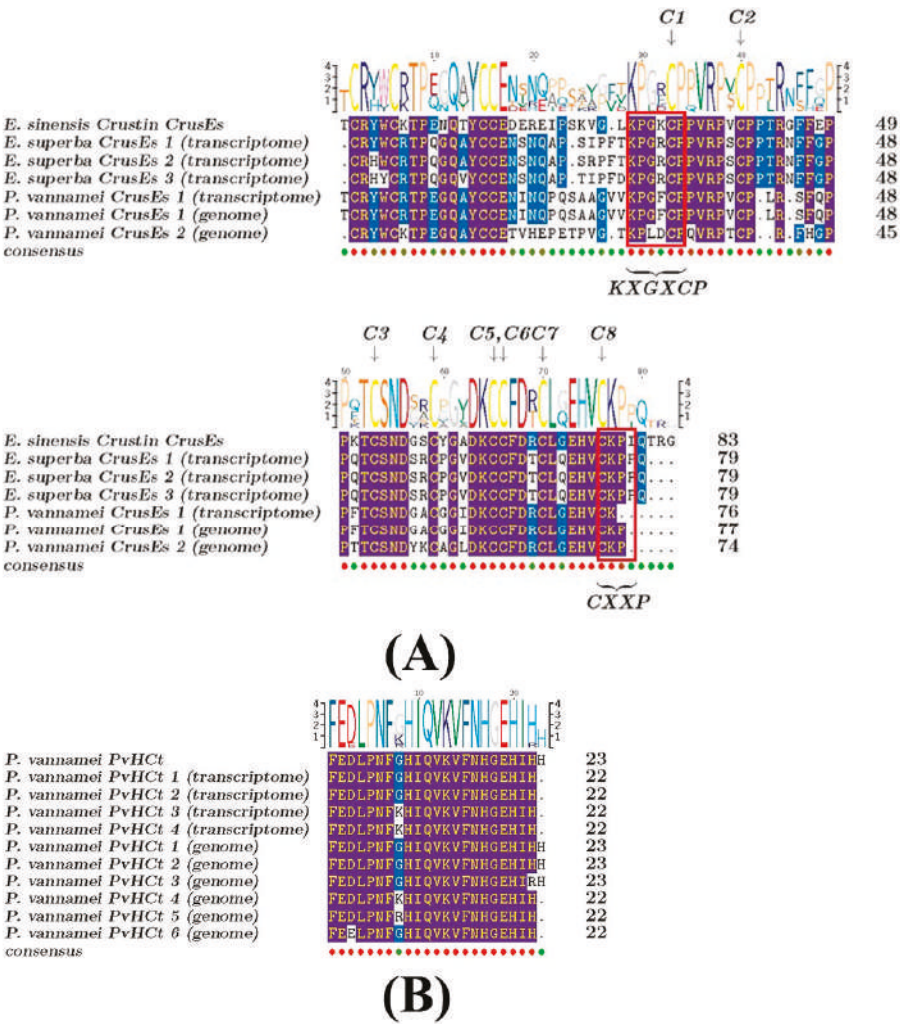


**Figure 6.** Predicted 3D structures of CcAMP1\_insect in insect *C. chinensis* (A) and the Antarctic krill (B). They were predicted by I-TASSER with high confidence (see more details in Section 3.2).

An important AMP category, crustin, abundantly existed in both crustaceans (Figure 5). Some of them, named CrusEs, belong to a group of cysteine-rich antibacterial peptides with whey acidic protein (WAP) domains, including two four-disulfide core domains and each domain with 8 conserved cysteine residues. The WAP domains also contain a KXGXCP motif [26,27]. Multiple sequence alignments of crustin (CrusEs; Figure 7A) demonstrated that both the Antarctic krill and the whiteleg shrimp possessed conserved cysteines. Another CXXP motif of the WAP domain could also be identified in the Antarctic krill, while it was incomplete in the whiteleg shrimp (see the detailed *P. vannamei* CrusEs



(genome) sequence in Figure 7A). A phylogenetic analysis of the representative CrusEs between the two crustaceans was performed for more comparison (Figure S3; data from Figure 7A).



**Figure 7.** Multiple sequence alignment of representative AMPs/AMP precursors. (A) Crustins from different species. The eight cysteine residues, conserved in all crustaceans with the consensus sequences of whey-acidic proteins [26], were also present in the CrusE sequences, as indicated by arrows and C1–C8. (B) PvHct from the whiteleg shrimp (*P. vannamei*). Red circles at the bottom stand for the same residues. Blue marks represent the alignment with identity >50%.

The transcription levels of crustin (such as CrusEs and MrCrs) were usually very high in the Antarctic krill, whereas they were not detectable in the whiteleg shrimp (see more details in Table S6). Interestingly, we observed three CrusEs in the former but only one in the latter. Similarly, another crustin category (MrCrs) was highly transcribed in the Antarctic krill but not detectable in the whiteleg shrimp; there were nine MrCrs in the former but only two in the latter (Table S6). There were also some *P. vannamei* unique crustins including CrustinPm1, CrustinPm7 as well as other AMPs including CqCrs,



SWDPM2, PvHCT, penaeidin, and waprin were obtained from the whiteleg shrimp transcriptome and genome, although their transcriptions were not detectable either (see Table S6). We noted that sylicin and thrombin were not identified in the transcriptome but only in the genome of the whiteleg shrimp in this study (Figure 5, Table S6). As expected, penaeidins of the whiteleg shrimp were the same as those of the reported penaeid shrimp [28]. The sequence of PvHCT identified in the present study was also highly conserved in comparison to that in previous studies [25] with minor variances (Figure 7B).

2.6. Prediction and Analysis of AHTPs in both Crustacean Species

To identify potential AHTPs in the translated proteomes (from the genome or transcriptome data) of the Antarctic krill and the whiteleg shrimp, we built a local AHTP-searching database [13]. Most of the known AHTPs searched in this database have been verified in reported studies, and they are usually tripeptides with less than 10 amino acids; the top 50 AHTPs with the highest activity were chosen to identify AHTPs in the two crustacean species, as reported in our previous study [14]. Finally, in the Antarctic krill, 23 AHTP sequences were identified from the transcriptomes; in the whiteleg shrimp, AHTP numbers were 20 and 29 from the reported transcriptomes [1] and genome assembly [8] (Table S9). The detailed location(s) of each matched AHTP sequence in its corresponding protein was listed in Table S7. It seems that AHTPs are almost overlapped between the two crustaceans (Figure 8, Table S9).

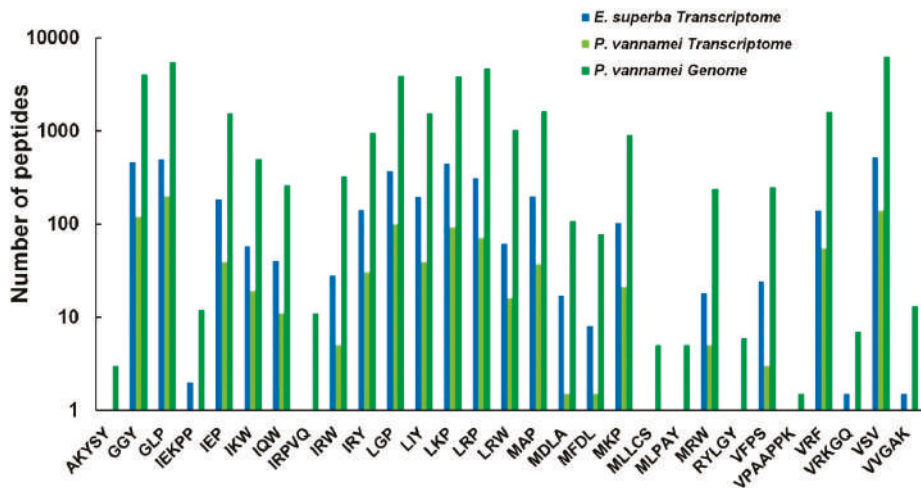


Figure 8. A comparative overview of the identified antihypertensive peptides (AHTPs) in both crustaceans. Blue bars denote the AHTPs identified from *E. superba* transcriptome [1]; green bars represent the *P. vannamei* AMPs retrieved from both transcriptome [24] and genome [8] data.

In the Antarctic krill, we observed that involucrin had the most abundant AHTP hit numbers (14; Table S8). In the whiteleg shrimp, however, it is the collagen alpha-1 chain-like protein that possessed the most AHTP hits (27; see Table S8). As shown in Figure 8, the richest AHTP categories were VSV, GLP, LRP, GGY, LGP, LKP in both crustacean species. Some AHTPs were identified only in the genome of whiteleg shrimp but were not detectable in the transcripts of Antarctic krill and whiteleg shrimp, such as AKYSY, IRPVQ, MLLCS, MLPAY, RYLGY, as well as VPAAPPK (Figure 8, Table S9).

### 3. Discussion

#### 3.1. Importance to Characterize the Genome Size, Mitochondrial Genome and SSRs in the Antarctic Krill

Our genome survey in the present study first calculated the estimated genome size of the Antarctic Krill as 42.1 Gb (Figure 1). This result is consistent with a previous report of 47.5 Gb from both flow cytometry and Feulgen image analysis densitometry [29]. However, such a large genome is beyond our present capacity to obtain a good assembly. We had to stop our genome project temporally, without wasting more time and money, until we figure out practicable assemble strategies.

Mitochondrial genes have been widely used for species identification. In the present study, sequence alignment and phylogenetic analysis of the representative *nad4L* between two sources of Antarctic krill and the whiteleg shrimp (Figures 2 and 3) revealed the phylogenetic relationship between Penaeidae and Euphausiacea (Figure 3). We also mapped the 13 typical protein-coding genes (Figure S1), which were similar to a previous report in *E. superba* (PB) [1]. It seems that the extraction of mitochondrial genes from the genome survey data can be used for origin determination, which will be informative for in-depth studies on various sources of Antarctic krill. Meanwhile, the mitochondrial roles for cold adaptation have been studied in cod. The overall COX activities in liver were reported to be higher in the cold-adapted population, although they were not affected by cold acclimation [30]. Similarly, the mitochondrial genes in the Antarctic krill may also benefit from the examination of cold adaptive mechanisms to polar environments.

SSRs, also called microsatellite markers, are a class of repetitive DNA sequences. They usually consist of tandem repeating units of mon-, di-, tri-, and tetra-nucleotide types. They have become well-known markers for identifying and classifying species from various resources [31]. In diverse shrimps, SSRs have been developed for potential applications in genetic studies, kinship analysis, origin determination, etc. [32]. Dinucleotide repeats were the most abundant type in reported Antarctic krill transcriptomes [1] and our partial genome raw data (Figure 4B). With the availability of more genome-wide SSRs from other resources of Antarctic krill, we may determine the origin of any commercial frozen products in the future.

#### 3.2. Similarities and Differences of AMPs between the Two Examined Crustacean Species

Our present study also provided a valuable genetic resource for AMP comparisons between Antarctic krill and whiteleg shrimp. It seems that AMPs and AMP precursors were generally conserved, while being differentially various between the two crustacean species, possibly due to their residency in significantly different waters.

The Antarctic krill unique CcAMP1 was originally extracted from *C. chinensis* [33]. However, there is no document revealing the correlation of CcAMP1 and environmental adaptation. According to previous reports, there were five hydrophobic amino acids (VAWVL) on its surface, which might construct an  $\alpha$ -helix to destroy the cell member integrity of bacteria [25] for stronger antimicrobial effects. However, since the predicted 3D structures of CcAMP1 of *E. superba* and *C. chinensis* in the present study were different (without the critical helix structures; Figure 6), thereby leading to uncertainty of the putative antimicrobial activity. As highly transcribed in the Antarctic krill, a specific protease was reported to be responsible for the generation of AMP buforin I from the histone 2 [34]. Buforin I was originally identified from Asian toad and showed strong antimicrobial activities against a broad spectrum of bacteria [35]. The AMP cgUbiquitin, mapped in the ubiquitin/ribosomal S27 fusion protein, was originally isolated from the gill of the Pacific oyster, and its precursor mRNA was reported to be significantly upregulated after *Vibrio* stimulation [36]. We therefore propose that these Antarctic krill's unique and highly transcribed AMPs were possibly important for the survival of aquatic animals in a cold environment.

For the crustin (CrusEs) from both Antarctic krill and whiteleg shrimp, the CXXP motif was identified completely from the former, while incomplete in the latter. This may cause non-functionality or neo-functionality in the whiteleg shrimp. Furthermore, the cDNA sequences of CrusEs, previously

identified from Chinese mitten crab with the validation of purified proteins to inhibit the growth of Gram-positive bacteria [26], and the cDNA encoding MrCr, with a first report in a freshwater prawn *Macrobrachium rosenbergii*, could be inductively expressed when the host was affected by bacteria [37]. Their high transcription levels and the greater number present in Antarctic krill compared to whiteleg shrimp suggest their more important roles in Antarctic krill.

The whiteleg shrimp's unique AMPs, identified in the present study, were from a preliminary exploration. It will be necessary to perform a double check when the genome assembly of the Antarctic krill is available. CrustinPm1, crustinPm7, CqCr, and stylicin were previously identified from black tiger shrimp (*Penaeus monodon*), red claw crayfish (*Cherax quadricarinatus*) and Pacific blue shrimp (*Litopenaeus stylirostris*), and exhibited antimicrobial activities against bacterial and fungal invasions [37–39]. SWDPm2, originally identified from hemocytes of the black tiger shrimp, is another group of WAP domains containing protein similar to crustin; it was up-regulated after an injection of white spot syndrome virus (WSSV) [40]. PvHCT, a histidine-rich antimicrobial peptide with antimicrobial activity to fungal cells, was originally found in whiteleg shrimp. It has potentially been derived in large quantities by the proteolytic cleavage of the hemocyanin protein [25]. Unlike gene-encoded cationic defense peptides such as crustins and penaeidins, PvHCT can be obtained massively by hemocyanin proteolytic cleavage without any recombinant production or purification system and is the most abundant plasma protein in crustaceans [25]. The whiteleg shrimp's unique AMPs identified in our present study were potentially more important for this species. Furthermore, those genes with high transcription levels, such as AMP precursor histone 2, ubiquitin/ribosomal S27 fusion protein, and the WAP-domain-containing proteins including crustin and waprin, as well as hemocyanins-derived PvHCT, may be promising antimicrobial candidates and potentially good sources for the development of AMP-based drugs. Regarding the stylicin [39] and thrombin [41], which were only identified in the *P. vannamei* genome in our present study, we guess that they may not be well transcribed.

Meanwhile, the environmental specificity of the AMPs in both Antarctic krill and whiteleg shrimp were also investigated. Interestingly, we found that some AMPs that are unique to the Antarctic krill or in both crustaceans may not show environmental specificity, because the habitats of their derived species and the bacteria inhibited by them were not coincident with Antarctic krill's distribution areas [35,36,38,42,43]. However, some AMPs only identified in whiteleg shrimp in the present study (such as crustinPm1) may play important roles in special responses to warm environments due to the fact that their originally sourced species were geographically consistent with whiteleg shrimp [44].

### 3.3. Conservations of AHTPs between the Two Crustacean Species

AHTPs were investigated in the present study for the potential development of antihypertensive drugs from the Antarctic krill. Although from different environments, unlike AMPs, the most abundant AHTPs (such as VSV) were the same, and most of the AHTPs can be found both in the datasets of the Antarctic krill as well as the whiteleg shrimp. These data indicate that the AHTPs may be highly conserved in both crustaceans, which is consistent with our previous report of marine mammals [14]. However, those AHTPs identified only in the genome of the whiteleg shrimp also need to be retrieved from the genome of the Antarctic krill once its good assembly is made available in future.

Interestingly, the AHTP mapping ratio in involucrin was higher than other proteins in the Antarctic krill, with AHTP hits to 14. The Involucrin with the most abundant AHTPs is a keratinocyte protein [45], and keratinocytes is the major constituent of the epidermis tissue [46] of the skin's outer layer [47]. As for the whiteleg shrimp, however, both collagen alpha-1(V) chain-like protein and collagen alpha-1(XI) chain-like protein were the most abundant AHTP-containing proteins, which were revealed previously by us in fishes [13]. In fact, ACE-inhibitory peptides had been obtained from the collagen hydrolysates of many animals [48–53]. Based on our present work, we propose to apply the epidermis tissues of the Antarctic krill and collagen alpha chain proteins of shrimps as a promising resource to obtain AHTP production. Of course, similarly to the AMPs, the ACE inhibitory activity can

be evaluated after the comprehensive prediction results are available, once the genome of the Antarctic krill is assembled with high quality.

## 4. Materials and Methods

### 4.1. Genomic DNA Extraction and Genome Sequencing for the Antarctic Krill

Our experimental procedures complied with the current laws on animal welfare and research in China. Alive Antarctic krill specimens were collected from the Argentine Sea area (45°92'S, 61°82'W). Genomic DNAs were extracted from the whole bodies of pooled specimens with a Qiagen GenomicTip100 kit (Qiagen, Germantown, MD, USA) according to the manufacturer's protocol. With the traditional whole-genome shotgun sequencing strategy [14], we used 1 µg of normalized DNA to prepare a paired-end short-insert library (400 bp). Quantification and size estimations of the library were performed on a Zebra Flowcell 3.1 chip. Finally, the library was normalized to 15 ng/µL for paired-end sequencing (100 bp in length) on a BGISEq500 platform (BGI, Shenzhen, China). Raw genome sequencing reads have been deposited in the NCBI and China National GeneBank (CNCB) under the project IDs PRJNA598052 and CNP0000808, respectively.

### 4.2. Assembly of the Antarctic Krill Mitochondrial Genome and Transcriptomes

At first, we estimated the genome size of the Antarctic krill using a routine K-mer analysis method [14] with the following formula:  $G = K\_num / K\_depth$ , where  $K\_num$  is the total number of K-mers, and  $K\_depth$  indicates the frequency of reads occurring more frequently than others [17].

BGI paired-end reads were filtered with SOAPnuke1.5.6 [54] and the common adapter sequences were trimmed. A roughly complete mitochondrial genome of the Antarctic krill was assembled. Firstly, the mitochondrial genome of a congeneric *E. superba* (downloaded from the NCBI with an accession number EU583500.1) was employed [6]. Those sequencing reads with a high similarity to the reference mitochondrial genome were identified by SOAP2 (version 2.21) [55]. Subsequently, SPAdes (version 3.10.0) was employed [56] to assemble all these highly similar reads. Finally, Blast (version 2.6.1) [57] was applied to compare the archived assembly with the reference mitochondrial genome. The scaffolds containing a low length (<200 bp) were removed and the filtered scaffolds were combined into one sequence as a mitochondrial genome sequence. The redundancy sequences were also manually deleted. Then, the mitochondrial genome sequence was annotated with AGORA [58] to get the 13 protein-coding genes nucleotide sequences.

The *E. superba* and *P. vannamei* transcriptome sequences were downloaded from the NCBI with accession numbers PRJNA307639 (SRR3089571) [1] and PRJNA288849 [24], respectively. SOAPnuke 1.5.6 [54] was employed to filter the paired-end short reads of transcriptomes with the removal of contaminants, adapters and those low-quality reads (with over 5% non-sequenced bases or more than 20% of bases with quality score  $\leq 10$ ). We then employed Trinity v2.5.1 [59] to assemble the remaining clean reads, which were clustered by using TGICL v2.1 [60] based on sequence similarity and assembled to consensus unigenes. Clean reads were aligned to the de novo assemblies with a Bowtie 2 read aligner [61] to calculate gene transcription values in the assembled transcriptomes. Finally, we used RNA-Seq by Expectation Maximization (RSEM) v1.2.31 [62] to estimate transcript abundance in term of FPKM (fragments per kilobase of transcript per million mapped reads) values. The candidate coding regions from the assembled transcripts were identified with TransDecoder (<http://transdecoder.sourceforge.net/>), and then were translated into amino acid sequences using the standard codon table.

### 4.3. Functional Annotation of the Extracted Mitochondrial Genome and the Reported Transcriptomes

The amino acid sequences of Antarctic krill mitochondrial protein-coding genes from AGORA [58] annotation results were mapped to KEGG [19] pathway annotations using Diamond [18] with an *E*-value threshold of  $1.0 \times 10^{-5}$ . Blast2GO v4.1 [63] was employed to perform GO [20] annotation of NCBI

Nr blast results. Unigene sequences from the Antarctic krill and the whiteleg shrimp transcriptomes were searched using Diamond [18] and blastn [57] against the NCBI Nr and UniProtKB/Swiss-Prot [64] databases ( $E$ -value  $\leq 1.0 \times 10^{-5}$ ) to retrieve protein functional annotations based on sequence similarity.

#### 4.4. Phylogenetic Analysis and Multiple Sequence Alignment

Along with the *nad4L* sequence extracted from the Antarctic krill mitochondrial genome, we also extracted several other malacostracan *nad4L* sequences from the NCBI for a subsequent phylogenetic analysis. Examined species include *Penaeus chinensis*, *P. vannamei*, *P. monodon*, *E. superba* (from the present study), *E. superba* (PB), and *Cherax destructor* (as the out group). The translated protein sequences from these species were aligned using mafft v7.158b [65] with default parameters. The phylogenetic tree was constructed with the Neighbor Joining (NJ) of pairwise distances using MEGA 7.0 [23]. Multiple sequence alignment was performed using MEGA 7.0 [23], and the archived results were further analyzed and visualized by TEXshade (version 2.12.14) [66].

#### 4.5. SSR Analysis

We employed our own script SSR.sh to search known SSRs from the reported transcriptome and our randomly selected partial genome raw data of the Antarctic krill. Our own script filter\_ssr.pl was used to calculate SSR ratio, and the SSR distribution map was plotted with our own script draw\_ssr.pl and Excel.

#### 4.6. AMP Analysis

A total of 3073 AMP sequences were used as a local AMPs searching list as previously reported [9,67]. Standard homology searches were performed against the *E. superba* [1] and *P. vannamei* transcriptomes [24] as well as *P. vannamei* genome [8] to predict putative AMP sequences. In brief, index transcriptome and genome databases were built by running a makeblastdb command in ncbi-blast-2.6.0 [57]. Subsequently, the tBLASTn ( $E$ -value of  $1.0 \times 10^{-5}$ ) in ncbi-blast-2.6.0 [57] was employed to search our reference AMP list from the index transcriptome and genome databases with filtering of those with a query align ratio less than 0.5.

#### 4.7. AHTP Analysis

The AHTPs with the top 50 inhibitory activities were compiled as a local searching reference as described in our previous study [13]. Employing a local custom Perl script pipeline, we identified matched AHTPs sequences and locations from target proteins in the transcriptomes of *E. superba* [1] and *P. vannamei* [24], as well as the genome of *P. vannamei* [8]. AHTPs hit numbers in the mapped proteins were summarized for comparison between the two crustacean species.

#### 4.8. Tertiary Structure Prediction

To predict the 3D structures of AMPs, I-TASSER [68] was employed and the high confidence model is supported by high C-score. The top ten starting threading templates for the predicted 3D structures of CcAMP1\_insect in *C. chinensis* were 3hiaB, 5lqwX, 1jy4A, 3mlqE, 6et5A, 1jy4A, 3hiaB, 1e0nA, 1jy4A and 3hiaB, and the first starting template was 3HIA, a crystal structure of the choline-binding domain of Spr1274 in *Streptococcus pneumoniae*. The top ten starting threading templates for the CcAMP1\_insect in the Antarctic krill were 5af7A, 5lqwX, 1jy4A, 3mlqE, 1udyA, 1jy4A, 3hiaB, 6pz9D, 5jscA and 3hiaB, and the first starting template was 5AF7 for the 3-Sulfinopropionyl-coenzyme A (3SP-CoA) desulfinate from *Advenella mimigardefordensis* DPN7T: crystal structure and function of a desulfinate with an acyl-CoA dehydrogenase fold. In our present work, the C-scores with a range between  $-5$  and  $2$  were collected as confidence indexes for model estimation.

## 5. Conclusions

At first, we reported a genome survey of Antarctic krill, the most fundamental animal in the Antarctic food chain. Partial mitochondrial genome and abundant SSRs were extracted from our archived partial genome raw data and reported transcriptomes, which may be useful for the species identification and origin determination of this important polar crustacean species. A high-throughput identification and comparison of AMPs/AMP precursors and AHTPs between Antarctic krill and its famous counterpart, the whiteleg shrimp from warm waters, revealed general conservation with interesting variations between the two species. In summary, as the first report of the estimated genome size of Antarctic krill, our present genome survey data provide a foundation for further biological research of this economically and ecologically important invertebrate species. Our primary investigations on bioactive peptides (including AMPs and AHTPs) on a large-scale from such a polar species will bring new a perspective for in-depth predictions and the development of novel marine drugs in the future.

**Supplementary Materials:** The following are available online at <http://www.mdpi.com/1660-3397/18/4/185/s1>. Figure S1. A sketch map for the 13 mitochondrial protein-coding genes of the Antarctic krill. The orders of these genes are in a clockwise direction, except for *nad1*, *nad4*, *nad4L*, and *nad5*. Figure S2. Functional classification of the *E. superba* mitochondrial genome. Figure S3. A phylogenetic analysis of the representative AMP precursors, CrusEs, from both crustaceans. File S1. Representative sequences of the 13 mitochondrial protein-coding genes of the Antarctic krill, using the reported entire mitochondrial genome sequence as the reference. Table S1. KEGG analysis of the Antarctic krill extracted mitochondrial genes. Table S2. KEGG2Gene of the *E. superba* extracted mitochondrial genes. Table S3. SSRs extracted from *E. superba* reported transcriptome sequences and part of our genome raw reads. Table S4. Collection of reported AMPs. Table S5. Putative AMPs identified from the *E. superba* and *P. vannamei* transcriptomes. Table S6. Summary of the identified AMPs/AMP precursors in both crustacean species with transcription levels (FPKM values). Table S7. Specific alignments of all mapped proteins and their corresponding matched AHTPs in both crustacean species. Table S8. Identified proteins with hit numbers of matched AHTPs in the Antarctic krill and whiteleg shrimp. Table S9. Number of mapped AHTPs in both crustacean species from transcriptome or genome data.

**Author Contributions:** L.S., C.X., H.H., and Q.S. conceived and designed the project. Y.H., C.B., and L.W. analyzed the data; Z.L., Y.Y., and X.Y. participated in data analysis and manuscript preparation. C.X., H.H., W.S., and X.M. collected samples. Y.H. and Q.S. wrote the manuscript. Q.S., L.W., C.X., and L.S. revised the manuscript. All authors have read and agreed to the published version of the manuscript.

**Acknowledgments:** The work was supported by China National Key R & D Program (No. 2018YFC0310802), Shenzhen Dapang Special Program for Industrial Development (Nos. KY20180205 and PT201901-08), and Shenzhen Special Project for High-Level Talents (No. SZYSGZZ-2018001).

**Conflicts of Interest:** The authors declare no conflict of interest.

## References

1. Ma, C.; Ma, H.; Xu, G.; Feng, C.; Ma, L.; Wang, L. De novo sequencing of the Antarctic krill (*Euphausia superba*) transcriptome to identify functional genes and molecular markers. *J. Genet.* **2018**, *97*, 995–999. [\[CrossRef\]](#)
2. Ikeda, T.; Dixon, P. The influence of feeding on the metabolic activity of Antarctic krill (*Euphausia superba* Dana). *Polar Biol.* **1984**, *3*, 1–9. [\[CrossRef\]](#)
3. Sales, G.; Deagle, B.E.; Calura, E.; Martini, P.; Biscontin, A.; De Pitta, C.; Kawaguchi, S.; Romualdi, C.; Meyer, B.; Costa, R. KrillDB: A *de novo* transcriptome database for the Antarctic krill (*Euphausia superba*). *PLoS ONE* **2017**, *12*, e0171908. [\[CrossRef\]](#)
4. Friedlaender, A.S.; Johnston, D.W.; Fraser, W.R.; Burns, J.; Costa, D.P. Ecological niche modeling of sympatric krill predators around Marguerite Bay, Western Antarctic Peninsula. *Deep Sea Res. Part II Top. Stud. Oceanogr.* **2011**, *58*, 1729–1740. [\[CrossRef\]](#)
5. Nicol, S.; Foster, J.; Kawaguchi, S. The fishery for Antarctic krill—recent developments. *Fish Fish.* **2012**, *13*, 30–40. [\[CrossRef\]](#)
6. Shen, X.; Wang, H.; Ren, J.; Tian, M.; Wang, M. The mitochondrial genome of *Euphausia superba* (Prydz Bay) (Crustacea: Malacostraca: Euphausiacea) reveals a novel gene arrangement and potential molecular markers. *Mol. Biol. Rep.* **2010**, *37*, 771. [\[CrossRef\]](#)



7. Machida, R.J.; Miya, M.U.; Yamauchi, M.M.; Nishida, M.; Nishida, S. Organization of the mitochondrial genome of Antarctic krill *Euphausia superba* (Crustacea: Malacostraca). *Mar. Biotechnol.* **2004**, *6*, 238–250. [\[CrossRef\]](#)
8. Zhang, X.; Yuan, J.; Sun, Y.; Li, S.; Gao, Y.; Yu, Y.; Liu, C.; Wang, Q.; Lv, X.; Zhang, X. Penaeid shrimp genome provides insights into benthic adaptation and frequent molting. *Nat. Commun.* **2019**, *10*, 356. [\[CrossRef\]](#)
9. Yi, Y.; You, X.; Bian, C.; Chen, S.; Lv, Z.; Qiu, L.; Shi, Q. High-throughput identification of antimicrobial peptides from amphibious mudskippers. *Mar. Drugs* **2017**, *15*, 364. [\[CrossRef\]](#)
10. Tincu, J.A.; Taylor, S.W. Antimicrobial peptides from marine invertebrates. *Antimicrob. Agents Chemother.* **2004**, *48*, 3645–3654. [\[CrossRef\]](#)
11. Sperstad, S.V.; Haug, T.; Blencke, H.-M.; Styrvoid, O.B.; Li, C.; Stensvag, K. Antimicrobial peptides from marine invertebrates: Challenges and perspectives in marine antimicrobial peptide discovery. *Biotechnol. Adv.* **2011**, *29*, 519–530. [\[CrossRef\]](#)
12. Zhao, L.; Yin, B.; Liu, Q.; Cao, R. Purification of antimicrobial peptide from Antarctic Krill (*Euphausia superba*) and its function mechanism. *J. Ocean. Univ. China* **2013**, *12*, 484–490. [\[CrossRef\]](#)
13. Yi, Y.; Lv, Y.; Zhang, L.; Yang, J.; Shi, Q. High throughput identification of antihypertensive peptides from fish proteome datasets. *Mar. Drugs* **2018**, *16*, 365. [\[CrossRef\]](#)
14. Jia, K.; Bian, C.; Yi, Y.; Li, Y.; Jia, P.; Gui, D.; Zhang, X.; Lin, W.; Sun, X.; Lv, Y.; et al. Whole genome sequencing of Chinese white dolphin (*Sousa chinensis*) for high-throughput screening of antihypertensive peptides. *Mar. Drugs* **2019**, *17*, 504. [\[CrossRef\]](#)
15. Park, S.Y.; Je, J.-Y.; Kang, N.; Han, E.J.; Um, J.H.; Jeon, Y.-J.; Ahn, G.; Ahn, C.-B. Antihypertensive effects of Ile-Pro-Ile-Lys from krill (*Euphausia superba*) protein hydrolysates: Purification, identification and in vivo evaluation in spontaneously hypertensive rats. *Eur. Food Res. Technol.* **2017**, *243*, 719–725. [\[CrossRef\]](#)
16. Zhao, Y.-Q.; Zhang, L.; Tao, J.; Chi, C.-F.; Wang, B. Eight antihypertensive peptides from the protein hydrolysate of Antarctic krill (*Euphausia superba*): Isolation, identification, and activity evaluation on human umbilical vein endothelial cells (HUVECs). *Food Res. Int.* **2019**, *121*, 197–204. [\[CrossRef\]](#)
17. Yu, Y.; Zhang, X.; Yuan, J.; Li, F.; Chen, X.; Zhao, Y.; Huang, L.; Zheng, H.; Xiang, J. Genome survey and high-density genetic map construction provide genomic and genetic resources for the Pacific White Shrimp *Litopenaeus vannamei*. *Sci. Rep.* **2015**, *5*, 15612. [\[CrossRef\]](#)
18. Buchfink, B.; Xie, C.; Huson, D.H. Fast and sensitive protein alignment using DIAMOND. *Nat. Methods* **2015**, *12*, 59–60. [\[CrossRef\]](#)
19. Kanehisa, M.; Goto, S. KEGG: Kyoto encyclopedia of genes and genomes. *Nucleic Acids Res.* **2000**, *28*, 27–30. [\[CrossRef\]](#)
20. Consortium, G.O. The Gene Ontology (GO) database and informatics resource. *Nucleic Acids Res.* **2004**, *32*, D258–D261. [\[CrossRef\]](#)
21. Saitou, N.; Nei, M. The neighbor-joining method: A new method for reconstructing phylogenetic trees. *Mol. Biol. Evol.* **1987**, *4*, 406–425.
22. Felsenstein, J. Confidence limits on phylogenies: An approach using the bootstrap. *Evolution* **1985**, *39*, 783–791. [\[CrossRef\]](#)
23. Kumar, S.; Stecher, G.; Tamura, K. MEGA7: Molecular evolutionary genetics analysis version 7.0 for bigger datasets. *Mol. Biol. Evol.* **2016**, *33*, 1870–1874. [\[CrossRef\]](#)
24. Gao, Y.; Zhang, X.; Wei, J.; Sun, X.; Yuan, J.; Li, F.; Xiang, J. Whole transcriptome analysis provides insights into molecular mechanisms for molting in *Litopenaeus vannamei*. *PLoS ONE* **2015**, *10*, e0144350. [\[CrossRef\]](#)
25. Petit, V.W.; Rolland, J.-L.; Blond, A.; Cazevielle, C.; Djediat, C.; Peduzzi, J.; Goulard, C.; Bachère, E.; Dupont, J.; Destoumieux-Garzon, D. A hemocyanin-derived antimicrobial peptide from the penaeid shrimp adopts an alpha-helical structure that specifically permeabilizes fungal membranes. *Biochim. Biophys. Acta* **2016**, *1860*, 557–568. [\[CrossRef\]](#)
26. Mu, C.; Zheng, P.; Zhao, J.; Wang, L.; Zhang, H.; Qiu, L.; Gai, Y.; Song, L. Molecular characterization and expression of a crustin-like gene from Chinese mitten crab, *Eriocheir sinensis*. *Dev. Comp. Immunol.* **2010**, *34*, 734–740. [\[CrossRef\]](#)
27. Ranganathan, S.; Simpson, K.J.; Shaw, D.C.; Nicholas, K.R. The whey acidic protein family: A new signature motif and three-dimensional structure by comparative modeling. *J. Mol. Graph. Model.* **1999**, *17*, 106–113. [\[CrossRef\]](#)

28. Destoumieux, D.; Munoz, M.; Bulet, P.; Bachere, E. Penaeidins, a family of antimicrobial peptides from penaeid shrimp (Crustacea, Decapoda). *Cell. Mol. Life Sci.* **2000**, *57*, 1260–1271. [\[CrossRef\]](#)
29. Jeffery, N.W. The first genome size estimates for six species of krill (Malacostraca, Euphausiidae): Large genomes at the north and south poles. *Polar Biol.* **2012**, *35*, 959–962. [\[CrossRef\]](#)
30. Lucassen, M.; Koschnick, N.; Eckerle, L.; Pörtner, H.-O. Mitochondrial mechanisms of cold adaptation in cod (*Gadus morhua* L.) populations from different climatic zones. *J. Exp. Biol.* **2006**, *209*, 2462–2471. [\[CrossRef\]](#)
31. Sundarar, J.K.; Rasal, K.D.; Chakrapani, V.; Swain, P.; Kumar, D.; Ninawe, A.S.; Nandi, S.; Jayasankar, P. Simple sequence repeats (SSRs) markers in fish genomic research and their acceleration via next-generation sequencing and computational approaches. *Aquacult. Int.* **2016**, *24*, 1089–1102. [\[CrossRef\]](#)
32. Perez, F.; Ortiz, J.; Zhinaula, M.; Gonzabay, C.; Calderon, J.; Volckaert, F.A. Development of EST-SSR markers by data mining in three species of shrimp: *Litopenaeus vannamei*, *Litopenaeus stylirostris*, and *Trachypenaeus birdy*. *Mar. Biotechnol.* **2005**, *7*, 554–569. [\[CrossRef\]](#)
33. Li, S.; Zhao, B. Isolation, purification, and detection of the antimicrobial activity of the antimicrobial peptide CcAMP1 from *Coridius chinensis* (Hemiptera: Dinidoridae). *Acta Entomol. Sin.* **2015**, *58*, 610–616.
34. Kim, H.S.; Park, C.B.; Kim, M.S.; Kim, S.C. cDNA cloning and characterization of buforin I, an antimicrobial peptide: A cleavage product of histone H2A. *Biochem. Biophys. Res. Commun.* **1996**, *229*, 381–387. [\[CrossRef\]](#)
35. Park, C.B.; Kim, M.S.; Kim, S.C. A novel antimicrobial peptide from *Bufo bufo* gargarizans. *Biochem. Biophys. Res. Commun.* **1996**, *218*, 408–413. [\[CrossRef\]](#)
36. Seo, J.-K.; Lee, M.J.; Go, H.-J.; Do Kim, G.; Do Jeong, H.; Nam, B.-H.; Park, N.G. Purification and antimicrobial function of ubiquitin isolated from the gill of Pacific oyster, *Crassostrea gigas*. *Mol. Immunol.* **2013**, *53*, 88–98. [\[CrossRef\]](#)
37. Krusong, K.; Poolpipat, P.; Supungul, P.; Tassanakajon, A. A comparative study of antimicrobial properties of crustinPm1 and crustinPm7 from the black tiger shrimp *Penaeus monodon*. *Dev. Comp. Immunol.* **2012**, *36*, 208–215. [\[CrossRef\]](#)
38. Yu, A.-Q.; Shi, Y.-H.; Wang, Q. Characterisation of a novel type i crustin involved in antibacterial and antifungal responses in the red claw crayfish, *Cherax quadricarinatus*. *Fish. Shellfish Immunol.* **2016**, *48*, 30–38. [\[CrossRef\]](#)
39. Rolland, J.A.M.; Dupont, J.; Lefevre, F.; Bachère, E.; Romestand, B. Stylicins, a new family of antimicrobial peptides from the Pacific blue shrimp *Litopenaeus stylirostris*. *Mol. Immunol.* **2010**, *47*, 1269–1277. [\[CrossRef\]](#)
40. Amparyup, P.; Donpuksa, S.; Tassanakajon, A. Shrimp single WAP domain (SWD)-containing protein exhibits proteinase inhibitory and antimicrobial activities. *Dev. Comp. Immunol.* **2008**, *32*, 1497–1509. [\[CrossRef\]](#)
41. Papareddy, P.; Rydengård, V.; Pasupuleti, M.; Walse, B.; Mörgelin, M.; Chalupka, A.; Malmsten, M.; Schmidtchen, A. Proteolysis of human thrombin generates novel host defense peptides. *PLoS Pathog.* **2010**, *6*, e1000857. [\[CrossRef\]](#)
42. Low, B.W.; Ng, N.K.; Yeo, D.C. First record of the invasive Chinese mitten crab, *Eriocheir sinensis* H. Milne Edwards, 1853 (Crustacea: Brachyura: Varunidae) from Singapore. *BiolInvas. Rec* **2013**, *2*, 73–78. [\[CrossRef\]](#)
43. Thanh, N.M.; Ponzoni, R.W.; Nguyen, N.H.; Vu, N.T.; Barnes, A.; Mather, P.B. Evaluation of growth performance in a diallel cross of three strains of giant freshwater prawn (*Macrobrachium rosenbergii*) in Vietnam. *Aquaculture* **2009**, *287*, 75–83. [\[CrossRef\]](#)
44. Benzie, J.; Ballment, E.; Forbes, A.; Demetriades, N.; Sugama, K.; Moria, S. Mitochondrial DNA variation in Indo-Pacific populations of the giant tiger prawn, *Penaeus monodon*. *Mol. Ecol.* **2002**, *11*, 2553–2569. [\[CrossRef\]](#)
45. Eckert, R.L.; Green, H. Structure and evolution of the human involucrin gene. *Cell* **1986**, *46*, 583–589. [\[CrossRef\]](#)
46. McGrath, J.; Eady, R.; Pope, F. Anatomy and organization of human skin. *Rook's Textb. Dermatol.* **2004**, *10*, 9781444317633.
47. Sotiropoulou, P.A.; Blanpain, C. Development and homeostasis of the skin epidermis. *Cold Spring Harb. Perspect. Biol.* **2012**, *4*, a008383. [\[CrossRef\]](#)
48. Saiga, A.; Iwai, K.; Hayakawa, T.; Takahata, Y.; Kitamura, S.; Nishimura, T.; Morimatsu, F. Angiotensin I-converting enzyme-inhibitory peptides obtained from chicken collagen hydrolysate. *J. Agric. Food Chem.* **2008**, *56*, 9586–9591. [\[CrossRef\]](#)
49. Kim, S.-K.; Byun, H.-G.; Park, P.-J.; Shahidi, F. Angiotensin I converting enzyme inhibitory peptides purified from bovine skin gelatin hydrolysate. *J. Agric. Food Chem.* **2001**, *49*, 2992–2997. [\[CrossRef\]](#)



50. Fu, Y.; Young, J.F.; Rasmussen, M.K.; Dalsgaard, T.K.; Lametsch, R.; Aluko, R.E.; Therkildsen, M. Angiotensin I-converting enzyme-inhibitory peptides from bovine collagen: Insights into inhibitory mechanism and transepithelial transport. *Food Res. Int.* **2016**, *89*, 373–381. [\[CrossRef\]](#)
51. Zhuang, Y.; Sun, L.; Li, B. Production of the angiotensin-I-converting enzyme (ACE)-inhibitory peptide from hydrolysates of jellyfish (*Rhopilema esculentum*) collagen. *Food. Bioproc. Tech.* **2012**, *5*, 1622–1629. [\[CrossRef\]](#)
52. Fahmi, A.; Morimura, S.; Guo, H.-C.; Shigematsu, T.; Kida, K.; Uemura, Y. Production of angiotensin I converting enzyme inhibitory peptides from sea bream scales. *Process. Biochem.* **2004**, *39*, 1195–1200. [\[CrossRef\]](#)
53. Liu, Z.-Y.; Chen, D.; Su, Y.-C.; Zeng, M.-Y. Optimization of hydrolysis conditions for the production of the angiotensin-I converting enzyme inhibitory peptides from sea cucumber collagen hydrolysates. *J. Aquat. Food Prod. Technol.* **2011**, *20*, 222–232. [\[CrossRef\]](#)
54. Chen, Y.; Chen, Y.; Shi, C.; Huang, Z.; Zhang, Y.; Li, S.; Li, Y.; Ye, J.; Yu, C.; Li, Z. SOAPnuke: A MapReduce acceleration-supported software for integrated quality control and preprocessing of high-throughput sequencing data. *Gigascience* **2017**, *7*, gix120. [\[CrossRef\]](#)
55. Li, R.; Yu, C.; Li, Y.; Lam, T.-W.; Yiu, S.-M.; Kristiansen, K.; Wang, J. SOAP2: An improved ultrafast tool for short read alignment. *Bioinformatics* **2009**, *25*, 1966–1967. [\[CrossRef\]](#)
56. Bankevich, A.; Nurk, S.; Antipov, D.; Gurevich, A.A.; Dvorkin, M.; Kulikov, A.S.; Lesin, V.M.; Nikolenko, S.I.; Pham, S.; Pribelski, A.D. SPAdes: A new genome assembly algorithm and its applications to single-cell sequencing. *J. Comput. Biol.* **2012**, *19*, 455–477. [\[CrossRef\]](#)
57. Mount, D.W. Using the basic local alignment search tool (BLAST). *Cold Spring Harb. Protoc.* **2007**, 2007, pdb.top17. [\[CrossRef\]](#)
58. Jung, J.; Kim, J.I.; Jeong, Y.-S.; Yi, G. AGORA: Organellar genome annotation from the amino acid and nucleotide references. *Bioinformatics* **2018**, *34*, 2661–2663. [\[CrossRef\]](#)
59. Haas, B.J.; Papanicolaou, A.; Yassour, M.; Grabherr, M.; Blood, P.D.; Bowden, J.; Couger, M.B.; Eccles, D.; Li, B.; Lieber, M. De novo transcript sequence reconstruction from RNA-seq using the Trinity platform for reference generation and analysis. *Nat. Protoc.* **2013**, *8*, 1494–1512. [\[CrossRef\]](#)
60. Pertea, G.; Huang, X.; Liang, F.; Antonescu, V.; Sultana, R.; Karamycheva, S.; Lee, Y.; White, J.; Cheung, F.; Parvizi, B. TIGR Gene Indices clustering tools (TGICL): A software system for fast clustering of large EST datasets. *Bioinformatics* **2003**, *19*, 651–652. [\[CrossRef\]](#)
61. Langmead, B.; Salzberg, S.L. Fast gapped-read alignment with Bowtie 2. *Nat. Methods* **2012**, *9*, 357–359. [\[CrossRef\]](#) [\[PubMed\]](#)
62. Li, B.; Dewey, C.N. RSEM: Accurate transcript quantification from RNA-Seq data with or without a reference genome. *BMC Bioinform.* **2011**, *12*, 323. [\[CrossRef\]](#) [\[PubMed\]](#)
63. Conesa, A.; Götz, S.; García-Gómez, J.M.; Terol, J.; Talón, M.; Robles, M. Blast2GO: A universal tool for annotation, visualization and analysis in functional genomics research. *Bioinformatics* **2005**, *21*, 3674–3676. [\[CrossRef\]](#) [\[PubMed\]](#)
64. Boeckmann, B.; Bairoch, A.; Apweiler, R.; Blatter, M.-C.; Estreicher, A.; Gasteiger, E.; Martin, M.J.; Michoud, K.; O'Donovan, C.; Phan, I. The SWISS-PROT protein knowledgebase and its supplement TrEMBL in 2003. *Nucleic Acids Res.* **2003**, *31*, 365–370. [\[CrossRef\]](#)
65. Katoh, K.; Standley, D.M. MAFFT multiple sequence alignment software version 7: Improvements in performance and usability. *Mol. Biol. Evol.* **2013**, *30*, 772–780. [\[CrossRef\]](#)
66. Beitz, E. TEXshade: Shading and labeling of multiple sequence alignments using LATEX2 epsilon. *Bioinformatics* **2000**, *16*, 135–139. [\[CrossRef\]](#)
67. Wang, G.; Li, X.; Wang, Z. APD3: The antimicrobial peptide database as a tool for research and education. *Nucleic Acids Res.* **2015**, *44*, D1087–D1093. [\[CrossRef\]](#)
68. Yang, J.; Yan, R.; Roy, A.; Xu, D.; Poisson, J.; Zhang, Y. The I-TASSER Suite: Protein structure and function prediction. *Nat. Methods* **2015**, *12*, 7–8. [\[CrossRef\]](#)





MDPI  
St. Alban-Anlage 66  
4052 Basel  
Switzerland  
Tel. +41 61 683 77 34  
Fax +41 61 302 89 18  
[www.mdpi.com](http://www.mdpi.com)

*Marine Drugs* Editorial Office  
E-mail: [marinedrugs@mdpi.com](mailto:marinedrugs@mdpi.com)  
[www.mdpi.com/journal/marinedrugs](http://www.mdpi.com/journal/marinedrugs)





MDPI  
St. Alban-Anlage 66  
4052 Basel  
Switzerland

Tel: +41 61 683 77 34  
Fax: +41 61 302 89 18

[www.mdpi.com](http://www.mdpi.com)



ISBN 978-3-0365-0565-7